Duc Hung NGUYEN

Valorization of natural drug products: from extraction to encapsulation

A thesis presented for the degree of

Doctor of Pharmacy

Speciality: Pharmaceutical Technology

Members of jury:

Prof. Dominique Laurain-Mattar	Université de Lorraine	President/ Rapporteur
Prof. Anne Sapin-Minet	Université de Lorraine	Rapporteur
Prof. Odile Chambin	UBFC	Supervisor
Prof. Anne-Claire Mitaine-Offer	UBFC	Co-supervisor

Dijon, 2020

THESE DE DOCTORAT DE L'ETABLISSEMENT UNIVERSITE BOURGOGNE FRANCHE-COMTE

PREPAREE AU LABORATOIRE DE PHARMACOGNOSIE PEPITE EA 4267

Ecole doctorale

Environnements - Santé

Doctorat de Pharmacie, spécialité Pharmacognosie

Par

Nguyen Duc Hung

Valorisation des produits médicamenteux naturels: de l'extraction à l'encapsulation

Thèse présentée et soutenue à l'UFR Sciences de Santé de Dijon, salle R46, le 09 Novembre 2020

Composition du Jury:

Prof. Dominique Laurain-Mattar	Université de Lorraine	Président/ Rapporteur
Prof. Anne Sapin-Minet	Université de Lorraine	Rapporteur
Prof. Odile Chambin	UBFC	Directeur de thèse
Prof. Anne-Claire Mitaine-Offer	UBFC	Co-Directeur de thèse

Dijon, 2020

Titre : Valorisation des produits médicamenteux naturels: de l'extraction à l'encapsulation

Mots clés : Saponine, Cytotoxicité, *Weigela*, *Cordyline*, *Dracaena*, Curcumine, Microencapsulation, Activité antioxydante.

Cette thèse s'inscrit dans la cadre de la thématique du Laboratoire de Pharmacognosie et du Laboratoire de Pharmacie Galénique de l'UFR Sciences de Santé, circonsription Pharmacie, au sein de l'Université de Bourgogne Franche-Comté, afin de trouver de nouvelles molécules naturelles bioactives à encaspuler. D'une part, nous nous sommes concentrés sur la recherche de saponines naturelles de plantes issues de la biodiversité vietnamienne et de l'horticulture française du genres *Dracaena*, *Cordyline* (Asparagaceae) et *Weigela* (Caprifoliaceae). Les travaux menés ont conduit à isolement de 35 saponines naturelles en utilisant différentes techniques chromatographiques. Les structures ont été déterminées par des méthodes de spectrométrie de masse en source ESI et de spectroscopie RMN. Parmi les 17 composés purs obtenus des 3 espèces appartenant au genre *Weigela*, 9 sont des glycosides de l'acide oléanolique et de l'hédéragénine de structure nouvelle. A partir des espèces *Dracaena braunii* et *Cordyline fruticosa* "Fairchild red", nous avons isolé et caractérisé 18 saponines stéroïdiques dont 7 nouvelles de type spirostane et 6 nouvelles de type furostane. Les activités cytotoxiques de la majorité des saponines isolées ont été évaluées sur trois lignées cellulaires : CT26 (cellules tumorales coliques murines), B16 (cellules de mélanome murin) et HepG2 (cellules d'hépatocarcinome) par le test de prolifération cellulaire MTS. Des relations structure/ activité ont ainsi été proposées.

D'autre part, nous avons sélectionné une molécule naturelle bien connue afin de mettre au point les essais d'encaspulation. La curcumine possède des propriétés thérapeutiques très intéressantes mais elle présente à la fois une faible solubilité et une faible biodisponibilité, limitant l'administration par voie orale. Dans cette partie de la thèse, nous avons cherché à améliorer la stabilité et la biodisponibilité de la curcumine ansi qu'une libération contrôlée dans le tractus gastro-intestinal. Des billes de pectinate de calcium ont préparées en utilisant la gélification ionique en présence de différents tensioactifs. Elles ont été caractérisées grâce à leur propriétés physico-chimiques et leur profils de dissolution *in vitro*. Leur activité antioxydante a été évaluée par le test DPPH. Le Kolliphor® HS 15 est le tensioactif le plus prometteur pour optimiser les propriétés de la curcumine.

Title : Valorization of natural drug products: from extraction to encapsulation

Keywords : Saponins, Cytotoxicity, *Weigela*, *Cordyline*, *Dracaena*, Curcumin, Microencapsulation, Antioxidant actitivy.

This thesis was carried out at the Laboratory of Pharmacognosy and the Laboratory of Pharmaceutical technology, at the UFR Sciences de Santé, circonscription Pharmacy, in the University of Burgundy Franche-Comté, to find new natural molecules to encapsulate. First of all, we focused on the natural saponins from plants of the Vietnam biodiversity and the French horticulture, belonging to the three genera *Dracaena*, *Cordyline* (Asparagaceae) and *Weigela* (Caprifoliaceae). The work led to the successful isolation and elucidation of 35 natural saponins using various chromatographic techniques. The structures were determined by ESI mass spectrometry and NMR spectroscopy. Among the 17 pure compounds obtained from three species of the *Weigela* genus, 9 oleanolic acid and hederagenin glycosides are previously undescribed ones. From the two species *Dracaena braunii* and *Cordyline fruticosa* "Fairchild red", we isolated and characterized 18 steroidal saponins including 7 new spirostane-types and 6 new furostane-types ones. The cytotoxic activities of the majority of isolated saponins were evaluated against mouse colon cancer (CT26 cells), mouse melanoma (B16 cells) and human liver cancer (HepG2 cells) by MTS assays. The structure / activity relationships were also proposed.

On the other hand, we selected a well-known natural molecule to develop encapsulation tests. Among the natural products, curcumin has very interesting therapeutic properties but exhibits both a poor solubility and a low bioavailability, limiting the administration by the oral route. The purpose of this study was to improve the solubility and bioavailability of curcumin as well as simultaneously achieve controlled release in gastrointestinal tract. Pectinate gel beads were prepared based on ionotropic gelation method with the presence of vaious surfactants. After drying, these beads were investigated for physicochemical characteristics (morphological aspects, encapsulation efficiency, stability, physical state), dissolution kinetics (*in vitro* release) and antioxidant activity was determined with DPPH assay. Kolliphor® HS 15 seems to be the best promising surfactant to increase stability and bioavailability of curcumin.

AKNOWLEDGEMENTS

I also warmly thank Mr. David Pertuit, a great technician, for supporting me during the fraction and isolation process. I am sincerely grateful for his patience and long hours spent to teach me how to use all equipments.

Futhermore, I am also greatful to the colleagues of laboratory of Pharmacognosy: Dr. Tomofumi Miyamoto, Dr. Chiaki Tanaka, Dr. Thomas Paululat for the measurements of the diverse NMR and MS experiments. Thankfulness is given to Dr. Bertrand Collin and Dr. Pierre-Simon Bellaye for help in cytotoxic activity.

To my lovely wife…

My wonderful wife Huyen could not be here during my PhD journey but she has always encouraged me and offered me the support that I needed to complete this thesis. I would have dropped out this journey and would not have written these words if I had lived without her. Huyen, my darling, you showed me what it means to love and to be loved, I am a lucky person with you. In the deepness of my heart, I give you a great love and appreciation for your faithful patience and all the moments we shared together, I thank you for being a half of my life.

…my sons…

Nam, my second son, I started my PhD journey while you were still in your mother's womb. I am sorry you, my son, for one reason that I could not be there when you were born. It can be the biggest regret of my life.

To Lam, my first son, I still remember the day I had to say goodbye to you. It has been an unforgettable in my mind. I hope you will understand my situation and excuse my absence at home.

…and my family!

My gratefulness address to my parents who have been supporting me in each and every step and breath I take, to my mother Ngan who gives me encouragement through her never-ended good wished, pray and emotional support, and to my father Hong whose kindness, inspiration always be in my heart. My gratitude is also forwarded to my big brother Ha and his wife Thao for their continuous tenderness and encouragement. To my mother-in-law Chien, my aunts-in-law Khay and Chin, my sister-in-law Ha and her husband Dat, receive my deep gratitude and love for your dedication and trust in me.

I thank to my aunt Hoa and two my uncles Tuan and Dung, you showed me the importance of education and helped me find the right way on every step of my life.

Last, but not least, to Madam Agnès Roy, receive my great gratitude and love for your supports during my whole schooling. Not only did you supply me with energy and motivation every time I depressed but also you taught me languages and the significance of life and love. Agnès, you have always been the one to make me better. For your love and endless support, I am happy to dedicate this thesis to you.

Finally, to someone who have not been here for any reason, I want you know that you have been always the ones to help me to reach this far in my career. Thank you for being a part of my life.

Duc Hung NGUYEN

Dijon, 2020

Dedication

I am so proud to dedicate this thesis

To my lovely wife and my children who have always encouraged me throughout my PhD journey…

To my whole family...

To Agnès Roy.

GENERAL INTRODUCTION

Nowadays, chemistry and biology laboratories around the world are studying on natural herbal medicines due to their safe to treat various diseases. There are several evidences to prove the use of traditional medicine in different cultures. Despite this historical importance of plants and considerable contemporary research into the identification of new naturally occurring chemical compounds, many of those are still not revealed both chemical structures and pharmacological activities. Saponin, a naturally occurring surface active glycoside, has been reported in recent years of publications about their properties. These compounds were discovered for their biological activities, from traditional uses to pharmaceutical applications. Saponins possess a various of pharmaceutical potentials, such as antitumor, anti-inflammatory, antiviral, antioxidant and antibacterial (Moghimipour and Handali, 2015). In this context, the Laboratory of Pharmacognosy, EA 4267, at the University of Burgundy Franche-Comté, is focusing on research of biologically active saponins from various plant families. Our research strategy consists in the selection of families and genera known for their richness in saponins, based essentially on chemotaxonomic criteria. Then, after extraction, isolation and structural characterization, the natural molecules are subjected to *in vitro* biological evaluation mainly in the field of cancerology. Due to these steps, three genera *Dracaena*, *Cordyline* and *Weigela* of two families Asparagaceae and Caprifoliaceae, were chosen for phytochemical investigation. It is interesting to note that many traditional uses of several species belonging to these genera present a potential in the pharmaceutical domain. Saponins were extracted and identified by using various chromatographic methods. These compounds were further evaluated for their cytotoxic activities and the analysis of relationships between structure and activity were carried out.

Aglycon (or sapogenin), an hydrophobic portion of saponin, has gained importance as a novel drug. But, their major limitation of its poor aqueous solubility leads to a relatively short half-life, low bioavailability and less permeability and degradation during human digestion. These problems are able to be overcome by various encapsulation method (Anand et al., 2007). However, extracted saponins is not enough to provide a good quantity,

so encapsulation are not carried out with this compound. Fortunately, curcumin, the principal curcuminoid found in turmeric which exhibits a wide spectrum of biological and pharmacological effects, is also a hydrophobic natural compound with low water solubility quite similar to saponins. We pointed out here an idea of encapsulation of curcumin instead of sapogenin in order to improve the solubility and bioavailability of hydrophobic compounds. This study was done using ionotropic gelation method with the presence of surfactants. Physicochemical characteristics, dissolution kinetics and antioxidant activity were further evaluated for efficacy of encapsulation to enhance the solubility and protect antioxidant capacity of curcumin, in view of future food applications.

This present thesis is structured by two parts:

- The first part will be carried out on saponin including three chapters. The first chapter will concern a literature review about botanical study and previous phytochemical works. The second chapter will give phytochemical investigations on selected plants. The third chapter corresponds to biological study on isolated compounds, in collaboration with Centre Georges-François Leclerc, ICMUB UMR CNRS 6302, using MTS colorimetric assay on different colon cancer cell lines.

- The second part will give a study on encapsulation of curcumin including three chapters. The first chapter will inform about chemical profile of curcumin and general background about some encapsulation methods. The second chapter will present the methodological and material tools used to manufacture beads, together with investigations of physicochemical characteristics, dissolution kinetics and antioxidant activity of beads. The third chapter will show the results and discussion.

A general conclusion also will be carried out at the end of this thesis providing an overview on results and propose perspectives.

SAPONIN PART

CONTENT

List of Figures

List of Tables

Abbreviations and Symbols

Ara	Arabinose
Fuc	Fucose
Glc	Glucose
Xyl	Xylose
Rha	Rhamnose
Agly	Aglycon
$CHCl_3$	Chloroform
MeOH	Methanol
EtOH	Ethanol
H_2O	Water
AcOH	Acetic acid
UV	Ultraviolet
CC	Column chromatography
GC	Gas chromatography
VLC	Vacuum liquid chromatography
MPLC	Medium pressure liquid chromatography
HPLC	High performance liquid chromatography
TLC	Thin layer chromatography
HPTLC	High performance thin layer chromatography

RPC	Reversed phase chromatography
MS	Mass spectrometry
RP	Reversed phase
NP	Normal phase
ESI	Electro spray ionization
NMR	Nuclear magnetic resonance
IR	Infrared spectroscopy
^{1}H NMR	Nuclear magnetic resonance of proton
^{13}C NMR	Nuclear magnetic resonance of carbon
COSY	Correlated spectroscopy
HSQC	Heteronuclear single quantum correlation
HMBC	Heteronuclear multiple bond correlation
TOCSY	Total correlation spectroscopy
ROESY	Rotating frame overhauser effect spectroscopy
NOESY	Nuclear overhauser effect spectroscopy
ppm	Part per million
s	Singulet
d	Duplet
t	Triplet
q	Quartet

dt	Doublet of triplets
td	Triplet of doublets
m	Multiplet
br	Broad
nd	Not determined
δ	Chemical shift in ppm
J	Coupling constant
IC_{50}	The half maximal inhibitory concentration
MTS	(3-(4,5-dimethylthiazol-2-yl)-5-(3-carboxymethoxyphenyl)-2-(4-sulfophenyl)-2H-tetrazolium)
5-FU	Fluorouracil

INTRODUCTION

Saponins are a class of phytochemical compounds which are found mainly but not exclusively in plants and normally foam when exposed in aqueous solution. In their structure, saponins are amphiphilic compounds composed of sugar chain(s) attached with an aglycon and as the result, this characteristic is cause of the foaming ability of saponins. The sugar chain(s) contains one or more linear oligosaccharides (L-arabinose, D-galactose, D-glucose, D-galactose, L-rhamnose and D-fructose) while aglycon (or sapogenin) is either a steroid (C27) or a triterpenoid (C30). When a single sugar chain normally attached at C-3 of aglycon, it is a mono-desmosidic saponin, while the other has two sugar chains which the one linked to C-3 and another one linked to C-22 of aglycon defined as bi-desmosidic saponins (Chaieb, 2010). Tri-desmosidic saponins have three sugar chains and are usually rare among others (Majinda, 2012).

In plants, saponins can be found in different parts of a number of plants, such as root, trunk, leaf, flower and seed, in both wild plants and cultivated crops. Their concentration, quantification and qualification depend on not only the cultivar, age and distribution, but also the part of plant species. Van et al. (2015) compared the content of saponin in different underground parts of *Panax vietnamensis* including radix, rhizome and roots.

Saponins possess strong pharmaceutical properties as anti-inflammatory, antimicrobial, anticancer, anti-cardiovascular, adjuvants and absorption enhancer (Moghimipour and Handali, 2015). Saponins are also known to possess mineral complexes of iron, zinc, and calcium. The beneficial effect of absorption activity is a significant consideration to sort of saponins (Milgate and Roberts, 1995). Not only is saponins' ability to extend the anticancer activity (Boutaghane et al., 2013; Pertuit et al., 2017; Wen et al., 2015), but these compounds also have important contributions in antibacterial (Fang et al., 2015; Mostafa et al., 2013, 2016), anti-inflammatory (Borges et al., 2013; Fu et al., 2017; Xiang et al., 2016), anti-oxydant (Chan et al., 2014) and immunological adjuvant activity (Cruz et al., 2016; Silva and Parente, 2013; Yendo et al., 2016).

During this thesis, three genera have been chosen, besed on chemotaxonomic data, for phytochemical investigations: one genus rich in triterpene glycosides, *Weigela*, and two rich in steroidal saponins, *Cordyline* and *Dracaena*.

The *Weigela* genus contains 10 species but over 200 cultivar names are recorded and still in cultivation. Phytochemical studies on *W. hortensis* (Murayama et al., 2003), *W. subsessilis* (Won et al., 2015), *W. stelzneri* (Rezgui et al., 2016), *W. florida* "rumba" (Champy-Tixier et al., 2018) and *Weigela* x "kosteriana variegata" (Andriamisaina et al., 2018) reported the presence of saponins.

Cordyline fruticosa "Fairchild red" is a cultivated dwarf evergreen shrub, belongs to a genus rich in saponins according to literature data (Mimaki et al., 1997, 1998a).

Dragon's blood, refers to a deep red resin, involve four genera including *Dracaena* (Asparagaceae), *Daemonorops* (Arecaceae), *Croton* (Euphorbiaceae) and *Pterocarpus* (Fabaceae). These plants have been used a traditional medicine for different diseases in many countries. Plants of genus *Dracaena* comprises approximately 60 species which are found nearly in tropical and subtropical of Africa (Marrero, 1998). Saponins extracted from species of genus *Dracaena*, i.e. *D. draco* L, *D. thalioides*, *D. cambodiana* and *D. angustifolia* Roxb., exhibit a cytostatic capacity against the cancer cells (González et al., 2003; Shen et al., 2014; Tang et al., 2014). *Dracaena braunii*, synonym *Dracaena sanderiana*, is an ornamental plant which can be found widely in Asia and Africa. In Vietnam, this plant is a popular indoor plant known as "Lucky bamboo" in common names. As a part of the *Dracaena* genus, this plant may contain saponins playing an interesting role in bioactivities.

In our continuing research for new biologically active saponins and completing the chemotaxonomic data about saponins from the genus *Weigela* (Caprifoliaceae), three species including *W.* x "Bristol ruby", *W. florida* "Pink poppet" and *W. florida* "Jean's gold" were phytochemically investigated, together with two species of the Asparagaceae family, *Cordyline fruticosa* "Fairchild red" and *Dracaena braunii*.

CHAPTER 1

BOTANICAL STUDIES AND PREVIOUS PHYTOCHEMICAL WORKS

1. Botanical study

1.1. Order Dipsacales

Dipsacales, an order of dicotyledon plants, includes only two families, Adoxaceae and Caprifoliaceae, containing 46 genera and 1090 species (The Angiosperm Phylogeny Group, 2009). They are distributed worldwide but the origin was probably in the Northern Hemisphere. Plants in Dipsacales have opposite, often gland-toothed leaves, petals fused into a corolla tube and inferior ovaries. Most members of the order are shrubby, but there are a few herbaceous members as well (Britanica, 1999).
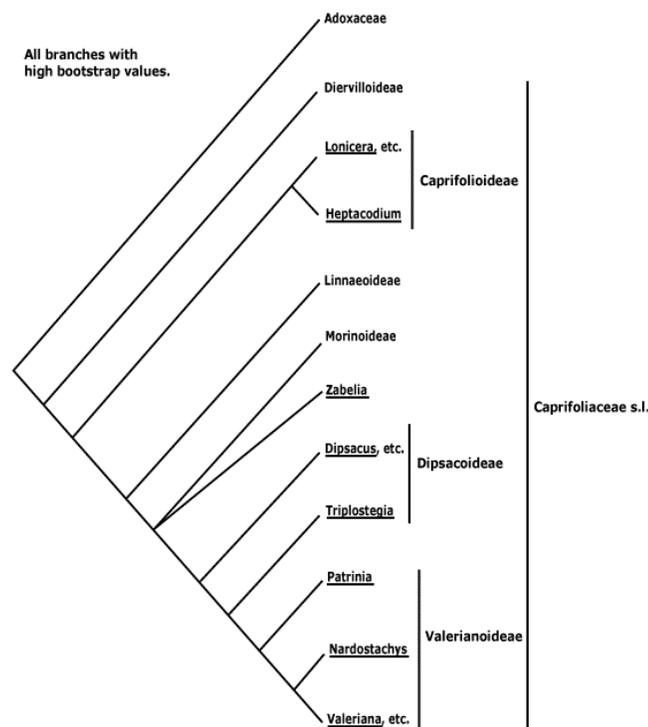
Figure 1. Phylogenetic classification of order Dipsacales (Missouri Botanical Garden)

1.1.1. Family Caprifoliaceae

Caprifoliaceae, one of two families of order Dipsacales, contains 42 genera and over 890 species contributed largely in warm temperate areas in the Northern Hemisphere (Britanica). They are trees or herbs that can be recognized by their opposite leaves and often rather weakly monosymmetric flowers with a more or less radially symmetric calyx; the ovary is inferior and the fruits are often few or one seeded. The bark in the woody taxa often comes off in thin flakes (Missouri Botanical Garden).
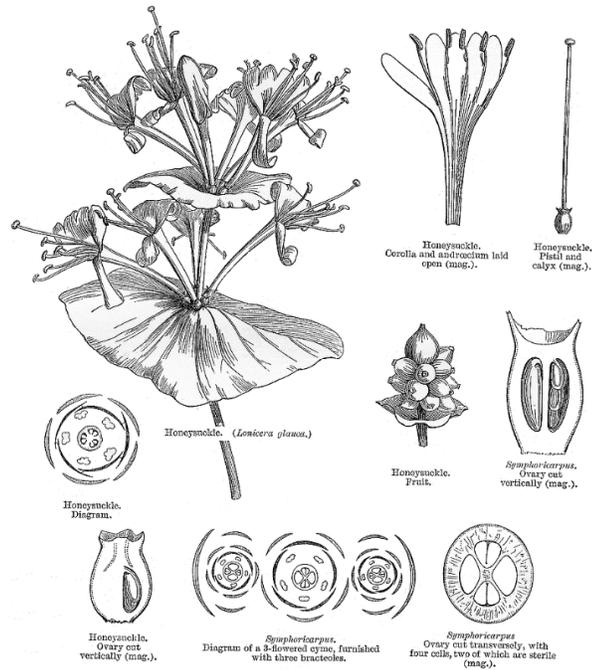
Figure 2. Diagram of Caprifoliaceae flower part (Watson, L., and Dallwitz, M.Z, 1992)

1.1.2. Genus Weigela

The genus *Weigela* is named after Christian Ehrenfried Weige (1748-1831), a Germanist Professor of Chemistry, Pharmacy, Botany, and Mineralogy at the University of Greifswald. The first species of the genus, *Weigela florida*, was introduced by Robert Fortune in 1845 (Sheffield Botanical Garden, 2019).

Weigela genus includes 52 species of deciduous shrubs in the family *Caprifoliaceae* which 7 of them are accepted as species names containing *Weigela decora* (Nakai) Nakai, *Weigela florida* (Bunge) A. DC., *Weigela fujisanensis* (Makino) Nakai, *Weigela grandiflora* (Siebold & Zucc.) Fortune, *Weigela japonica* Thunb., *Weigela praecox* (Lemoine) Bailey and *Weigela sanguinea* (Nakai) Nakai (The Plan list, 2019).

The species *Weigela florida* has ovate-oblong in leaves with 5-15 cm in length which an acuminate tip and a serrated margin are included. The flowers have a length of 2-4 cm, with a five-lobed white, pink, or red corolla which are produced in small corymbs of several together in early summer. The fruits appear like dry capsules containing small winged seeds (Lamarck, 1808).

1.1.3. Some horticultural species of genus Weigela

a. Weigela x "Bristol Ruby"

Weigela x "Bristol Ruby" is a hybrid deciduous shrub of upright habit with narrowly ovate, dark green leaves. Flowers are ruby-red produced and cover the foliage. The bell-shaped flowers attract hummingbirds. This plants can grow up to 120-140cm in height and 120-180 cm in width and may flower during the summer into fall (Gardenia, 2019).

Figure 3. *Weigela* x "Bristol Ruby"

b. Weigela florida "Jean's Gold"

Weigela florida "Jean's Gold" is a cultivar deciduous shrub which are highly appreciated and cultivated for the diversity of shapes and colors of flower. This plant has red flower and can grow up to 2-3 m in height and may flower from May to September (Jardinland, 2019).

Figure 4. *Weigela florida* "Jean's Gold"

c. Weigela florida "Pink Poppet"

The cultivar *Weigela florida* "Pink Poppet" was selected in 1991 as a shrub noted for its dwarf growth habit, early-blooming pink flowers and winter hardiness. Funnel-shaped, light pink flowers bloom profusely in late spring, with a sparse and scattered repeat bloom often occurring in mid to late summer. This plant can grow up to 2-3 m in height (Missouri Botanical Garden, 2019a).

Figure 5. *Weigela florida* "Pink Poppet"

1.2. Order Asparagales

Asparagales, an order of monocot plants, has been classified by Angiosperm Phylogeny Group. It was introduced firstly by Huber in 1977 (Huber, 1977) and later by Krikorian (1986) and then by the APG 1998, 2003, 2009 and 2016. In the past, many families of the order were distributed in old order Liliales which contains almost of monocot plants. But, it has then redistributed by DNA sequence analysis to three orders including Liliales, Asparagales and Dioscoreales that Asparagales becomes the largest order of monocots with 14 families, 1122 genera and 36205 species (Missouri Botanical Garden, 2019b).
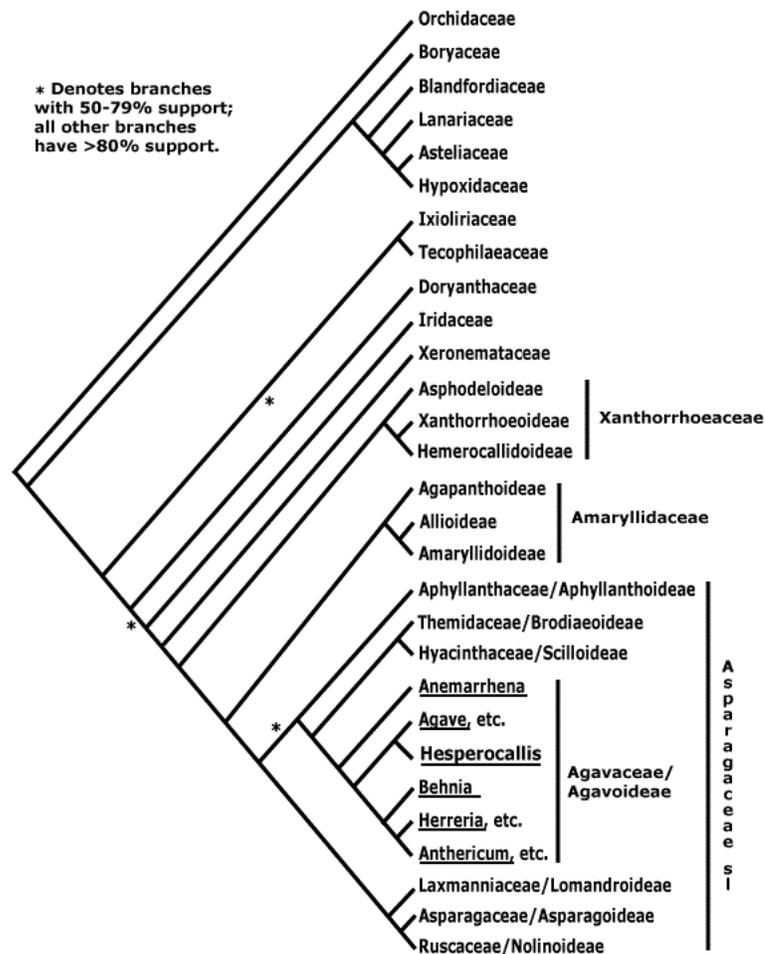
Figure 6. Phylogenetic classification of order Asparagales
(Missouri Botanical Garden, 2019b)

1.2.1. Family Asparagaceae

Placed in the order Asparagales, Asparagaceae is a family of flowering plants which includes 114 genera with 2900 known species (Christenhusz and Byng, 2016). Species in this family are herbaceous plants, with rhizomatous roots, fibrous, or thickened in tuber. They develop branched, erect or climbing stems, thorny and sometimes high as in *Asparagus umbellatus*. Their leaves are small, thorny and completely devoid of stipules. The flowers are small, occur cyclically which have 6 tepals, 2 whorls of 3 stamens and a gynoecium with 3 carpels. These plants have superior ovaries and three compartments that mature into dry capsules. This family posscess phytomelanin which create black colored seed coats. The fruits are small berries (Willamette Botany, 2001).

8

1.2.2. Genus Dracaena

The botanical name of *Dracaena* comes from ancient Greek "drakaina" which means dragon. It refers to a deep red resin and comprises approximately 60 species which are found nearly in tropical and subtropical of Africa (Marrero, 1998). This genus is placed in the family Asparagaceae, subfamily Nolinoideae (formerly the family Ruscaceae) (Sennikov et al., 2016; W. Chase et al., 2009). These are very common green plants, prized for their variegated foliage. Most are shrubs with erect stems, little branched, with broad or narrow leaves, usually grouped together with stems.

Species *Dracaena braunii*

Dracaena braunii, synonym *Dracaena sanderiana* Sander, is an ornamental plant which can be found widely in Africa and Asia. In Vietnam, this plant also known as "Lucky bamboo" in common names and also a popular indoor plant. *Dracaena braunii* is a vertical, woody, evergreen shrubby species with slender stems and flexible strap-shaped leaves that grow as understory plants in rainforests. It is an upright shrub growing to 1.5 m in height, with leaves 15-25 cm in length and 1.5-4 cm breadth at the base. Indoor height rarely exceeds 90cm. This species can grow in water and have a bright green, cane-like stem, green leaves and roots with different colors (black, white, orange, red) (PlantsRescue, 2019).

Figure 7. *Dracaena braunii*

1.2.3. Genus Cordyline

Cordyline is derived from the ancient Greek "kordyle", meaning club which is a reference to the enlarged underground stems or rhizomes (Ho, 2006). This genus is found natively in Western Pacific Ocean region which consists of about 26 species of woody monocots plants which is accepted by World Checklist of Selected Plant Families (Zonneveld, 2019).

These are evergreen shrubs and tree-like, woody perennials. The larger perennials resemble palm trees. Long, leathery leaves are produced in tufts or rosettes. Flowers are cup-shaped and sweet-smelling, sometimes produced in large terminal panicles. Round white, red, blue, or purple berries follow. Cabbage palms are good as houseplants or grown in a greenhouse. In warmer areas, they can be used as specimen plants, in a border, or in a courtyard garden (Finegardening, 2019).

Species *Cordyline fruticosa* "Fairchild Red"

Cordyline fruticosa "Fairchild Red" is a dwarf evergreen shrub that averages 60-90 cm in height with a spread of 45-60 cm. It has an upright, fountain-shaped growth habit. Leaves are evergreen, linear in shape, narrow, spiral in arrangement, simple, somewhat glossy and medium green with pink margins. Some older foliage can become very dark green with pink or red margins. As plants get older and depending on the amount of light, newer foliage can be predominantly red. It has parallel veins. This plant has pink flower and blooms from spring to fall. Fruit are small, round berries (Looking at plant, 2014).

Figure 8. *Cordyline fruticosa* "Fairchild Red"

2. Previous phytochemical analysis

2.1. Saponin generalities

Saponins, which is derived from Latin word "*sapo*" which means "*soap*" and have a form soap-like foams upon shaking, are known as a non-volatile and surfactant compound. Due to this property, saponin dissolve easily in water and form soap-like. Some of plants which have this ability are named with a word "*sapo*", such examples soapwort (*Saponaria officinalis* L.) (Bruneton, 2016; Sparg et al., 2004), soapberry (Naidu, 2000). Most saponins have haemolytic properties and are toxic to most cold-blooded animals. (Herlt et al., 2002) reported that saponins extracted from seeds of *Barringtonia asiatica* Kurz., a "fish killer tree" in tropical Asia and Pacific, exhibit piscicidal activity to fish when thrown into water.

In structure, saponin contain sugar chain(s) attached with an aglycon (or sapogenin). These sugars could be attached to aglycon one, two or three side chains and the term mono-desmosidic, bi-desmosidic and tri-desmosidic are named for these saponins, respectively (in Greek, *desmos* means *chain*) (Naidu, 2000). Aglycons (or sapogenins) are divided into two groups based on their skeleton: steroidal and triterpenoid. Steroidal saponins almost present in the monocotyledonous angiosperms, while triterpenoid saponins occur mainly in dicotyledonous angiosperms (Bruneton, 2016).

Lacaille-Dubois and Wagner (1996) reported biological and pharmacological activities of saponins in several reviews. The biological role of saponins are not completely figured. Saponins are considered as a part of plants' defense systems and often have antifungal and antimicrobial activities in molecules of plants (Morrissey and Osbourn, 1999). Besides that, a wide number of plants containing saponins are used in traditional medicine, in example, root of *Panax notoginseng* (Burk.) F. H. Chen. which is utilized in treating injury (Zhang et al., 2013). The genus *Bupleurum*, officially recognized in Chinese and Japanese pharmacopoeia, is utilized widely to treat different diseases. The main anti-inflammatory compounds in dry root of *Bupleurum fruticescens* L. (Apiaceae) are saikosaponins (J Just et al., 1998). Active constituents of *Achyranthes bidentata*, a Chinese traditional medicine which used for strengthening bones and muscles and ensuring proper downward flow of blood, have been shown to be saponins named Bidentatoside II and chikusetsusaponin V

methyl ester (Mitaine-Offer et al., 2001). Another example, *Momordica charantia* utilized to reduce blood glucose and lipids, protect β cells, enhance insulin sensitivity and reduce oxidative stress contains saponins (Keller et al., 2011).

Due to the chemical properties and soap-like foaming, saponins are also used in food industry and cosmetics. In example, the saponin of *Quillaja saponaria* is accepted to be used in food as "Generally Recognized as Safe" (GRAS) in the USA (Zhao et al., 2012).

As pointed out above, saponins can be divided into two groups due to the nature of their aglycon skeletons which are either steroidal or triterpenoid. Saponins are classed on the base of number of sugars (saccharide chain). Sugar could be attached one, two or three side chains to aglycon and the term are named mono-desmosidic, bi-desmosidic and tri-desmosidic, respectively.

a. Structure of aglycon (sapogenin)

Steroidal aglycon

Steroidal saponins are available in monocotyledonous angiosperms, not only in the families of Asparagaceae, Dioscoreaceae and Amaryllidaceae but also in the dicotyledonous angiosperm *Solanaceae*. In structure, steroidal saponins are mainly compounds containing 27 carbon atoms forming the core structures, ie, spirostane-type (16β, 22:22α, 26-diepoxy-cholestan) and furostane-type (16β, 22-epoxycholestan) (Fig.9).

a   b
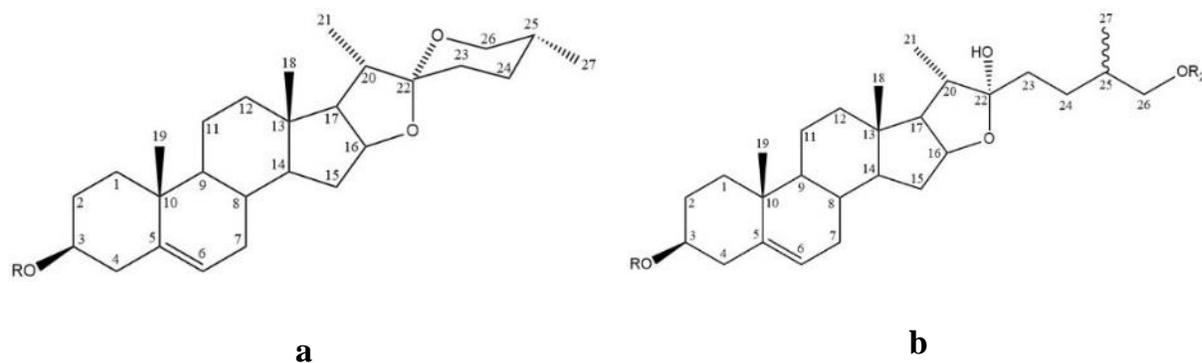
Figure 9. Structure of spirostane aglycon (**a**) and furostane aglycon (**b**)

(P. Munafo Jr and Gianfagna, 2014)

In nature, the saponins mainly consist of (25S)-spirostane derivatives (neosaponins), (25R)-spirostane derivatives (isosaponins), and (25S)- and (25R)-furostane derivatives. There are

rare reports of aglycon derivatives from furostane [spirofuran, (22R)-16β, 22:22, 25-diepoxy-cholestan] and spirostane [(22R)-22, 26-epoxy-cholestan], as well as derivatives of cholestane without a fused *O*-heterocycle, cholestan-23-on-derivatives or pregnane derivatives. The ring systems A/B/C/D are linked together in the order trans-trans-trans (5α derivatives) or cis/trans/trans (5β derivatives) (Thakur et al., 2011).

Table 1. Structural features of spirostane derivatives for saponins

Type of sapogenin	Substituent at different C-positions						
	1β	3β	25	Double bonds	Configuration at		Reference
					C-5	C-25	
Australigenin	OH	OH	$=CH_2$		α		(Blunden et al., 1984)
Diosgenin			CH_3	Δ^5		R	(Tsukamoto and Ueno, 1936)

<u>Triterpenoid aglycon</u>

Triterpenoid saponins mainly contain aglycons with 30 carbon atoms. The most commonly occurring core structures are pentacyclic oleananes and tetracyclic dammarans. Other aglycons of triterpenoid saponins are of the ursane-, lupane-, and hopane-type. The ring systems A/B/C/D/E for oleanane and ursane derivatives are linked together in the order trans-trans-trans-trans, for lupane derivatives in the order trans-trans-trans-cis, and for the rings A/B/C/D in dammarane derivatives in the order trans-trans-trans.
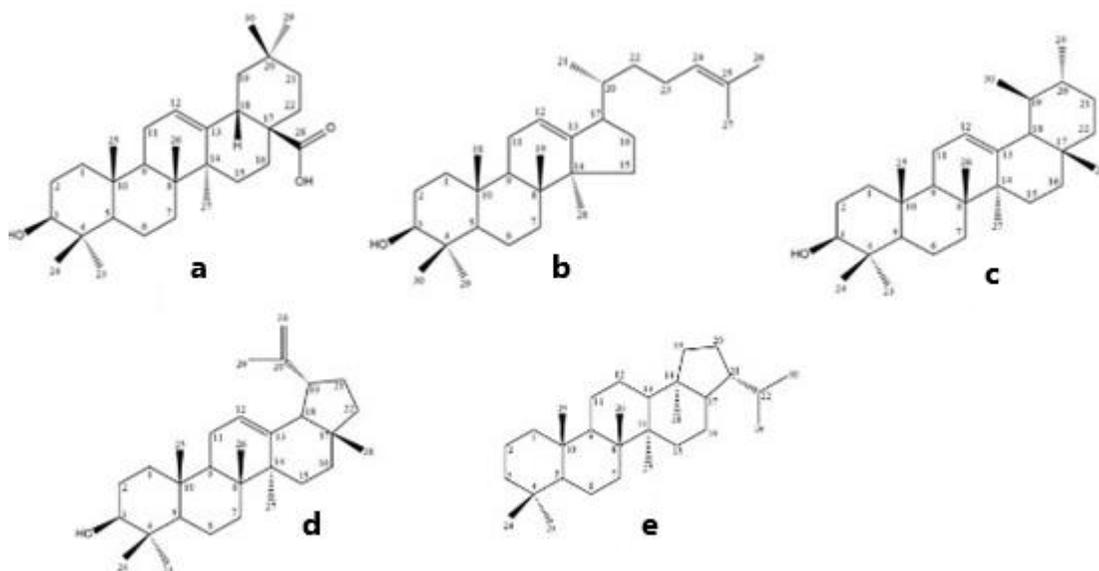
Figure 10. Structure of oleanane- (**a**), dammarane- (**b**), ursane- (**c**), lupane- (**d**) and hopane-type aglycon (**e**) (Moses et al., 2014)

Substituents on the frequently occurring aglycons derived from the oleanane structure of saponins are showed in Table 2. The hydroxyl group at position C-3 is found in all structures; very often hydroxyl groups are also reported at positions C-16, C-21, and C-22, and less often in positions C-2 and C-15. The methyl groups in positions C-23, C-24, C-28, C-29, and C-30 can be oxidized to CH_2OH- or COOH- moieties, and in some cases also to a CHO- group. Epoxide groups, keto functions and double bonds between C-12 and C-13 are also reported. The hydroxyl groups can be acylated, and this leads to the formation of ester saponins. Acidic components in such cases are formic, acetic, n- and iso-butyric, iso-valerianic, α-methyl butyric, angelic, tiglic, benzoic, cinnamic, and ferulic acid, and, in some cases, sulfuric acid.

Table 2. Types of aglycons substituted at carbon positions (Thakur et al., 2011)

Type of sapogenin	Substitution at carbon positions						
	3β	R^1	R^2	R^3	R^4	R^5	Δ^{12}
Hederagenin	OH	CH_2OH	H	COOH	CH_3	H	+
Oleanolic acid	OH	CH_3	H	COOH	CH_3	H	+

b. Sugars (carbohydrate chains)

Saponins consisting of one or more carbohydrate chains frequently attached to the C-1, C-3, C-28 of aglycon are showed in Fig.11 below.

D-galacturonic acid
(GalA)

D-glucuronic acid
(GlcA)

D-fucopyranose
(Fuc)

D-galactopyranose
(Gal)

D-glucopyranose
(Glc)

D-xylopyranose
(Xyl)

L-arabinopyranose
(Ara)

L-rhamnopyranose
(Rha)

D-apiofuranose
(Apif)

L-arabinofuranose
(Araf)
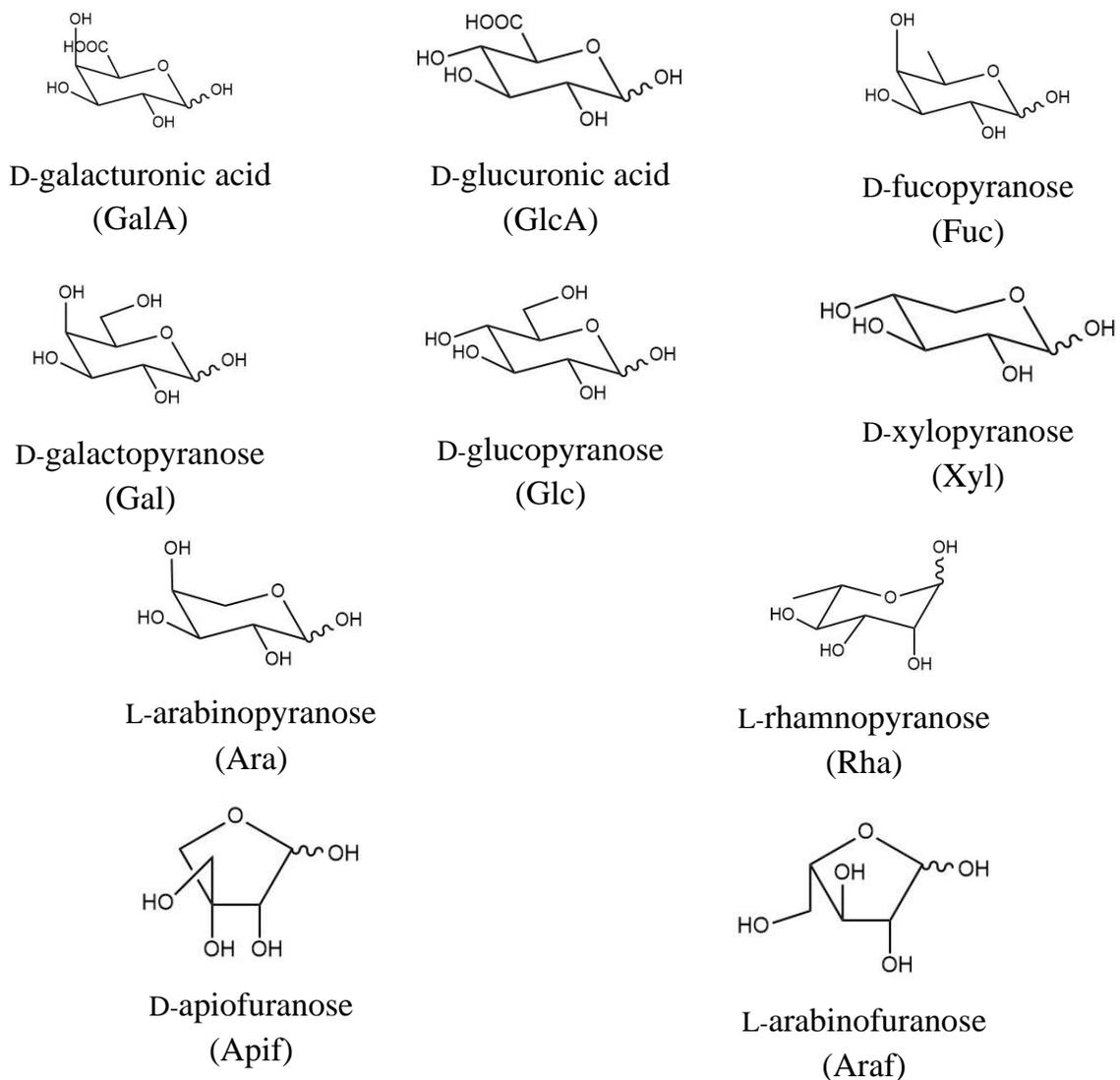
Figure 11. Available different sugars in saponins

2.2. Saponins isolated from genus *Weigela*

Plants of genus *Weigela* contains 10 species but over 200 cultivar names are recorded and still in cultivation. Several species of *Weigela* plants were investigated and structures of compounds isolated were also elucidated which are triterpenoid saponins of oleanane-type and hederagenin-type. Fig.12 shows different triterpenoid saponins elucidated from species of *Weigela* genus.
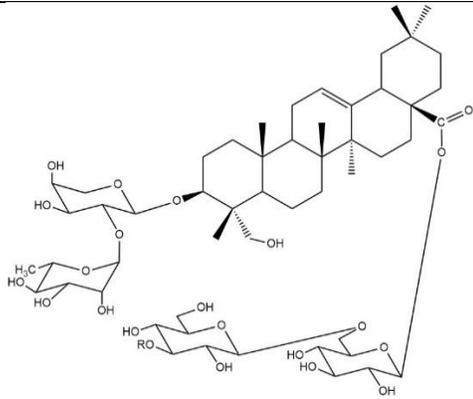
	R
Weigela hortensis (Murayama et al., 2003)	H
	Ac

	R₁	R₂
Weigela subsessilis (Won et al., 2015)	H	β-D-Xyl
	H	β-D-Glc
		H
		H

	R₁	R₂	R₃
Weigela stelzneri (Rezgui et al., 2016)		H	H
		H	H
		H	H
			H
			OH

	R
Weigela florida "rumba"
(Champy-Tixier et al., 2018) |

H |
|
Weigela x "kosteriana variegata"
(Andriamisaina et al., 2018) | R
 |
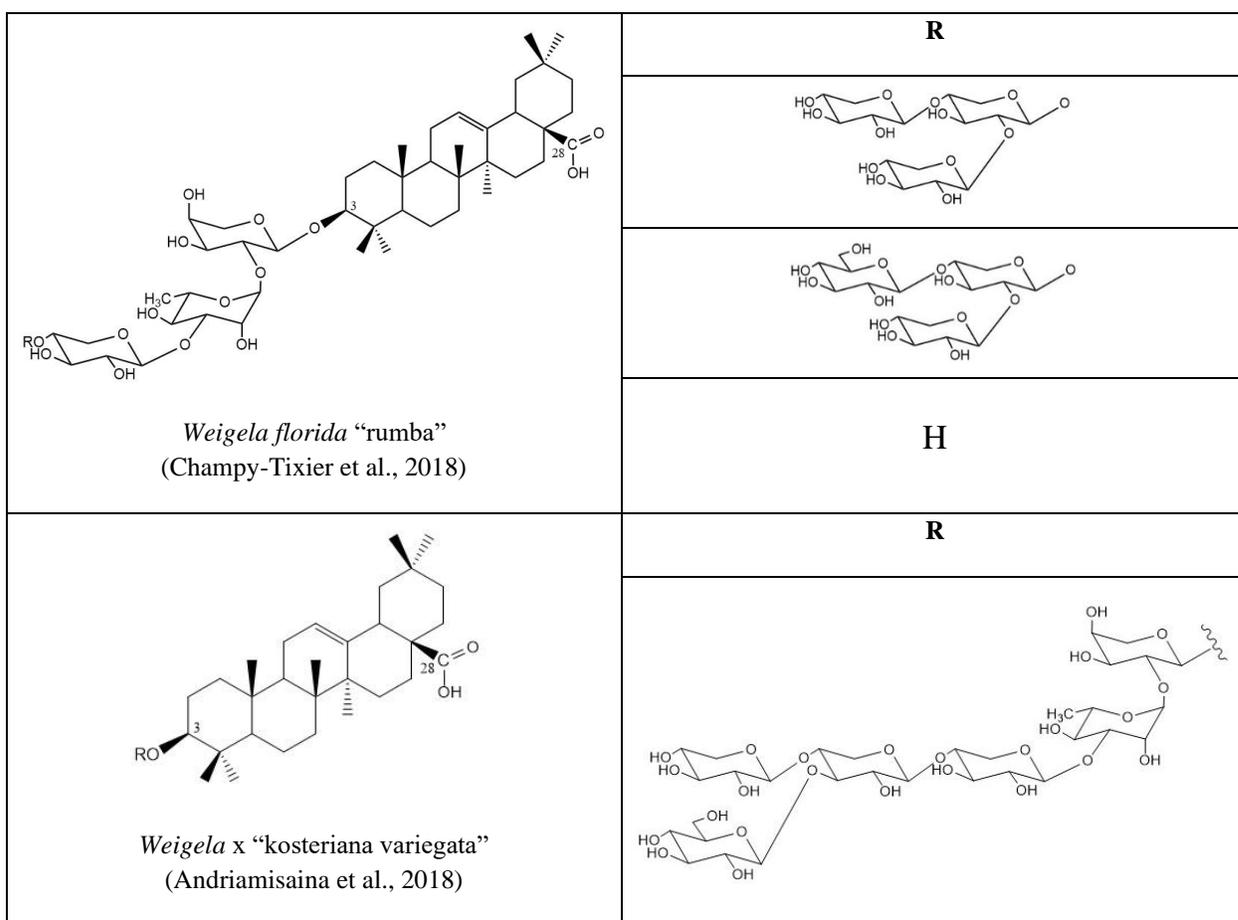
Figure 12. Some triterpenoid saponins elucidated from species of *Weigela* genus

2.3. Saponins isolated from genus *Cordyline*

Plants of genus *Cordyline* are found natively in Western Pacific Ocean region which consists of about 26 species of woody monocots plants which is accepted by World Checklist of Selected Plant Families. Some species of *Cordyline* plants were investigated and structures of compounds isolated were also elucidated which are steroidal saponins of spirostane-type and furostane-type. Different steroidal saponins elucidated from species of *Cordyline* genus are showed in Fig.13.

	R1	R2	R3	R4	R5
Cordyline cannifolia (Jewers et al., 1974)	OH	H	OH	H	Me
	OH	OH	H	Me	H
	Ac	Ac	H	Me	H
	Ac	OH	H	Me	H
	H	OH	H	Me	H

Cordyline cannifolia (Jewers et al., 1974)	R1	R2
	Me	H
	H	Me

Cordyline rubra
(Yang et al., 1990)

Cordyline rubra
(Yang et al., 1990)

Cordyline stricta
(Mimaki et al., 1997)

Cordyline stricta
(Mimaki et al., 1997)

Cordyline stricta
(Mimaki et al., 1997)

Cordyline stricta
(Mimaki et al., 1997)

Cordyline stricta (Mimaki et al., 1997) **R** H OH	*Cordyline stricta* (Mimaki et al., 1997)
Cordyline stricta (Mimaki et al., 1998a)	*Cordyline stricta* (Mimaki et al., 1998a)
Cordyline stricta (Mimaki et al., 1998a)	*Cordyline stricta* (Mimaki et al., 1998a)
Cordyline stricta (Mimaki et al., 1998a)	*Cordyline fruticosa* (Fouedjou et al., 2013) **R** **1** H $\Delta^{5(6)}$ **2** SO_3H
Cordyline fruticosa (Fouedjou et al., 2013)	*Cordyline fruticosa* var. strawberries (Ponou et al., 2019)

	R₁	R₂	R₃
Cordyline fruticosa var. strawberries (Ponou et al., 2019)	SO₃H	SO₃Na	H
		SO₃H	H
		SO₃H	OH

Figure 13. Steroidal saponins elucidated from species of *Cordyline* genus

2.4. Saponins isolated from genus *Dracaena*

The botanical name of *Dracaena* comes from ancient Greek "*drakaina*" which means dragon. It refers to a deep red resin and comprises approximately 60 species which are found nearly in tropical and subtropical of Africa (Marrero, 1998). The genus *Dracaena* contains both spirostane-type and furostane-type steroidal saponins possessing bioactivities. Different steroidal saponins elucidated from species of *Cordyline* genus are showed in Fig.14.

Dracaena concinna (Mimaki et al., 1998b)	R1	R2
	H	α-L-Rha
	β-D-Glc	H

	R1	R2	R3	R4
Dracaena concinna (Mimaki et al., 1998b)	H	H	H	H
	H	H	H	SO₃⁻
	OH	OH	β-D-Xyl	H
	OH	O-β-D-fuc	β-D-Xyl	H

	R1	R2
Dracaena concinna (Mimaki et al., 1998b)	H	α-L-Rha
	β-D-fuc	H

	R1	R2	R3
Dracaena concinna (Mimaki et al., 1998b)	H	β-D-Xyl	Me
	H	H	Me
	H	H	H
	OH	H	Me
	OH	H	Me

	R1	R2
Dracaena concinna (Mimaki et al., 1998b)	H	Me
	H	H
	OH	Me

	R1	R2	R3	R4
Dracaena draco L. (González et al., 2003)	Ac	Ac	Ac	H
	Ac	Ac	H	H
	Ac	H	H	H
	H	H	H	H
	H	H	Ac	H
	Ac	Ac	Ac	β-D-fuc

	R1	R2	R3
Dracaena draco L. (González et al., 2003)	H	H	α-L-Rha
	H	H	α-L-Rha
	α-L-Rha	β-D-Fuc	H

	R1	R2	R3
Dracaena draco L. (González et al., 2003)	α-L-Rha	β-D-Fuc	H
	α-L-Rha	H	α-L-Rha

Dracaena draco L. (Hernández et al., 2006)

	R
Dracaena surculosa (Yokosuka et al., 2000)	H
	Ac

Dracaena surculosa (Yokosuka et al., 2000)	**R**
	H
	α-L-Rha*p*

Dracaena surculosa
(Yokosuka et al., 2000)

Dracaena surculosa (Yokosuka et al., 2000)	**R**
	H
	β-D-Glc

Dracaena surculosa
(Yokosuka et al., 2000)

Dracaena surculosa (Yokosuka et al., 2002)	**R**
	β-D-Fuc*p*
	β-D-Glc*p*

Dracaena surculosa (Yokosuka et al., 2002)	**R**
	β-D-Glc*p*
	β-D-Fuc*p*

Dracaena cambodiana
(Shen et al., 2014)

| *Dracaena cambodiana* (Shen et al., 2014) | **R1** | **R2** |
| | | |

	R1	R2
Dracaena angustifolia Roxb. (Huang et al., 2013)	H	
	H	
		H

	R1	R2	R3	R4	R5	R6
Dracaena cambodiana (Shen et al., 2014)	S_4	H	H	OH	CH_2OH	H
	S_4	H	H	H	CH_2OH	H
	S_4	H	H	H	CH_3	H
	S_4	H	OH	H	CH_3	H
	H	OS_5	H	H	H	CH_3

S_4	S_5

	R
Dracaena cambodiana (Shen et al., 2014)	

	R
Dracaena cambodiana (Shen et al., 2014)	

	R1	R2	R3
Dracaena cambodiana (Shen et al., 2014)	SO_3H	H	H
	H	H	S_2
	H	S_3	S_2
	SO_3H	H	S_2

S_2	S_3

Dracaena marginata (Rezgui et al., 2013)

	R1	R2
Dracaena thalioides (Tang et al., 2014)	H	H
	Rha	Xyl
	Rha	H

	R1	R2
Dracaena thalioides (Tang et al., 2014)	H	H
	Rha	H
	Rha	Xyl

	R1	R2	R3
Dracaena thalioides (Tang et al., 2014)	Glc	Ac	Ac
	Fuc	Ac	Ac
	Fuc	Ac	H
	Fuc	H	H
	Glc	Ac	H
	H	Ac	H

	R1	R2	R3
Dracaena thalioides (Tang et al., 2014)	Rha	Ac	H
	Rha	Ac	Ac
	H	H	H
	Rha	H	H

Figure 14. Steroidal saponins elucidated from species of *Dracaena* genus

24

CHAPTER 2

PHYTOCHEMICAL STUDY

1. Materials and methods

1.1. Materials and extraction

Weigela x "Bristol Ruby" was provided in 2016 from Jardiland® (Chenôve, France). A voucher specimen (N° 20160110) was deposited in the herbarium of the Laboratory of Pharmacognosy, Université de Bourgogne Franche-Comté, Dijon, France.

Weigela florida "Pink Poppet" and *Weigela florida* "Jean's Gold" were provided in 2018 from Jardiland® (Chenôve, France). The voucher specimens (N° 2018/05/1 for *W. florida* "Pink Poppet" and N° 2018/05/2 for *W. florida* "Jean's Gold") were deposited in the herbarium of the Laboratory of Pharmacognosy, Université de Bourgogne Franche-Comté, Dijon, France.

Cordyline fruticosa "Fairchild Red" was collected in a flower shop in Thainguyen city, Vietnam in 2018. The voucher specimen (N° 2018/10/8) was deposited in the herbarium of the Laboratory of Pharmacognosy, Université de Bourgogne Franche-Comté, Dijon, France.

Dracaena braunii (synonym: *Dracaena sanderiana* hort. ex Mast.) used in this study were collected in a garden-shop in Can Tho, Vietnam. A small dried specimen of *Dracaena braunii* was deposited in our laboratory (N° 2019/03/20).

The dried and powdered roots of *Weigela* x "Bristol Ruby" (49 g) were submitted to ultrasounds three times with 1 L of the solvent $EtOH/H_2O$ (75/35), 30 min/time. The solvent was evaporated to give 7 g of crude extract.

The dried and powdered of aerial parts of *Weigela florida* "Jean's Gold" (56.78 g) were submitted to a microwaves extraction three times with the solvent $EtOH/H_2O$ (75/35, 400 mL each one, 200 W, 60°C, 45 min). After filtration and evaporation, 21.49 g of crude extract was yielded.

The dried roots (26.52 g) and aerial parts (28.97 g) of *Weigela florida* "Pink Poppet" were extracted separately by microwaves three times for each part with 300 mL of solvent $EtOH/H_2O$ (60°C, 30 min, 200W, 75/35, 250 mL of solvent x 3 times). After removal of the solvent, 2.25 g of roots' residue and 7.7 g of aerial parts' residue were obtained.

The dried roots (74.18 g) and aerial parts (103.87 g) of *Cordyline fruticosa* "Fairchild red" were submitted separately to microwaves (60°C, 30 min, 200W, 300 mL of solvent EtOH/H_2O 75/35 x 3 times). After evaporation of the solvents under vacuum, 24.88 g of roots' residue and 15.34 g of aerial parts' residue were obtained.

The roots of *D. braunii* (6.16 g) were extracted by microwaves (60°C, 30 min, 200W, 250 mL of solvent EtOH/H_2O 75/35 x 2 times). After filtration and evaporation, 1.22 g dried crude extract was collected.

1.2. Methods of isolation

Several chromatographic techniques are used to identify and separate the crude extract and obtain pure saponins including TLC (Thin Layer Chromatography), HPTLC (High Performance Thin Layer Chromatography), VLC (Vacuum liquid chromatography), MPLC (Medium Pressure Liquid Chromatography) and HPLC (High Pressure Liquid Chromatography).

1.2.1. Chromatographic methods of analysis

a. Thin Layer Chromatography (TLC)

TLC is a simple, quick and inexpensive procedure used to identify how many components are in a mixture. A TLC plate is a sheet of glass coated with a thin layer of a solid absorbent. A small amount of mixture which need to be analysed is spotted near the bottom of this plate. The TLC plate is placed in a rectangular TLC developing tank with a solvent. This solvent is the mobile phase and it slowly rises on the TLC plate by capillary action. The outcome depends upon a balance among three polarities - that of the plate, the development solvent and the spot material. Different components in the original spot, having different polarities, will move different distances from the original spot location and show up as separate spots (Oleszek and Bialy, 2006).

Chromatographic conditions

- Stationary phase:

Silica plate for normal phase: 60 Å F_{254}, Silicycle.

Silica plate high performance HPTLC: 60 Å F_{254}, Merck.

- Mobile phase:

Chloroform ($CHCl_3$)-Methanol (MeOH)-Water (H_2O)

$CHCl_3$/MeOH/H_2O 85/15/2; 75/25/3; 70/30/5; 65/31/6; 60/32/7

TLC plates are observed on UV light from 254 to 366 nm before revelation.

Revelation

Vanillin sulfuric reagent: Solution consisting of 1 g vanillin, 2 mL sulfuric acid and 95% ethanol up to 100 mL.

After soaking the plates in a dip tank containing the reagent, the plates are then dried at 110°C for a few minutes. Several colorations appear depending on the type of compounds.

Detection spots of saponin

The saponin spot forms mainly green on TLC plate, but in some cases, it is the spot of sugar.

b. High Performance Thin Layer Chromatography (HPTLC)

High-performance thin-layer chromatography (HPTLC) is an enhanced form of thin-layer chromatography (TLC). Various enhancements can be made to the basic method of thin-layer chromatography to automate the different steps, to increase the resolution achieved and to allow more accurate quantitative measurements. Chromatographic conditions for HPTLC are similar to TLC (Reich and Maire-Widmer, 2019).

1.2.2 Preparative chromatographic methods

a. Column Chromatography (CC)

Column Chromatography is a method used to purify individual chemical compounds from mixtures of compounds depending on molecular mass or special structure. A column is filled by a stationary phase and an organic solvent or a mixture of solvents flows down through the column. Sample is placed on the top of column and the eluent is then added. Components of the sample are separated from each other by partitioning between the

stationary packing material and the mobile eluent. Molecules with different polarity partition to different extents are moved through the column at different rates. The eluent is collected in fractions. Fractions are typically analysed by TLC to see if separation of the components was successful (Hostettmann and Wolfender, 2000).

Chromatographic conditions

- Stationary phase:

Sephadex LH-20 is prepared by hydroxypropylation of Sephadex G-25 to give a Dextran gel with both hydrophilic and lipophilic properties. It is stable in all solvents which are not strongly acidic and do not contain strong oxidizing agents. Separation depends on molecular size (gel filtration), adsorption, partition, ion exclusion and retardation, and probably other mechanisms still unknown (Murphy and D'Aux, 1975).

- Mobile phase: MeOH 100%, EtOH 100%

b. Vacuum-liquid chromatography (VLC)

VLC may be considered as a preparative TLV run as a column with a vacuum applied to speed up eluent flow rates. VLC is mainly used for the fractionation of natural products prior to other separation steps such as RPC, MPLC and HPLC (Sticher, 2008). VLC is carried out by using a sintered glass and a vacuum pump. Stationary phase is washed by MeOH and equilibrated by the solvent used as an eluent. Sample is dissolved in water (if stationary phase is reversed phase) or in mixture Chloroform: Methanol: Water (if stationary phase is normal phase).

Chromatographic conditions

- Stationary phase:

Silica for normal phase: 60 Å, 15-40 µm, Merck.

Silica for reversed phase: RP-18 Spherical C18 (300 Å, 75-200 µm, Silicycle).

- Mobile phase:

In case of normal phase:

CHCl$_3$/MeOH/H$_2$O 75/25/3; 70/30/5, 60/32/7. Tannin are stayed on the silica and interesting compounds are eluted.

In case of reversed phase RP-18: MeOH/H$_2$O 0/1, 1/1, 1/0; EtOH/H$_2$O 0/1, 1/1, 1/0. In this case, saponins are eluted in the methanolic or ethanolic solution, while sugars are eluted in water.

c. Flash chromatography

Flash chromatography is a rapid form of preparative column chromatography based upon an air pressure driven hybrid of medium and short column chromatography optimized for rapid separation. This is a process in which a vertical column (plastic or glass) is placed and that column is packed with the solid stationary phase from which the mobile phase is passed through it by gravity or some external pressure. Stationary phase is washed by MeOH and equilibrated by the solvent used as an eluent. Sample is dissolved in mixture Chloroform: Methanol: Water (Hostettmann and Wolfender, 2000).

Chromatographic conditions

- Material: Stationary phase: RediSep Rf Normal phase Silica Flash Columns (60 Å, 35-70µm).

- Mobile phase: CHCl$_3$/MeOH/H$_2$O 70:30:5; 60:32:7 (v/v).

d. Medium Pressure Liquid Chromatography (MPLC)

Medium-pressure liquid chromatography (MPLC) is one of the various preparative column chromatography techniques which separate samples under pressure to render the use of smaller particle size supports possible and increases the diversity of usable stationary phases. MPLC allows purification of large compound quantities, faster and improved separations. Packing of material with lower particle size under pressure enhances separation quality and moreover the solid phase can be re-used (Hostettmann and Terreaux, 2000).

Chromatographic conditions

- Material:

+ Separation column using silica: 110 x 15 mm, 460 x 25 mm, 460 x 15 mm, 230 x 15 mm.

+ Pump for equipment MPLC normal phase: HPLC pump 426 (Alltech); Fraction collector: Biophamacia.

+ Pump for equipment MPLC reverse-phase RP-18: Büchi® Pump manager C-605, Büchi® Pump module C-601; Fraction collector: C-660, 4 rack, 240 tubes.

- Stationary phase

Silica for normal phase: 60 Å, 15-40 µm, Merck.

Silica for reversed phase: RP-18 Spherical C18 (300 Å, 75-200 µm, Silicycle).

- Mobile phase

Silica for normal phase: $CHCl_3$/MeOH/H_2O 75/25/3; 70/30/5, 60/32/7

Silica for reversed phase RP-18: Several gradients of MeOH/H_2O and EtOH/H_2O can be utilized (20/80, 30/70, 40/60, 50/50).

e. High Pressure Liquid Chromatography (HPLC)

HPLC is the more useful technique used to analyse substances of plant under a maximum pressure of 300 bars in analytical mode and 100 bars in semi-preparative mode. This technique is applied to isolate, separate and purify compounds in a mixture, as well as to display botanical relationships between different species based on a chromatographic comparison of their chemical compositions (Hostettmann and Wolfender, 2000).

- Apparatus: Agilent Technologies Seri 1260 Infinity.
- Analytical mode: Column Luna 5µ C18(2) 100A 250 x 4.6 mm, 5 µm, flow rate 1mL/min.
- Semi-preparative mode: Column Luna 5µ C18(2) 100A 250 x 10 mm, 5 µm, flow rate 3mL/min.
- Eluent: Acetonitrile-Water (TFA 0.01%).

1.3. Methods of structural determination

1.3.1. Mass spectrometry (MS)

Mass spectrometry (MS) is an analytical method used to identify the mass of charged substances when they move in an electric filed. This technique is useful to identify molecular and isotopic composition of elements and detemine structure of compounds. A

mass spectrometer generates multiple ions from the sample under investigation, it then separates them according to their specific mass-to-charge ratio (*m/z*), and then records the relative abundance of each ion type. A mass spectrum of the molecule is thus produced. It provides this result as a plot of ion abundance versus mass-to-charge ratio (Hoffmann and Stroobant, 2007).

1.3.2. Electro-Spray Ionization (ESI)

Electro-Spray Ionization (ESI) is a technique used in mass spectrometry for production of ions using an electrospray in which a high voltage is applied to a liquid to create an aerosol. It is applied to structural determination because of its rapidity, sensitivity, higher accuracy than others traditional techniques of mass determination (Cech and Enke, 2001; Ho et al., 2003).
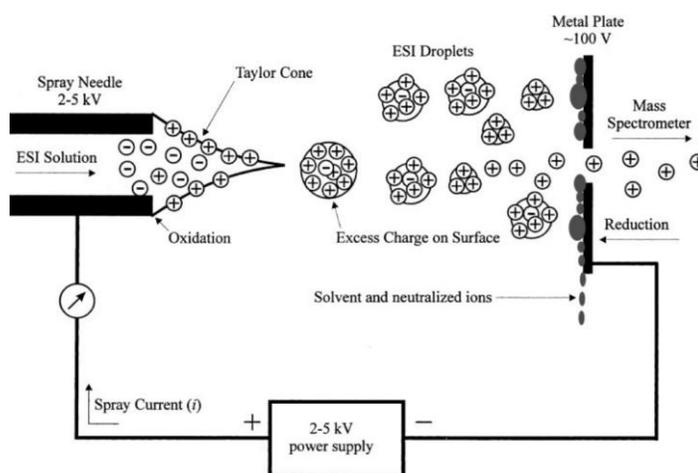
Figure 15. Mechanism of electrospray ionization (Cech and Enke, 2001)

1.3.3. Nuclear magnetic resonance (NMR) spectrometry

Nuclear magnetic resonance (NMR) spectrometry is another form of absorption spectrometry related to IR or UV spectrometry. Under appropriate condition in a magnetic field, a sample can absorb electromagnetic radiation in the radio frequency (Rf) region at frequencies governed by the characteristics of the sample. Absorption is a function of certain nuclei in the molecule. A plot of the frequencies of the absorption peaks versus peak intensities constitutes an NMR spectrum. The results of NMR are presented as one-dimensional NMR such as ^{1}H (Proton NMR) and ^{13}C; and two-dimensional NMR such as

COSY (Correlated Spectroscopy: through bond H-H correlation), TOCSY (Total Correlation Spectroscopy: extended through bond H-H correlation), ROESY (Rotating Frame Overhauser Effect Spectroscopy: determine the signals coming from protons that are close in space), HSQC (Heteronuclear Single Quantum Correlation: interpret precisely the direct H-C (^{1}H-C) heteronuclear couplings), HMBC (Heteronuclear Multiple-Bond Correlation: show the long-range H-C heteronuclear couplings) (Elyashberg, 2015).

a. One-dimensional Nuclear Magnetic Resonance spectroscopy (1D NMR)

<u>^{1}H NMR</u>

The ^{1}H NMR spectrum contains several resonance signals representing the chemical shifts of the different types of protons of the molecule. A saponin has three zones of resonance:

- From 0.5 to 3 ppm: the protons of aglycon, with methyl, methylene and methane groups.

- From 3 to 4.5 ppm: the osidic protons except anomers.

- From 4.5 to 6 ppm: the anomeric protons (No.1 of the sugars) in the form of enlarged doublets or singlets and the ethylenic protons of aglycon (Massiot and Lavaud, 1995).

<u>^{13}C NMR</u>

In the same way as the ^{1}H NMR spectrum, the ^{13}C spectrum is divided into the following three resonance zones:

- From 10 to 60 ppm: the carbons of aglycon.

- From 60 to 90 ppm: the osidic carbons (except anomers) and some hydroxyl carbons of aglycon.

- From 90 to 110 ppm: the carbons of anomers.

- Above 110 ppm: ethylenic carbons, carbons of carboxylic acids, aldehydes, esters and ketones (Agrawal et al., 1995, 1985; Massiot and Lavaud, 1995).

b. Two-dimensional nuclear magnetic resonance spectroscopy (2D NMR)

Heteronuclear Single Quantum Correlation (HSQC)

The HSQC spectrum allows to interpret precisely the direct H-C ($^{1}J_{H-C}$) heteronuclear couplings. In case of comparison to 1D ^{13}C NMR and 1D ^{1}H NMR spectra, the ^{1}H, ^{13}C HSQC spectrum reduces spectral overlap which highly benefits compound identification. It allows to identify CH, CH_2, CH_3 groups with the chemical shift assignment (Elyashberg, 2015).
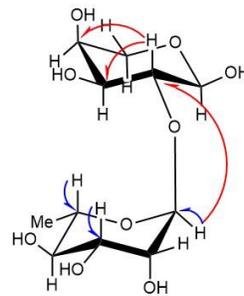
Figure 16. Correlations of HSQC (blue) and HMBC (red) between α-L-rhamnose and α-L-arabinose

Heteronuclear Multiple-Bond Correlation (HMBC)

The data provided by HMBC show the long-range H-C heteronuclear couplings with $^{2}J_{H-C}$ or $^{3}J_{H-C}$ coupling constants. This spectrum is very useful for determining the structure of the aglycon, but above all for elucidating the sequence of sugars in the oligosaccharide chains and their position of attachment to the aglycon (Reynolds and Enríquez, 2002).

Correlated Spectroscopy (COSY)

The COSY demonstrates the protons with $^{2}J_{H-H}$ geminal couplings and $^{3}J_{H-H}$ vicinal couplings. They are used to determine the structure of sugars and to verify the position of certain protons of the aglycon (Elyashberg, 2015).

Total Correlation Spectroscopy (TOCSY)

TOCSY allows to observe the correlations of all the protons of the same spin system, as for the COSY experiment, to extended through bond H-H correlation (Elyashberg, 2015).
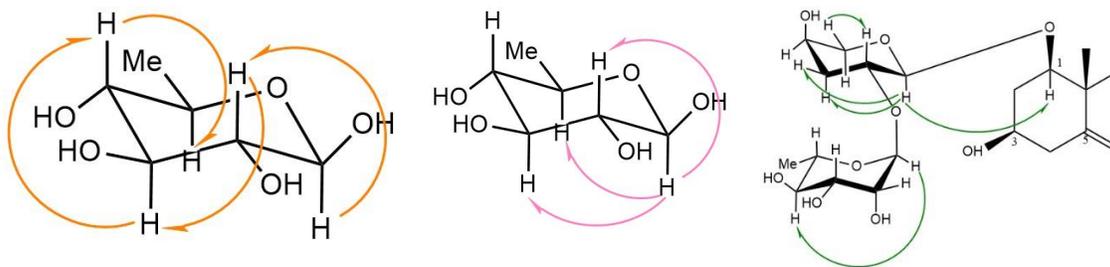
Figure 17. Correlations of COSY (orange), TOCSY (pink) and ROESY (green)

Rotating Frame Overhauser Effect Spectroscopy (ROESY)

The ROESY spectrum is used to determine the signals coming from protons that are close in space. This spectrum can verify the data analysed by HMBC (Elyashberg, 2015).

1.3.4. Acid hydrolysis and GC analysis

Each pure compound (3 mg) was hydrolysed with 2N aq. CF_3COOH (5 mL) for 3 h at 95°C. After extraction with CH_2Cl_2 (3 x 5 mL), the aqueous layer was repeatedly evaporated to dryness with MeOH until neutral, and then analysed by TLC over silica gel ($CHCl_3$/MeOH/H_2O 8/5/1) by comparison with authentic samples. Furthermore, the sugars residue was dissolved in anhydrous pyridine (100 µL), and L-cysteine methyl ester hydrochloride (0.06 mol/L) was added. The mixture was stirred at 60 °C for 1 h, then 150 µL of HMDS-TMCS (hexamethyldisilazane/trimethylchlorosilane 3/1) was added, and the mixture was stirred at 60 °C for another 30 min. The precipitate was centrifuged off, and the supernatant was concentrated under a N_2 stream. The residue was partitioned between *n*-hexane and H_2O (0.1 mL each), and the hexane layer (1 µL) was analysed by GC (Hara et al., 1987). The absolute configurations were determined by comparing the retention times with thiazolidine derivatives prepared in a similar way from standard sugars (Sigma-Aldrich).

2. Phytochemical investigation

2.1. Phytochemical study of *Weigela* x "Bristol Ruby"

Seven oleanane-type triterpenoid saponins were obtained from an aqueous-ethanolic extract of the roots of *Weigela* x "Bristol Ruby" and fractionated by vacuum-liquid chromatography (VLC) and purified by several solid/liquid chromatographic methods. Six of them are previously undescribed (**1-6**) in addition to one known compound (**7**).

2.1.1. Isolation and purification

The dried and powdered roots of *Weigela* x "Bristol Ruby" (49 g) were submitted to an ultrasound assisted extraction three times with EtOH/H_2O (75/35, 3 x 1L, 1 h each). The resulting extracts were combined and concentrated under vacuum to give a crude extract (3 g), which was fractionated by VLC (Silica gel 60, $CHCl_3$/MeOH/H_2O 70/30/5) yielding 12

fractions (F1-F12). The fractions F3 and F4 were combined (780 mg) and then submitted to CC (Sephadex LH-20, MeOH) to give 4 fractions. The fraction rich in saponins (103 mg) was fractionated by MPLC on silica gel 60 (CHCl$_3$/MeOH/H$_2$O 80/20/2, 70/30/5) yielding compounds **1** (4.4 mg), **2** (3.8 mg), **3** (3.7 mg), **4** (3.6 mg), **5** (3.6 mg), and **7** (8.6 mg). The combined fractions F5 and F6 (130.4 mg) were fractionated by MPLC on silica gel 60 (CHCl$_3$/MeOH/H$_2$O 80/20/2, 70/30/5) to give compound **6** (3.1 mg).

Figure 18. Purification scheme of compounds in roots of *Weigela* x "Bristol Ruby"

2.1.2. Structural determination of isolated saponins

a. Compound 1 (WBR2311)

Mass spectrometry

Compound **1** showed a pseudo-molecular ion peak [M+Na]$^+$ at *m/z* 1183.5882 in the HR-ESIMS (positive-ion mode) spectrum, indicating a molecular weight of 1160 and a molecular formula of $C_{57}H_{92}O_{24}$. This was confirmed by the ESIMS (negative-ion mode) spectrum with *m/z* 1160.1 [M–H]$^-$.

NMR spectroscopy

Structure of aglycon

The aglycon was identified by analysing spectra NMR ^{1}H, ^{13}C, HSQC and HMBC. In spectra of NMR ^{1}H and ^{13}C, characteristic signals of oleanolic acid were showed:

- 7 methyl groups with singlet signals at δ_H 1.28, 1.12, 0.86, 0.99, 1.32, 0.97 and 1.02 confirmed the presence of triterpene.

- 1 olefinic proton at δ_H 5.48 (br t, $J = 3.6$ Hz) corresponds to proton H-12.

The ^{13}C NMR spectrum showed:

- 5 tertiary carbons (CH), 10 secondary carbons (CH$_2$), 7 primary carbons (CH$_3$) and 8 quaternary carbons (C).

- 2 signals at δ_C 122.5 and 144.8 correspond to the double bond Δ^{12}.

The ^{1}H and ^{13}C NMR signals of the aglycon assigned from the 2D NMR spectra, were in good agreement with those of oleanolic acid commonly encountered in the *Weigela* genus (Andriamisaina et al., 2018; Champy-Tixier et al., 2018; Rezgui et al., 2016). The downfield shift at δ_C 88.7 and upfield shift at δ_C 180.2, due to the glycosylation shift, suggested that compound **1** was a monodesmosidic glycoside.

Structure of sugar moieties

The monosaccharides were identified by acid hydrolysis and extensive 2D NMR analysis as α-L-arabinopyranosyl (Ara), α-L-rhamnopyranosyl (Rha), β-D-xylopyranosyl (Xyl) and

β-D-glucopyranosyl (Glc) in the case of **1**–**3**, and Rha, Xyl and Glc in the case of **4**–**7**. The absolute configurations of the sugars were determined to be D for glucose (Glc), and xylose (Xyl), and L for arabinose (Ara) and rhamnose (Rha), by GC analysis (see Section 1.3.4). The relatively large $^3J_{H-1,H-2}$ values of the Glc, Xyl, and Ara (6.0–8.0 Hz) indicated a β anomeric orientation for Glc and Xyl, and an α anomeric orientation for Ara. For compound **3**, the broad singlet observed for the anomeric proton of the terminal arabinopyranosyl moiety is consistent with the $^1C_4$ conformation of Ara with an α-orientation of the anomeric center (Ishii et al., 1981). The large $^1J_{H-1,C-1}$ values of the Rha (165–168 Hz), confirmed that the anomeric protons were equatorial (α-pyranoid anomeric form).

For the sugar part of the molecule, the ^1H NMR spectrum of **1** showed five anomeric proton signals at δ_H 4.88 (d, J = 6.0 Hz), 4.99 (d, J = 7.6 Hz), 5.09 (d, J = 7.6 Hz), 5.26 (d, J = 7.6 Hz) and 6.18 (br s), which gave correlations in the HSQC spectrum with their corresponding anomeric carbons at δ_C 105.0, 103.2, 105.5, 107.0 and 101.5, respectively. All protons and carbons signals were identified by 2D NMR experiments, starting mainly by the TOCSY experiment (Table 3). Five sugar moieties are identified:

- 1 α-L-arabinopyranosyl Ara-1 at δ_H 4.88 (d, J = 6.0 Hz),

- 1 α-L-rhamnopyranosyl Rha-1 at δ_H 6.18 (br s),

- 1 β-D-glucopyranosyl Glc-1 at δ_H 4.99 (d, J = 7.6 Hz),

- 2 β-D-xylopyranosyl Xyl I-1 at δ_H 5.26 (d, J = 7.6 Hz) and Xyl II-1 at δ_H 5.09 (d, J = 7.6 Hz).

The sequence of the oligosaccharide was established by analysing the HMBC and ROESY spectra:

- α-L-arabinopyranosyl showed to be attached to the C-3 position of the aglycon by observation of an HMBC correlation between δ_H 4.88 (Ara I H-1) and δ_C 88.7 (C-3) (Fig.19).

- The HMBC correlation between δ_H 4.55 (Ara I H-2) and δ_C 101.5 (Rha C-1) and in ROESY at δ_H 4.55 (Ara I H-2) and δ_H 6.18 (Rha H-1) proved that Rha was attached to the Ara at C-2.

- The HMBC correlation between δ_H 5.26 (Xyl I H-1) and δ_C 83.1 (Rha C-3) and in ROESY at δ_H 5.26 (Xyl I H-1) and δ_H 4.67 (Rha H-3) proved that Xyl I was attached to the Rha at C-3.

- The HMBC correlation between δ_H 4.99 (Glc H-1) and δ_C 77.6 (Xyl I C-4) and in ROESY at δ_H 4.99 (Glc H-1) and δ_H 4.27 (Xyl I H-4) proved that Glc was attached to the Xyl I at C-4.

- The HMBC correlation between δ_H 5.09 (Xyl II H-1) and δ_C 80.7 (Glc C-4) and in ROESY at δ_H 5.09 (Xyl II H-1) and δ_H 4.26 (Glc H-4) proved that Xyl II was attached to the Glc at C-4.

Conclusion

Based on the above results, the structure of **1** was elucidated as 3-O-β-D-xylopyranosyl-(1→4)-β-D-glucopyranosyl-(1→4)-β-D-xylopyranosyl-(1→3)-α-L-rhamnopyranosyl-(1→2)-α-L-arabinopyranosyloleanolic acid.
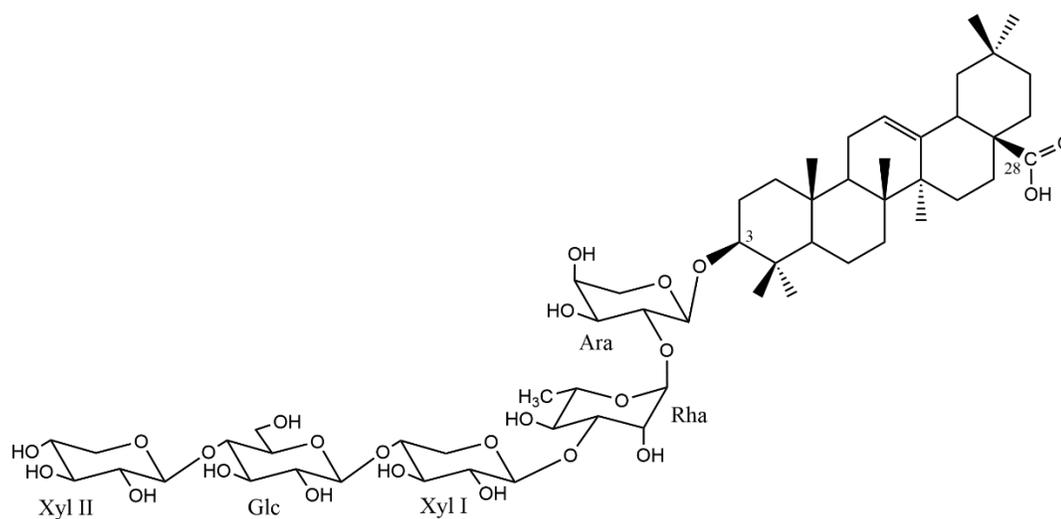
Figure 19. Structure of compound **1**
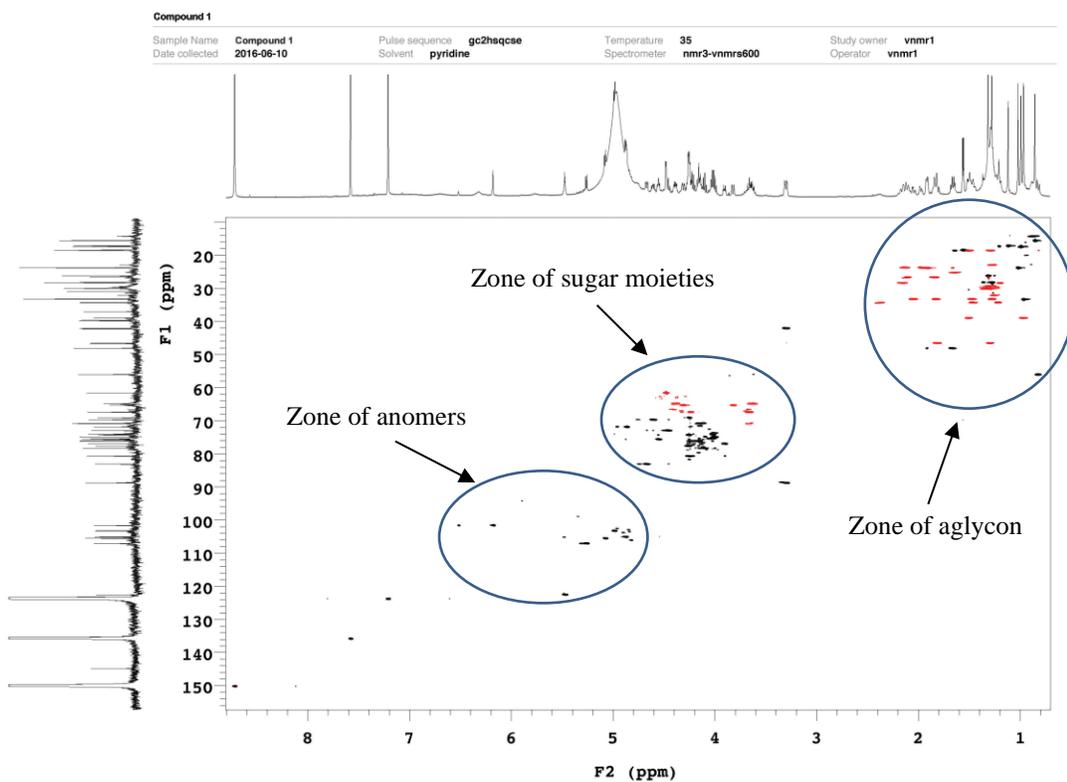
Figure 20. HSQC spectrum of compound **1**
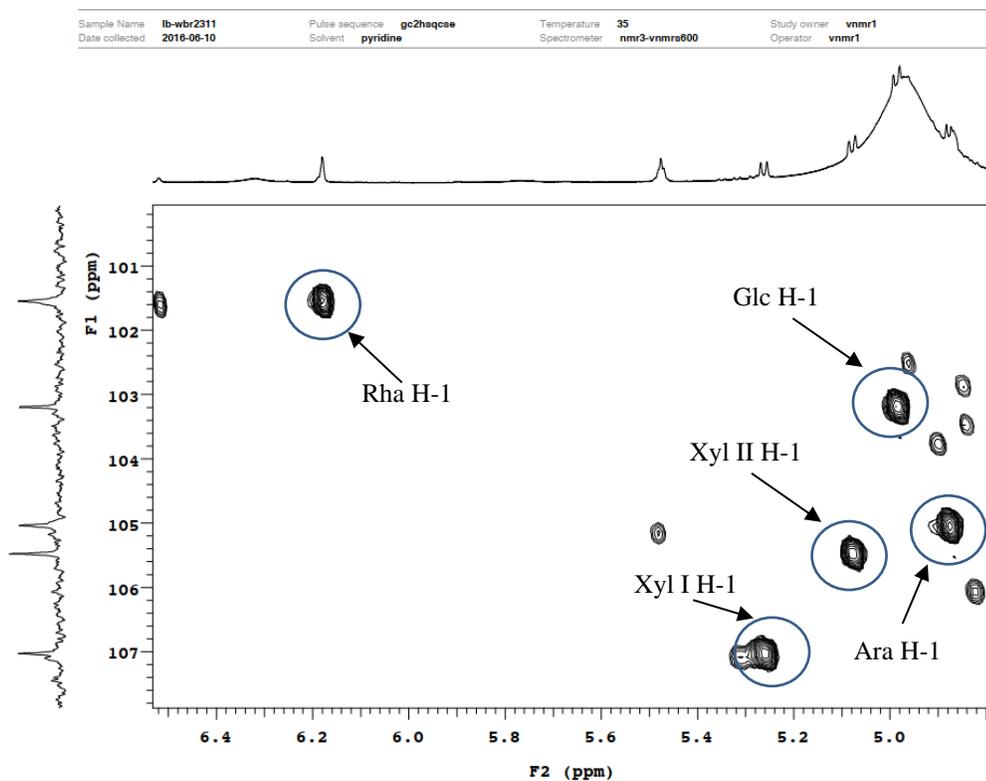
Figure 21. HSQC spectrum of sugar anomers of compound **1**
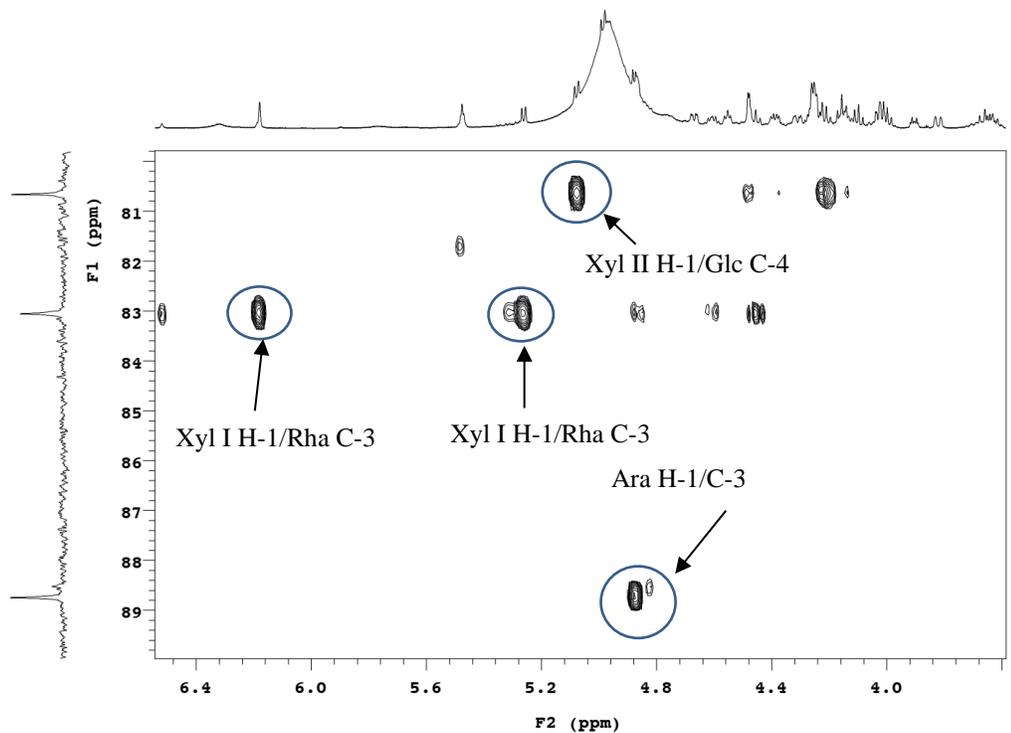
Figure 22. HMBC spectrum of sugar moieties of compound **1**
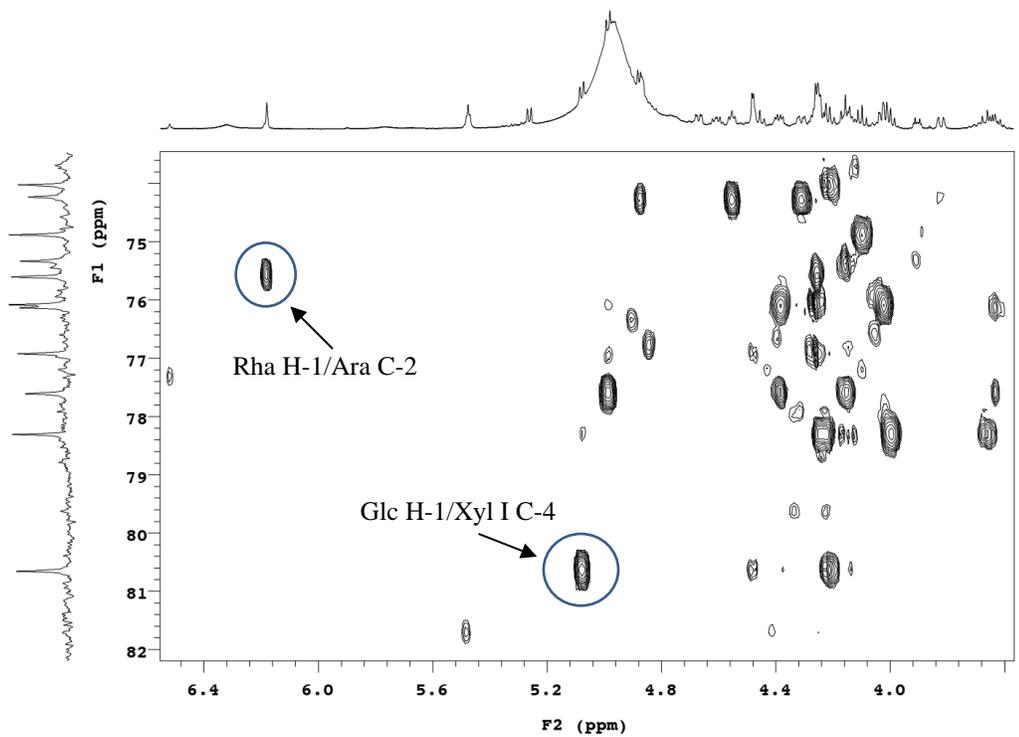
Figure 23. HMBC spectrum of sugar moieties of compound **1**
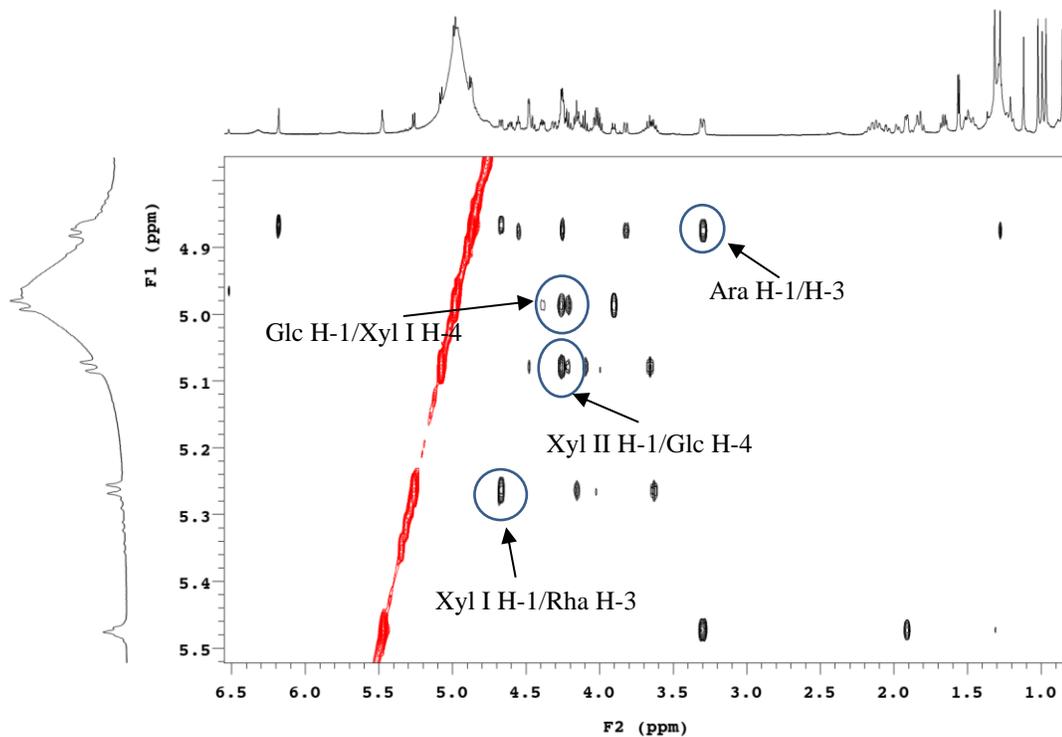
Figure 24. ROESY spectrum of sugar moieties of compound **1**
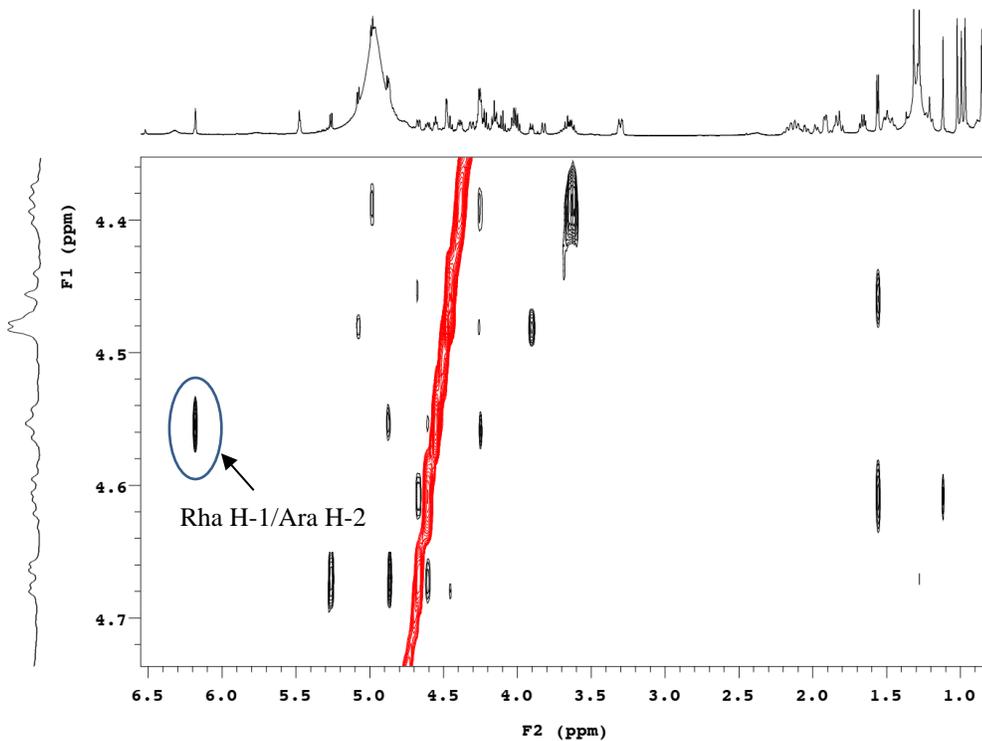
Figure 25. ROESY spectrum of sugar moieties of compound **1**

Combine	<78-80>	Count	3483	Data Source Name	Compound 1	Data Type	c		Date	09 Aug 2016
File Name	E:\NMR-Daten\Lacaille-Dubois\MS-Aug2016\Compound1.RAW					Ion Mode	+		Mass Spec Model	LCQ\LCQ Deca
Plot Type	Stick	Retention Time	4.087	Scan	78	Scan Filter	+ c Full ms [50.00-2000.00]			
Scan Mode	ms	Scan Type	Full	TIC	6014.97	Total Signal	1121236480			
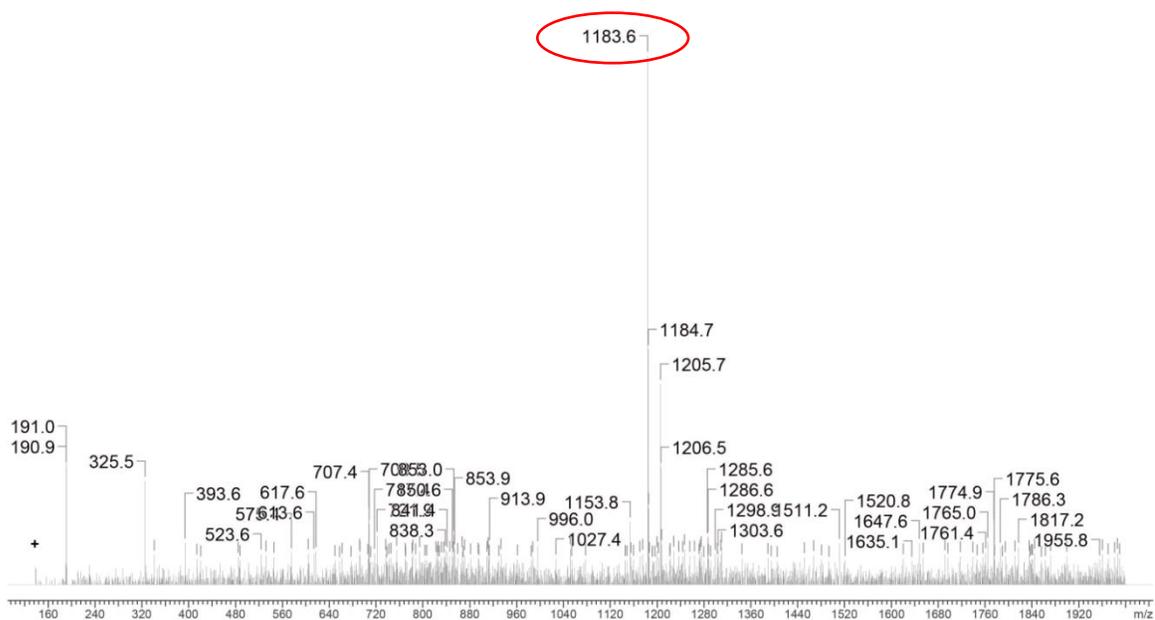
Figure 26. Mass spectrum of compound **1**

b. Compound 2 (WBR2320_1)
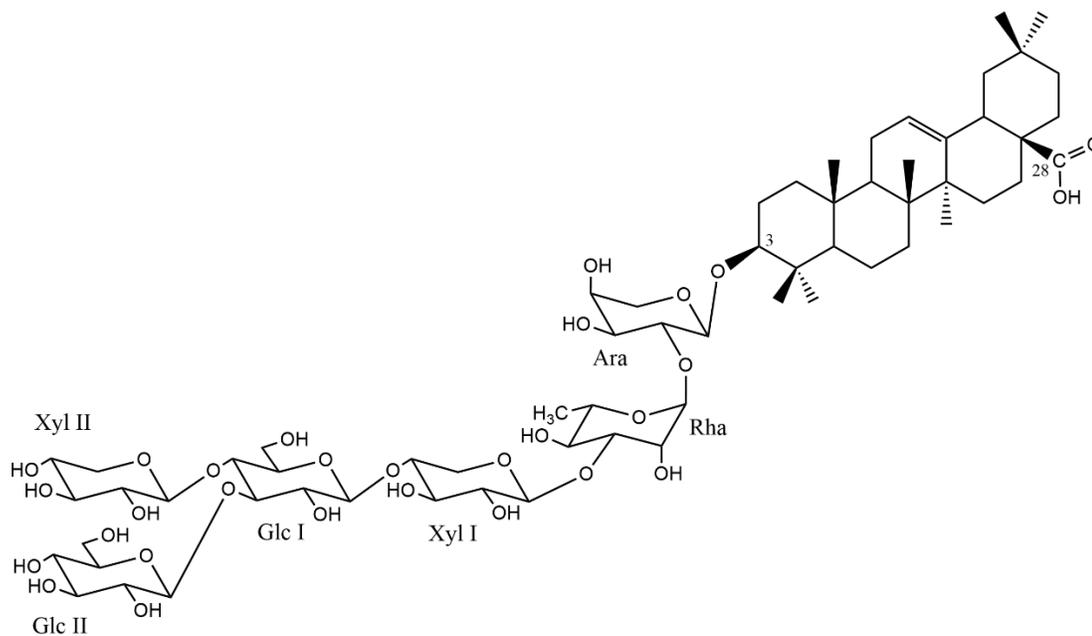
Figure 27. Structure of compound **2**

43

Mass spectrometry

Compound **2**, the molecular formula $C_{63}H_{102}O_{29}$, and thus a molecular weight of 1322, was obtained according to its HR-ESIMS (positive-ion mode) spectrum which displayed a pseudo-molecular ion peak at *m/z* 1345.6409 $[M+Na]^+$. This was in accordance with the ESIMS (negative-ion mode) spectrum with *m/z* 1322.3 $[M–H]^-$.

NMR spectroscopy

Structure of aglycon

The analysis of the NMR spectra of compound **2** showed that the aglycon was almost identified to those of compound **1**. The correlations of HSQC, HMBC and ROESY allowed to identify the genin of compound **2** as the oleanolic acid which was characterised to compound **1** (Table 3).

Structure of sugar moieties

The molecular weight of compound **2** differs from **1** by only 162 amu, corresponding to a supplementary hexosyl group. The part of the HSQC spectrum corresponding to the osidic chain showed cross-peaks at δ_H/δ_C 4.88/105.0, 4.94/102.8, 5.25 (d, *J* = 7.2 Hz)/107.0, 5.48 (d, *J* = 6.4 Hz)/102.9, 5.52 (d, *J* = 7.6 Hz)/104.7 and 6.16 (br s)/101.6, indicating the presence of six sugar units. After analysing the spectre of HSQC, HMBC, COSY, TOCSY and ROESY, the sugar moieties of compound **2** was identified as:

- 1 α-L-arabinopyranosyl Ara-1 at δ_H 4.88 (d, *J* = 6.0 Hz),

- 1 α-L-rhamnopyranosyl Rha-1 at δ_H 6.16 (br s),

- 2 β-D-glucopyranosyl Glc I-1 at δ_H 4.94 and Glc II-1 at δ_H 5.52 (d, *J* = 7.6 Hz)

- 2 β-D-xylopyranosyl Xyl I-1 at δ_H 5.25 (d, *J* = 7.2 Hz) and Xyl II-1 at δ_H 5.09 (d, *J* = 6.4 Hz).

The sequence of the oligosaccharide was established by analysing the HMBC and ROESY spectra:

- α-L-arabinopyranosyl showed to be attached to the C-3 position of the aglycon by observation of an HMBC correlation between δ_H 4.88 (Ara I H-1) and δ_C 88.7 (C-3) (Fig.28).

- The HMBC correlation between δ_H 4.54 (Ara I H-2) and δ_C 101.6 (Rha C-1) and in ROESY at δ_H 4.54 (Ara I H-2) and δ_H 6.16 (Rha H-1) proved that Rha was attached to the Ara at C-2.

- The HMBC correlation between δ_H 5.25 (Xyl I H-1) and δ_C 83.1 (Rha C-3) and in ROESY at δ_H 5.25 (Xyl I H-1) and δ_H 4.67 (Rha H-3) proved that Xyl I was attached to the Rha at C-3.

- The HMBC correlation between δ_H 4.94 (Glc I H-1) and δ_C 77.9 (Xyl I C-4) and in ROESY at δ_H 4.94 (Glc H-1) and δ_H 4.22 (Xyl I H-4) proved that Glc I was attached to the Xyl I at C-4.

- The HMBC correlation between δ_H 5.52 (Glc II H-1) and δ_C 82.2 (Glc I C-3) and in ROESY at δ_H 5.52 (Glc II H-1) and δ_H 4.45 (Glc I H-3) proved that Glc II was attached to the Glc I at C-3.

- The HMBC correlation between δ_H 5.48 (Xyl II H-1) and δ_C 74.2 (Glc I C-4) and in ROESY at δ_H 5.48 (Xyl II H-1) and δ_H 4.54 (Glc I H-4) proved that Xyl II was attached to the Glc I at C-4.

Conclusion

The structure of **2** was elucidated as 3-*O*-β-D-xylopyranosyl-(1→4)-[β-D-glucopyranosyl-(1→3)]-β-D-glucopyranosyl-(1→4)-β-D-xylopyranosyl-(1→3)-α-L-rhamnopyranosyl-(1→2)-α-L-arabinopyranosyloleanolic acid.

Figure 28. HSQC spectrum of compound **2**

Figure 29. HSQC spectrum of sugar anomers of compound **2**

Figure 30. HMBC spectrum of sugar moieties of compound **2**

Figure 31. ROESY spectrum of sugar moieties of compound **2**

Figure 32. ROESY spectrum of sugar moieties of compound **2**

Figure 33. Mass spectrum of compound **2**

48

c. Compound 3 (WBR2317)

Mass spectrometry

The HR-ESIMS (positive-ion mode) spectrum of compound **3** showed a pseudo-molecular ion peak $[M+Na]^+$ at *m/z* 1315.6306, indicating a molecular weight of 1292 and a molecular formula of $C_{62}H_{100}O_{28}$. This was confirmed by the ESIMS (negative-ion mode) spectrum with *m/z* 1292.4 $[M–H]^-$.

NMR spectroscopy

Structure of aglycon

The analysis of the NMR spectra of compound **3** showed that the aglycon was almost identified to those of compounds **1** and **2**. The correlations of HSQC, HMBC and ROESY allowed to identify the genin of compound **2** as the oleanolic acid which was characterised to compounds **1** and **2** (Table 3).

Structure of sugar moieties

The molecular weight of compound **3** is lower than **2** by 30 amu, corresponding to a pentosyl group instead of an hexosyl one. The HSQC spectrum of the sugar part showed cross-peaks at δ_H/δ_C 4.88 (d, $J = 6.2$ Hz)/105.0, 4.90 (d, $J = 7.8$ Hz)/102.9, 5.24 (d, $J = 7.6$ Hz)/107.0, 5.35 (d, $J = 6.8$ Hz)/103.7, 5.92 (br s)/103.4, and 6.16 (br s)/101.6, indicating the presence of six sugar units. Starting mainly the TOCY and NOESY spectra, the sugar moieties of compound **3** was identified as:

- 2 α-L-arabinopyranosyl Ara I-1 at δ_H 4.88 (d, $J = 6.2$ Hz) and Ara II-1 at δ_H 5.92 (br s). According to the coupling constant of their anomeric protons, (d, $J = 6.2$ Hz) for Ara I-1 and (br s) for Ara II-1, the $^4C_1$ conformation was proposed for Ara I, and $^1C_4$ for Ara II.

- 1 α-L-rhamnopyranosyl Rha-1 at δ_H 6.16 (br s),

- 1 β-D-glucopyranosyl Glc-1 at δ_H 4.90 (d, $J = 7.8$ Hz),

- 2 β-D-xylopyranosyl Xyl I-1 at δ_H 5.24 (d, $J = 7.6$ Hz) and Xyl II-1 at δ_H 5.35 (d, $J = 6.8$ Hz).

The sequence of the oligosaccharide was established by analysing the HMBC and ROESY spectra:

- α-L-arabinopyranosyl showed to be attached to the C-3 position of the aglycon by observation of an HMBC correlation between δ_H 4.88 (Ara I H-1) and δ_C 88.8 (C-3) (Fig.34).

- The HMBC correlation between δ_H 4.88 (Ara I H-2) and δ_C 101.6 (Rha C-1) and in ROESY at δ_H 4.88 (Ara I H-2) and δ_H 6.16 (Rha H-1) proved that Rha was attached to the Ara at C-2.

- The HMBC correlation between δ_H 5.24 (Xyl I H-1) and δ_C 83.0 (Rha C-3) and in ROESY at δ_H 5.24 (Xyl I H-1) and δ_H 4.66 (Rha H-3) proved that Xyl I was attached to the Rha at C-3.

- The HMBC correlation between δ_H 4.90 (Glc H-1) and δ_C 77.4 (Xyl I C-4) and in ROESY at δ_H 4.90 (Glc H-1) and δ_H 4.21 (Xyl I H-4) proved that Glc was attached to the Xyl I at C-4.

- The HMBC correlation between δ_H 5.92 (Ara II H-1) and δ_C 79.8 (Glc C-3) and in ROESY at δ_H 5.92 (Ara II H-1) and δ_H 4.44 (Glc H-3) proved that Xyl II was attached to the Glc at C-3.

- The HMBC correlation between δ_H 5.35 (Xyl II H-1) and δ_C 74.0 (Glc I C-4) and in ROESY at δ_H 5.35 (Xyl II H-1) and δ_H 4.48 (Glc H-4) proved that Xyl II was attached to the Glc at C-4.

Conclusion

Thus, on the basis of the above results, the structure of compound **3** was established as 3-*O*-β-D-xylopyranosyl-(1→4)-[α-L-arabinopyranosyl-(1→3)]-β-D-glucopyranosyl-(1→4)-β-D-xylopyranosyl-(1→3)-α-L-rhamnopyranosyl-(1→2)-arabinopyranosyloleanolic acid.
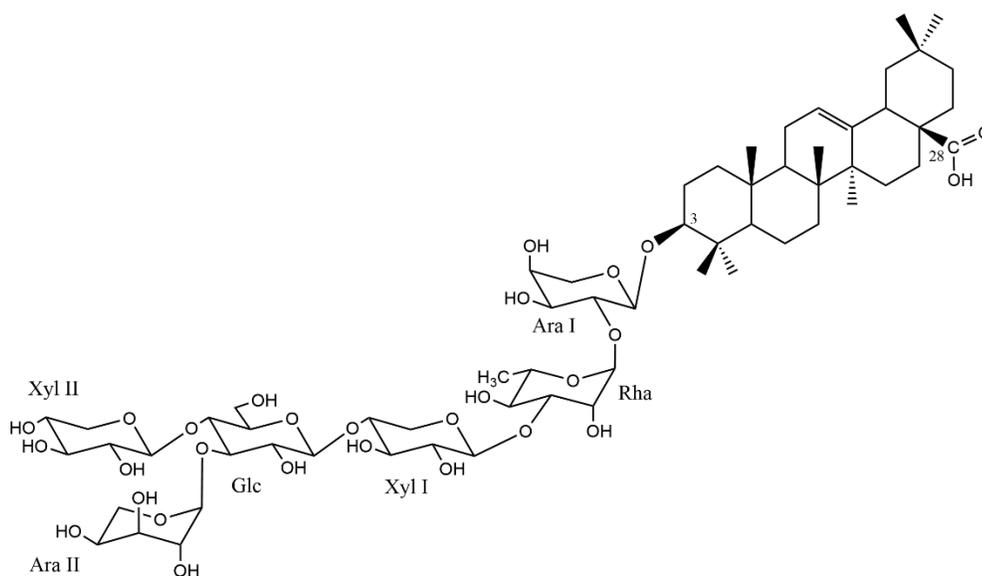
Figure 34. Structure of compound **3**
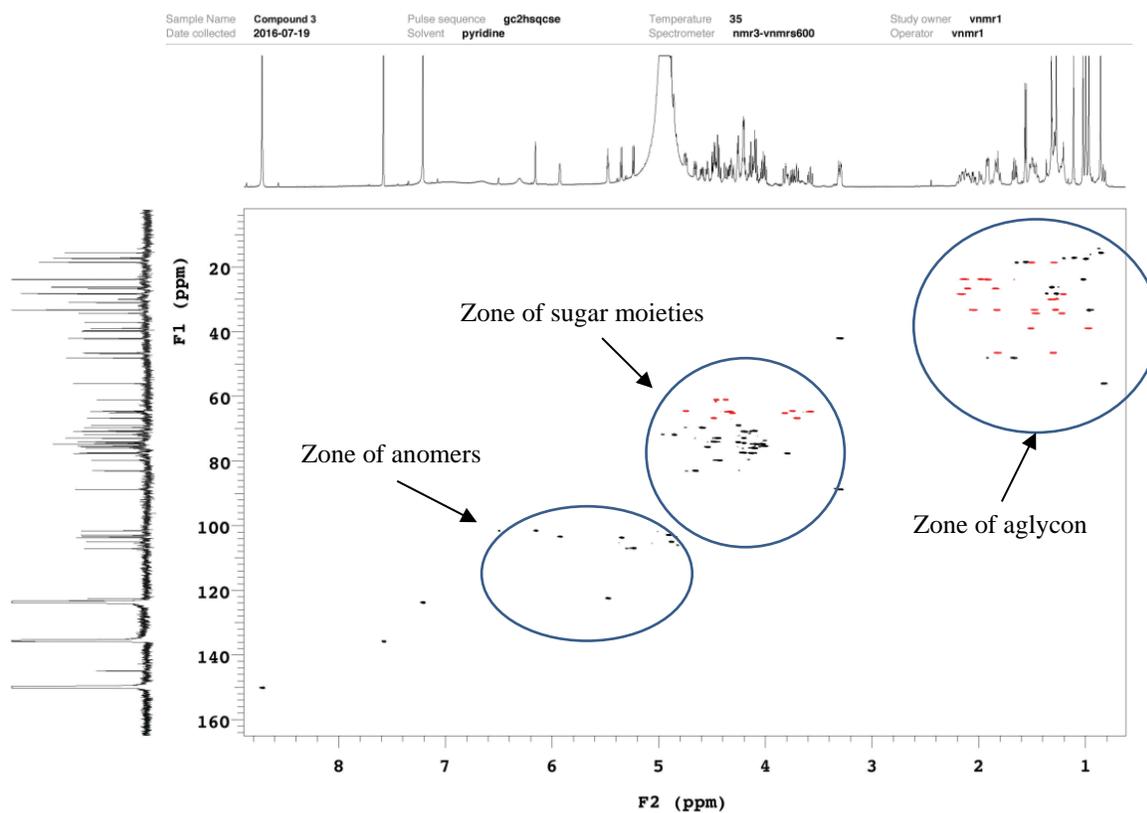
Figure 35. HSQC spectrum of compound **3**
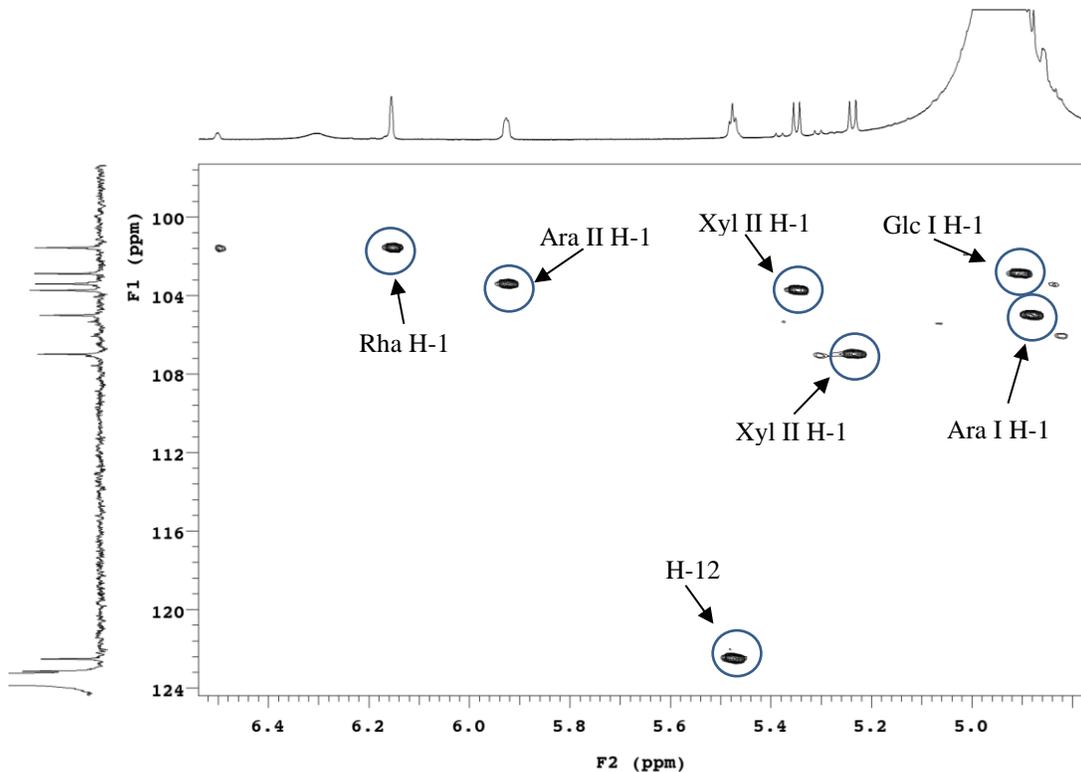
Figure 36. HSQC spectrum of sugar anomers of compound **3**
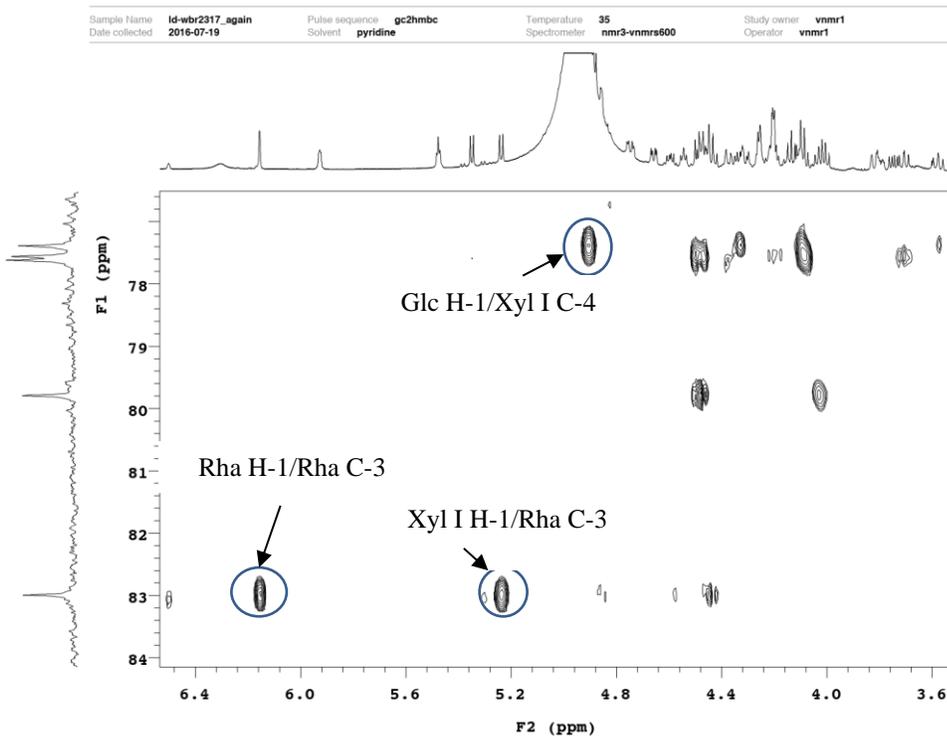
**Figure 37.** HMBC spectrum of sugar moieties of compound **3**

Xyl II H-1/Glc C-4

Rha H-1/Ara I C-2

Glc H-1/Xyl I C-4

Figure 38. HMBC spectrum of sugar moieties of compound **3**

Ara I H-1/C-3

Figure 39. HMBC spectrum of sugar moieties of compound **3**

53

Figure 40. ROESY spectrum of sugar moieties of compound **3**

Figure 41. Mass spectrum of compound **3**

d. Compound 4 (WBR2321)

Mass spectrometry

For compound **4**, the same molecular formula as **2** ($C_{63}H_{102}O_{29}$) was obtained according to its HR-ESIMS (positive-ion mode) spectrum which displayed a pseudo-molecular ion peak at *m/z* 1345.6409 [M+Na]$^+$, and its ESIMS (negative-ion mode) spectrum with *m/z* 1322.1 [M–H]$^-$.

NMR spectroscopy

Structure of aglycon

The analysis of the NMR spectra of compound **4** showed that the aglycon was almost identified to those of compounds **1, 2** and **3**. The correlations of HSQC, HMBC and ROESY allowed to identify the genin of compound **4** as the oleanolic acid which was characterised to compounds **1, 2** and **3** (Table 3).

Structure of sugar moieties

The HSQC spectrum of the sugar part showed six cross-peaks at δ_H/δ_C 4.83 (d, *J* = 7.6 Hz)/106.1, 4.94/102.8, 5.29 (d, *J* = 7.6 Hz)/107.1, 5.49 (d, *J* = 6.0 Hz)/102.9, 5.52 (d, *J* = 8.0 Hz)/104.7 and 6.50 (br s)/101.6, indicating the presence of six sugar units. Starting mainly the TOCY and NOESY spectra, the sugar moieties of compound **4** was identified as:

- 1 α-L-rhamnopyranosyl Rha-1 at δ_H 6.50 (br s),

- 2 β-D-glucopyranosyl Glc I-1 at δ_H 4.94 and Glc II-1 at δ_H 5.52 (d, *J* = 8.0 Hz),

- 3 β-D-xylopyranosyl Xyl I-1 at δ_H 4.83 (d, *J* = 7.6 Hz), Xyl II-1 at δ_H 5.29 (d, *J* = 7.6 Hz) and Xyl III-1 at δ_H 5.49 (d, *J* = 6.0 Hz).

The sequence of the oligosaccharide was established by analysing the HMBC and ROESY spectra:

- The HMBC correlation between δ_H 4.83 (Xyl I H-1) and δ_C 88.3 (C-3) and in ROESY at δ_H 4.83 (Xyl I H-1) and δ_H 3.31 (H-3) proved that Xyl I was attached to the C-3 position of the aglycon (Fig.42).

- The HMBC correlation between δ_H 4.21 (Xyl I H-2) and δ_C 101.6 (Rha C-1) and in ROESY at δ_H 4.21 (Xyl I H-2) and δ_H 6.50 (Rha H-1) proved that Rha was attached to the Xyl I at C-2.

- The HMBC correlation between δ_H 5.29 (Xyl II H-1) and δ_C 83.2 (Rha C-3) and in ROESY at δ_H 5.29 (Xyl II H-1) and δ_H 4.73 (Rha H-3) proved that Xyl II was attached to the Rha at C-3.

- The HMBC correlation between δ_H 4.94 (Glc I H-1) and δ_C 77.9 (Xyl II C-4) and in ROESY at δ_H 4.94 (Glc I H-1) and δ_H 4.23 (Xyl II H-4) proved that Glc I was attached to the Xyl II at C-4.

- The HMBC correlation between δ_H 5.52 (Glc II H-1) and δ_C 82.3 (Glc I C-3) and in ROESY at δ_H 5.52 (Glc II H-1) and δ_H 4.45 (Glc I H-3) proved that Glc II was attached to the Glc I at C-3.

- The HMBC correlation between δ_H 5.49 (Xyl III H-1) and δ_C 74.2 (Glc I C-4) and in ROESY at δ_H 5.49 (Xyl III H-1) and δ_H 4.54 (Glc I H-4) proved that Xyl III was attached to the Glc I at C-4.

Conclusion

Thus, on the basis of the above results, the structure of **4** was established as 3-*O*-β-D-xylopyranosyl-(1→4)-[β-D-glucopyranosyl-(1→3)]-β-D-glucopyranosyl-(1→4)-β-D-xylopyranosyl-(1→3)-α-L-rhamnopyranosyl-(1→2)-β-D-Xylopyranosyloleanolic acid.

Figure 42. Structure of compound **4**
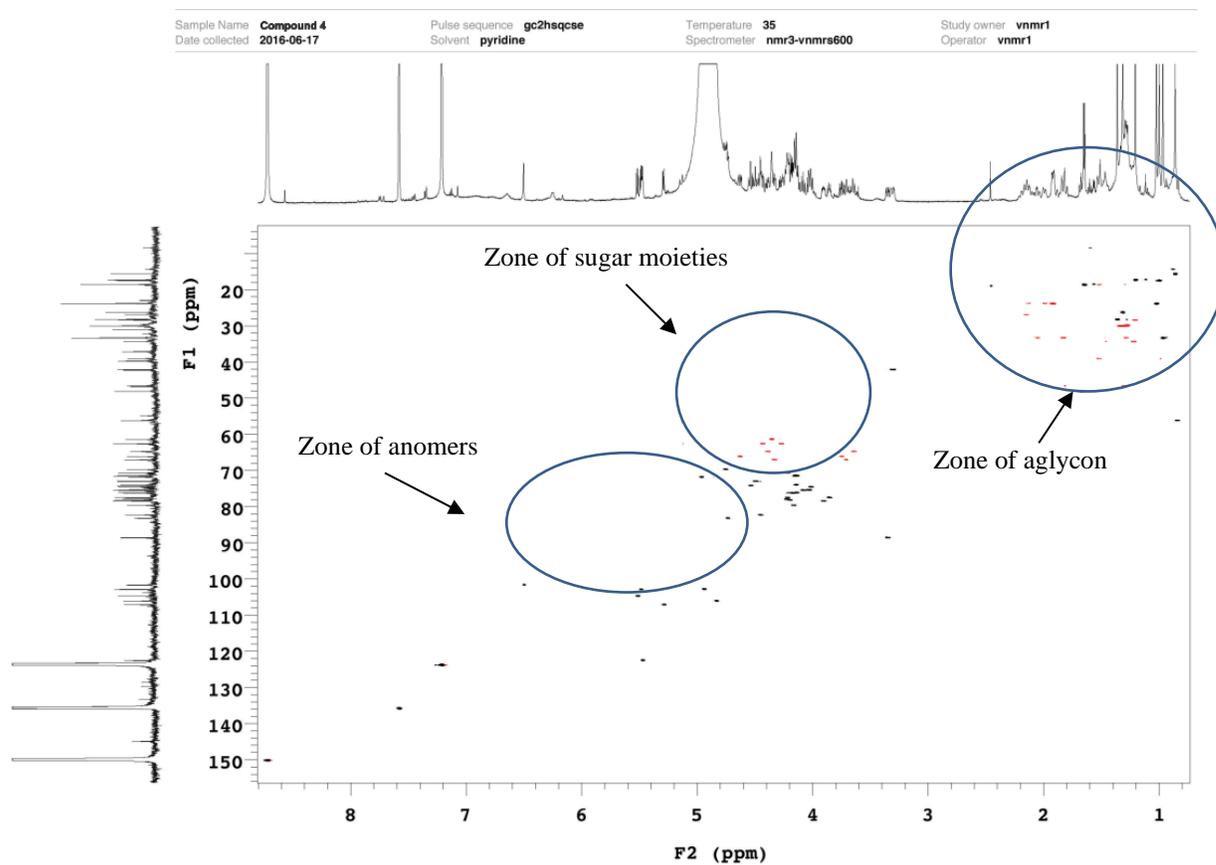
**Figure 43.** HSQC spectrum of compound **4**
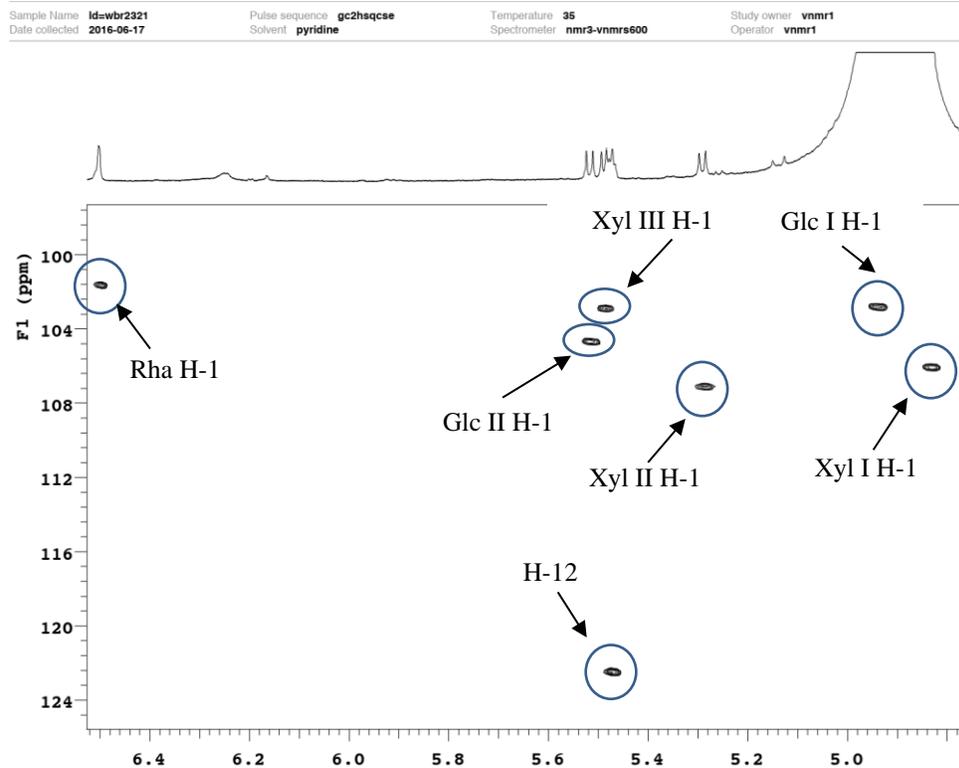
Figure 44. HSQC spectrum of sugar anomers of compound **4**
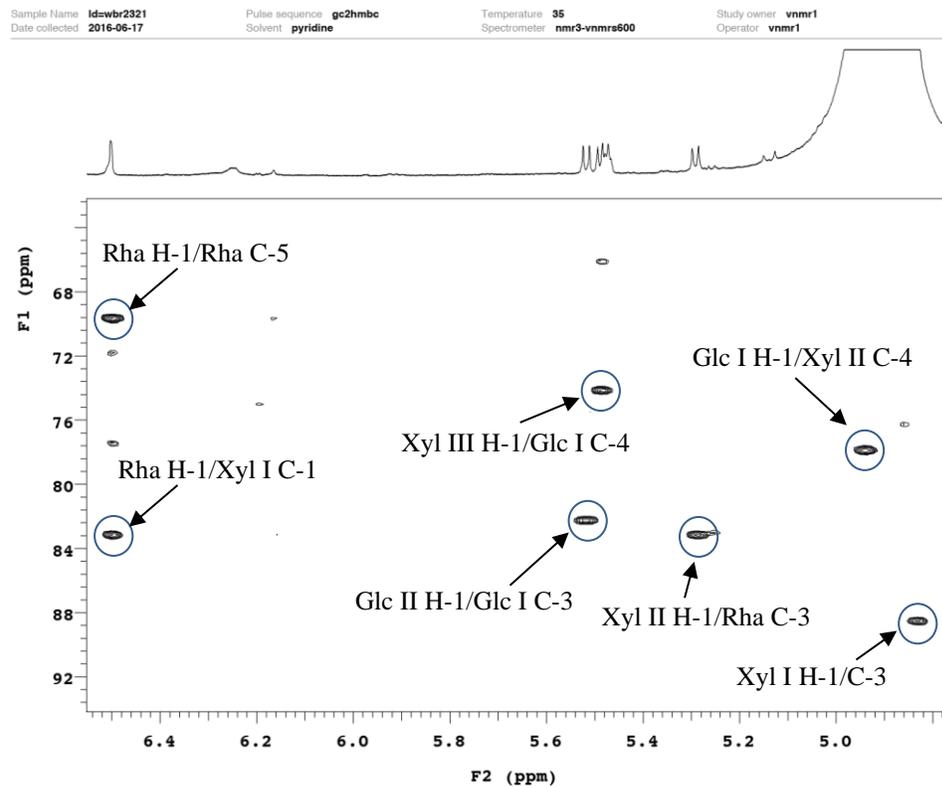
Figure 45. HMBC spectrum of sugar moieties of compound **4**
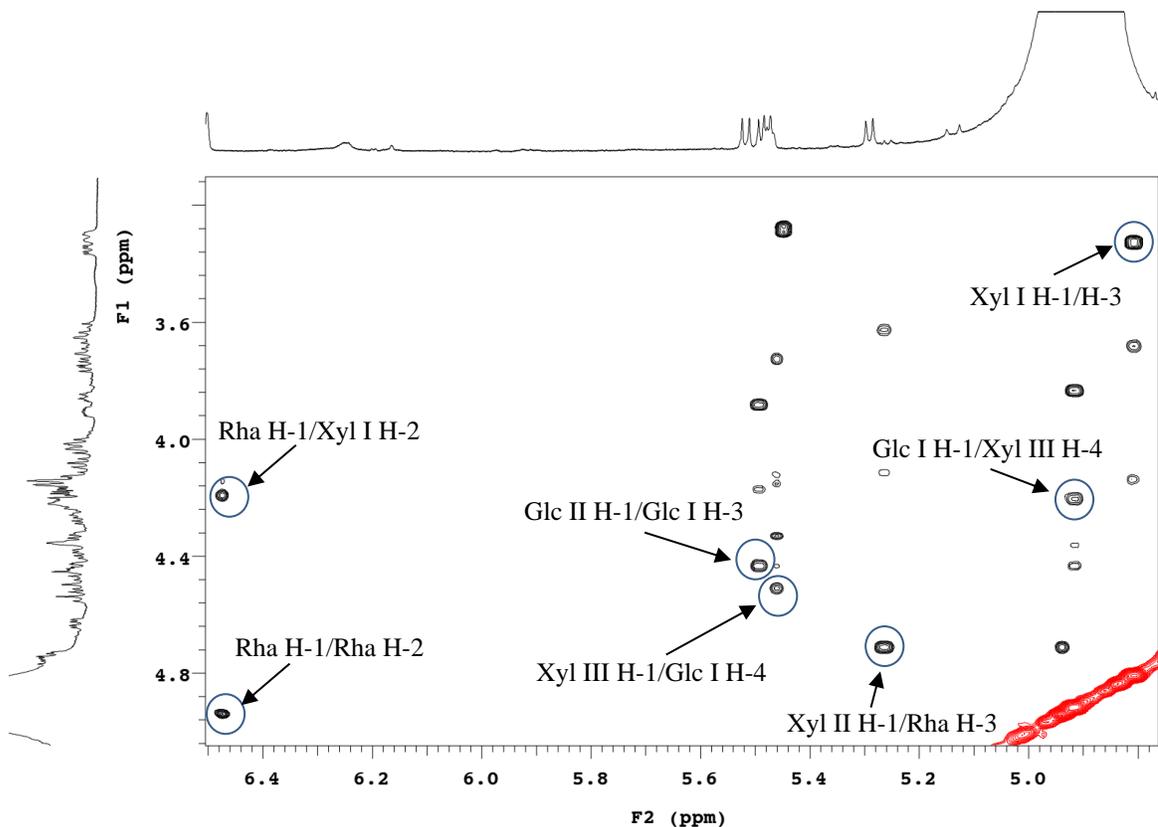
**Figure 46.** ROESY spectrum of sugar moieties of compound **4**
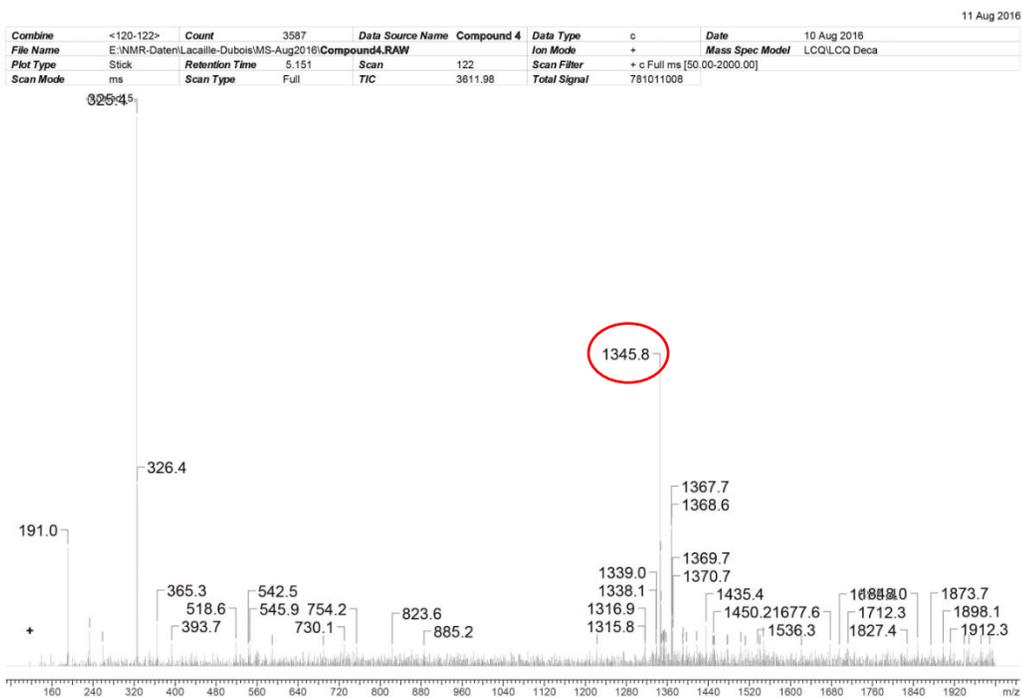
Figure 47. Mass spectrum of compound **4**

59

e. Compound 5 (WBR2320_2)

Mass spectrometry

The quasi-molecular ion peak [M+Na]$^+$ at *m/z* 1315.6306 observed in the HR-ESIMS (positive-ion mode) spectrum of compound **5**, suggested a molecular formula of $C_{62}H_{100}O_{28}$, and a molecular weight of 1292. This was in accordance with the ESIMS (negative-ion mode) spectrum with *m/z* 1292.0 [M–H]$^-$.

NMR spectroscopy

Structure of aglycon

The analysis of the NMR spectra of compound **5** showed that the aglycon was almost identified to those of compounds **1, 2, 3** and **4**. The correlations of HSQC, HMBC and ROESY allowed to identify the genin of compound **5** as the oleanolic acid which was characterised to compounds **1, 2, 3** and **4** (Table 3).

Structure of sugar moieties

The HSQC spectrum of the sugar part showed six cross-peaks at δ_H/δ_C 4.82 (d, *J* = 7.6 Hz)/106.1, 4.86 (d, *J* = 7.6 Hz)/103.8, 4.97/103.2, 5.03 (d, *J* = 8.0 Hz)/105.1, 5.28 (d, *J* = 7.2 Hz)/107.1, and 6.50 (br s)/101.6, indicating the presence of six sugar units. Starting mainly the TOCY and ROESY spectra, the sugar moieties of compound **5** was identified as:

- 1 α-L-rhamnopyranosyl Rha-1 at δ_H 6.50 (br s),

- 1 β-D-glucopyranosyl Glc-1 at δ_H 4.97,

- 4 β-D-xylopyranosyl Xyl I-1 at δ_H 4.82 (d, *J* = 7.6 Hz), Xyl II-1 at δ_H 5.28 (d, *J* = 7.2 Hz), Xyl III-1 at δ_H 5.03 (d, *J* = 8.0 Hz) and Xyl IV-1 at δ_H 4.86 (d, *J* = 7.6 Hz).

The sequence of the oligosaccharide was established by analysing the HMBC and ROESY spectra:

- The HMBC correlation between δ_H 4.82 (Xyl I H-1) and δ_C 88.5 (C-3) and in ROESY at δ_H 4.82 (Xyl I H-1) and δ_H 3.30 (H-3) proved that Xyl I was attached to the C-3 position of the aglycon (Fig.48).

- The HMBC correlation between δ_H 4.22 (Xyl I H-2) and δ_C 101.6 (Rha C-1) and in ROESY at δ_H 4.22 (Xyl I H-2) and δ_H 6.50 (Rha H-1) proved that Rha was attached to the Xyl I at C-2.

- The HMBC correlation between δ_H 5.28 (Xyl II H-1) and δ_C 83.1 (Rha C-3) and in ROESY at δ_H 5.28 (Xyl II H-1) and δ_H 4.72 (Rha H-3) proved that Xyl II was attached to the Rha at C-3.

- The HMBC correlation between δ_H 4.97 (Glc H-1) and δ_C 77.6 (Xyl II C-4) and in ROESY at δ_H 4.97 (Glc H-1) and δ_H 4.26 (Xyl II H-4) proved that Glc was attached to the Xyl II at C-4.

- The HMBC correlation between δ_H 5.03 (Xyl III H-1) and δ_C 80.5 (Glc C-4) and in ROESY at δ_H 5.03 (Xyl III H-1) and δ_H 4.21 (Glc H-4) proved that Xyl III was attached to the Glc at C-4.

- The HMBC correlation between δ_H 4.86 (Xyl IV H-1) and δ_C 76.1 (Xyl III C-4) and in ROESY at δ_H 4.86 (Xyl IV H-1) and δ_H 4.22 (Xyl III H-4) proved that Xyl IV was attached to the Xyl III at C-4.

Conclusion

Due to the evidences above, the structure of **5** was elucidated as 3-*O*-β-D-xylopyranosyl-(1→4)-β-D-xylopyranosyl-(1→4)-β-D-glucopyranosyl-(1→4)-β-D-xylopyranosyl-(1→3)-α-L-rhamnopyranosyl-(1→2)-β-D-xylopyranosyloleanolic acid.
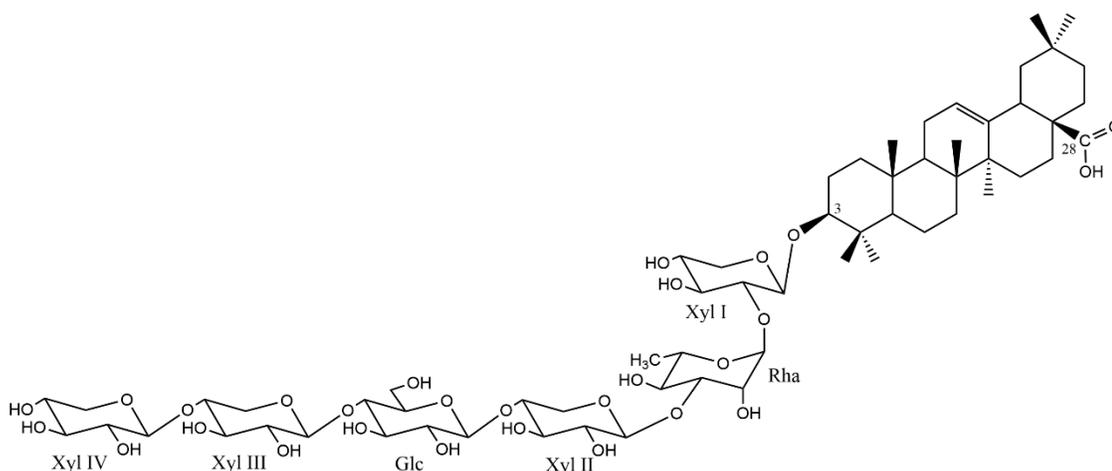
Figure 48. Structure of compound **5**
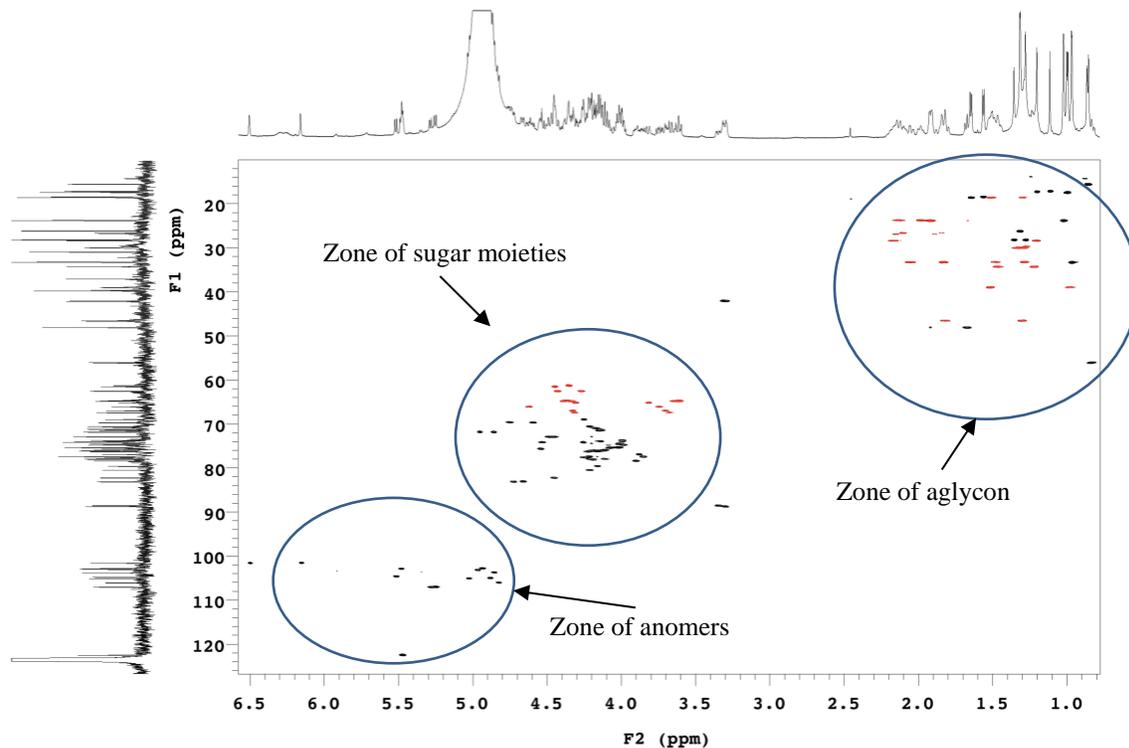
Figure 49. HSQC spectrum of compound **5**
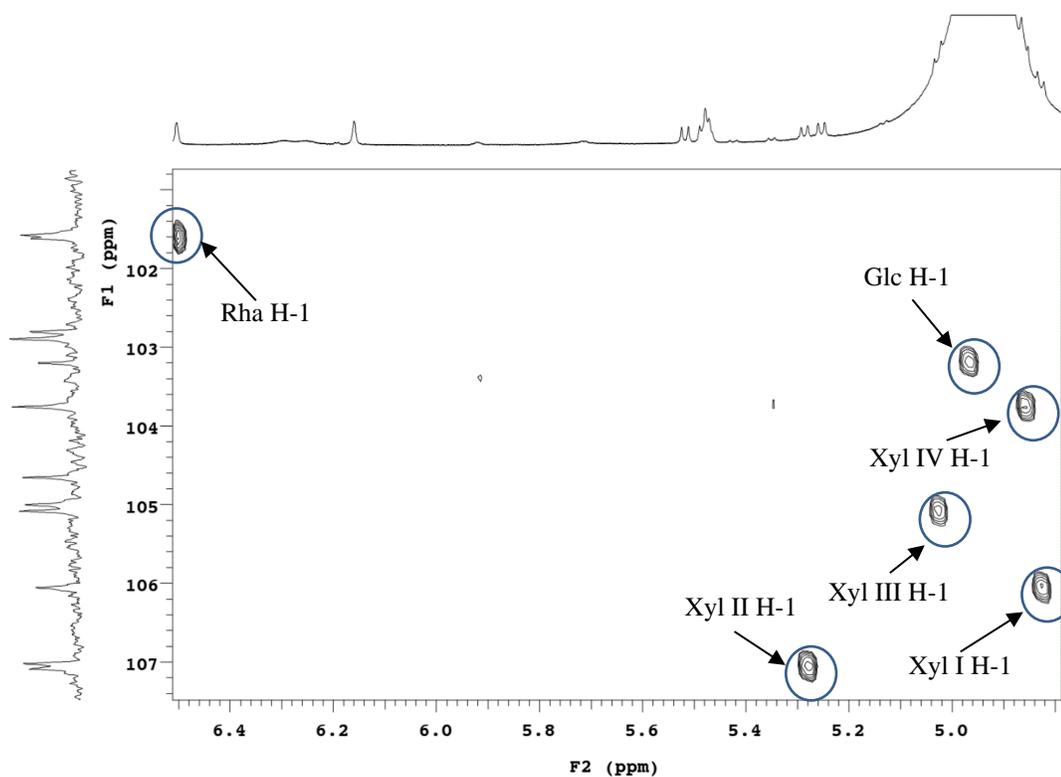
Figure 50. HSQC spectrum of sugar anomers of compound **5**
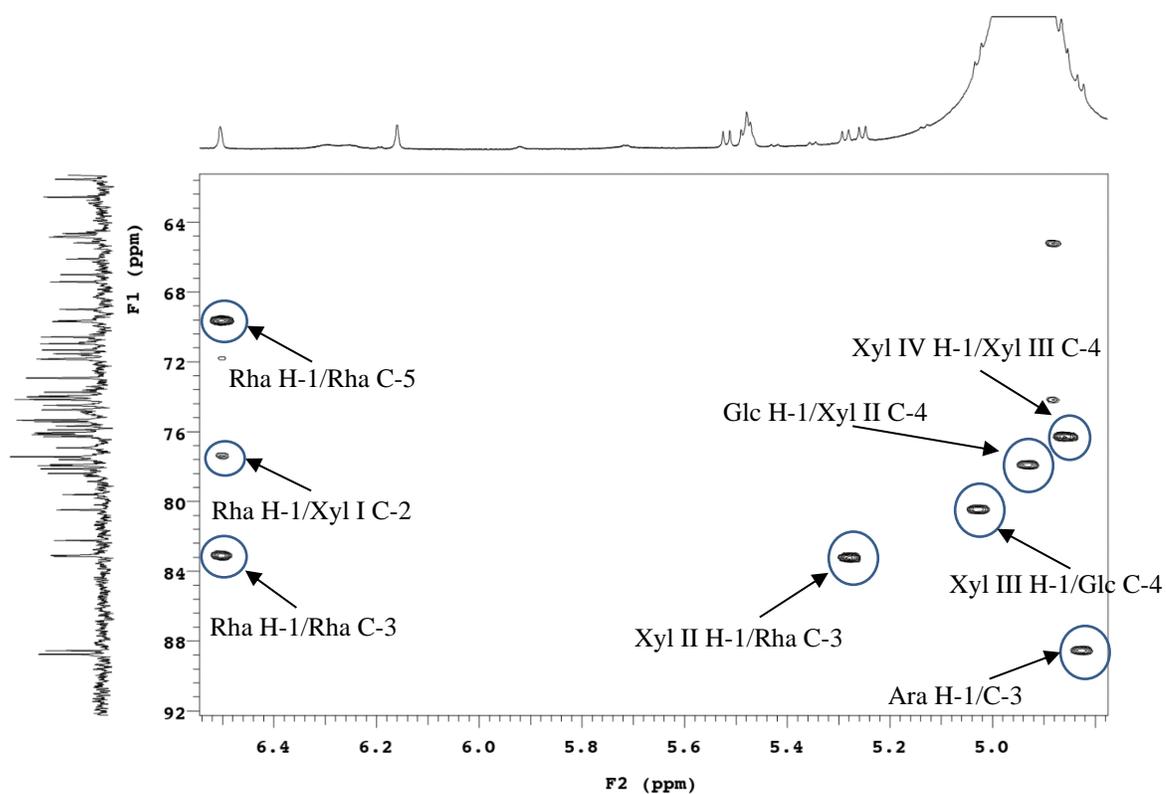
**Figure 51.** HMBC spectrum of sugar moieties of compound **5**
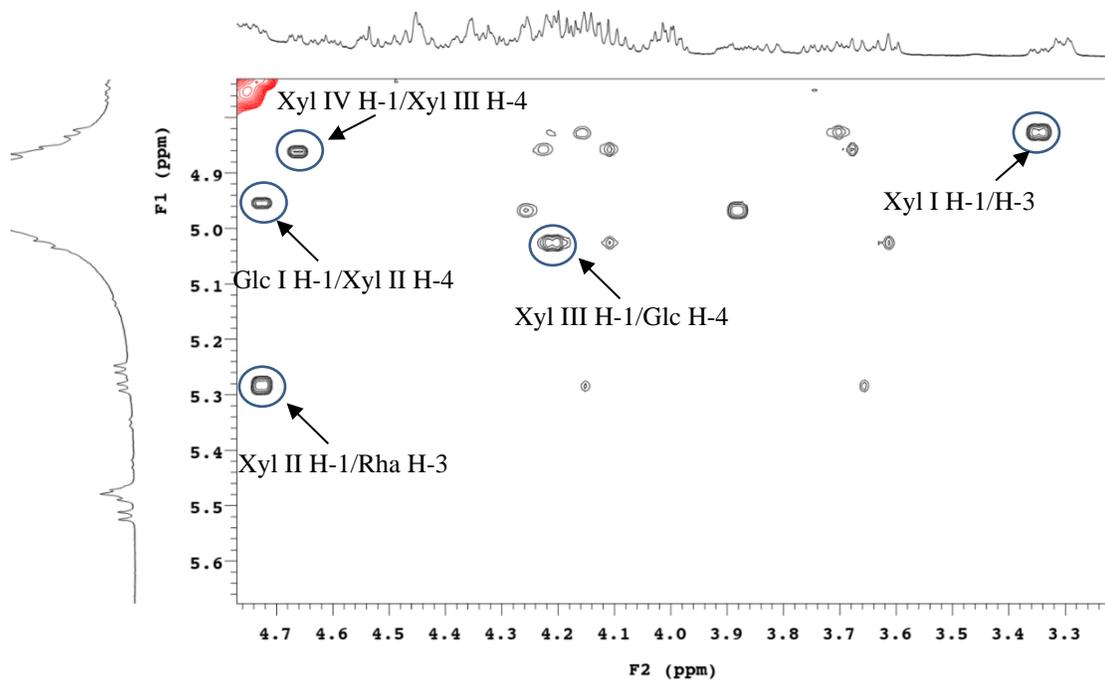

Figure 52. ROESY spectrum of sugar moieties of compound **5**

Figure 53. ROESY spectrum of sugar moieties of compound **5**

Figure 54. Mass spectrum of compound **5**

f. Compound 6 (WBR1518)

Mass spectrometry

The HR-ESIMS (positive-ion mode) spectrum of compound **6** showed a pseudo-molecular ion peak HR-ESIMS (positive-ion mode) at *m/z* 1346.3724 [M+Na]$^+$, indicating a molecular weight of 1322 and a molecular formula of $C_{63}H_{102}O_{29}$.

NMR spectroscopy

Structure of aglycon

The analysis of the NMR spectra of compound **6** showed that the aglycon was almost identified to those of compounds **1, 2, 3, 4** and **5**. The correlations of HSQC, HMBC and ROESY allowed to identify the genin of compound **6** as the oleanolic acid which was characterised to compounds **1, 2, 3, 4** and **5** (Table 3).

Structure of sugar moieties

Six sugar units were detected by HSQC correlations in the sugar region between protons at δ_H 4.69 (d, *J* = 5.2 Hz), 4.79 (d, *J* = 7.6 Hz), 5.14 (d, *J* = 6.9 Hz), 5.19 (d, *J* = 7.6 Hz), 6.00 (d, *J* = 7.3 Hz) and 6.33 (br s), and carbons at δ_C 104.8, 101.2, 102.2, 105.3, 92.1 and 100.1, respectively. The 2D NMR spectroscopic analyses enabled the full assignments of the resonances of these sugars as:

- 1 α-L-rhamnopyranosyl Rha-1 at δ_H 6.33 (br s),

- 2 β-D-glucopyranosyl Glc I-1 at δ_H 4.79 and Glc II-1 at δ_H 6.00,

- 3 β-D-xylopyranosyl Xyl I-1 at δ_H 4.69 (d, *J* = 6.0 Hz), Xyl II-1 at δ_H 5.19 (d, *J* = 7.6 Hz) and Xyl III-1 at δ_H 5.14 (d, *J* = 6.9 Hz).

The sequence of the oligosaccharide was established by analysing the HMBC and NOESY spectra:

- The HMBC correlation between δ_H 4.69 (Xyl I H-1) and δ_C 87.4 (C-3) and in NOESY at δ_H 4.69 (Xyl I H-1) and δ_H 3.23 (H-3) proved that Xyl I was attached to the C-3 position of the aglycon (Fig.55).

- The HMBC correlation between δ_H 4.09 (Xyl I H-2) and δ_C 100.1 (Rha C-1) and in NOESY at δ_H 4.09 (Xyl I H-2) and δ_H 6.33 (Rha H-1) proved that Rha was attached to the Xyl I at C-2.

- The HMBC correlation between δ_H 5.19 (Xyl II H-1) and δ_C 80.9 (Rha C-3) and in NOESY at δ_H 5.19 (Xyl II H-1) and δ_H 4.63 (Rha H-3) proved that Xyl II was attached to the Rha at C-3.

- The HMBC correlation between δ_H 4.79 (Glc I H-1) and δ_C 76.1 (Xyl II C-4) and in NOESY at δ_H 4.79 (Glc I H-1) and δ_H 4.14 (Xyl II H-4) proved that Glc I was attached to the Xyl II at C-4.

- The HMBC correlation between δ_H 5.14 (Xyl III H-1) and δ_C 79.0 (Glc C-4) and in NOESY at δ_H 5.14 (Xyl III H-1) and δ_H 4.31 (Glc H-4) proved that Xyl III was attached to the Glc I at C-4.

- The shielded chemical shift at δ_C 92.1 (Glc II C-1) and the shielded at δ_C 177.0 (C-28), suggested an ester linkage of Glc II with C-28 of the aglycon.

Conclusion

These evidences led to the elucidation of **6** as 3-*O*-β-D-xylopyranosyl-(1→4)-β-D-glucopyranosyl-(1→4)-β-D-xylopyranosyl-(1→3)-α-L-rhamnopyranosyl-(1→2)-β-D-xylopyranosyloleanolic acid 28-*O*-β-D-glucopyranosyl ester.
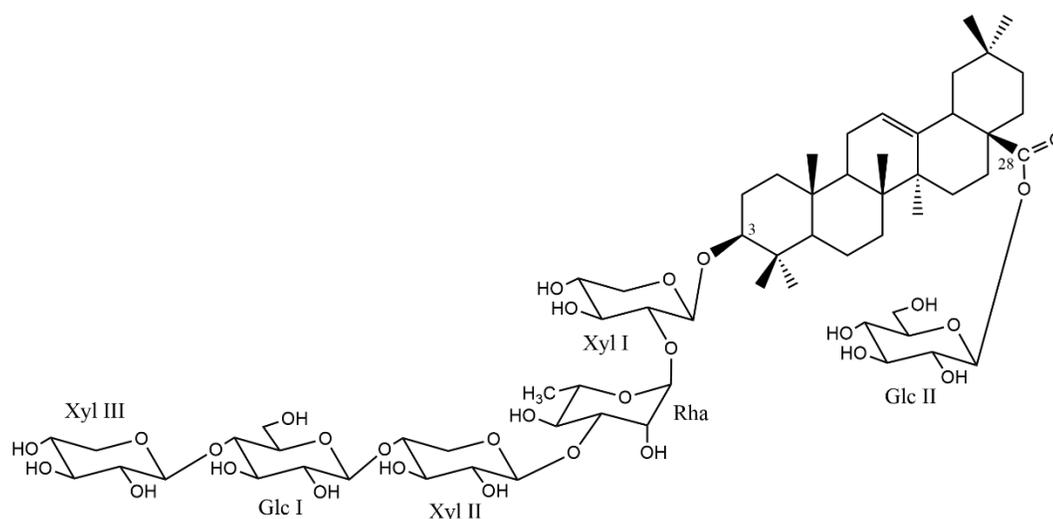
Figure 55. Structure of compound **6**
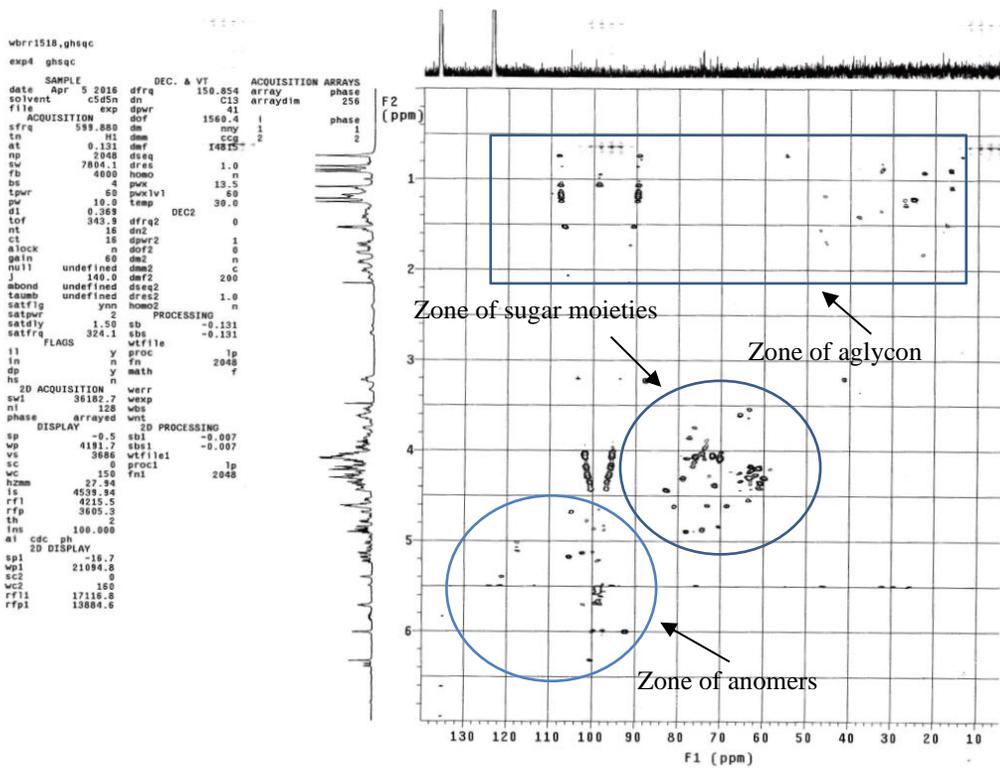
Figure 56. HSQC spectrum of compound **6**
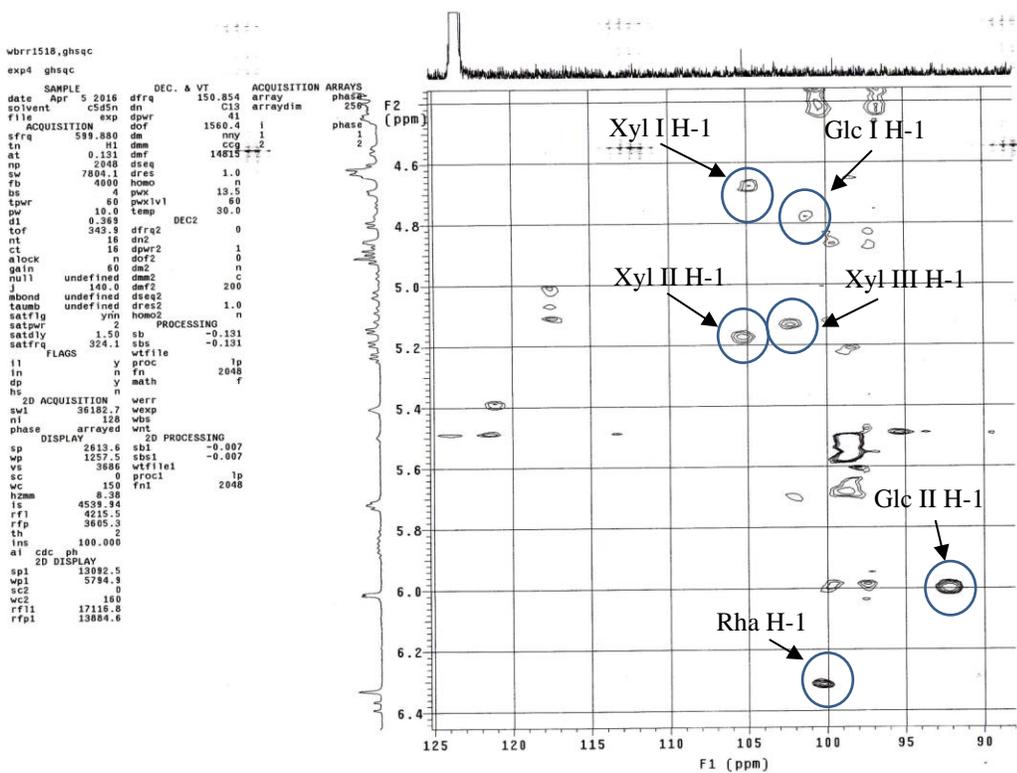
Figure 57. HSQC spectrum of sugar anomers of compound **6**
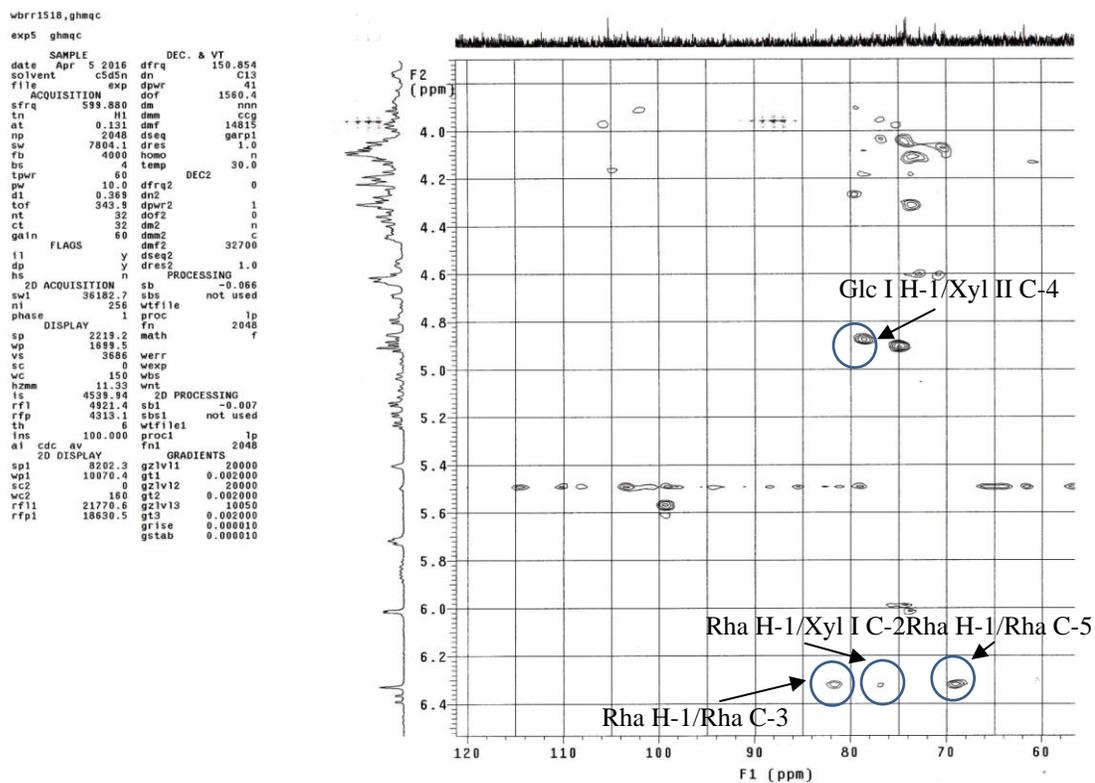
Figure 58. HMBC spectrum of sugar moieties of compound **6**
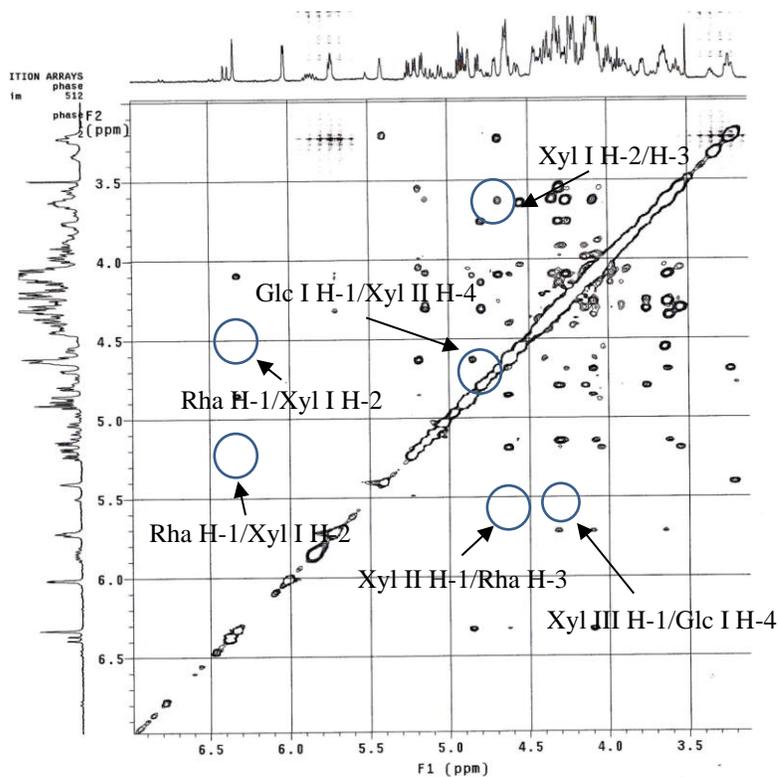
Figure 59. ROESY spectrum of sugar moieties of compound **6**

Mass Spectrum List Report

Figure 60. Mass spectrum of compound **6**

g. Compound 7 (WBR2314)

Figure 61. Structure of compound **7**

The structure of compound **7** was characterized as oleanolic acid 3-*O*-β-D-xylopyranosyl-(1→4)-β-D-glucopyranosyl-(1→4)-β-D-xylopyranosyl-(1→3)-α-L-rhamnopyranosyl-(1→2)-β-D-xylopyranoside. This compound was already isolated from the whole plant of *Pterocephalus hookeri* (Jun et al., 1993).

In conlusion, seven oleanolic acid glycosides (**1–7**) were obtained from an aqueous-ethanolic extract of the roots of *Weigela* x "Bristol Ruby" by several solid/liquid chromatographic methods. Most of those compounds posscess a bidesmosidic form with an *O*-heterosidic linkage at the C-3 position of the oleanolic acid by an oligosaccharidic chain which is composed by a sequence β-D-xylopyranosyl-(1→3)-α-L-rhamnopyranosyl-(1→2)-α-L-arabinopyranosyl or β-D-xylopyranosyl-(1→3)-α-L-rhamnopyranosyl-(1→2)-β-D-xylopyranosyl. Exception is for compound **6** which exhibits a bidesmosidic hegeragenin with an ester linkage of a β-D-glucopyranosyl at C-28 of the aglycone.

Table 3. ^{13}C and ^{1}H NMR spectroscopic data of the aglycon moieties of **1-6** in pyridine-d_5 (δ in ppm, J in Hz)

	1		2		3		4		5		6	
	δ_C	δ_H	δ_C	δ_H	δ_C	δ_H	δ_C	δ_H	δ_C	δ_H	δ_C	δ_H
1	38.9	0.96 m, 1.50 m	38.9	0.98 m, 1.52 m	38.9	0.98 m, 1.51 m	39.0	0.98 m, 1.52 m	38.9	0.98 m, 1.52 m	38.0	0.89 m, 1.40 m
2	26.6	1.85 m, 2.11 m	26.6	1.85 m, 2.10 m	26.6	1.85 m, 2.10 m	26.8	1. 89 m, 2.14 m	26.9	1.89 m, 2.15 m	26.6	1.91 m, 2.09 m
3	88.7	3.30 dd (12.1, 3.6)	88.7	3.30	88.8	3.30	88.3	3.31 dd (12.4, 4.0)	88.5	3.30	87.4	3.23
4	39.6	–	39.6	–	39.6	–	39.6	–	39.6	–	39.0	–
5	56.0	0.83 br d (11.7)	56.0	0.83	56.0	0.82 br d (12.0)	56.2	0.84	56.2	0.83	55.2	0.75
6	18.5	1.29, 1.50 m	18.5	1.29, 1.51 m	18.6	1.30, 1.50 m	18.6	1.30, 1.50 m	18.5	1.28, 1.48	nd	nd
7	33.2	1.28, 1.47 m	33.2	1.28, 1.48 m	33.2	1.28, 1.48 m	33.3	1.28, 1.48 m	33.2	1.28, 1.48	33.2	1.32, 1.50 m
8	39.8	–	39.8	–	39.8	–	39.8	–	39.8	–	39.2	–
9	48.1	1.68 dd (15.2, 8.8)	48.1	1.67	48.1	1.68 dd (17.2, 8.8)	48.1	1.68	48.1	1.67	47.3	1.59
10	37.1	–	37.1	–	37.1	–	37.1	–	37.1	–	37.0	–
11	23.8	1.89, 1.94	23.8	1.90, 1.92	23.8	1.90, 1.92	23.8	1.90, 1.92	23.8	1.90, 1.92	23.9	1.90, 1.93
12	122.5	5.48 br t (3.6)	122.5	5.48 br t (4.4)	122.5	5.48 br t (3.6)	122.5	5.47 br t (3.6)	122.5	5.48 br t (4.4)	122.5	5.40 br t (3.6)

#	δC	δH	δC	δH	δC	δH	δC	δH	δC	δH	δC	δH
13	144.8	–	144.8	–	144.9	–	144.9	–	144.8	–	144.0	–
14	42.2	–	42.2	–	42.2	–	42.2	–	42.2	–	42.0	–
15	28.3	1.20 m, 2.16	28.3	1.20 m, 2.17	28.3	1.21 m, 2.16	28.4	1.21 m, 2.15	28.3	1.20 m, 2.17	28.0	1.21 m, 2.15
16	23.7	1.97 m, 2.15	23.7	1.98 m, 2.14	23.7	1.97 m, 2.15	23.7	1.98 m, 2.15	23.7	1.98 m, 2.14	23.7	1.98 m, 2.13
17	46.7	–	46.7	–	46.7	–	46.7	–	46.7	–	46.4	–
18	42.0	3.34 dd (12.0, 4.0)	42.0	3.35	42.0	3.34	42.0	3.35 dd (11.8, 4.2)	42.0	3.35 dd (12.1, 4.0)	41.0	3.23
19	46.5	1.30, 1.82	46.5	1.30, 1.82	46.5	1.30, 1.82	46.5	1.30, 1.82	46.5	1.30, 1.82	46.0	1.18, 1.70
20	31.0	–	31.0	–	31.0	–	31.0	–	31.0	–	31.0	–
21	34.2	1.22 m, 1.46 m	34.3	1.22 m, 1.46 m	34.3	1.22 m, 1.46 m	34.3	1.22 m, 1.46 m	34.3	1.22 m, 1.46 m	34.0	1.20 m, 1.43 m
22	33.2	1.83, 2.05 m	33.3	1.83, 2.05 m	33.2	1.83, 2.05 m	33.2	1.83, 2.05 m	33.3	1.83, 2.05 m	33.1	1.83, 2.00 m
23	28.2	1.28 s	28.2	1.28 s	28.2	1.27 s	28.2	1.36 s	28.2	1.36 s	28.0	1.26 s
24	17.1	1.12 s	17.1	1.12 s	17.1	1.11 s	17.2	1.21 s	17.2	1.20 s	16.5	1.09 s
25	15.5	0.86 s	15.5	0.85 s	15.5	0.86 s	15.6	0.86 s	15.6	0.86 s	14.0	0.76 s
26	17.4	0.99 s	17.4	0.99 s	17.4	0.99 s	17.4	1.00 s	17.4	1.00 s	16.5	0.90 s
27	26.2	1.32 s	26.2	1.32 s	26.2	1.32 s	26.2	1.31 s	26.2	1.32 s	25.0	1.22 s
28	180.2	–	180.2	–	180.2	–	180.3	–	180.2	–	177.0	–
29	33.3	0.97 s	33.3	0.97 s	33.3	0.97 s	33.3	0.97 s	33.3	0.97 s	33.0	0.86 s
30	23.8	1.02 s	23.8	1.02 s	23.8	1.02 s	23.8	1.02 s	23.8	1.02 s	23.8	0.92 s

Overlapped proton signals are reported without designated multiplicity.

Table 4. ^{13}C and ^{1}H NMR spectroscopic data of the sugar moieties of **1-6** in pyridine-d_5 (δ in ppm, J in Hz)

	1		2		3		4		5		6	
	δ_C	δ_H	δ_C	δ_H	δ_C	δ_H	δ_C	δ_H	δ_C	δ_H	δ_C	δ_H
Ara I-1	105.0	4.88 d (6.0)	105.0	4.88 d (6.0)	105.0	4.88 d (6.2)						
2	75.6	4.55 t (6.0)	75.7	4.54 t (6.0)	75.6	4.54 t (6.2)						
3	74.2	4.26	74.2	4.26	74.1	4.25						
4	69.0	4.25 m	69.0	4.25 m	69.0	4.25 m						
5	65.2	3.82 dd (11.6, 1.2), 4.31 dd (11.6, 3.6)	65.2	3.82 dd (11.6, 1.2), 4.31 dd (11.6, 4.0)	65.2	3.81 dd (11.2, 1.6), 4.31 dd (11.2, 3.6)						
Rha-1	101.5	6.18 br s	101.6	6.16 br s	101.6	6.16 br s	101.6	6.50 br s	101.6	6.50 br s	100.1	6.33 br s
2	71.8	4.87 br s	71.9	4.86 br s	71.8	4.84 br s	71.8	4.96 br s	71.7	4.95 br s	70.3	4.85 br s
3	83.1	4.67 dd (9.6, 2.8)	83.1	4.66 dd (9.6, 3.2)	83.0	4.66 dd (9.2, 2.8)	83.2	4.73 dd (9.6, 3.6)	83.1	4.72	80.9	4.63
4	72.9	4.46 dd (9.6, 9.2)	72.9	4.45	72.9	4.44	72.9	4.49 dd (9.6, 9.2)	72.9	4.49 dd (9.6, 9.2)	71.2	4.39
5	69.7	4.61 dq (9.2, 6.0)	69.7	4.59	69.7	4.59	69.6	4.75 dq (9.2, 6.0)	69.6	4.75 dq (9.2, 6.4)	68.4	4.61
6	18.4	1.56 d (6.0)	18.4	1.56 d (6.0)	18.4	1.56 d (6.0)	18.6	1.65 d (6.0)	18.6	1.64 d (6.4)	18.0	1.54 d (6.0)
Xyl I-1	107.0	5.26 d (7.6)	107.0	5.25 d (7.2)	107.0	5.24 d (7.6)	106.1	4.83 d (7.6)	106.1	4.82 d (7.6)	104.8	4.69 d (5.2)
2	75.3	4.03	75.3	4.02	75.3	4.01	77.5	4.21	77.4	4.22	78.0	4.09
3	76.1	4.16	76.1	4.13	76.0	4.10	79.6	4.16	79.6	4.16	75.9	4.10
4	77.6	4.27	77.9	4.22	77.4	4.21	71.5	4.16	71.6	4.15	70.1	4.10
5	64.8	3.63 t (10.6), 4.39 dd (11.2, 5.2)	64.8	3.62 t (10.8), 4.37	64.7	3.58 t (11.3), 4.33	67.0	3.71 t (10.4), 4.33	67.0	3.70 t (10.0), 4.33	65.4	3.62 t (10.2), 4.25

Position	C	H	C	H	C	H	C	H	C	H	C	H
Xyl II-1	105.5	5.09 d (7.6)	102.9	5.48 d (6.4)	103.7	5.35 d (6.8)	107.1	5.29 d (7.6)	107.1	5.28 d (7.2)	105.3	5.19 d (7.6)
2	74.9	4.00	73.9	4.14	74.7	4.08	75.3	4.04	75.3	4.04	73.8	3.98
3	78.3	4.10	76.2	4.18	77.5	4.14	76.1	4.14	76.2	4.15	75.1	4.04
4	70.8	4.15	70.6	4.21	70.9	4.20	77.9	4.23	77.6	4.26	76.1	4.14
5	67.3	3.66 t (10.6), 4.24	66.1	3.75 t (11.2), 4.62	66.7	3.70 t (11.2), 4.48	64.7	3.65 t (11.4), 4.39 dd (11.4, 5.0)	64.8	3.66, 4.39	63.2	3.55 t (10.7), 4.29
Xyl III-1							102.9	5.49 d (6.0)	105.1	5.03 d (8.0)	102.2	5.14 d (6.9)
2							73.9	4.14	74.7	3.99	73.8	3.97
3							76.2	4.17	75.9	4.11	75.9	4.08
4							70.6	4.22	76.1	4.22	70.0	4.10
5							66.1	3.75 t (11.7), 4.63 dd (11.7, 4.4)	64.8	3.62 t (10.8), 4.34	65.3	3.61 t (11.9), 4.34
Xyl IV-1									103.8	4.86 d (7.6)		
2									73.7	4.00		
3									77.9	4.12		
4									71.0	4.17		
5									67.4	3.68, 4.32		
Glc I-1	103.2	4.99 d (7.6)	102.8	4.94	102.9	4.90 d (7.8)	102.8	4.94	103.2	4.97	101.2	4.79 d (7.6)
2	74.0	4.02	74.5	4.02	74.7	4.03	74.5	4.02	74.0	4.00	73.1	3.91
3	76.1	4.21	82.2	4.45	79.8	4.44	82.3	4.45	76.1	4.19	78.8	4.27

74

Position	C	H	C	H	C	H	C	H	C	H	C	H
4	80.7	4.26	74.2	4.54	74.0	4.48	74.2	4.54 dd (9.6, 9.2)	80.5	4.21	79.0	4.31
5	76.9	3.91 m	77.4	3.85 m	77.6	3.79 m	77.4	3.85 m	76.9	3.88 m	76.0	3.75 m
6	61.5	4.47, 4.48	61.3	4.34, 4.35	61.0	4.37, 4.46	61.3	4.36, 4.37	61.5	4.44, 4.45	60.0	4.28, 4.29
Glc II-1			104.7	5.52 d (7.6)			104.7	5.52 d (8.0)			92.1	6.00 d (7.3)
2			75.4	4.08			75.4	4.08			71.9	4.07
3			78.1	4.20			78.1	4.19			73.0	nd
4			71.3	4.14			71.4	4.14			70.1	4.04
5			78.4	3.90 m			78.4	3.91 m			77.2	3.87 m
6			62.5	4.27, 4.43			62.5	4.27 dd (12.0, 5.6), 4.43			61.0	4.20, 4.36
Ara II-1					103.4	5.92 br s						
2					72.9	4.20						
3					74.4	4.20						
4					70.7	4.10						
5					64.5	3.74 dd (11.6, 6.4), 4.75 dd (11,6, 3.6)						

Overlapped proton signals are reported without designated multiplicity. Nd: Not determined

Cytotoxic glycosides from the roots of *Weigela* x "Bristol Ruby"

Duc Hung Nguyen[a,b,c], Anne-Claire Mitaine-Offer[a,*], Sveva Maroso[d], Anna-Maria Papini[d], Thomas Paululat[e], Pierre-Simon Bellaye[f], Bertrand Collin[g], Odile Chambin[c], Marie-Aleth Lacaille-Dubois[a]

[a] PEPITE EA 4267, Laboratoire de Pharmacognosie, UFR des Sciences de Santé, Université de Bourgogne Franche-Comté, BP 87900, 21079 Dijon, Cedex, France
[b] Department of Biology, Thainguyen University of Education, Thainguyen University, 24000 Thainguyen, Viet Nam
[c] Department of Pharmaceutical Technology, PAM UMR A 02.102, PCAV team, Université de Bourgogne Franche-Comté, Dijon, France
[d] Department of Chemistry "Ugo Schiff", University of Florence, 50019 Sesto Fiorentino, Italy
[e] OC-II, Naturwissenschaftlich-Technische Fakultät, Universität Siegen, D-57076 Siegen, Germany
[f] Plateforme d'Imagerie et de Radiothérapie Précliniques, Service de Médecine Nucléaire, Centre Georges-François Leclerc, BP77980, 21079 Dijon, Cedex, France
[g] Plateforme d'Imagerie et de Radiothérapie Précliniques, ICMUB UMR CNRS 6302, Service de Médecine Nucléaire, Centre Georges-François Leclerc, BP77980, 21079 Dijon, Cedex, France

ARTICLE INFO

ABSTRACT

Seven oleanane-type glycosides were extracted and isolated by various chromatographic methods from the roots of *Weigela* x "Bristol Ruby" (**1–7**), six previously undescribed (**1–6**) and a known one (**7**). Their structures were assigned by spectroscopic analysis mainly 2D NMR and mass spectrometry (ESIMS). Selected triterpenoid glycosides (**1–3, 6, 7**) displayed a good cytotoxic activity against a mouse colon cancer cell line CT26.

1. Introduction

Weigela Thumb. (or *Weigelia* Schreb.) species, cultivars and hybrids, are known for their richness in bioactive oleanane-type glycosides as *W. stelzneri* [1], *W. florida* "rumba" [2], *W.* x "kosteriana variegata" [3], *W. hortensis* [4], and *W. subsessilis* [5]. These glycosides have been already tested for their cytotoxicity and anti-inflammatory effect [1], their capacity in the antibody recognition [2], their stimulatory activity on melanogenesis [5], and their toxicological property [3]. We have thus decided to choose another source for a phytochemical investigation of this genus. *Weigela* x "Bristol Ruby" (Caprifoliaceae) is a hybrid shrub of upright habit with dark green leaves and red flowers belonging to the Caprifoliaceae family from the Dipsacales order [6,7]. In our continuing search for new biologically active glycosides and to complete the chemotaxonomic data of the genus *Weigela,* and the Caprifoliaceae family, the phytochemical study of *Weigela* x "Bristol Ruby" was achieved, and the cytotoxicity of five isolated molecules evaluated.

Seven oleanane-type glycosides (**1–7**) (Fig. 1) were obtained from an aqueous-ethanolic extract of the roots of *W.* x "Bristol Ruby" by several solid/liquid chromatographic methods. Their structures were established by 1D and 2D NMR analysis (¹H, ¹³C, COSY, TOCSY, ROESY, HSQC, HMBC) in combination with mass spectrometry

(ESIMS), and by comparison of their spectral data with literature values as: 3-*O*-β-D-xylopyranosyl-(1 → 4)-β-D-glucopyranosyl-(1 → 4)-β-D-xylopyranosyl-(1 → 3)-α-L-rhamnopyranosyl-(1 → 2)-α-L-arabinopyranosyloleanolic acid (**1**), 3-*O*-β-D-xylopyranosyl-(1 → 4)-[β-D-glucopyranosyl-(1 → 3)]-β-D-glucopyranosyl-(1 → 4)-β-D-xylopyranosyl-(1 → 3)-α-L-rhamnopyranosyl-(1 → 2)-α-L-arabinopyranosyloleanolic acid (**2**), 3-*O*-β-D-xylopyranosyl-(1 → 4)-[α-L-arabinopyranosyl-(1 → 3)]-β-D-glucopyranosyl-(1 → 4)-β-D-xylopyranosyl-(1 → 3)-α-L-rhamnopyranosyl-(1 → 2)-arabinopyranosyloleanolic acid (**3**), 3-*O*-β-D-xylopyranosyl-(1 → 4)-[β-D-glucopyranosyl-(1 → 3)]-β-D-glucopyranosyl-(1 → 4)-β-D-xylopyranosyl-(1 → 3)-α-L-rhamnopyranosyl-(1 → 2)-β-D-xylopyranosyloleanolic acid (**4**), 3-*O*-β-D-xylopyranosyl-(1 → 4)-β-D-xylopyranosyl-(1 → 4)-β-D-glucopyranosyl-(1 → 4)-β-D-xylopyranosyl-(1 → 3)-α-L-rhamnopyranosyl-(1 → 2)-β-D-xylopyranosyloleanolic acid (**5**), 3-*O*-β-D-xylopyranosyl-(1 → 4)-β-D-glucopyranosyl-(1 → 4)-β-D-xylopyranosyl-(1 → 3)-α-L-rhamnopyranosyl-(1 → 2)-β-D-xylopyranosyloleanolic acid 28-*O*-β-D-glucopyranosyl ester (**6**), and 3-*O*-β-D-xylopyranosyl-(1 → 4)-β-D-glucopyranosyl-(1 → 4)-β-D-xylopyranosyl-(1 → 3)-α-L-rhamnopyranosyl-(1 → 2)-β-D-xylopyranosyloleanolic acid (**7**). Compounds **1–6** were previously undescribed and compound **7** was already isolated from the whole plant of *Pterocephalus hookeri* [8]. Moreover, the cytotoxicity of glycosides **1–3, 6** and **7** was evaluated against a mouse colon
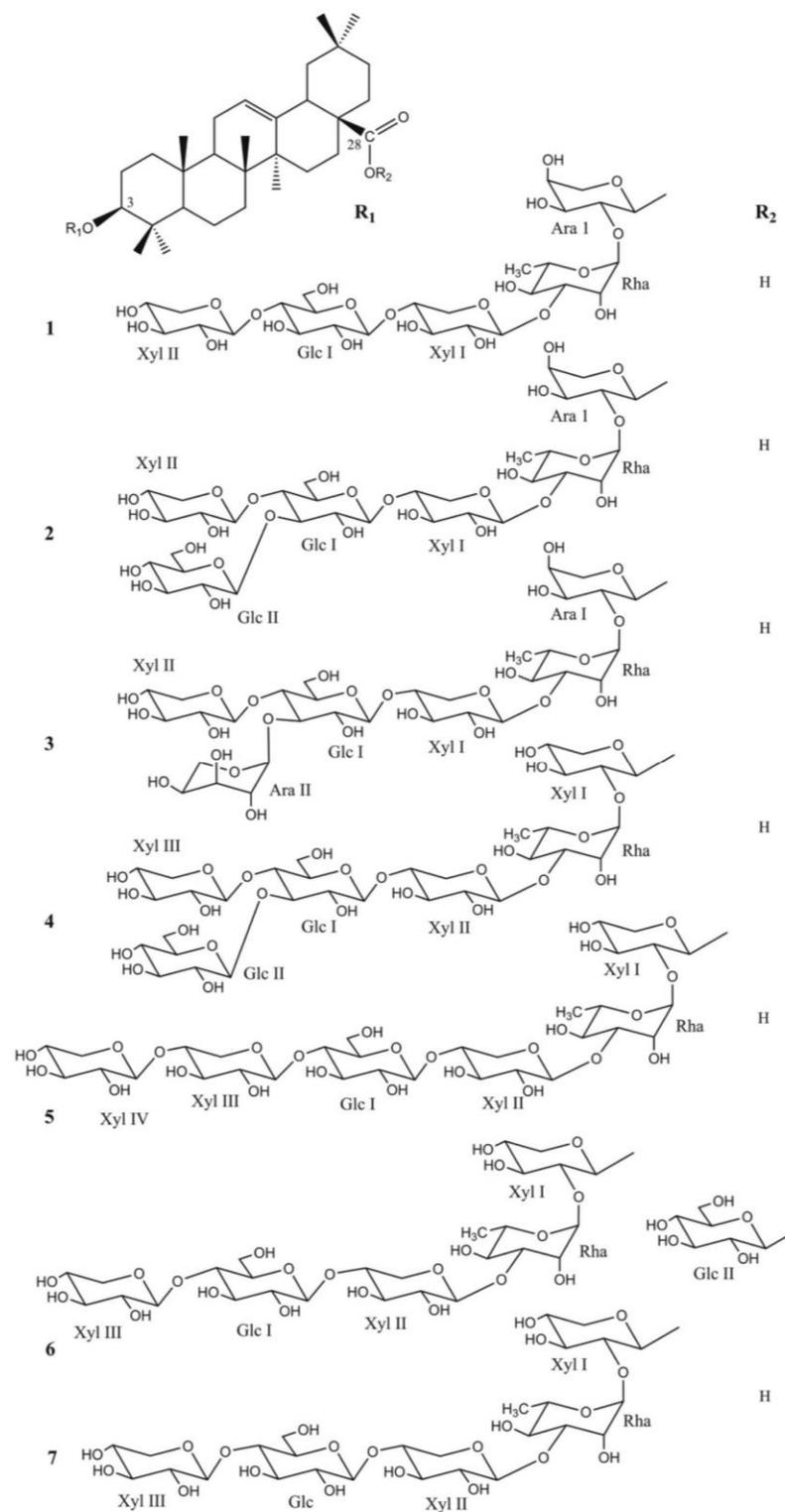
Fig. 1. Structures of compounds **1–7**.

cancer cell line CT26, with fluorouracil (5-FU) as positive control.

2. Experimental

2.1. General

Optical rotation values were recorded on a AA-10R automatic polarimeter (Optical Activity LTD). The 1D and 2D spectra (^{1}H and ^{13}C NMR, ^{1}H–^{1}H COSY, TOCSY, ROESY, HSQC and HMBC) were performed using a Varian VNMR-S 600 MHz spectrometer equipped with 3 mm triple resonance inverse and 3 mm dual broadband probeheads. Spectra are recorded in pyridine-d_5. Solvent signals were used as internal standard (pyridine-d_5: $\delta_H = 7.21$, $\delta_C = 123.5$ ppm), and all spectra were recorded at $T = 35$ °C. Pulse sequences were taken from Varian pulse sequence library (gCOSY; gHSQCAD and gHMBCAD with adiabatic pulses CRISIS-HSQC and CRISIS-HMBC). TOCSY spectra are acquired using DIPSI spin-lock and 150 ms mixing time. Mixing time in ROESY experiments: 300 ms. The carbon type (CH$_3$, CH$_2$, CH) was determined by DEPT experiments, and coupling constants (J) were measured in Hz. HRESIMS (positive-ion mode) were carried out on a Bruker microOTOF II spectrometer, and ESIMS (negative-ion mode) on a Finnigan LCQ Deca. A R.E.U.S. ultrasonic apparatus was used for the extraction (US frequency 24 KHz, Power 200 W). Compound isolations were carried out using column chromatography (CC) on Sephadex LH-20 (550 mm × 20 mm, GE Healthcare Bio-Sciences AB), and vacuum liquid chromatography (VLC) on silica gel 60 (Merck, 60–200 μm). Medium-pressure liquid chromatography (MPLC) was performed on silica gel 60 (15–40 μm, Merck) with a Gilson M 305 pump (25 SC head pump, M 805 manometric module), a Büchi glass column (460 mm × 25 mm and 460 mm × 15 mm) and a Büchi precolumn (110 mm × 15 mm). Thin-layer chromatography (TLC, Silicycle) and high-performance thin-layer chromatography (HPTLC, Merck) were carried out on precoated silica gel plates 60F$_{254}$, solvent system CHCl$_3$/MeOH/H$_2$O/AcOH (70:30:5:1). The spray reagent for saponins was vanillin reagent (1% vanillin in EtOH/H$_2$SO$_4$, 50:1).

2.2. Plant material

Weigela x "Bristol Ruby" was provided in 2016 from Jardiland® (Chenôve, France). A voucher specimen (N°20,160,110) was deposited in the herbarium of the Laboratory of Pharmacognosy, Université de Bourgogne Franche-Comté, Dijon, France.

2.3. Extraction and isolation

The dried and powdered roots of *Weigela* x "Bristol Ruby" (49 g) were submitted to an ultrasound-assisted extraction three times with EtOH/H$_2$O (75:35, 3 × 1 L, 1 h each). The resulting extracts were combined and concentrated under vacuum to give a crude extract (3 g), which was fractionated by VLC (Silica gel 60, CHCl$_3$/MeOH/H$_2$O 70:30:5) yielding 12 fractions (F1–F12). The fractions F3 and F4 were combined (780 mg) and then submitted to CC (Sephadex LH-20, MeOH) to give 4 fractions. The fraction rich in saponins (103 mg) was fractionated by MPLC (silica gel 60, CHCl$_3$/MeOH/H$_2$O 80:20:2, 70:30:5) yielding compounds **1** (4.4 mg), **2** (3.8 mg), **3** (3.7 mg), **4** (3.6 mg), **5** (3.6 mg), and **7** (8.6 mg). The combined fractions F5 and F6 (130.4 mg) were fractionated by MPLC (silica gel 60, CHCl$_3$/MeOH/H$_2$O 80:20:2, 70:30:5) to give compound **6** (3.1 mg).

2.3.1. 3-O-β-D-xylopyranosyl-(1 → 4)-β-D-glucopyranosyl-(1 → 4)-β-D-xylopyranosyl-(1 → 3)-α-L-rhamnopyranosyl-(1 → 2)-α-L-arabinopyranosyloleanolic acid (1)

White, amorphous powder; $[\alpha]_D^{25} = -6$ (c 0.15, MeOH); ^{1}H and ^{13}C NMR data (600 MHz and 150 MHz, pyridine-d_5), see Tables 1 and 2; HR-ESIMS (positive-ion mode) m/z 1183.5882 [M + Na]$^+$ (calcd. For C$_{57}$H$_{92}$NaO$_{24}$, 1183.5876). ESIMS (negative-ion mode) m/z 1159 [M–H]$^-$.

2.3.2. 3-O-β-D-xylopyranosyl-(1 → 4)-[β-D-glucopyranosyl-(1 → 3)]-β-D-glucopyranosyl-(1 → 4)-β-D-xylopyranosyl-(1 → 3)-α-L-rhamnopyranosyl-(1 → 2)-α-L-arabinopyranosyloleanolic acid (2)

White, amorphous powder; $[\alpha]_D^{25} = -10$ (c 0.15, MeOH); ^{1}H and ^{13}C NMR data (600 MHz and 150 MHz, pyridine-d_5), see Tables 1 and 2; HR-ESIMS (positive-ion mode) m/z 1345.6409 [M + Na]$^+$ (calcd. For C$_{63}$H$_{102}$NaO$_{29}$, 1345.6404). ESIMS (negative-ion mode) m/z 1321 [M–H]$^-$.

2.3.3. 3-O-β-D-xylopyranosyl-(1 → 4)-[α-L-arabinopyranosyl-(1 → 3)]-β-D-glucopyranosyl-(1 → 4)-β-D-xylopyranosyl-(1 → 3)-α-L-rhamnopyranosyl-(1 → 2)-arabinopyranosyloleanolic acid (3)

White, amorphous powder; $[\alpha]_D^{25} = -8$ (c 0.15, MeOH); ^{1}H and ^{13}C NMR data (600 MHz and 150 MHz, pyridine-d_5), see Tables 1 and 2; HR-ESIMS (positive-ion mode) m/z 1315.6306 [M + Na]$^+$ (calcd. For C$_{62}$H$_{100}$NaO$_{28}$, 1315.6299). ESIMS (negative-ion mode) m/z 1291 [M–H]$^-$.

2.3.4. 3-O-β-D-xylopyranosyl-(1 → 4)-[β-D-glucopyranosyl-(1 → 3)]-β-D-glucopyranosyl-(1 → 4)-β-D-xylopyranosyl-(1 → 3)-α-L-rhamnopyranosyl-(1 → 2)-β-D-xylopyranosyloleanolic acid (4)

White, amorphous powder; $[\alpha]_D^{25} = -6$ (c 0.15, MeOH); ^{1}H and ^{13}C NMR data (600 MHz and 150 MHz, pyridine-d_5), see Tables 1 and 2; HR-ESIMS (positive-ion mode) m/z 1345.6409 [M + Na]$^+$ (calcd. For C$_{63}$H$_{102}$NaO$_{29}$, 1345.6404). ESIMS (negative-ion mode) m/z 1321 [M–H]$^-$.

2.3.5. 3-O-β-D-xylopyranosyl-(1 → 4)-β-D-xylopyranosyl-(1 → 4)-β-D-glucopyranosyl-(1 → 4)-β-D-xylopyranosyl-(1 → 3)-α-L-rhamnopyranosyl-(1 → 2)-β-D-xylopyranosyloleanolic acid (5)

White, amorphous powder; $[\alpha]_D^{25} = -3$ (c 0.15, MeOH); ^{1}H and ^{13}C NMR data (600 MHz and 150 MHz, pyridine-d_5), see Tables 1 and 2; HR-ESIMS (positive-ion mode) m/z 1315.6306 [M + Na]$^+$ (calcd. For C$_{62}$H$_{100}$NaO$_{28}$, 1315.6299). ESIMS (negative-ion mode) m/z 1291 [M–H]$^-$.

2.3.6. 3-O-β-D-xylopyranosyl-(1 → 4)-β-D-glucopyranosyl-(1 → 4)-β-D-xylopyranosyl-(1 → 3)-α-L-rhamnopyranosyl-(1 → 2)-β-D-xylopyranosyloleanolic acid 28-O-β-D-glucopyranosyl ester (6)

White, amorphous powder; $[\alpha]_D^{25} = -8$ (c 0.15, MeOH); ^{1}H and ^{13}C NMR data (600 MHz and 150 MHz, pyridine-d_5), see Tables 1 and 2; HR-ESIMS (positive-ion mode) m/z 1345.6409 [M + Na]$^+$ (calcd. For C$_{63}$H$_{102}$NaO$_{29}$, 1345.6404).

2.4. Acid hydrolysis and GC analysis

Each compound (3 mg) was hydrolyzed with 2 N aq. CF$_3$COOH (5 mL) for 3 h at 95 °C. After extraction with CH$_2$Cl$_2$ (3 × 5 mL), the aqueous layer was repeatedly evaporated to dryness with MeOH until neutral, and then analyzed by TLC over silica gel (CHCl$_3$/MeOH/H$_2$O 8:5:1) by comparison with authentic samples. Furthermore, the sugars residue was dissolved in anhydrous pyridine (100 μL), and L-cysteine methyl ester hydrochloride (0.06 mol/L) was added. The mixture was stirred at 60 °C for 1 h, then 150 μL of HMDS-TMCS (hexamethyldisilazane/trimethylchlorosilane 3:1) was added, and the mixture was stirred at 60 °C for another 30 min. The precipitate was centrifuged off, and the supernatant was concentrated under a N$_2$ stream. The residue was partitioned between *n*-hexane and H$_2$O (0.1 mL each), and the hexane layer (1 μL) was analyzed by GC [9]. The absolute configurations were determined by comparing the retention times with thiazolidine derivatives prepared in a similar way from standard sugars (Sigma-Aldrich).

2.5. Cytotoxicity assay

CT26 cells (mouse colon cancer, ATCC® CRL-2638™) were seeded at

Table 1
^{13}C and ^1H NMR spectroscopic data of the aglycone moieties of **1–6** in pyridine-d_5 (δ in ppm, J in Hz).

	1		2		3		4		5		6	
	δ_C	δ_H	δ_C	δ_H	δ_C	δ_H	δ_C	δ_H	δ_C	δ_H	δ_C	δ_H
1	38.9	0.96 m, 1.50 m	38.9	0.98 m, 1.51 m	38.9	0.98 m, 1.52 m	39.0	0.98 m, 1.52 m	38.9	0.98 m, 1.52 m	38.0	0.89 m, 1.40 m
2	26.6	1.85 m, 2.11 m	26.6	1.85 m, 2.10 m	26.6	1.85 m, 2.10 m	26.8	1.89 m, 2.14 m	26.9	1.89 m, 2.15 m	26.6	1.91 m, 2.09 m
3	88.7	3.30 dd (12.1, 3.6)	88.7	3.30	88.8	3.30	88.3	3.31 dd (12.4, 4.0)	88.5	3.30	87.4	3.23
4	39.6	–	39.6	–	39.6	–	39.6	–	39.6	–	39.0	–
5	56.0	0.83 br d (11.7)	56.0	0.83	56.0	0.82 br d (12.0)	56.2	0.84	56.2	0.83	55.2	0.75
6	18.5	1.29, 1.50 m	18.5	1.29, 1.51 m	18.6	1.30, 1.50 m	18.6	1.30, 1.50 m	18.5	1.28, 1.48	nd	nd
7	33.2	1.28, 1.47 m	33.2	1.28, 1.48 m	33.2	1.28, 1.48 m	33.3	1.28, 1.48 m	33.2	1.28, 1.48	33.2	1.32, 1.50 m
8	39.8	–	39.8	–	39.8	–	39.8	–	39.8	–	39.2	–
9	48.1	1.68 dd (15.2, 8.8)	48.1	1.67	48.1	1.68 dd (17.2, 8.8)	48.1	1.68	48.1	1.67	47.3	1.59
10	37.1	–	37.1	–	37.1	–	37.1	–	37.1	–	37.0	–
11	23.8	1.89, 1.94	23.8	1.90, 1.92	23.8	1.90, 1.92	23.8	1.90, 1.92	23.8	1.90, 1.92	23.9	1.90, 1.93
12	122.5	5.48 br t (3.6)	122.5	5.48 br t (4.4)	122.5	5.48 br t (3.6)	122.5	5.47 br t (3.6)	122.5	5.48 br t (4.4)	122.5	5.40 br t (3.6)
13	144.8	–	144.8	–	144.9	–	144.9	–	144.8	–	144.0	–
14	42.2	–	42.2	–	42.2	–	42.2	–	42.2	–	42.0	–
15	28.3	1.20 m, 2.16	28.3	1.20 m, 2.17	28.3	1.21 m, 2.16	28.4	1.21 m, 2.15	28.3	1.20 m, 2.17	28.0	1.21 m, 2.15
16	23.7	1.97 m, 2.15	23.7	1.98 m, 2.14	23.7	1.97 m, 2.15	23.7	1.98 m, 2.15	23.7	1.98 m, 2.14	23.7	1.98 m, 2.13
17	46.7	–	46.7	–	46.7	–	46.7	–	46.7	–	46.4	–
18	42.0	3.34 dd (12.0, 4.0)	42.0	3.35	42.0	3.34	42.0	3.35 dd (11.8, 4.2)	42.0	3.35 dd (12.1, 4.0)	41.0	3.23
19	46.5	1.30, 1.82	46.5	1.30, 1.82	46.5	1.30, 1.82	46.5	1.30, 1.82	46.5	1.30, 1.82	46.0	1.18, 1.70
20	31.0	–	31.0	–	31.0	–	31.0	–	31.0	–	31.0	–
21	34.2	1.22 m, 1.46 m	34.3	1.22 m, 1.46 m	34.3	1.22 m, 1.46 m	34.3	1.22 m, 1.46 m	34.3	1.22 m, 1.46 m	34.0	1.20 m, 1.43 m
22	33.2	1.83, 2.05 m	33.3	1.83, 2.05 m	33.2	1.83, 2.05 m	33.2	1.83, 2.05 m	33.3	1.83, 2.05 m	33.1	1.83, 2.00 m
23	28.2	1.28 s	28.2	1.28 s	28.2	1.27 s	28.2	1.36 s	28.2	1.36 s	28.0	1.26 s
24	17.1	1.12 s	17.1	1.12 s	17.1	1.11 s	17.2	1.21 s	17.2	1.20 s	16.5	1.09 s
25	15.5	0.86 s	15.5	0.85 s	15.5	0.86 s	15.6	0.86 s	15.6	0.86 s	14.0	0.76 s
26	17.4	0.99 s	17.4	0.99 s	17.4	0.99 s	17.4	1.00 s	17.4	1.00 s	16.5	0.90 s
27	26.2	1.32 s	26.2	1.32 s	26.2	1.32 s	26.2	1.31 s	26.2	1.32 s	25.0	1.22 s
28	180.2	–	180.2	–	180.2	–	180.3	–	180.2	–	177.0	–
29	33.3	0.97 s	33.3	0.97 s	33.3	0.97 s	33.3	0.97 s	33.3	0.97 s	33.0	0.86 s
30	23.8	1.02 s	23.8	1.02 s	23.8	1.02 s	23.8	1.02 s	23.8	1.02 s	23.8	0.92 s

Overlapped proton signals are reported without designated multiplicity. Nd: Not determined.

the density of 5×10^3 cells in 96 well plates (Falcon), cultivated for 48 h before treatments in RPMI 1640 medium (Corning) with 10% FBS (Dutcher). Cells were then treated with the isolated compounds at the concentrations from 1 to 50 μM, for 36 h in RPMI1640 medium without FBS (200 μL per well). Viability was measured using a MTS colorimetric assay (Abcam) following the manufacturer recommendations. Briefly, 20 μL of MTS reagent was added into each well and optical density at 490 nm was read using a microplate reader (Spark®, Tecan) after 1 h incubation at 37 °C, 5% CO_2, in the dark. The results were expressed as concentrations of compound producing 50% toxicity (IC_{50} value). Fluorouracil (5-FU) was used as positive control and exhibited IC_{50} values of 11.7 μM. The experiment was done in quintuplet.

3. Results and discussion

From an aqueous-ethanolic (35:75) extract of the roots of *Weigela* x "Bristol Ruby", seven triterpene glycosides **1–7** (Fig. 1) were isolated by various solid/liquid chromatographic methods. Their structural analysis was performed mainly by 2D NMR and mass spectrometry.

For all the isolated compounds **1–7**, the ^1H and ^{13}C NMR signals of the aglycone assigned from the 2D NMR spectra, were in good agreement with those of oleanolic acid commonly encountered in the *Weigela* genus [1–3]. The differences were located at the osidic moieties linked to the C-3 and C-28 of the aglycone. The monosaccharides were identified by acid hydrolysis and extensive 2D NMR analysis as α-L-arabinopyranosyl (Ara), α-L-rhamnopyranosyl (Rha), β-D-xylopyranosyl (Xyl) and β-D-glucopyranosyl (Glc) in the case of **1–3**, and Rha, Xyl and Glc in the case of **4–7**. The absolute configurations of the sugars were determined to be D for glucose (Glc), and xylose (Xyl), and L for arabinose (Ara) and rhamnose (Rha), by GC analysis (see Experimental

section). The relatively large $^3J_{H-1,H-2}$ values of the Glc, Xyl, and Ara (6.0–8.0 Hz) indicated a β anomeric orientation for Glc and Xyl, and an α anomeric orientation for Ara. For compound **3**, the broad singlet observed for the anomeric proton of the terminal arabinopyranosyl moiety is consistent with the $^1C_4$ conformation of Ara with an α-orientation of the anomeric center [10]. The large $^1J_{H-1,C-1}$ values of the Rha (165–168 Hz), confirmed that the anomeric protons were equatorial (α-pyranoid anomeric form). The complete structural analysis is detailed below, only for the previously undescribed glycosides **1–6**.

For compound **1**, the HR-ESIMS (positive-ion mode) spectrum showed a pseudo-molecular ion peak $[M + Na]^+$ at m/z 1183.5882, indicating a molecular weight of 1160 and a molecular formula of $C_{57}H_{92}O_{24}$. This was confirmed by the ESIMS (negative-ion mode) spectrum with m/z 1159 $[M–H]^-$.

The ^1H and ^{13}C spectra of the aglycone part of **1** (Table 1) were in good accordance with the signals of oleanolic acid [1–3]. The chemical shifts at δ_C 88.7 for C-3 and 180.2 for C-28 suggested a monodesmosidic structure.

For the sugar part of the molecule, the ^1H NMR spectrum of **1** showed five anomeric proton signals at δ_H 4.88 (d, J = 6.0 Hz), 4.99 (d, J = 7.6 Hz), 5.09 (d, J = 7.6 Hz), 5.26 (d, J = 7.6 Hz) and 6.18 (br s), which gave correlations in the HSQC spectrum with their corresponding anomeric carbons at δ_C 105.0, 103.2, 105.5, 107.0 and 101.5, respectively. All protons and carbons signals were identified by 2D NMR experiments, starting mainly by the TOCSY experiment (Table 2). The α-L-arabinopyranosyl moiety was shown to be attached at the C-3 position of the aglycone by observation of an HMBC correlation between δ_H 4.88 (Ara I H-1) and δ_C 88.7 (C-3). Moreover, the HMBC spectrum of **1** displayed long-range correlations at δ_H/δ_C 6.18 (Rha H-1)/75.6 (Ara I C-2), 5.26 (Xyl I H-1)/83.1 (Rha C-3), 4.99 (Glc I H-1)/77.6 (Xyl I C-4),

Table 2

^{13}C and ^{1}H NMR spectroscopic data of the sugar moieties of **1–6** in pyridine-d_5 (δ in ppm, J in Hz).

	1 δC	1 δH	2 δC	2 δH	3 δC	3 δH	4 δC	4 δH	5 δC	5 δH	6 δC	6 δH
Ara I-1	105.0	4.88 d (6.0)	105.0	4.88 d (6.0)	105.0	4.88 d (6.2)						
2	75.6	4.55 t (6.0)	75.7	4.54 t (6.0)	75.6	4.54 t (6.2)						
3	74.2	4.26	74.2	4.26	74.1	4.25						
4	69.0	4.25 m	69.0	4.25 m	69.0	4.25 m						
5	65.2	3.82 dd (11.6, 1.2),	65.2	3.82 dd (11.6, 1.2),	65.2	3.81 dd (11.2, 1.6),						
		4.31 dd (11.6, 3.6)		4.31 dd (11.6, 4.0)		4.31 dd (11.2, 3.6)						
Rha-1	101.5	6.18 br s	101.6	6.16 br s	101.6	6.16 br s	101.6	6.50 br s	101.6	6.50 br s	100.1	6.33 br s
2	71.8	4.87 br s	71.9	4.86 br s	71.8	4.84 br s	71.8	4.96 br s	71.7	4.95 br s	70.3	4.85 br s
3	83.1	4.67 dd (9.6, 2.8)	83.1	4.66 dd (9.6, 3.2)	83.0	4.66 dd (9.2, 2.8)	83.2	4.73 dd (9.6, 3.6)	83.1	4.72	80.9	4.63
4	72.9	4.46 dd (9.6, 9.2)	72.9	4.45	72.9	4.44	72.9	4.49 dd (9.6, 9.2)	72.9	4.49 dd (9.6, 9.2)	71.2	4.39
5	69.7	4.61 dq (9.2, 6.0)	69.7	4.59	69.7	4.59	69.6	4.75 dq (9.2, 6.0)	69.6	4.75 dq (9.2, 6.4)	68.4	4.61
6	18.4	1.56 d (6.0)	18.4	1.56 d (6.0)	18.4	1.56 d (6.0)	18.6	1.65 d (6.0)	18.6	1.64 d (6.4)	18.0	1.54 d (6.0)
Xyl I-1	107.0	5.26 d (7.6)	107.0	5.25 d (7.2)	107.0	5.24 d (7.6)	106.1	4.83 d (7.6)	106.1	4.82 d (7.6)	104.8	4.69 d (6.0)
2	75.3	4.03	75.3	4.02	75.3	4.01	77.5	4.21	77.4	4.22	78.0	4.09
3	76.1	4.16	76.1	4.13	76.0	4.10	79.6	4.16	79.6	4.16	75.9	4.10
4	77.6	4.27	77.9	4.22	77.4	4.21	71.5	4.16	71.6	4.15	70.1	4.10
5	64.8	3.63 t (10.6), 4.39 dd (11.2, 5.2)	64.8	3.62 t (10.8), 4.37	64.7	3.58 t (11.3), 4.33	67.0	3.71 t (10.4), 4.33	67.0	3.70 t (10.0), 4.33	65.4	3.62 t (10.2), 4.25
Xyl II-1	105.5	5.09 d (7.6)	102.9	5.48 d (6.4)	103.7	5.35 d (6.8)	107.1	5.29 d (7.6)	107.1	5.28 d (7.2)	105.3	5.19 d (7.6)
2	74.9	4.00	73.9	4.14	74.7	4.08	75.3	4.04	75.3	4.04	73.8	3.98
3	78.3	4.10	76.2	4.18	77.5	4.14	76.1	4.14	76.2	4.14	75.1	4.04
4	70.8	4.15	70.6	4.21	70.9	4.20	77.9	4.23	77.6	4.26	76.1	4.14
5	67.3	3.66 t (10.6), 4.24	66.1	3.75 t (11.2), 4.62	66.7	3.70 t (11.2), 4.48	64.7	3.65 t (11.4), 4.39 dd (11.4, 5.0)	64.8	3.66, 4.39	63.2	3.55 t (10.7), 4.29
Xyl III-1							102.9	5.49 d (6.0)	105.1	5.03 d (8.0)	102.2	5.14 d (6.9)
2							73.9	4.14	74.7	3.99	73.8	3.97
3							76.2	4.17	75.9	4.11	75.9	4.08
4							70.6	4.22	76.1	4.22	70.0	4.10
5							66.1	3.75 t (11.7), 4.63 dd (11.7, 4.4)	64.8	3.62 t (10.8), 4.34	65.3	3.61 t (11.9), 4.34
Xyl IV-1									103.8	4.86 d (7.6)		
2									73.7	4.00		
3									77.9	4.12		
4									71.0	4.17		
5									67.4	3.68, 4.32		
Glc I-1	103.2	4.99 d (7.6)	102.8	4.94	102.9	4.90 d (7.8)	102.8	4.94	103.2	4.97	101.2	4.79 d (7.6)
2	74.0	4.02	74.5	4.02	74.7	4.03	74.5	4.02	74.0	4.00	73.1	3.91
3	76.1	4.21	82.2	4.45	79.8	4.44	82.3	4.45	76.1	4.19	78.8	4.27
4	80.7	4.26	74.2	4.54	74.0	4.48	74.2	4.54 dd (9.6, 9.2)	80.5	4.21	79.0	4.31
5	76.9	3.91 m	77.4	3.85 m	77.6	3.79 m	77.4	3.85 m	76.9	3.88 m	76.0	3.75 m
6	61.5	4.47, 4.48	61.3	4.34, 4.35	61.0	4.37, 4.46	61.3	4.36, 4.37	61.5	4.44, 4.45	60.0	4.28, 4.29
Glc II-1			104.7	5.52 d (7.6)			104.7	5.52 d (8.0)			92.1	6.00 d (7.3)
2			75.4	4.08			75.4	4.08			71.9	4.07
3			78.1	4.20			78.1	4.19			73.0	nd
4			71.3	4.14			71.4	4.14			70.1	4.04
5			78.4	3.90 m			78.4	3.91 m			77.2	3.87 m
6			62.5	4.27, 4.43			62.5	4.27 dd (12.0, 5.6), 4.43			61.0	4.20, 4.36
Ara II-1					103.4	5.92 br s						
2					72.9	4.20						
3					74.4	4.20						
4					70.7	4.10						
5					64.5	3.74 dd (11.6, 6.4), 4.75 dd (11.6, 3.6)						

Overlapped proton signals are reported without designated multiplicity. Nd: Not determined.

and 5.09 (Xyl II H-1)/80.7 (Glc I C-4), which suggested the structure of the oligosaccharidic part as 3-O-β-D-xylopyranosyl-(1 → 4)-β-D-glucopyranosyl-(1 → 4)-β-D-xylopyranosyl-(1 → 3)-α-L-rhamnopyranosyl-(1 → 2)-α-L-arabinopyranosyl. The linkages were ensured by the ROESY cross-peaks at δ_H/δ_H 4.88 (Ara I H-1)/3.30 (dd, J = 12.1, 3.6 Hz, H-3), 6.18 (Rha H-1)/4.55 (t, J = 6.0 Hz, Ara H-2), 5.26 (Xyl I H-1)/4.67 (dd, J = 9.6, 2.8 Hz, Rha H-3), 4.99 (Glc I H-1)/4.27 (Xyl I H-4), and 5.09 (Xyl II H-1)/4.26 (Glc I H-4). Based on the above results, the structure of **1** was elucidated as 3-O-β-D-xylopyranosyl-(1 → 4)-β-D-

glucopyranosyl-(1 → 4)-β-D-xylopyranosyl-(1 → 3)-α-L-rhamnopyranosyl-(1 → 2)-α-L-arabinopyranosyloleanolic acid (Fig. 1).

For compound **2**, the molecular formula $C_{63}H_{102}O_{29}$, and thus a molecular weight of 1322, was obtained according to its HR-ESIMS (positive-ion mode) spectrum which displayed a pseudo-molecular ion peak at m/z 1345.6409 $[M + Na]^+$. This was in accordance with the ESIMS (negative-ion mode) spectrum with m/z 1321 $[M–H]^-$.

This molecular weight differs from **1** by only 162 amu, corresponding to a supplementary hexosyl group. The part of the HSQC

spectrum corresponding to the osidic chain showed cross-peaks at δ_H/δ_C 4.88 (d, J = 6.0 Hz)/105.0, 4.94/102.8, 5.25 (d, J = 7.2 Hz)/107.0, 5.48 (d, J = 6.4 Hz)/102.9, 5.52 (d, J = 7.6 Hz)/104.7 and 6.16 (br s)/101.6, indicating the presence of six sugar units which were identified as Ara I, Xyl I, Xyl II, Glc I, Glc II and Rha. The NMR data of **2** were assigned and compared to **1**, and similarities appeared: The structure of the common sequence was determined as 3-O-β-D-xylopyranosyl-(1 → 4)-β-D-glucopyranosyl-(1 → 4)-β-D-xylopyranosyl-(1 → 3)-α-L-rhamnopyranosyl-(1 → 2)-α-L-arabinopyranosyloleanolic acid (Tables 1 and 2). The only difference was located at the Glc I moiety, at the C-3 position, which was linked to a terminal osidic group. Its ring protons were defined starting from the H-1 at δ_H 5.52 in the TOCSY spectrum, and was identified as a β-D-glucopyranosyl moiety (Glc II) by extensive 2D NMR analysis. The linkage at the Glc I-3 position was proved by the HMBC correlation at δ_H/δ_C 5.52 (Glc II H-1)/82.2 (Glc I C-3) and by the ROESY cross-peak at δ_H/δ_H 5.52 (Glc II H-1)/4.45 (Glc I H-3). Hence, the structure of **2** was elucidated as 3-O-β-D-xylopyranosyl-(1 → 4)-[β-D-glucopyranosyl-(1 → 3)]-β-D-glucopyranosyl-(1 → 4)-β-D-xylopyranosyl-(1 → 3)-α-L-rhamnopyranosyl-(1 → 2)-α-L-arabinopyranosyloleanolic acid (Fig. 1).

The HR-ESIMS (positive-ion mode) spectrum of compound **3** showed a pseudo-molecular ion peak [M + Na]$^+$ at m/z 1315.6306, indicating a molecular weight of 1292 and a molecular formula of $C_{62}H_{100}O_{28}$. This was confirmed by the ESIMS (negative-ion mode) spectrum with m/z 1291 [M–H]$^-$. It is lower than **2** by 30 amu, suggesting the presence of a pentosyl group instead of an hexosyl one.

The HSQC spectrum of the sugar part showed cross-peaks at δ_H/δ_C 4.88 (d, J = 6.2 Hz)/105.0, 4.90 (d, J = 7.8 Hz)/102.9, 5.24 (d, J = 7.6 Hz)/107.0, 5.35 (d, J = 6.8 Hz)/103.7, 5.92 (br s)/103.4, and 6.16 (br s)/101.6, indicating the presence of six sugar units. Starting mainly by the TOCSY and ROESY spectra, they were identified as Ara, I and II, Xyl, I and II, Glc I, and Rha. According to the coupling constant of their anomeric protons, (d, J = 6.2 Hz) for Ara I-1 and (br s) for Ara II-1, the $^4C_1$ conformation was proposed for Ara I, and $^1C_4$ for Ara II [10]. The oligosaccharidic part of **2** and **3** were almost similar, except for the osisidic group linked at the Glc I-3 position. The ROESY correlation at δ_H/δ_H 5.92 (Ara II H-1)/4.44 (Glc I H-3) and the HMBC correlation at δ_H/δ_C 4.44 (Glc I H-3)/103.4 (Ara II C-1) suggested the α-L-arabinopyranosyl-(1 → 3)-β-D-glucopyranosyl sequence in **3** instead of β-D-glucopyranosyl-(1 → 3)-β-D-glucopyranosyl in **2**.

Thus, on the basis of the above results, the structure of compound **3** was established as 3-O-β-D-xylopyranosyl-(1 → 4)-[α-L-arabinopyranosyl-(1 → 3)]-β-D-glucopyranosyl-(1 → 4)-β-D-xylopyranosyl-(1 → 3)-α-L-rhamnopyranosyl-(1 → 2)-arabinopyranosyloleanolic acid (Fig. 1).

For compound **4**, the same molecular formula as **2** ($C_{63}H_{102}O_{29}$) was obtained according to its HR-ESIMS (positive-ion mode) spectrum which displayed a pseudo-molecular ion peak at m/z 1345.6409 [M + Na]$^+$, and its ESIMS (negative-ion mode) spectrum with m/z 1321 [M–H]$^-$.

The HSQC spectrum of the sugar part showed six cross-peaks at δ_H/δ_C 4.83 (d, J = 7.6 Hz)/106.1, 4.94/102.8, 5.29 (d, J = 7.6 Hz)/107.1, 5.49 (d, J = 6.0 Hz)/102.9, 5.52 (d, J = 8.0 Hz)/104.7 and 6.50 (br s)/101.6, indicating the presence of six sugar units. They were recognized as Xyl I, Xyl II, Xyl III, Glc I, Glc II and Rha (Table 2). All the NMR signals observed for **4** was similar to those of **2**, except for the pentosyl moiety linked to the C-3 of the aglycone which is Xyl I in **4** instead of Ara I in **2**. This was confirmed by the HMBC correlation at δ_H/δ_C 4.83 (Xyl I H-1)/88.3 (C-3), and by the ROESY correlation at δ_H/δ_H 4.83 (Xyl I H-1)/3.31 (dd, J = 12.4, 4.0 Hz, H-3). Hence, the structure of **4** was established as 3-O-β-D-xylopyranosyl-(1 → 4)-[β-D-glucopyranosyl-(1 → 3)]-β-D-glucopyranosyl-(1 → 4)-β-D-xylopyranosyl-(1 → 3)-α-L-rhamnopyranosyl-(1 → 2)-β-D-xylopyranosyloleanolic acid (Fig. 1).

The quasi-molecular ion peak [M + Na]$^+$ at m/z 1315.6306 observed in the HR-ESIMS (positive-ion mode) spectrum of compound **5**, suggested a molecular formula of $C_{62}H_{100}O_{28}$, and a molecular weight of 1292. This was in accordance with the ESIMS (negative-ion mode) spectrum with m/z 1291 [M–H]$^-$.

The HSQC spectrum of the sugar part showed six cross-peaks at δ_H/δ_C 4.82 (d, J = 7.6 Hz)/106.1, 4.86 (d, J = 7.6 Hz)/103.8, 4.97/103.2, 5.03 (d, J = 8.0 Hz)/105.1, 5.28 (d, J = 7.2 Hz)/107.1, and 6.50 (br s)/101.6, indicating the presence of six sugar units, Xyl I, Xyl II, Xyl III, Xyl IV, Glc I, and Rha (Table 2). The Xyl I moiety was shown to be attached at C-3 of the aglycone by observation of an HMBC correlation between δ_H 4.82 (Xyl H-1) and δ_C 88.5 (C-3), and a ROESY correlation between δ_H 4.82 (Xyl I H-1) and δ_H 3.30 (H-3). Moreover, HMBC correlations at δ_H/δ_C 4.86 (Xyl IV H-1)/76.1 (Xyl III C-4), 5.03 (Xyl III H-1)/80.5 (Glc I C-4), 4.97 (Glc I H-1)/77.6 (Xyl II C-4), 5.28 (Xyl II H-1)/83.1 (Rha C-3), and 6.50 (Rha H-1)/77.4 (Xyl I C-2), were used to establish the structure of the osidic chain as 3-O-β-D-xylopyranosyl-(1 → 4)-β-D-xylopyranosyl-(1 → 4)-β-D-glucopyranosyl-(1 → 4)-β-D-xylopyranosyl-(1 → 3)-α-L-rhamnopyranosyl-(1 → 2)-β-D-xylopyranosyl. This was ensured by the ROESY cross-peaks at δ_H/δ_H 4.86 (Xyl IV H-1)/4.22 (Xyl III H-4), 5.03 (Xyl III H-1)/4.21 (Glc I H-4), 4.97 (Glc I H-1)/4.26 (Xyl II H-4), 5.28 (Xyl II H-1)/4.72 (Rha H-3), and 6.50 (Rha H-1)/4.22 (Xyl I H-2). Accordingly, the structure of **5** was elucidated as 3-O-β-D-xylopyranosyl-(1 → 4)-β-D-xylopyranosyl-(1 → 4)-β-D-glucopyranosyl-(1 → 4)-β-D-xylopyranosyl-(1 → 3)-α-L-rhamnopyranosyl-(1 → 2)-β-D-xylopyranosyloleanolic acid (Fig. 1).

The HR-ESIMS (positive-ion mode) spectrum of compound **6** showed a pseudo-molecular ion peak HR-ESIMS (positive-ion mode) at m/z 1345.6409 [M + Na]$^+$, indicating a molecular weight of 1322 and a molecular formula of $C_{63}H_{102}O_{29}$.

Six sugar units were detected by HSQC correlations in the sugar region between protons at δ_H 4.69 (d, J = 6.0 Hz), 4.79 (d, J = 7.6 Hz), 5.14 (d, J = 6.9 Hz), 5.19 (d, J = 7.6 Hz), 6.00 (d, J = 7.3 Hz) and 6.33 (br s), and carbons at δ_C 104.8, 101.2, 102.2, 105.3, 92.1 and 100.1, respectively. The 2D NMR spectroscopic analyses enabled the full assignments of the chemical shifts of Xyl I, Xyl II, Xyl III, Glc I, Glc II and Rha (Tables 1 and 2). The 3-O-heterosidic linkage and the structure of the oligosaccharidic chain, the same as **7**, were identified using mainly the ROESY spectrum. The ROESY correlations showed long-range correlations at δ_H/δ_H 5.14 (Xyl III H-1)/4.31 (Glc I H-4), 4.79 (Glc I H-1)/4.14 (Xyl II H-4), 5.19 (Xyl II H-1)/4.63 (Rha H-3), 6.33 (Rha H-1)/4.09 (Xyl I H-2) and 4.69 (Xyl I H-1)/3.23 (H-3). The shielded chemical shifts at δ_C 92.1 (Glc II C-1) and at 177.0 (C-28), suggested an ester linkage of Glc II with C-28 of the aglycone, in accordance with the literature data [1]. These evidences led to the elucidation of **6** as 3-O-β-D-xylopyranosyl-(1 → 4)-β-D-glucopyranosyl-(1 → 4)-β-D-xylopyranosyl-(1 → 3)-α-L-rhamnopyranosyl-(1 → 2)-β-D-xylopyranosyloleanolic acid 28-O-β-D-glucopyranosyl ester (Fig. 1).

Compounds **1–3**, **6** and **7**, monodesmoside and bidesmoside saponins, were tested to evaluate their cytotoxic activity against a mouse colon cancer cell line (CT26), in concentrations ranging from 1 to 50 μM (Fig. 2). All the tested glycosides showed potent cytotoxicities, with IC$_{50}$ from 1.09 to 1.97 μM, comparing to 5-FU with an IC$_{50}$ of 11.7 μM (Table 3). First of all, to propose clear structure / activity relationships, oleanolic acid is important for the cytotoxicity. In the literature, a substitution for example by a primary alcoholic function at C-23, as hederagenin, seems to decrease the activity [1,11]. For the osidic part, the presence of the common sequences α-L-rhamnopyranosyl-(1 → 2)-β-D-xylopyranosyloleanolic or α-L-rhamnopyranosyl-(1 → 2)-α-L-arabinopyranosyloleanolic acid, have a role in the cytotoxicity [1,11], but in our study, we can propose more precisely the key sequence β-D-xylopyranosyl-(1 → 3)-α-L-rhamnopyranosyl-(1 → 2)-β-D-xylopyranosyloleanolic acid or β-D-xylopyranosyl-(1 → 3)-α-L-rhamnopyranosyl-(1 → 2)-α-L-arabinopyranosyloleanolic acid. Moreover, a linear oligosaccharidic chain linked at the C-3 position in **1** and **7**, instead of a branched one in **2** and **3**, seems to weakly decrease the activity. Compound **6** shows the more potent activity, even if its structure contains a linear oligosaccharidic chain, but it's the only one with an ester function
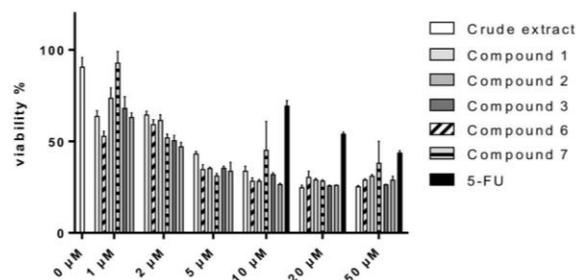
Fig. 2. Evaluation of the cytotoxic activity of compounds **1–3**, **6** and **7** against mouse colon cancer cells (CT26), in concentrations ranging from 1 to 50 μM. Fluorouracil (5-FU) was used as positive control.

Table 3
IC_{50} of compounds **1–3**, **6** and **7** against mouse colon cancer cells (CT26).

Compounds	IC_{50} (μM)
1	1.97
2	1.22
3	1.48
6	1.09
7	1.87
5-FU	11.7

at the position 28. More studies are necessary to propose strong structure / activity relationships.

4. Conclusion

Seven oleanolic acid glycosides (**1–7**) were obtained from an aqueous-ethanolic extract of the roots of *Weigela* x "Bristol Ruby" by several solid/liquid chromatographic methods. Compounds **1–6** were previously undescribed and **7** was a known one. Compounds **1–3**, **6** and **7** exert a potent cytotoxicity against a mouse colon cancer cell line CT26, with IC_{50} from 1.09 to 1.97 μM. A key sequence was proposed to complete previous structure / activity relationships as β-D-xylopyranosyl-(1 → 3)-α-L-rhamnopyranosyl-(1 → 2)-β-D-xylopyranosyloleanolic acid or β-D-xylopyranosyl-(1 → 3)-α-L-rhamnopyranosyl-(1 → 2)-α-L-arabinopyranosyloleanolic acid.

Appendix A. Supplementary data

Supplementary data to this article can be found online at https://doi.org/10.1016/j.fitote.2019.104242.

References

[1] A. Rezgui, A.C. Mitaine-Offer, T. Miyamoto, C. Tanaka, S. Delemasure, P. Dutartre, M.A. Lacaille-Dubois, Oleanolic acid and hederagenin glycosides from *Weigela stelzneri*, Phytochemistry 123 (2016) 40–47.
[2] A.-S. Champy-Tixier, A.-C. Mitaine-Offer, F. Real Fernández, T. Miyamoto, C. Tanaka, A.-M. Papini, M.-A. Lacaille-Dubois, Oleanane-type glycosides from the roots of *Weigela florida* "rumba" and evaluation of their antibody recognition, Fitoterapia 128 (2018) 198–203.
[3] N. Andriamisaina, A.-C. Mitaine-Offer, B. Pruvot, J. Chluba, T. Miyamoto, C. Tanaka, M.-A. Lacaille-Dubois, Phytochemistry of *Weigela* x "kosteriana variegata"(Caprifoliaceae), Nat. Prod. Commun. 13 (2018) 403–406.
[4] T. Murayama, A. Kasahara, Y. Shiono, M. Ikeda, Structure elucidation of a triterpene glycoside isolated from *Weigela hortensis*, Nat. Med. 57 (2003) 181–184.
[5] Y.-M. Won, Z.-K. Seong, J.-L. Kim, H.-S. Kim, H.-H. Song, D.-Y. Kim, J.-H. Kim, S.-R. Oh, H.-W. Cho, J.-H. Cho, H.-K. Lee, Triterpene glycosides with stimulatory activity on melanogenesis from the aerial parts of *Weigela subsessilis*, Arch. Pharmacal. Res. 38 (2015) 1541–1551.
[6] The Angiosperm Phylogeny Group, An update of the angiosperm phylogeny group classification for the orders and families of flowering plants: APG III, Bot. J. Linn. Soc. 161 (2009) 105–121.
[7] Friends of the Botanical Gardens, http://www.fobssheffield.co.uk/weigelas.html, (2019).
[8] J. Tian, F.E. Wu, M.H. Qiu, R.L. Nie, Triterpenoid saponins from *Pterocephalus hookeri*, Phytochemistry 32 (1993) 1535–1538.
[9] S. Hara, H. Okabe, K. Mihashi, Gas-liquid chromatographic separation of aldose enantiomers as trimethylsilyl ethers of methyl 2-(polyhydroxyalkyl)thiazolidine-4(R)-carboxylates, Chem. Pharm. Bull. 35 (1987) 501–506.
[10] H. Ishii, I. Kitagawa, K. Matsushita, K. Shirakawa, K. Tori, T. Tozyo, M. Yoshikawa, Y. Yoshimura, The configuration and conformation of the arabinose moiety in platycodins, saponins isolated from *Platycodon grandiflorum*, and mi-saponins from *Madhuca longifolia* based on Carbon-13 and Hydrogen-1 NMR spectroscopic evidence: the total structures of the saponins, Tetrahedron Lett. 22 (1981) 1529–1532.
[11] S.-C. Bang, J.-H. Lee, G.-Y. Song, D.-H. Kim, M.-Y. Yoon, B.-Z. Ahn, Antitumor activity of *Pulsatilla koreana* saponins and their structure-activity relationship, Chem. Pharm. Bull. 53 (2005) 1451–1454.

2.2. Phytochemical study of *Weigela florida* "Pink Poppet"

Phytochemical investigation on aqueous-ethanolic extract of the roots and aerial parts of *Weigela florida* "Pink Poppet" led to the isolation of one previously undescribed triterpenoid saponin (**8**) along with three known compounds (**9-11**).

2.2.1. Isolation and purification

The dried and powdered of roots (26.5 g) and aerial parts (29.0 g) of *Weigela florida* "Pink Poppet" were submitted to microwaves three times with the solvent $EtOH/H_2O$ (200 W, 60°C, 45 min, 75/35, 400 mL each), separately. After evaporation of the solvent, an aliquot of the roots extract (1.7 g) was dissolved in water and partitioned with *n*-BuOH saturated with H_2O (1/1, 200 mL x 3). The dried *n*-BuOH phase (142.3 mg) was submitted to MPLC on silica gel 60 ($CHCl_3/MeOH/H_2O$ 70/30/5) affording compound **8** (4.0 mg). The remaining residue of roots extract (1.5 g) was presented to VLC (RP-18 silica gel, H_2O, $EtOH/H_2O$ 50/50, EtOH) yielding 3 fractions (R1-R3). Fractions R2 (85.2 mg), rich in saponins, was fractionated by successive MPLC on silica gel 60 ($CHCl_3/MeOH/H_2O$ 75/25/3; 70/30/5; 60/32/7) resulting compounds **9** (3.9 mg) and **10** (2.0 mg). Then 7.7 g crude of extract of aerial parts was subjected to VLC (RP-18 silica gel, H_2O, $EtOH/H_2O$ 50:50, EtOH) to give 3 fractions (AP1-AP3). Fraction AP2 was submitted to a MPLC on silica gel 60 ($CHCl3/MeOH/H_2O$ 75/25/3) affording compound **11** (8.5 mg).
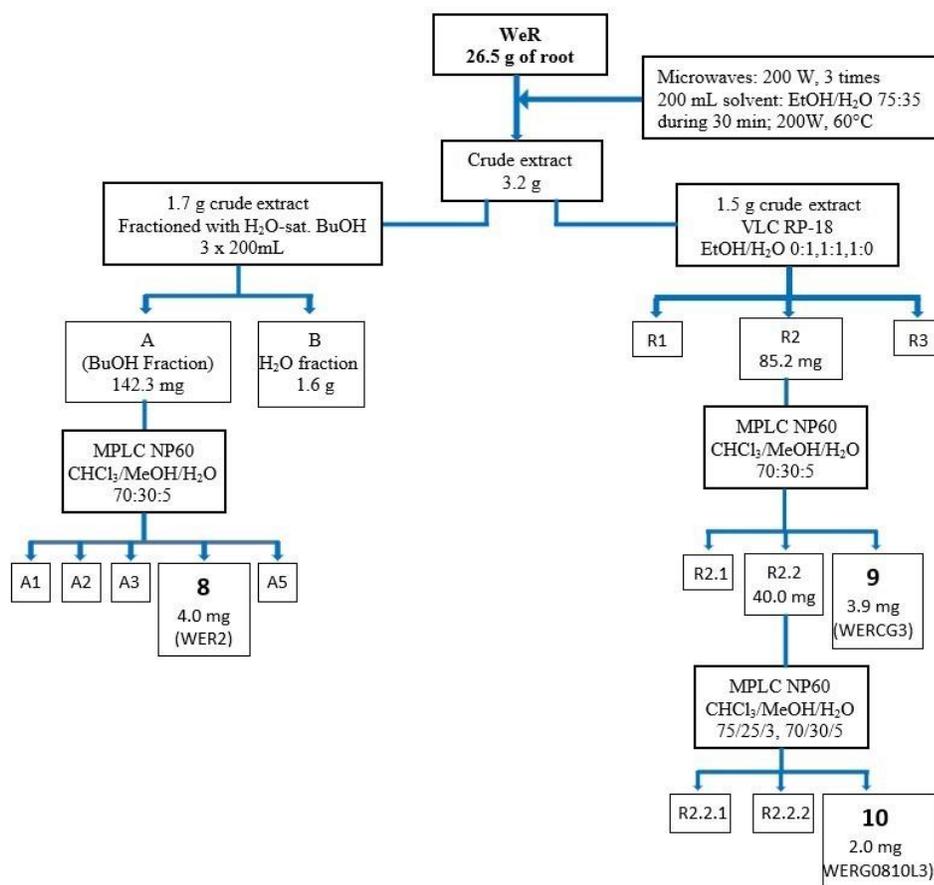
Figure 62. Purification of compounds in roots of *Weigela florida* "Pink Poppet"
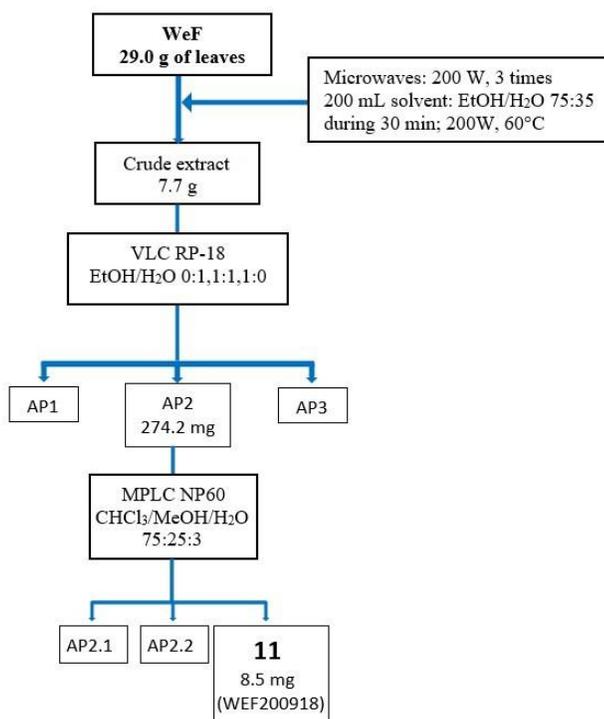
Figure 63. Purification of compounds in aerial parts of *Weigela florida* "Pink Poppet"

78

2.2.2. Structural determination of isolated saponins

Compounds 8-11 were isolated as white amorphous powders and assigned as monodesmosidic structures by means of the 1D and 2D spectra (^{1}H and ^{13}C NMR, ^{1}H-^{1}H COSY, TOCSY, ROESY, HSQC and HMBC).

a. Compound 8 (WER2)

Mass spectrometry

The HR-ESIMS (positive-ion mode) spectrum of compound **8** showed a pseudo-molecular ion peak [M+Na]$^+$ at 1315.6029 *m/z*, indicating a molecular weight of 1292 and a molecular formula of $C_{62}H_{100}O_{28}$.

NMR spectroscopy

Structure of aglycon

The analysis of the NMR spectra of compound **8** showed that the aglycon was almost identified to those of compounds isolated from *W*. x "Bristol Ruby". The correlations of HSQC, HMBC and ROESY allowed to identify the genin of compound **8** as the oleanolic acid which was characterised to compounds **1, 2, 3, 4** and **5** (**Table 3** and **5**). The downfield shift at δ_C 88.5 and upfield shift at δ_C 180.0, due to the glycosylation shift, suggested that compound **8** was a monodesmosidic glycoside.

Structure of sugar moieties

The monosaccharides were identified by acid hydrolysis and extensive 2D NMR analysis as α-L-arabinopyranosyl (Ara), α-L-rhamnopyranosyl (Rha), β-D-xylopyranosyl (Xyl) and β-D-glucopyranosyl (Glc) in the case of **8**, **11** and Rha, Xyl and Glc in the case of **9, 10**. The absolute configurations of the sugars were determined to be D for glucose (Glc), and xylose (Xyl), and L for arabinose (Ara) and rhamnose (Rha), by GC analysis (see Section 1.3.4). The relatively large $^3J_{\text{H-1, H-2}}$ values of the Glc, Xyl, and Ara (5.0-8.2 Hz) indicated a ß anomeric orientation for Glc and Xyl, and an α anomeric orientation for Ara. The large $^1J_{\text{H-1,C-1}}$ values of the Rha (165-168 Hz), confirmed that the anomeric protons were equatorial (α-pyranoid anomeric form).

The sugar parts of **8** contains six residues as evidenced by ^{1}H spectrum which displayed six anomeric protons at δ_H 4.80 (d, J = 4.7 Hz), 4.91 (d, J = 7.6 Hz), 5.28 (d, J = 7.0 Hz), 5.31 (d, J = 7.6 Hz), 5.85 (d, J = 4.6 Hz) and 6.48 (br s) which gave correlation, in the HSQC spectrum, with six anomeric carbon signals at δ_C 105.8, 102.5, 103.4, 106.4, 103.2 and 101.2, respectively. Starting mainly the TOCY and ROESY spectra, the sugar moieties of compound **8** was identified as:

- 1 α-L-arabinopyranosyl Ara-1 at δ_H 5.85 (d, J = 4.6 Hz),

- 1 α-L-rhamnopyranosyl Rha-1 at δ_H 6.48 (br s),

- 1 β-D-glucopyranosyl Glc-1 at δ_H 4.91 (d, J = 7.6 Hz),

- 3 β-D-xylopyranosyl Xyl I-1 at δ_H 4.80 (d, J = 4.7 Hz), Xyl II-1 at δ_H 5.31 (d, J = 7.6 Hz) and Xyl III-1 at δ_H 4.91 (d, J = 7.6 Hz).

The sequence of the oligosaccharide was established by analysing the HMBC and ROESY spectra:

- The HMBC correlation between δ_H 4.80 (Xyl I H-1) and δ_C 88.5 (C-3) and in ROESY at δ_H 4.80 (Xyl I H-1) and δ_H 3.35 (H-3) proved that Xyl I was attached to the C-3 position of the aglycon (Fig.64).

- The HMBC correlation between δ_H 4.21 (Xyl I H-2) and δ_C 101.2 (Rha C-1) and in ROESY at δ_H 4.21 (Xyl I H-2) and δ_H 6.48 (Rha H-1) proved that Rha was attached to the Xyl I at C-2.

- The HMBC correlation between δ_H 5.31 (Xyl II H-1) and δ_C 82.1 (Rha C-3) and in ROESY at δ_H 5.31 (Xyl II H-1) and δ_H 4.75 (Rha H-3) proved that Xyl II was attached to the Rha at C-3.

- The HMBC correlation between δ_H 4.91 (Glc H-1) and δ_C 77.2 (Xyl II C-4) and in ROESY at δ_H 4.91 (Glc H-1) and δ_H 4.26 (Xyl II H-4) proved that Glc was attached to the Xyl II at C-4.

- The HMBC correlation between δ_H 5.85 (Ara H-1) and δ_C 79.8 (Glc C-3) and in ROESY at δ_H 5.85 (Ara H-1) and δ_H 4.43 (Glc H-3) proved that Ara was attached to the Glc at C-3.

- The HMBC correlation between δ_H 5.28 (Xyl III H-1) and δ_C 73.8 (Glc C-4) and in ROESY at δ_H 5.28 (Xyl III H-1) and δ_H 4.42 (Glc H-4) proved that Xyl III was attached to the Glc at C-4.

Conclusion

Based on the above results, the structure of **8** was elucidated as 3-*O*-β-D-xylopyranosyl-(1→4)-[α-L-arabinopyranosyl-(1→3)]-β-D-glucopyranosyl-(1→4)-β-D-xylopyranosyl-(1→3)-α-L-rhamnopyranosyl-(1→2)-xylopyranosyloleanolic acid.
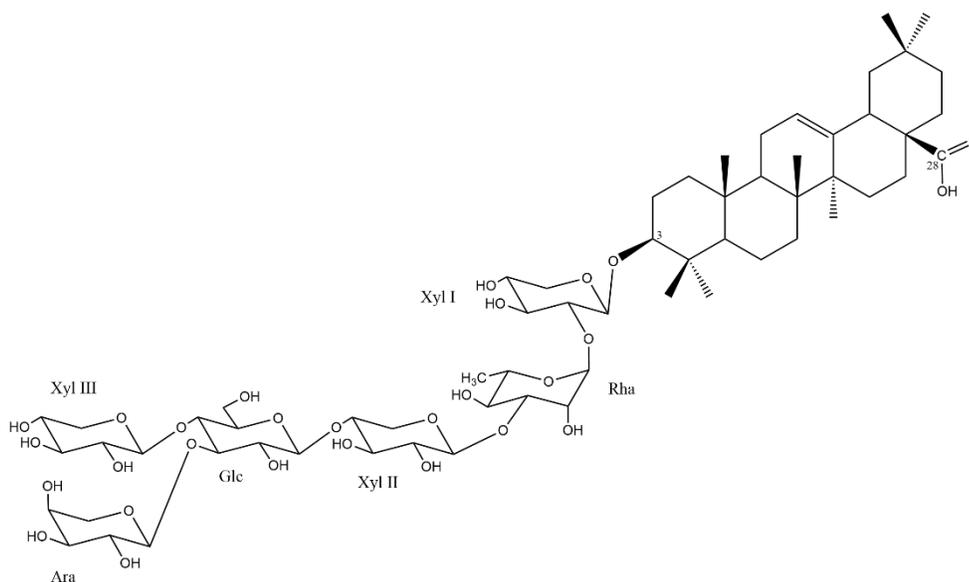
Figure 64. Structure of compound **8**
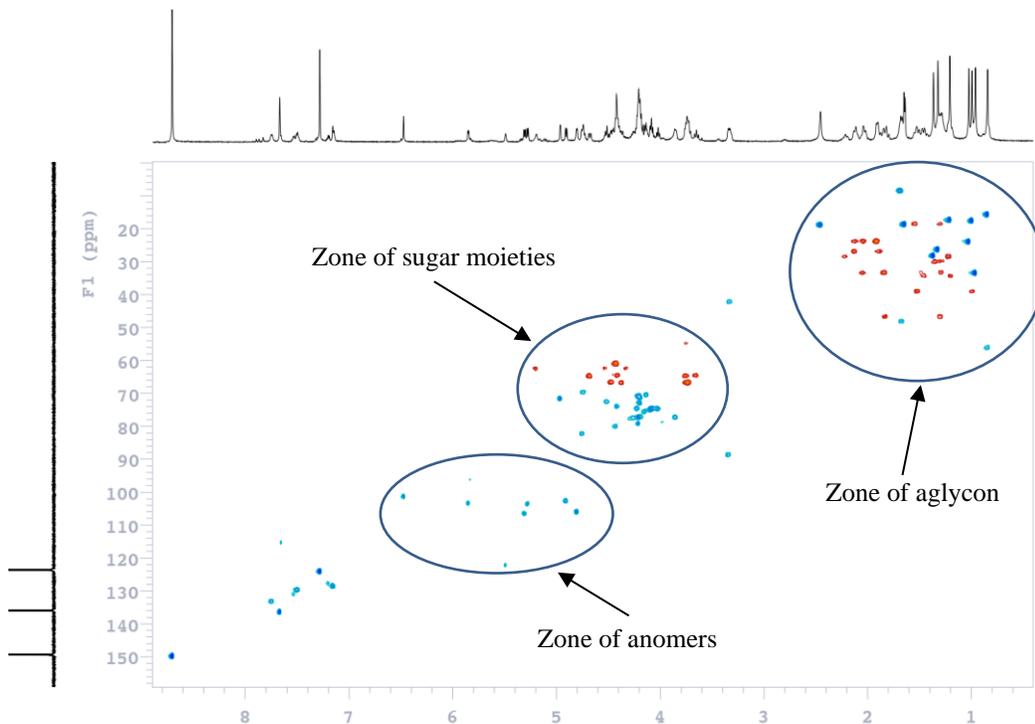
Figure 65. HSQC spectrum of compound **8**

Figure 66. HSQC spectrum of sugar anomers of compound **8**

Figure 67. HMBC spectrum of sugar moieties of compound **8**

Figure 68. ROESY spectrum of sugar moieties of compound **8**

Figure 69. Mass spectrum of compound **8**

b. Compound 9 (WERCG3)

Figure 70. Structure of compound **9**

For compound 9, the HR-ESIMS (positive-ion mode) spectrum showed a pseudo-molecular ion peak [M+Na]$^+$ at *m/z* 1345.6367, indicating a molecular weight of 1322 and a molecular

formula of $C_{63}H_{102}O_{29}$. This compound was isolated from the roots of *Weigela* x "Bristol Ruby" identified as compound **4**.

c. Compound 10 (WERG0810L3)

The HR-ESIMS (positive-ion mode) spectrum of **10** showed a pseudo-molecular ion peak [M+Na]$^+$ at *m/z* 1315.6274, indicating a molecular weight of 1292 and a molecular formula of $C_{62}H_{100}O_{28}$. This compound was isolated from the roots of *Weigela* x "Bristol Ruby" identified as compound **5**.
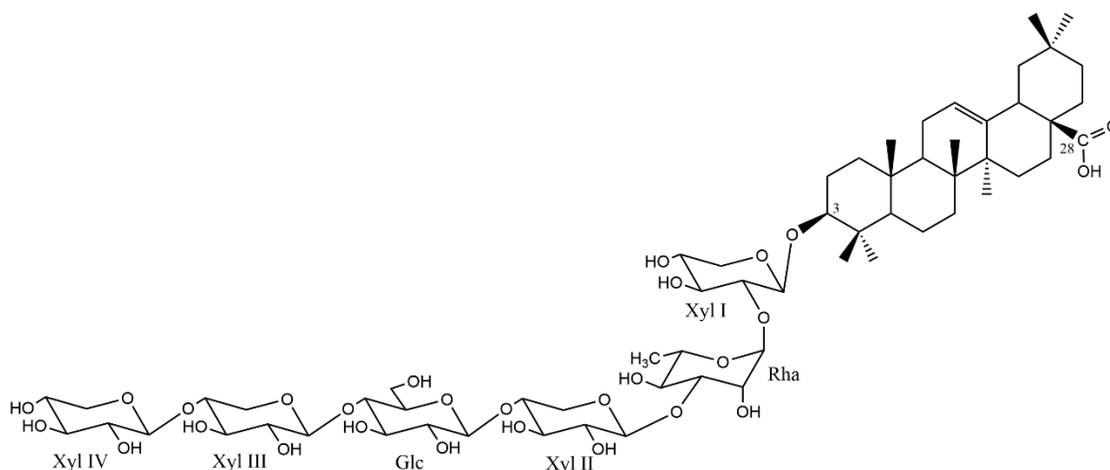
Figure 71. Structure of compound **10**

d. Compound 11 (WEF200918)

For compound **11**, the HR-ESIMS (positive-ion mode) spectrum showed a pseudo-molecular ion peak [M+Na]$^+$ at *m/z* 1067.5389, indicating a molecular weight of 1044 and a molecular formula of $C_{52}H_{84}O_{21}$. By working on literature data, the structure of **11** was identified as 3-*O*-α-L-arabinopyranosylhederagenin 28-*O*-α-L-rhamnopyranosyl-(1→2)-[β-D-xylopyranosyl-(1→6)]-β-D-glucopyranosyl ester. This saponin was isolated from the aerial parts of *Lonicera japonica* (Ho Son et al., 1994).
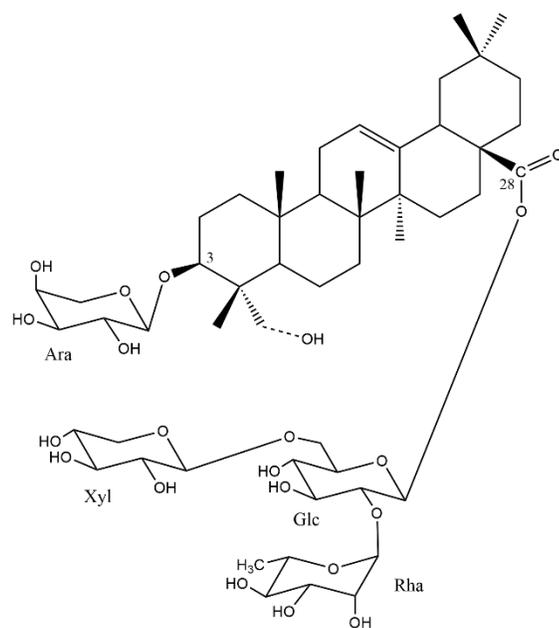
Figure 72. Structure of compound **11**

Table 5. ^{13}C and ^{1}H NMR spectroscopic data of the aglycon and sugar moieties of **8** in pyridine-d_5 (δ in ppm, J in Hz)

	Aglycon			Sugar moieties	
	δ_C	δ_H		δ_C	δ_H
1	38.5	1.53 m, 0.98 m	Ara-1	103.2	5.85 d (4.6)
2	26.5	1.88 m, 2.13 m	2	72.8	4.19
3	88.5	3.35	3	74.6	4.22
4	39.4	–	4	70.2	4.14
5	56.0	0.86 overlapped	5	66.4	3.74, 4.48
6	18.5	1.21, 1.55 m	Rha-1	101.2	6.48 br s
7	33.0	1.30, 1.39	2	71.4	4.96 br s
8	39.5	–	3	82.1	4.75 dd (9.3, 2.8)
9	47.9	1.67 dd (15.8, 8.8)	4	72.5	4.51 dd (9.3, 9.3)
10	37.0	–	5	69.5	4.73 dq (9.3, 5.2)
11	23.6	1.92, 2.10	6	18.5	1.65 d (5.2)
12	122.0	5.49 br t (3.6)	Xyl I-1	105.8	4.80 d (4.7)
13	145.0	–	2	77.1	4.21
14	42.0	–	3	77.1	4.18
15	28.3	1.37, 2.21	4	70.5	4.19
16	23.6	1.92 m, 2.20	5	64.6	3.75, 4.68
17	47.9	–	Xyl II-1	106.4	5.31 d (7.6)
18	42.1	3.34	2	74.6	4.09
19	46.5	1.30, 1.82	3	75.5	4.16
20	30.8	–	4	77.2	4.26
21	34.2	1.20, 1.46 m	5	64.4	3.66 t (10.5), 4.41
22	33.0	1.82 m, 2.05 m	Xyl III-1	103.4	5.28 d (7.0)
23	27.9	1.37 s	2	74.7	4.10
24	17.1	1.21 s	3	79.1	4.21

25	15.4	0.85 s	4	70.9	4.21
26	17.3	0.99 s	5	66.5	3.75, 4.36
27	26.0	1.32 s	Glc I-1	102.5	4.91 d (7.6)
28	180.0	–	2	74.6	4.02
29	33.2	0.96 s	3	79.8	4.43
30	23.7	1.02 s	4	73.8	4.42
			5	77.1	3.86 m
			6	60.8	4.42, 4.43

Overlapped proton signals are reported without designated multiplicity.

2.3. Phytochemical study of *Weigela florida* "Jean's Gold"

Phytochemical investigation on aqueous-ethanolic extract of the aerial parts of *Weigela florida* "Jean's Gold" led to the isolation of two previously undescribed triterpenoid saponins (**12, 13**) along with four known compounds (**14-17**).

2.3.1. Isolation and purification

The dried and powdered of aerial parts of *Weigela florida* "Jean's Gold" (56.8 g) were submitted to microwaves three times with the solvent $EtOH/H_2O$ (200 W, 60°C, 45 min, 75/35 400 mL each). After filtration and evaporation, 21.5 g of crude of extract were obtained. An aliquot (17.5 g) was fractionated using successive VLC on silica gel 60, ($CHCl_3/MeOH/H_2O$ 60/32/7), and on RP-18 silica gel (H_2O, $EtOH/H_2O$ 50/50, EtOH), yielding 4 fractions (A1-A4). Fraction A3 (309.1 mg) was submitted to MPLC on silica gel 60 ($CHCl_3/MeOH/H_2O$ 70/30/5) yielding two pure compounds, **13** (3.2 mg) and **15** (2.8 mg) among the 5 fractions obtained (A3.1 to A3.5). The remaining extract (4.0 g) was fractionated by flash chromatography ($CHCl_3/MeOH/H_2O$ 60/32/7) to give 4 fractions. The fractions rich in saponins were further separated using MPLC on silica gel 60 ($CHCl_3/MeOH/H_2O$ 80/20/2, 75/25/3) yielding compound **12** (3.2 mg) and compound **14** (8.0 mg) which was previously obtained from the leaves extract of *W. florida* "Pink Poppet". The remaining fractions were combined and chromatographed again on silica gel

60 by MPLC (CHCl$_3$/MeOH/H$_2$O 70/30/5), yielding compound **16** (4.4 mg), compound **17** (8.6 mg) and compound **14** (2.8 mg).
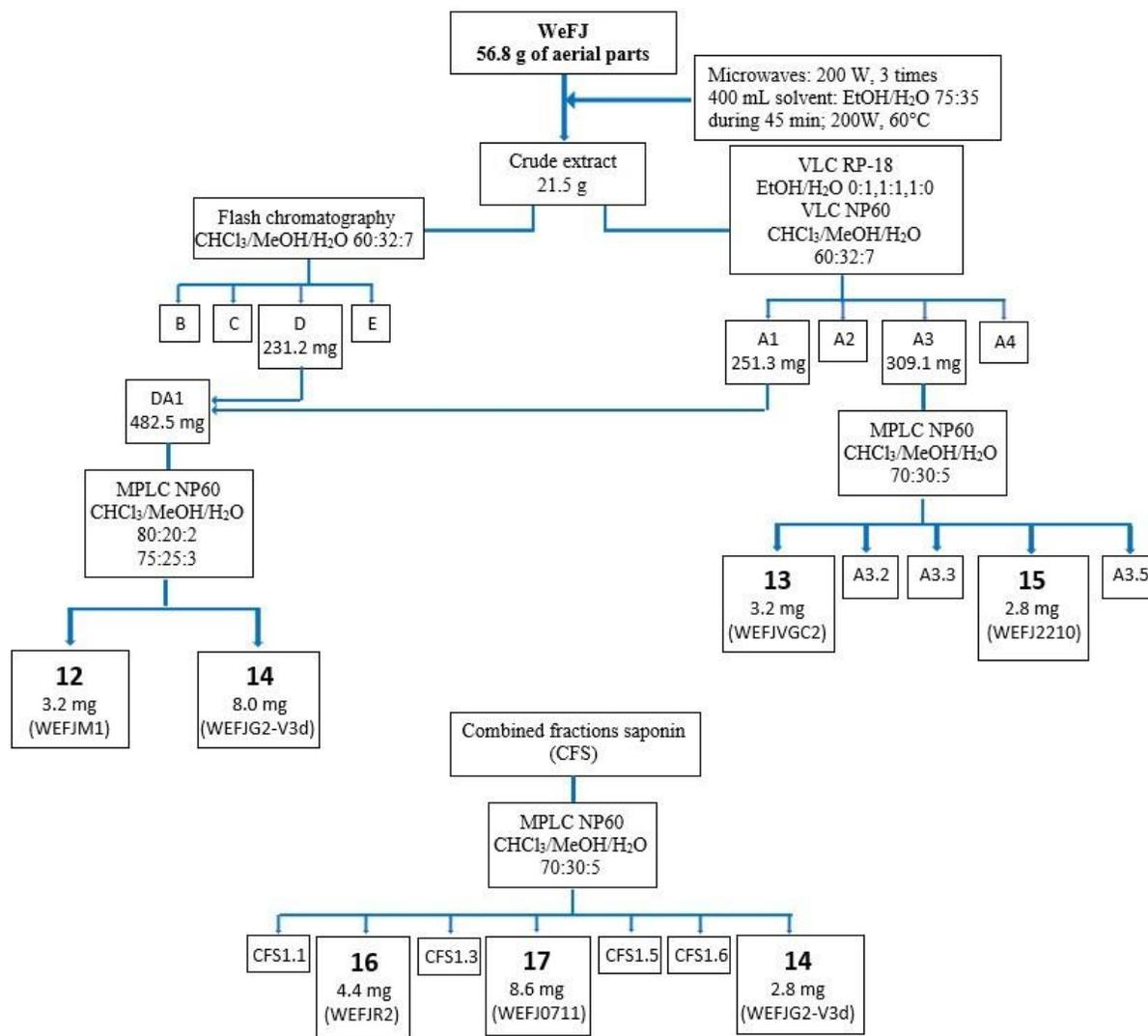
Figure 73. Purification of compounds in leaves of *W. florida* "Jean's Gold"

2.3.2. Structural determination of isolated saponins

All compounds **12-17** were isolated as white amorphous powders and assigned as bidesmosidic structures by means of the 1D and 2D spectra (^{1}H and ^{13}C NMR, ^{1}H-^{1}H COSY, TOCSY, ROESY, HSQC and HMBC).

a. Compound 12 (WEFJM1)

Mass spectrometry

The HR-ESIMS (positive-ion mode) spectrum of compound **12** showed a pseudo-molecular ion peak HR-ESIMS (positive-ion mode) at *m/z* 1051.5427 $[M+Na]^+$, indicating a molecular weight of 1028 and a molecular formula of $C_{52}H_{84}O_{20}$.

NMR spectroscopy

Structure of aglycon

The structure of aglycon was identified by analysing spectra NMR ^1H, ^{13}C, HSQC and HMBC. In spectra of NMR ^1H and ^{13}C, characteristic signals of oleanolic acid were showed:

- 7 methyl groups with singlet signals at δ_H 1.15, 0.87, 0.85, 1.02, 1.21, 0.83 and 0.80 confirmed the presence of triterpene.

- 1 olefinic proton at δ_H 5.40 (br t, $J = 3.6$ Hz) corresponds to proton H-12.

The ^{13}C NMR spectrum showed:

- 5 tertiary carbons (CH), 10 secondary carbons (CH_2), 7 primary carbons (CH_3) and 8 quaternary carbons (C).

- 2 signals at δ_C 124.1 and 145.4 correspond to the double bond Δ^{12}.

The ^1H and ^{13}C NMR signals of the aglycon assigned from the 2D NMR spectra, were in good agreement with those of oleanolic acid commonly encountered in the *Weigela* genus (Andriamisaina et al., 2018; Champy-Tixier et al., 2018; Rezgui et al., 2016). The observed downfield shift at δ_C 90.0 for C-3 and upfield shift at δ_C 178.0 for C-28, due to the glycosylation shift, suggested that compound **12** was a bidesmosidic glycoside.

Structure of sugar moieties

The monosaccharides were identified by acid hydrolysis and extensive 2D NMR analysis as α-L-arabinopyranosyl (Ara), α-L-rhamnopyranosyl (Rha), β-D-xylopyranosyl (Xyl) and β-D-glucopyranosyl (Glc) in the case of **12-14, 17**, Rha, Xyl and Glc in the case of **15** and Ara, Rha and Ara in the case of **16**. The absolute configurations of the sugars were determined to be D for glucose (Glc), and xylose (Xyl), and L for arabinose (Ara) and rhamnose (Rha), by GC analysis (see Section 1.3.4). The relatively large $^3J_{H-1, H-2}$ values of

the Glc, Xyl, and Ara (5.0-8.2 Hz) indicated a ß anomeric orientation for Glc and Xyl, and an α anomeric orientation for Ara. The large $^1J_{\text{H-1,C-1}}$ values of the Rha (165-168 Hz), confirmed that the anomeric protons were equatorial (α-pyranoid anomeric form).

The sugar part of **12** in the HSQC spectrum corresponding to the osidic chain showed cross-peaks at δ_H/δ_C 4.73 (d, J = 6.4 Hz)/108.4, 4.79 (d, J = 7.0 Hz)/106.6, 6.02 (d, J = 7.6 Hz)/96.0 and 6.35 (br s)/102.6, indicating the presence of four sugar units which identified as:

- 1 α-L-arabinopyranosyl Ara-1 at δ_H 4.73 (d, J = 6.4 Hz),

- 1 α-L-rhamnopyranosyl Rha-1 at δ_H 6.39 (br s),

- 1 β-D-glucopyranosyl Glc-1 at δ_H 6.02 (d, J = 7.6 Hz),

- 1 β-D-xylopyranosyl Xyl-1 at δ_H 4.79 (d, J = 7.0 Hz).

The sequence of the oligosaccharide was established by analysing the HMBC and ROESY spectra:

- The HMBC correlation between δ_H 4.73 (Ara H-1) and δ_C 90.0 (C-3) and in ROESY at δ_H 4.73 (Ara H-1) and δ_H 3.25 (H-3) proved that Ara was attached to the C-3 position of the aglycon (Fig.74).

- The shielded chemical shift at δ_C 96.0 (Glc C-1) and the shielded at δ_C 178.0 (C-28) suggested an ester linkage of Glc with C-28 of the aglycon.

- The HMBC correlation between δ_H 4.29 (Glc H-2) and δ_C 102.6 (Rha C-1) and in ROESY at δ_H 4.29 (Glc H-2) and δ_H 6.39 (Rha H-1) proved that Rha was attached to the Glc at C-2.

- The HMBC correlation between δ_H 4.79 (Xyl H-1) and δ_C 70.1 (Glc C-6) and in ROESY at δ_H 4.79 (Xyl H-1) and δ_H 4.19 (Glc H-6) proved that Xyl was attached to the Glc at C-6.

Conclusion

All the evidences above led to the elucidation of **12** as 3-*O*-α-L-arabinopyranosyloleanolic acid 28-*O*-β-D-xylopyranosyl-(1→6)-[α-L-rhamnopyranosyl-(1→2)]-β-D-glucopyranosyl ester.

Figure 74. Structure of compound **12**

Figure 75. HSQC spectrum of compound **12**

Figure 76. HSQC spectrum of sugar anomers of compound **12**

Figure 77. HMBC spectrum of sugar moieties of compound **12**

Figure 78. ROESY spectrum of sugar moieties of compound **12**

Figure 79. Mass spectrum of compound **12**

b. Compound 13 (WEFJVGC2)

Mass spectrometry

Compound **13**, the molecular formula of $C_{58}H_{94}O_{25}$, and thus a molecular weight of 1190, was obtained according to its HR-ESIMS (positive-ion mode) which showed a pseudo-molecular ion peak at *m/z* 1213.6004 $[M + Na]^+$.

NMR spectroscopy

Structure of aglycon

The analysis of the NMR spectra of compound **13** showed that the aglycon was almost identified to those of compound **12**. The correlations of HSQC, HMBC and ROESY allowed to identify the genin of compound **13** as the oleanolic acid which was characterised to compound **12** (**Table 6**).

Structure of sugar moieties

The molecular weight of compound **13** differs from **12** by only 162 amu, corresponding to a supplementary hexosyl group. The HSQC spectrum of sugar part of **7** showed five cross-peaks at δ_H/δ_C 4.78 (d, *J* = 7.6 Hz)/106.4, 4.87 (d, *J* = 5.8 Hz)/106.0, 5.13 (d, *J* = 7.6 Hz)/106.5, 6.00 (d, *J* = 8.2 Hz)/ 96.0 and 6.35 (br s*)*/102.6, indicating the presence of five sugar units. After analysing the spectre of HSQC, HMBC, COSY, TOCSY and ROESY, the sugar moieties of compound **13** was characterised as:

- 1 α-L-arabinopyranosyl Ara-1 at δ_H 4.87 (d, *J* = 5.8 Hz),

- 1 α-L-rhamnopyranosyl Rha-1 at δ_H 6.35 (br s),

- 2 β-D-glucopyranosyl Glc I-1 at δ_H 5.13 (d, *J* = 7.6 Hz) and Glc II-1 at δ_H 6.00 (d, *J* = 8.2 Hz),

- 1 β-D-xylopyranosyl Xyl-1 at δ_H 4.78 (d, *J* = 7.6 Hz).

The sequence of the oligosaccharide was established by analysing the HMBC and ROESY spectra:

- The HMBC correlation between δ_H 4.87 (Ara H-1) and δ_C 90.5 (C-3) and in ROESY at δ_H 4.87 (Ara H-1) and δ_H 3.12 (H-3) proved that Ara was attached to the C-3 position of the aglycon (Fig.80).

- The HMBC correlation between δ_H 4.54 (Ara H-2) and δ_C 106.5 (Glc I C-1) and in ROESY at δ_H 4.54 (Ara H-2) and δ_H 5.13 (Glc I H-1) proved that Glc I was attached to the Ara at C-2.

- The shielded chemical shift at δ_C 96.0 (Glc II C-1) and the shielded at δ_C 178.1 (C-28) suggested an ester linkage of Glc II with C-28 of the aglycon.

- The HMBC correlation between δ_H 4.28 (Glc II H-2) and δ_C 102.6 (Rha C-1) and in ROESY at δ_H 4.28 (Glc II H-2) and δ_H 6.35 (Rha H-1) proved that Rha was attached to the Glc II at C-2.

- The HMBC correlation between δ_H 4.78 (Xyl H-1) and δ_C 70.0 (Glc II C-6) and in ROESY at δ_H 4.78 (Xyl H-1) and δ_H 4.19 (Glc II H-6) proved that Xyl was attached to the Glc II at C-6.

Conclusion

Based on the above evidences, the structure of compound **13** was elucidated as 3-*O*-β-D-glucopyranosyl-(1→2)-α-L-arabinopyranosyloleanolic acid 28-*O*-β-D-xylopyranosyl-(1→6)-[α-L-rhamnopyranosyl-(1→2)]-β-D-glucopyranosyl ester.
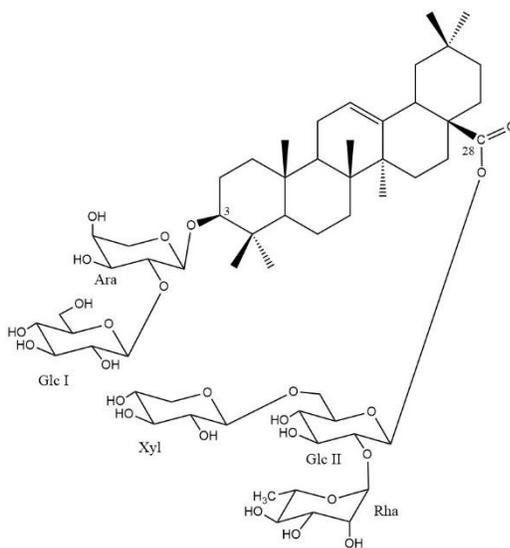
Figure 80. Structure of compound **13**
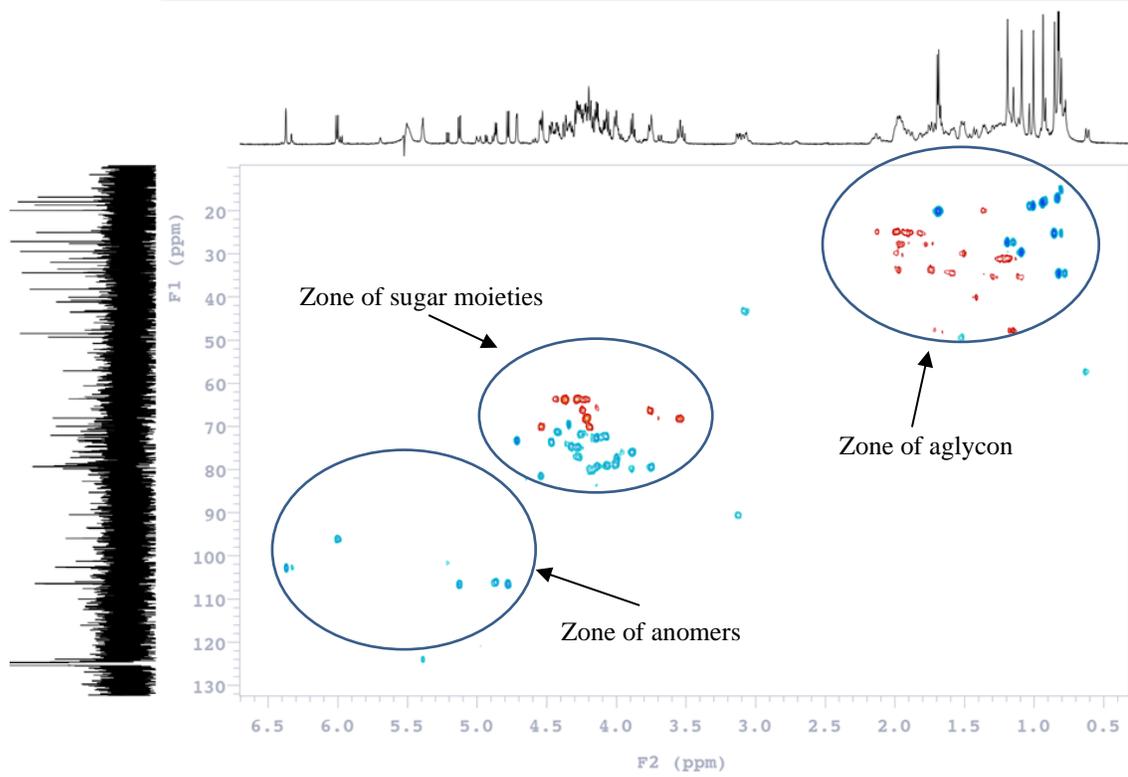
Figure 81. HSQC spectrum of compound **13**
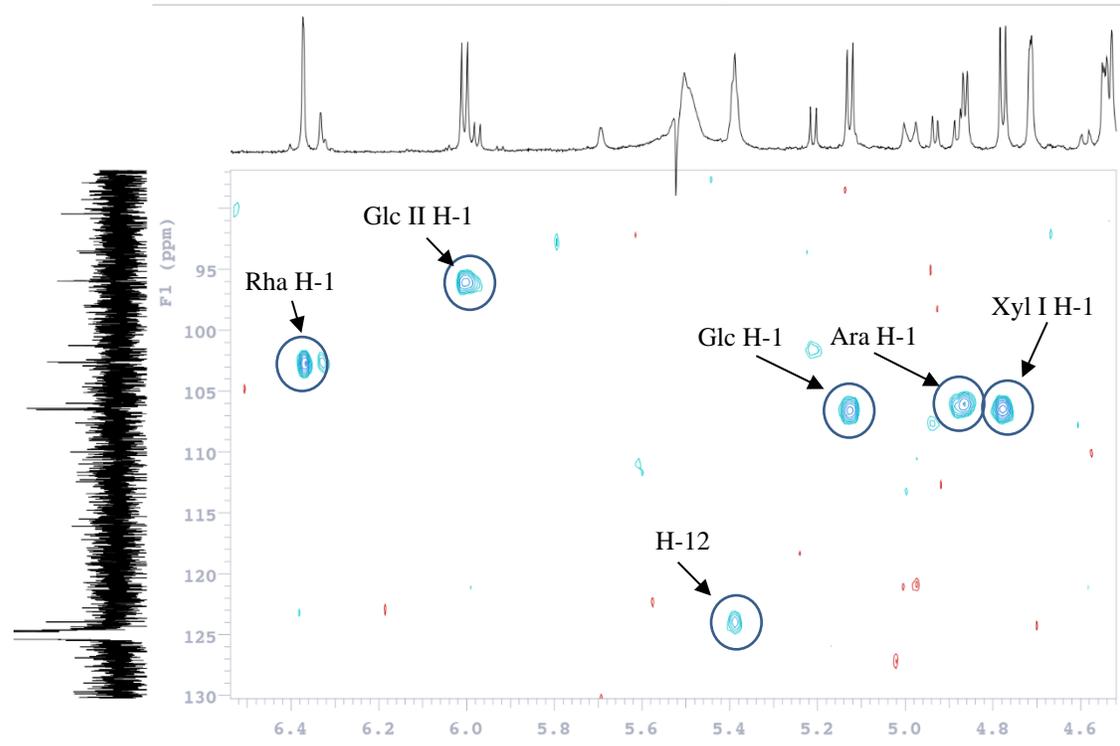
Figure 82. HSQC spectrum of sugar anomers of compound **13**

97
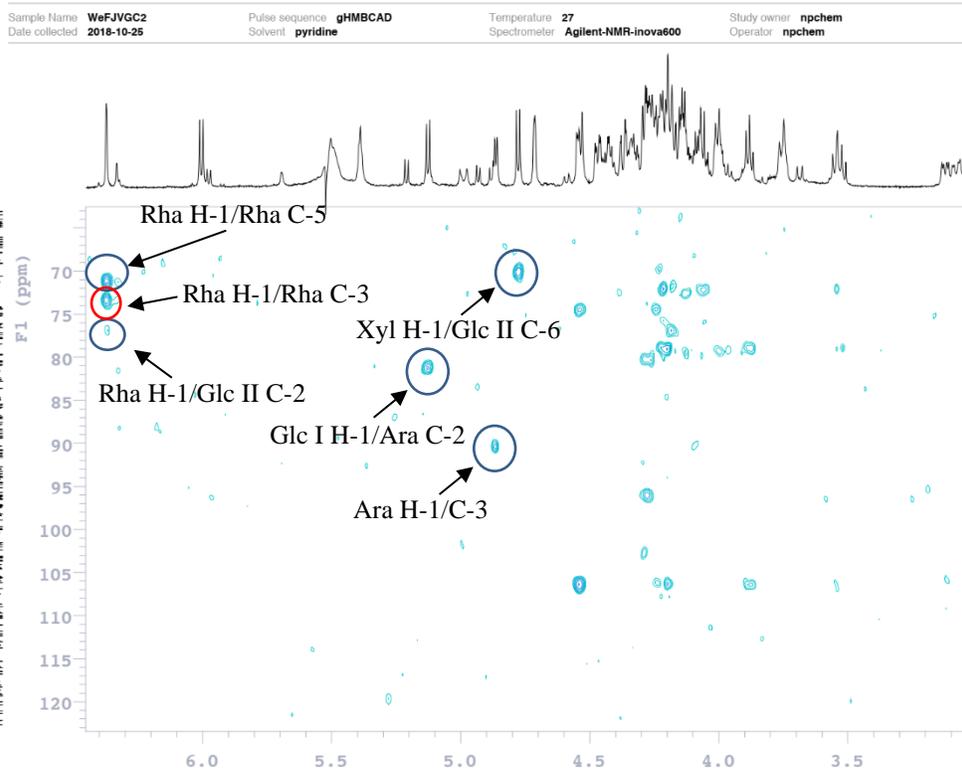
Figure 83. HMBC spectrum of sugar moieties of compound **13**
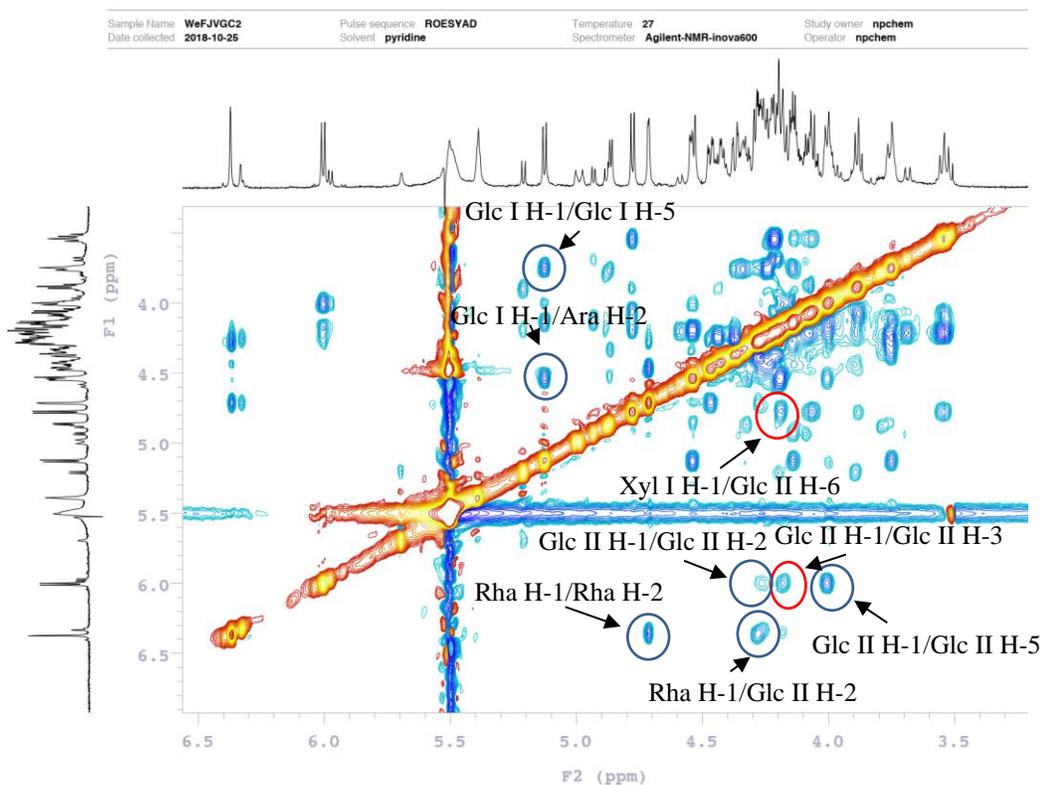
Figure 84. ROESY spectrum of sugar moieties of compound **13**

+MS, 0.6min #36

1213.6004

1097.5514

618.2963   774.4516 871.7026   1468.4704 1587.7151

Meas. m/z   #   Formula   Score   m/z   err [mDa]   err [ppm]   mSigma   rdb   e⁻ Conf   N-Rule
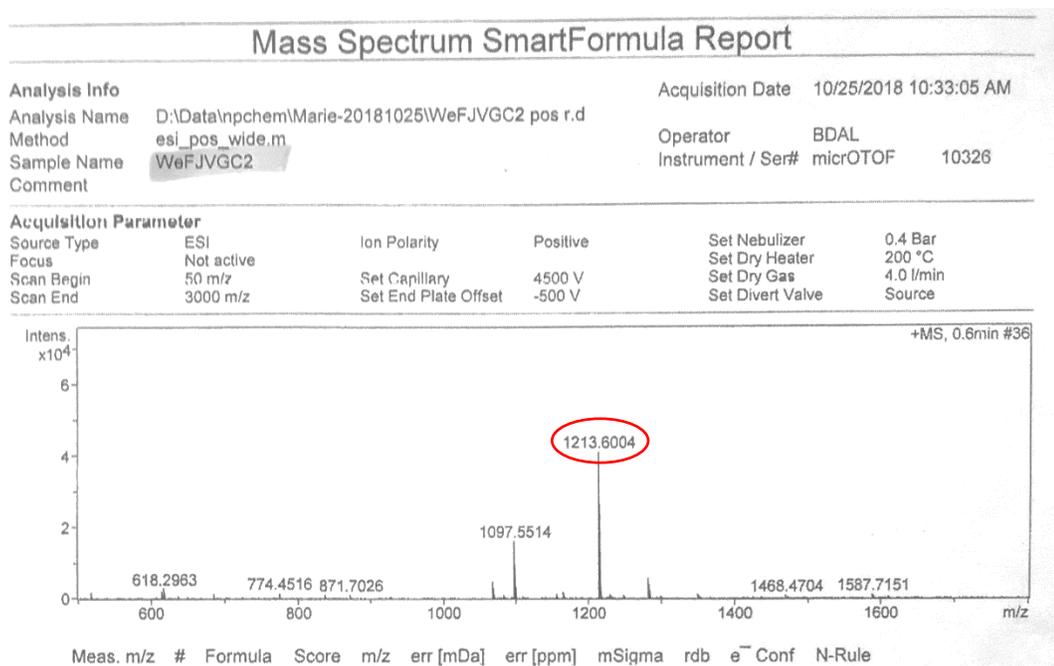
Figure 85. Mass spectrum of compound **13**

c. Compound 14 (WEFJG2V3D)

For compound **14**, the HR-ESIMS (positive-ion mode) spectrum showed a pseudo-molecular ion peak $[M+Na]^+$ at *m/z* 921.4839, indicating a molecular weight of 898 and a molecular formula of $C_{46}H_{74}O_{17}$. By working on literature data, the structure of **14** was identified as 3-*O*-α-L-arabinopyranosylhederagenin 28-*O*-β-D-xylopyranosyl-(1→6)-[α-L-rhamnopyranosyl-(1→2)]-β-D-glucopyranosyl ester. This saponin was isolated from the aerial parts of *Lonicera japonica* (Ho Son et al., 1994).
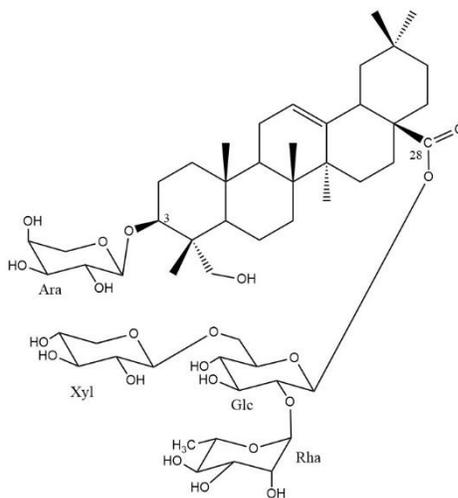
Figure 86. Structure of compound **14**

d. Compound 15 (WEFJ2210)

For compound **15**, the HR-ESIMS (positive-ion mode) spectrum showed a pseudo-molecular ion peak [M+Na]$^+$ at *m/z* 921.4839, indicating a molecular weight of 898 and a molecular formula of $C_{46}H_{74}O_{17}$. By working on literature data, the structure of **15** was identified as 3-*O*-α-L-arabinopyranosylhederagenin 28-*O*-β-D-xylopyranosyl-(1→6)-β-D-glucopyranosyl ester. This saponin was isolated from the aerial parts of *Lonicera japonica* (Ho Son et al., 1994).
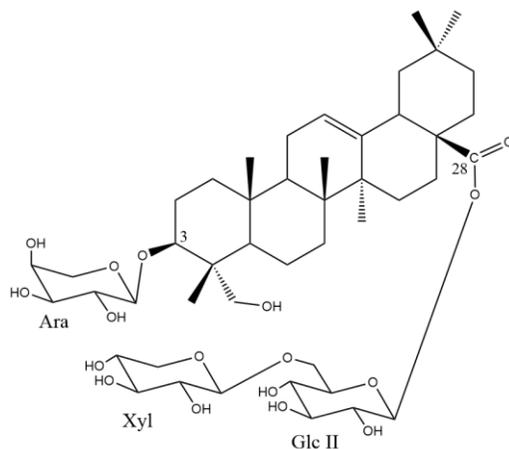
Figure 87. Structure of compound **15**

e. Compound 16 (WEFJR2)

For compound **16**, the HR-ESIMS (positive-ion mode) spectrum showed a pseudo-molecular ion peak [M+Na]$^+$ at *m/z* 1097.5513, indicating a molecular weight of 1074 and a molecular formula of $C_{53}H_{86}O_{22}$. By working on literature data, the structure of **16** was identified as 3-*O*-α-L-arabinopyranosylhederagenin 28-*O*-α-L-rhamnopyranosyl-(1→2)-[β-D-xylopyranosyl-(1→6)]-β-D-glucopyranosyl ester. This saponin was isolated from the aerial parts of *Weigela subsessilis* (Won et al., 2015).
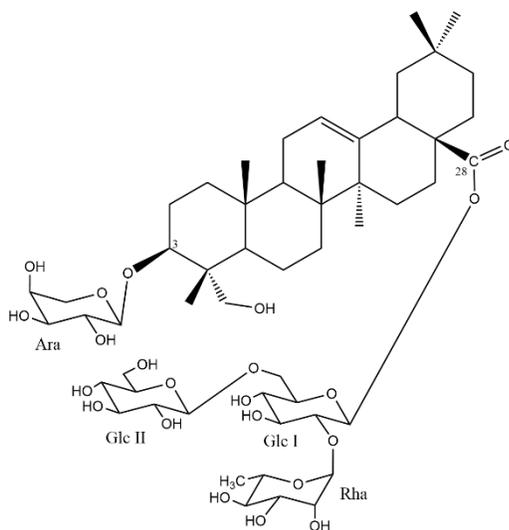
Figure 88. Structure of compound **16**

f. Compound 17 (WEFJ0711)

The HR-ESIMS (positive-ion mode) spectrum of **17** showed a pseudo-molecular ion peak [M+Na]$^+$ at *m/z* 1229.5954, indicating a molecular weight of 1206 and a molecular formula of $C_{58}H_{94}O_{26}$. By working on literature data, the structure of **17** was identified as 3-*O*-β-D-glucopyranosyl-(1→2)-α-L-arabinopyranosylhederagenin 28-*O*-α-L-rhamnopyranosyl-(1→2)-[β-D-xylopyranosyl-(1→6)]-β-D-glucopyranosyl ester. This saponin was isolated from the roots of *Weigela stelzneri* (Rezgui et al., 2016).
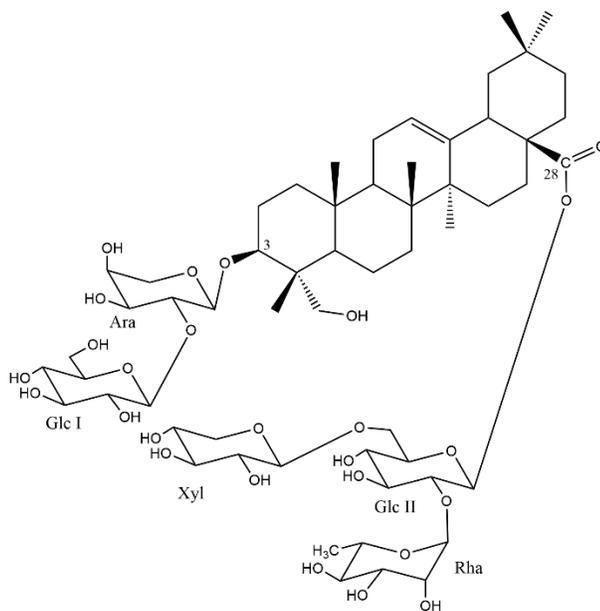
Figure 89. Structure of compound **17**

101

From a chemotaxonomic point of view, most of the saponins isolated from the roots of the investigated *Weigela* species as compounds **8-10** and molecules isolated from various hybrids and cultivars of *Weigela* (Andriamisaina et al., 2018; Champy-Tixier et al., 2018; Rezgui et al., 2016), possess a monodesmosidic form with an *O*-heterosidic linkage at the C-3 position of the oleanolic acid by an oligosaccharidic chain. This chain is composed by a common sequence β-D-xylopyranosyl-(1→3)-α-L-rhamnopyranosyl-(1→2)-β-D-xylopyranosyl or β-D-xylopyranosyl-(1→3)-α-L-rhamnopyranosyl-(1→2)-α-L-arabinopyranosyl. In contrast, the glycosides isolated from the leaves are mainly bidesmosidic saponins with hederagenin as aglycone. A common sequence may be proposed as α-L-arabinopyranosylhederagenin 28-*O*-β-D-glucopyranosyl ester, as in compounds **6-9** and saponins from *W*. x "stelzneri" (Rezgui et al., 2016).

Table 6. ^{13}C and ^{1}H NMR spectroscopic data of the aglycon moieties of compounds **12** and **13** in pyridine-d_5 (δ in ppm, J in Hz)

	12		**13**	
	δ_C	δ_H	δ_C	δ_H
1	40.2	0.87 m, 1.47 m	123.9	5.39 br t (3.6)
2	27.9	1.79 m, 2.06 m	145.5	–
3	90.0	3.25 dd (11.7, 4.1)	43.5	–
4	41.0	–	30.1	1.50 m, 1.94
5	57.2	0.71 br d (11.1)	24.8	1.98, 2.12
6	19.8	1.26, 1.37 m	48.4	–
7	34.4	1.39, 1.60 m	43.2	3.08
8	41.2	–	47.9	1.16, 1.69
9	49.1	1.57	32.0	–
10	38.2	–	35.2	1.10 m, 1.30 m
11	25.0	1.85, 1.89	33.6	1.74, 1.97
12	124.1	5.40 br t (3.6)	29.5	1.09 s
13	145.4	–	18.0	0.94 s
14	43.6	–	16.8	0.83 s
15	29.9	1.52 m, 2.00	18.7	1.00 s
16	24.6	2.00, 2.15	27.2	1.20 s
17	48.4	–	178.1	–
18	43.2	3.09	34.4	0.82 s
19	47.6	1.16, 1.72	25.1	0.85 s
20	32.2	–	123.9	5.39 br t (3.6)
21	35.2	1.11 m, 1.30 m	145.5	–
22	33.5	1.76, 1.98	43.5	–
23	29.5	1.15 s	30.1	1.50 m, 1.94
24	18.3	0.87 s	24.8	1.98, 2.12
25	16.9	0.85 s	48.4	–
26	18.8	1.02 s	43.2	3.08
27	27.3	1.21 s	47.9	1.16, 1.69
28	178.0	–	32.0	–
29	34.4	0.83 s	35.2	1.10 m, 1.30 m
30	24.9	0.80 s	33.6	1.74, 1.97

Overlapped proton signals are reported without designated multiplicity.

Table 7. ^{13}C and ^{1}H NMR spectroscopic data of the sugar moieties of compounds **12** and **13** in pyridine-d_5

	12		**13**	
	δ_C	δ_H	δ_C	δ_H
Ara-1	108.4	4.73 d (6.4)	106.0	4.87 d (5.8)
2	73.9	4.38	81.2	4.54 t (5.8)
3	75.6	4.17	74.7	4.33
4	70.5	4.33	69.5	4.34 m
5	67.8	3.79 dd (12.3, 1.2), 4.27	66.2	3.76 dd (11.1, 1.2), 4.24
Rha-1	102.6	6.39 br s	102.6	6.35 br s
2	73.3	4.72 br s	73.2	4.72 br s
3	73.5	4.48 dd (9.3, 2.9)	73.5	4.47 dd (9.3, 2.9)
4	74.9	4.28	74.9	4.28
5	71.2	4.44	71.1	4.42
6	20.0	1.69 d (5.8)	19.9	1.69 d (5.8)
Xyl-1	106.6	4.79 d (7.0)	106.4	4.78 d (7.6)
2	75.8	3.89	76.0	3.88
3	79.0	4.08	79.0	4.06
4	72.3	4.09	72.1	4.08
5	68.1	3.57, 4.22	68.1	3.55 t (11.1), 4.21
Glc I-1	96.0	6.02 d (7.6)	106.5	5.13 d (7.6)
2	76.9	4.29	77.2	4.00
3	80.2	4.19	79.1	4.14
4	71.9	4.27	72.5	4.15
5	78.6	4.01	79.3	3.75 m
6	70.1	4.19, 4.55	63.7	4.28, 4.36
Glc II-1			96.0	6.00 d (8.2)
2			77.0	4.28
3			80.1	4.18
4			71.8	4.24
5			78.7	4.01 m
6			70.0	4.19, 4.54

Overlapped proton signals are reported without designated multiplicity. dt: not determined
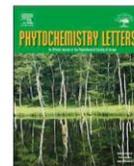
Phytochemical analysis of two *Weigela florida* cultivars, "Pink Poppet" and "Jean's Gold"

Duc Hung Nguyen[a,b,c], Anne-Claire Mitaine-Offer[a,*], Tomofumi Miyamoto[d], Chiaki Tanaka[d], Pierre-Simon Bellaye[e], Bertrand Collin[f], Odile Chambin[c], Marie-Aleth Lacaille-Dubois[a]

[a] PEPITE EA 4267, Laboratoire de Pharmacognosie, UFR des Sciences de Santé, Université de Bourgogne Franche-Comté, BP 87900, 21079, Dijon cedex, France
[b] Department of Biology, Thainguyen University of Education, Thainguyen University, 24000 Thainguyen, Viet Nam
[c] Department of Pharmaceutical Technology, PAM UMR A 02.102, PCAV Team, Université de Bourgogne Franche-Comté, Dijon, France
[d] Graduate School of Pharmaceutical Sciences, Kyushu University, Fukuoka, Japan
[e] Plateforme d'Imagerie et de Radiothérapie Précliniques, Service de Médecine Nucléaire, Centre Georges-François Leclerc, BP77980, 21079, Dijon cedex, France
[f] Plateforme d'Imagerie et de Radiothérapie Précliniques - ICMUB UMR CNRS 6302, Service de Médecine Nucléaire, Centre Georges-François Leclerc, BP77980, 21079 Dijon cedex, France

ARTICLE INFO

ABSTRACT

Nine different oleanane-type glycosides were extracted and isolated by various chromatographic methods from two *Weigela florida* cultivars, "Pink Poppet" and "Jean's Gold". From the roots of *W. florida* "Pink Poppet", three monodesmosidic oleanolic acid saponins 1, 4, 5 were obtained, together with one hederagenin ester 6 from the leaves, and six bidesmosidic saponins 2, 3, 6-9 were isolated from the leaves of *W. florida* "Jean's Gold". Among compounds 1-9, three were previously undescribed (1-3) and six (4-9) were already published in the literature. Their structures were assigned by spectroscopic analysis mainly 2D NMR and mass spectrometry (ESI-MS).

The cytotoxicity of the isolated compounds 1, 3, 4, 6, 7, 9, against mouse colon carcinoma (CT26), mouse melanoma (B16) and human liver cancer (HepG2) cell lines, was evaluated by MTS assay. The ester group at C-28 and/or the primary alcohol function at C-23 led to a negative effect, whereas monodesmosidic oleanolic acid glycosides displayed a good cytotoxicity with IC_{50} ranging from 2.19 to 2.83 μM. A key sequence in the structure of the molecules was proposed for the cytotoxicity.

1. Introduction

As part of our research on bioactive glycosides from the Caprifoliaceae family, we have already investigated hybrids and cultivars of the *Weigela* Thunb. (or *Weigelia* Schreb.) genus. From a chemotaxonomic point of view, monodesmosidic oleanolic acid glycosides were mainly found in the roots and bidesmosidic glycosides, mostly of hederagenin, in the leaves. These types of glycosides have already been tested for their cytotoxicity (Nguyen et al., 2019), their anti-inflammatory effect (Rezgui et al., 2016), their capacity in the antibody recognition (Champy-Tixier et al., 2018), and their toxicological property (Andriamisaina et al., 2018), highlighting the key role of the nature of the aglycone.

To complete the chemotaxonomic data of the genus *Weigela,* and to establish structure/activity relationships, the phytochemical study of two *Weigela florida* (Bunge) A. DC. cultivars, "Pink Poppet" and "Jean's Gold", was achieved, and the cytotoxicity of some isolated glycosides was evaluated.

Herein, we report the isolation of nine different glycosides from an aqueous-ethanolic (35:75) extract of the roots and the leaves of *W. florida* "Pink Poppet", and the leaves of *W. florida* "Jean's Gold", by several solid/liquid chromatographic methods. Their structures were established by 1D and 2D NMR analysis (^{1}H, ^{13}C, COSY, TOCSY, ROESY, HSQC, HMBC) in combination with mass spectrometry (ESI-MS), and by comparison of their spectral data with literature values. From the roots of *W. florida* "Pink Poppet", three monodesmosidic oleanolic acid glycosides 1, 4, 5 were obtained, together with one hederagenin ester 6 from the leaves, and six bidesmosidic glycosides 2, 3, 6-9 were isolated from the leaves of *W. florida* "Jean's Gold". Three were previously undescribed (1-3) and six (4-9) were already published in the literature.

The cytotoxicity of the isolated compounds 1, 3, 4, 6, 7, 9, against mouse colon carcinoma (CT26), mouse melanoma (B16) and human liver cancer (HepG2) cell lines, was evaluated by MTS assay.

---

* Corresponding author.
   E-mail address: anne-claire.offer@u-bourgogne.fr (A.-C. Mitaine-Offer).
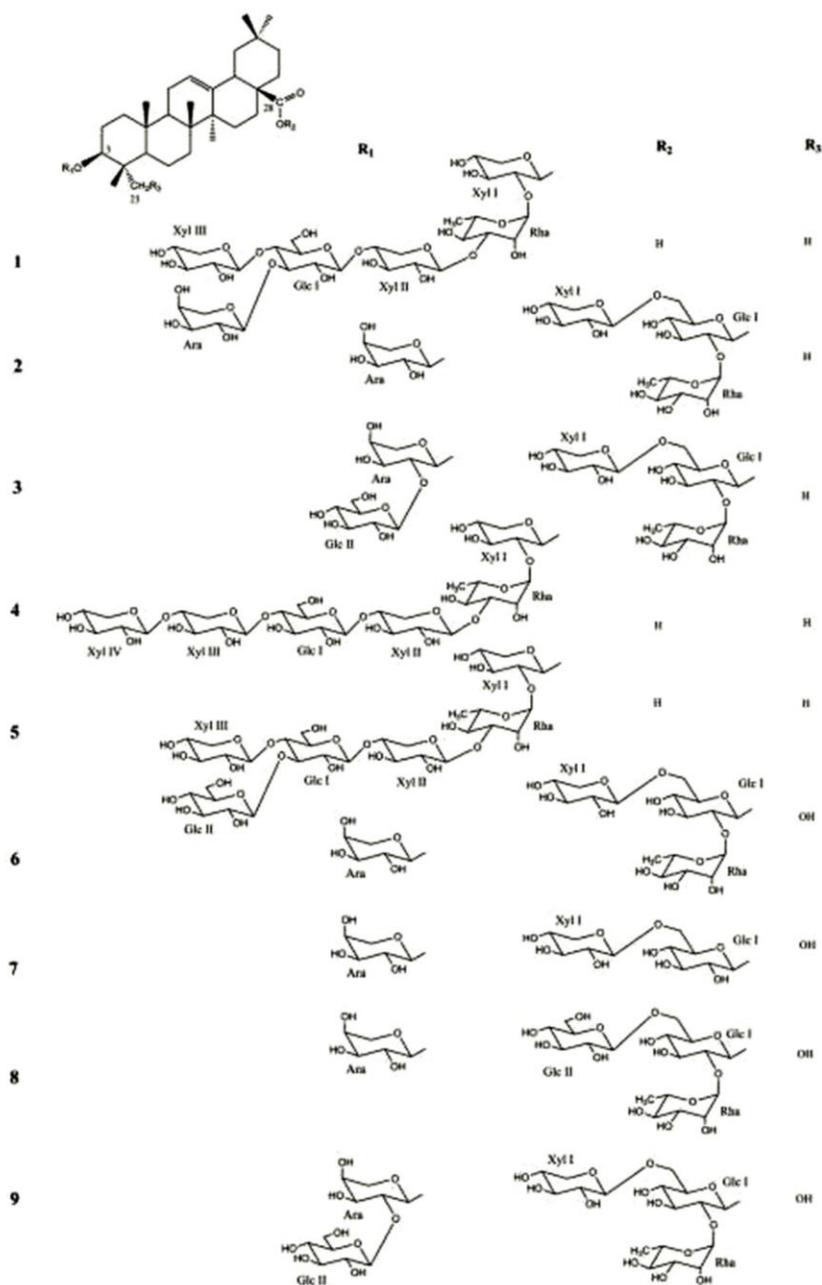
Fig. 1. Structures of compounds 1-9.

2. Results and discussion

For all the isolated compounds **1-9** (Fig. 1), the ^{1}H- and ^{13}C-NMR signals of the aglycone assigned from the 2D NMR spectra, were in good agreement with those of oleanolic acid commonly encountered in the *Weigela* genus (Andriamisaina et al., 2018; Champy-Tixier et al., 2018; Nguyen et al., 2019; Rezgui et al., 2016). The differences were located at the oligosaccharidic chain linked to the C-3 and C-28 positions of the aglycone, together with the presence of the primary alcoholic function

at C-23. The monosaccharides were identified by acid hydrolysis and GC analysis (see Experimental section), and by extensive 2D NMR analysis as α-ʟ-arabinopyranosyl (Ara), α-ʟ-rhamnopyranosyl (Rha), β-ᴅ-xylopyranosyl (Xyl) and β-ᴅ-glucopyranosyl (Glc) in the case of **1-3**, **6**, **9**, Ara, Xyl and Glc in the case of **7**, Ara, Rha and Glc in the case of **8**, and Rha, Xyl and Glc in the case of **4**, **5**. The relatively large $^3J_{H-1, H-2}$ values of the Glc, Xyl, and Ara (5.0–8.2 Hz) indicated a ß anomeric orientation for Glc and Xyl, and an α anomeric orientation for Ara. The large $^1J_{H-1,C-1}$ values of the Rha (165−168 Hz), confirmed that the

Table 1

^{13}C- and ^{1}H-NMR spectroscopic data of the aglycone moieties of **1-3** in pyridine-d_5 (δ in ppm, J in Hz).

	1		2		3	
	δ_C	δ_H	δ_C	δ_H	δ_C	δ_H
1	38.5	0.98 m, 1.53 m	40.2	0.87 m, 1.47 m	40.1	0.78 m, 1.42 m
2	26.5	1.88 m, 2.13 m	27.9	1.79 m, 2.06 m	27.6	1.78 m, 1.96 m
3	88.5	3.35	90.0	3.25 dd (11.7, 4.1)	90.5	3.12 dd (11.7, 4.1)
4	39.4	–	41.0	–	41.1	–
5	56.0	0.86	57.2	0.71 br d (11.1)	57.1	0.62 br d (11.7)
6	18.5	1.21, 1.55 m	19.8	1.26, 1.37 m	19.9	1.24, 1.36 m
7	33.0	1.30, 1.39	34.4	1.39, 1.60 m	34.4	1.36, 1.58 m
8	39.5	–	41.2	–	41.2	–
9	47.9	1.67 dd (15.8, 8.8)	49.1	1.57	49.3	1.52
10	37.0	–	38.2	–	38.2	–
11	23.6	1.92, 2.10	25.0	1.85, 1.89	25.0	1.82, 1.90
12	122.0	5.49 br t (3.6)	124.1	5.40 br t (3.6)	123.9	5.39 br t (3.6)
13	145.0	–	145.4	–	145.5	–
14	42.0	–	43.6	–	43.5	–
15	28.3	1.37, 2.21	29.9	1.52 m, 2.00	30.1	1.50 m, 1.94
16	23.6	1.92 m, 2.20	24.6	2.00, 2.15	24.8	1.98, 2.12
17	47.9	–	48.4	–	48.4	–
18	42.1	3.34	43.2	3.09 dd (13.4, 4.0)	43.2	3.08 dd (14.0, 4.1)
19	46.5	1.30, 1.82	47.6	1.16, 1.72	47.9	1.16, 1.69
20	30.8	–	32.2	–	32.0	–
21	34.2	1.20, 1.46 m	35.2	1.11 m, 1.30 m	35.2	1.10 m, 1.30 m
22	33.0	1.82 m, 2.05 m	33.5	1.76, 1.98	33.6	1.74, 1.97
23	27.9	1.37 s	29.5	1.15 s	29.5	1.09 s
24	17.1	1.21 s	18.3	0.87 s	18.0	0.94 s
25	15.4	0.85 s	16.9	0.85 s	16.8	0.83 s
26	17.3	0.99 s	18.8	1.02 s	18.7	1.00 s
27	26.0	1.32 s	27.3	1.21 s	27.2	1.20 s
28	180.0	–	178.0	–	178.1	–
29	33.2	0.96 s	34.4	0.83 s	34.4	0.82 s
30	23.7	1.02 s	24.9	0.80 s	25.1	0.85 s

Overlapped proton signals are reported without designated multiplicity.

Table 2

^{13}C and ^{1}H NMR spectroscopic data of the sugar moieties of **1-3** in pyridine-d_5 (δ in ppm, J in Hz).

	1		2		3	
	δ_C	δ_H	δ_C	δ_H	δ_C	δ_H
Ara-1	103.2	5.85 d (5.0)	108.4	4.73 d (6.4)	106.0	4.87 d (5.8)
2	72.8	4.19	73.9	4.38	81.2	4.54 t (5.8)
3	74.6	4.22	75.6	4.17	74.7	4.33
4	70.2	4.14 m	70.5	4.33 m	69.5	4.34 m
5	66.4	3.74, 4.48	67.8	3.79 dd (11.2, 1.1), 4.27	66.2	3.76 dd (11.1, 1.2), 4.24
Rha-1	101.2	6.48 br s	102.6	6.39 br s	102.6	6.35 br s
2	71.4	4.96 br s	73.3	4.72 br s	73.2	4.72 br s
3	82.1	4.75 dd (9.3, 2.8)	73.5	4.48 dd (9.3, 2.9)	73.5	4.47 dd (9.3, 2.9)
4	72.5	4.51 t (9.3)	74.9	4.28 t (9.3)	74.9	4.28 t (9.3)
5	69.5	4.73 dq (9.3, 5.2)	71.2	4.44 dq (9.3, 5.8)	71.1	4.42 dq (9.3, 5.8)
6	18.5	1.65 d (5.2)	20.0	1.69 d (5.8)	19.9	1.69 d (5.8)
Xyl I-1	105.8	4.80 d (5.0)	106.6	4.79 d (7.0)	106.4	4.78 d (7.6)
2	77.1	4.21	75.8	3.89	76.0	3.88
3	77.1	4.18	79.0	4.08	79.0	4.06
4	70.5	4.19	72.3	4.09	72.1	4.08
5	64.6	3.75, 4.68	68.1	3.57 t (10.0), 4.22	68.1	3.55 t (11.1), 4.21
Xyl II-1	106.4	5.31 d (7.6)				
2	74.6	4.09				
3	75.5	4.16				
4	77.2	4.26				
5	64.4	3.66 t (10.5), 4.41				
Xyl III-1	103.4	5.28 d (7.0)				
2	74.7	4.10				
3	79.1	4.21				
4	70.9	4.21				
5	66.5	3.75, 4.36				
Glc I-1	102.5	4.91 d (7.6)	96.0	6.02 d (7.6)	96.0	6.00 d (8.2)
2	74.6	4.02	76.9	4.29	77.0	4.28
3	79.8	4.43	80.2	4.19	80.1	4.18
4	73.8	4.42	71.9	4.27	71.8	4.24
5	77.1	3.86 m	78.6	4.01	78.7	4.01 m
6	60.8	4.42, 4.43	70.1	4.19, 4.55	70.0	4.19, 4.54
Glc II-1					106.5	5.13 d (7.6)
2					77.2	4.00
3					79.1	4.14
4					72.5	4.15
5					79.3	3.75 m
6					63.7	4.28, 4.36

Overlapped proton signals are reported without designated multiplicity.

anomeric protons were equatorial (α-pyranoid anomeric form). The complete structural analysis is detailed below only for the previously undescribed glycosides **1-3**.

Compound **1** was obtained as a white amorphous powder. The molecular formula was defined as $C_{62}H_{100}O_{28}$ by HR-ESI-MS (positive-ion mode) spectrum, at m/z 1315.6029 [M + Na]$^{+}$.

The ^{1}H- and ^{13}C-NMR spectra of the aglycone part of **1** (Table 1) were in good accordance with the signals of oleanolic acid (Andriamisaina et al., 2018; Champy-Tixier et al., 2018; Nguyen et al., 2019; Rezgui et al., 2016). This was clear in the HSQC spectrum, with signals of seven classical angular methyl groups of a triterpene skeleton at δ_C / δ_H 27.9/1.37 (s) (CH$_3$-23), 17.1/1.21 (s) (CH$_3$-24), 15.4/0.85 (s) (CH$_3$-25), 17.3/0.99 (s) (CH$_3$-26), 26.0/1.32 (s) (CH$_3$-27), 33.2/0.96 (s) (CH$_3$-29), 23.7/1.02 (s) (CH$_3$-30), and signals of an ethylene bond at δ_C / δ_H 122.0/5.49 (br t J = 3.6 Hz) (CH-12). The signal of a carboxylic acid function at the C-28 position at δ_C 180.0 ppm and the chemical shift of the C-3 at δ_C 88.5 ppm, due to a O-heterosidic linkage, suggested that compound **1** was a monodesmosidic glycoside.

Six sugar units were detected by HSQC correlations in the anomeric region between protons at δ_H 4.80 (d, J = 5.0 Hz), 4.91 (d, J = 7.6 Hz), 5.28 (d, J = 7.0 Hz), 5.31 (d, J = 7.6 Hz), 5.85 (d, J = 5.0 Hz) and 6.48 (br s), and carbons at δ_C 105.8, 102.5, 103.4, 106.4, 103.2 and 101.2, respectively. The 2D extensive NMR spectroscopic analyses enabled the full assignments of the chemical shifts of Xyl I, Xyl II, Xyl III, Glc, Ara and Rha (Table 2). The β-D-xylopyranosyl moiety was shown to be attached at the C-3 position of the aglycone by observation of an HMBC correlation between δ_H 4.80 (Xyl I H-1) and δ_C 88.5 (C-3). Moreover, the HMBC spectrum of **1** displayed long-range correlations at δ_H/δ_C 6.48 (Rha H-1)/77.1 (Xyl I C-2), 5.31 (Xyl II H-1)/82.1 (Rha C-3), 4.91

(Glc H-1)/77.2 (Xyl II C-4), 5.85 (Ara H-1)/79.8 (Glc C-3) and 5.28 (Xyl III H-1)/73.8 (Glc C-4), which suggested the structure of the oligosaccharidic part as 3-O-β-D-xylopyranosyl-(1→4)-[α-L-arabinopyranosyl-(1→3)]-β-D-glucopyranosyl-(1→4)-β-D-xylopyranosyl-(1→3)-α-L-rhamnopyranosyl-(1→2)-β-D-xylopyranosyl. The linkages were ensured by the ROESY cross-peaks at δ_H/δ_H 4.80 (Xyl I H-1)/3.35 (H-3), 6.48 (Rha H-1)/4.21 (Xyl I H-2), 5.31 (Xyl II H-1)/4.75 (dd, J = 9.3, 2.8 Hz, Rha H-3), 4.91 (Glc H-1)/4.26 (Xyl II H-4), 5.85 (Ara H-1)/4.43 (Glc H-3) and 5.28 (Xyl III H-1)/4.42 (Glc H-4). Based on the above results, the structure of **1** was elucidated as 3-O-β-D-xylopyranosyl-(1→4)-[α-L-arabinopyranosyl-(1→3)]-β-D-glucopyranosyl-(1→4)-β-D-xylopyranosyl-(1→3)-α-L-rhamnopyranosyl-(1→2)-β-D-xylopyranosyloleanolic acid (Fig. 1).

The HR-ESI-MS (positive-ion mode) spectrum of compound **2**, a white amorphous powder, showed a pseudo-molecular ion peak at m/z 1051.5427 [M + Na]$^{+}$, indicating a molecular weight of 1028 and a molecular formula of $C_{52}H_{84}O_{20}$.

For the aglycone analysis, HSQC signals were in accordance with oleanolic acid, with for example, seven angular methyl groups at δ_C / δ_H 29.5/1.15 (s) (CH$_3$-23), 18.3/0.87 (s) (CH$_3$-24), 16.9/0.85 (s) (CH$_3$-25), 18.8/1.02 (s) (CH$_3$-26), 27.3/1.21 (s) (CH$_3$-27), 34.4/0.83 (s) (CH$_3$-29),

24.9/0.80 (s) (CH$_3$-30), and signals of an ethylene bond at δ_C / δ_H 124.1/5.40 (br t J = 3.6 Hz) (CH-12). The signal of an ester function at the C-28 position at δ_C 178.0 ppm and the chemical shift of the C-3 at δ_C 90.0 ppm, suggested that compound **2** was a bidesmosidic glycoside.

The HSQC spectrum of the sugar part of **2** showed four cross-peaks at δ_H/δ_C 4.73 (d, J = 6.4 Hz)/108.4, 4.79 (d, J = 7.0 Hz)/106.6, 6.02 (d, J = 7.6 Hz)/96.0 and 6.39 (br s)/102.6, corresponding to anomeric signals of four osidic units, which were identified as Ara, Xyl, Glc and Rha, respectively (Table 2). The 3-*O*-heterosidic linkage and the structure of the oligosaccharidic chain were identified using mainly the ROESY and HMBC spectra. A HMBC correlation at δ_H 4.73 (Ara H-1)/δ_C 90.0 (C-3), confirmed by a ROESY correlation at δ_H 4.73 (Ara H-1)/δ_H 3.25 (dd, J = 11.7, 4.1 Hz, H-3), showed that the Ara moiety was linked to the aglycone at C-3 position. Moreover, the chemical shift of the aglycone C-28 at 178.0 ppm, and the Glc I C1 signal at δ_C 96.0 ppm, suggested an ester linkage between C-28 and Glc I (Nguyen et al., 2019; Rezgui et al., 2016). The HMBC correlations at δ_H/δ_C 4.79 (Xyl I H-1)/ 70.1 (Glc I C-6), 6.39 (Rha H-1)/ 76.9 (Glc I C-2), and the ROESY correlations at δ_H/δ_H 4.79 (Xyl I H-1)/4.19 (Glc I H-6), 6.39 (Rha H-1)/ 4.29 (Glc I H-2) were used to establish the structure of the oligosaccharidic chain as β-ᴅ-xylopyranosyl-(1→6)-[α-ʟ-rhamnopyranosyl-(1→2)]-β-ᴅ-glucopyranosyl.

All the conclusions above led to the elucidation of the structure of **2** as 3-*O*-α-ʟ-arabinopyranosyloleanolic acid 28-*O*-β-ᴅ-xylopyranosyl-(1→6)-[α-ʟ-rhamnopyranosyl-(1→2)]-β-ᴅ-glucopyranosyl ester (Fig. 1).

For compound **3**, a white amorphous powder, the molecular formula of C$_{58}$H$_{94}$O$_{25}$, and thus a molecular weight of 1190, was obtained according to its HR-ESI-MS (positive-ion mode) which showed a pseudo-molecular ion peak at *m/z* 1213.6004 [M + Na]$^+$.

This molecular weight differs from **2** by only 162 amu, corresponding to a supplementary hexosyl group. The HSQC spectrum of the osidic part of **3** showed five correlations corresponding to anomeric signals at δ_H/δ_C 4.78 (d, J = 7.6 Hz)/106.4, 4.87 (d, J = 5.8 Hz)/106.0, 5.13 (d, J = 7.6 Hz)/106.5, 6.00 (d, J = 8.2 Hz)/ 96.0 and 6.35 (br s)/ 102.6. These osidic units were identified as Xyl I, Ara, Glc II, Glc I, and Rha, respectively (Table 2). The complete assignment of the NMR data of **3** was achieved and the structure of a common sequence with **2** appeared as α-ʟ-arabinopyranosyloleanolic acid 28-*O*-β-ᴅ-xylopyranosyl-(1→6)-[α-ʟ-rhamnopyranosyl-(1→2)]-β-ᴅ-glucopyranosyl ester (Tables 1 and 2). The only difference between **2** and **3** was located at the C-2 position of the Ara moiety, which was linked to a terminal β-ᴅ-glucopyranosyl moiety. This was proved by a HMBC correlation at δ_H/ δ_C 5.13 (Glc II H-1)/81.2 (Ara C-2) and a ROESY cross-peak at δ_H/δ_H 5.13 (Glc II H-1)/4.54 (t, J = 5.8 Hz) (Ara H-2). Thus, the structure of **3** was elucidated as 3-*O*-β-ᴅ-glucopyranosyl-(1→2)-α-ʟ-arabinopyranosyloleanolic acid 28-*O*-β-ᴅ-xylopyranosyl-(1→6)-[α-ʟ-rhamnopyranosyl-(1→2)]-β-ᴅ-glucopyranosyl ester (Fig. 1).

The structure of six known compounds were also identified, based on the NMR and MS data and comparison with the literature, as 3-*O*-β-ᴅ-xylopyranosyl-(1→4)-β-ᴅ-xylopyranosyl-(1→4)-β-ᴅ-glucopyranosyl-(1→4)-β-ᴅ-xylopyranosyl-(1→3)-α-ʟ-rhamnopyranosyl-(1→2)-β-ᴅ-xylopyranosyloleanolic acid (**4**) (Nguyen et al., 2019), 3-*O*-β-ᴅ-xylopyranosyl-(1→4)-[β-ᴅ-glucopyranosyl-(1→3)]-β-ᴅ-glucopyranosyl-(1→4)-β-ᴅ-xylopyranosyl-(1→3)-α-ʟ-rhamnopyranosyl-(1→2)-β-ᴅ-xylopyranosyloleanolic acid (**5**) (Nguyen et al., 2019), 3-*O*-α-ʟ-arabinopyranosylhederagenin 28-*O*-β-ᴅ-xylopyranosyl-(1→6)-[α-ʟ-rhamnopyranosyl-(1→2)]-β-ᴅ-glucopyranosyl ester (Loniceroside A) (**6**) (Ho Son et al., 1994), 3-*O*-α-ʟ-arabinopyranosylhederagenin 28-*O*-β-ᴅ-xylopyranosyl-(1→6)-β-ᴅ-glucopyranosyl ester (**7**) (Ho Son et al., 1994), 3-*O*-α-ʟ-arabinopyranosylhederagenin 28-*O*-β-ᴅ-glucopyranosyl-(1→6)-[α-ʟ-rhamnopyranosyl-(1→2)]-β-ᴅ-glucopyranosyl ester (Loniceroside K) (**8**) (Won et al., 2015), and 3-*O*-β-ᴅ-glucopyranosyl-(1→2)-α-ʟ-arabinopyranosylhederagenin 28-*O*-α-ʟ-rhamnopyranosyl-(1→2)-[β-ᴅ-xylopyranosyl-(1→6)]-β-ᴅ-glucopyranosyl ester (**9**) (Rezgui et al., 2016).

From a chemotaxonomic point of view, most of the saponins isolated from the roots of the investigated *Weigela* species as compounds 1,

4, 5, and molecules isolated from various hybrids and cultivars of *Weigela* (Andriamisaina et al., 2018; Champy-Tixier et al., 2018; Nguyen et al., 2019; Rezgui et al., 2016), possess a monodesmosidic form with an *O*-heterosidic linkage at the C-3 position of the oleanolic acid by an oligosaccharidic chain. This chain is composed by a common sequence β-ᴅ-xylopyranosyl-(1→3)-α-ʟ-rhamnopyranosyl-(1→2)-β-ᴅ-xylopyranosyl- or β-ᴅ-xylopyranosyl-(1→3)-α-ʟ-rhamnopyranosyl-(1→2)-α-ʟ-arabinopyranosyl. In contrast, the glycosides isolated from the leaves are mainly bidesmosidic saponins with hederagenin as aglycone. A common sequence may be proposed as α-ʟ-arabinopyranosylhederagenin 28-*O*-β-ᴅ-glucopyranosyl ester, as in compounds **6-9** and saponins from *W.* x "stelzneri" (Rezgui et al., 2016).

The cytotoxicity of the isolated compounds **1, 3, 4, 6, 7, 9** was evaluated by MTS assay against mouse melanoma (B16), mouse colon cancer (CT26), and human liver cancer (HepG2) cells, in concentrations ranging from 1 to 50 μM in comparison with fluorouracil as a positive control. The bidesmosidic oleanolic acid derivative **3** and hederagenin derivatives **6, 7, 9** were inactive on the three cell lines. The ester group at C-28 and/or the primary alcohol function at C-23 led to a negative effect, which was previously described by Bang et al. (2005), and confirmed by Rezgui et al. (2016). On the other hand, the two monodesmosidic oleanolic acid glycosides **1** and **4** exhibited a good cytotoxic activity on the three cell lines, with IC$_{50}$ (μM) at 2.35 (B16), 2.45 (CT26), 2.78 (HepG2) for **1**, and 2.32 (B16), 2.19 (CT26), 2.83 (HepG2) for **4**.

This activity is related to the presence of the sequence β-ᴅ-xylopyranosyl-(1→3)-α-ʟ-rhamnopyranosyl-(1→2)-β-ᴅ-xylopyranosyloleanolic acid, which was previously described as a key sequence for the cytotoxicity.

3. Experimental

3.1. General experimental procedures

Optical rotation values were recorded on an AA-10R automatic polarimeter. NMR spectra of compounds **1-9** were performed using a Varian INOVA 600 (Agilent Technologies) at the operating frequency of 600 MHz. The operating conditions were as follows: ^{1}H: frequency, 600 MHz; sweep width, 8 kHz; sampling point, 66 k; spectral width, 7804 Hz, accumulation, 32 pulses; temperature, 304 K. ^{13}C: frequency, 150 MHz; sweep width, 32 kHz; sampling point, 160 k; spectral width, 30,000 Hz, accumulation, 8000 pulses; temperature, 304 K. Samples were dissolved in C$_5$D$_5$N (200 μL) using a 5 mm micro-sample tube (SHIGEMI Co., Ltd., Japan). Chemical shifts were referenced to C$_5$D$_5$N signals (δ_H 7.22, δ_C 123.8). Conventional pulse sequences were used for gMQF-COSY, TOCSY, ROESY, gHSQC, and gHMBC. The mixing time in the ROESY experiment was set to 500 ms. TOCSY spectra were acquired using the standard MLEV17 spin-locking sequence and 60 ms mixing time. TOCSY, ROESY and HSQC spectra were recorded using phase-sensitive mode. The size of the acquisition data matrix was 2048 × 256 words in f2 and f1, respectively, and zero filling up to 2k in f1 was made prior to Fourier transformation. Sine-bell or Shifted sine-bell window functions, with the corresponding shift optimized for every spectrum, were used for resolution enhancement, and baseline correction was applied in both dimensions.

HR-ESI-MS and ESI-MS (positive-ion mode) were carried out on a Bruker micrOTOF II mass spectrometer. For the extractions, a MARS 6 microwave apparatus (CEM) was used. Compound isolations were carried out using vacuum liquid chromatography (VLC) on silica gel 60 (Merck, 60–200 μm), reversed-phase RP-18 silica gel (75–200 μm, Silicycle), and on a Teledyne Isco CombiFlash Retrieve (RediSep Rf columns, normal phase silicagel). Medium-pressure liquid chromatography (MPLC) was performed on silica gel 60 (15–40 μm, Merck) with a Gilson M 305 pump (25 SC head pump, M 805 manometric module), a Büchi glass column (460 mm × 25 mm and 460 mm × 15 mm) and a Büchi precolumn (110 mm × 15 mm). Thin-layer chromatography

(TLC, Silicycle) and high-performance thin-layer chromatography (HPTLC, Merck) were carried out on precoated silica gel plates 60F$_{254}$, solvent system CHCl$_3$/MeOH/H$_2$O/AcOH (70:30:5:1). The spray reagent for saponins was vanillin reagent (1 % vanillin in EtOH/H$_2$SO$_4$, 50:1).

3.2. Plant material

Weigela florida "Pink Poppet" and *Weigela florida* "Jean's Gold" were provided in 2018 from Jardiland® (Chenôve, France). The voucher specimens (N° 2018/05/1 for *W. florida* "Pink Poppet" and N° 2018/05/2 for *W. florida* "Jean's Gold") were deposited in the herbarium of the Laboratory of Pharmacognosy, Université de Bourgogne Franche-Comté, Dijon, France.

3.3. Extraction and isolation

The dried powdered roots (26.5 g) and aerial parts (29.0 g) of *W. florida* "Pink Poppet" were submitted to microwaves three times with the solvent EtOH/H$_2$O (75:35) (200 W, 60 °C, 45 min, 400 mL each), separately. After evaporation of the solvent, an aliquot of the roots extract (1.5 g) was submitted to VLC (RP-18 silica gel, H$_2$O, EtOH/H$_2$O 50:50, EtOH) yielding 3 fractions (R1-R3). Fractions R2 (85.2 mg), rich in saponins, was fractionated by successive MPLC on silica gel 60 (CHCl$_3$/MeOH/H$_2$O 75:25:3; 70:30:5; 60:32:7) yielding compounds **1** (4.0 mg) and **4** (2.0 mg). The remaining residue of the roots extract was dissolved in water and partitioned with *n*-BuOH saturated with H$_2$O (1:1, 200 mL x 3). The dried *n*-BuOH phase (142.3 mg) was submitted to MPLC on silica gel 60 (CHCl$_3$/MeOH/H$_2$O 70:30:5) affording compound **5** (3.9 mg). Then 7.7 g of the crude extract of the aerial parts were subjected to VLC (RP-18 silica gel, H$_2$O, EtOH/H$_2$O 50:50, EtOH) to give 3 fractions (AP1-AP3). Fraction AP2 was submitted to a MPLC on silica gel 60 (CHCl$_3$/MeOH/H$_2$O 75:25:3) affording compound **6** (8.5 mg).

The same protocol was used for the extraction of the aerial parts of *W. florida* "Jean's Gold" (56.8 g). After filtration and evaporation, 21.5 g of crude of extract were obtained. An aliquot (17.5 g) was fractionated using successive VLC on silica gel 60, (CHCl$_3$/MeOH/H$_2$O 60:32:7), and on RP-18 silica gel (H$_2$O, EtOH/H$_2$O 50:50, EtOH), yielding 4 fractions (A1-A4). Fraction A3 (309.1 mg) was submitted to MPLC on silica gel 60 (CHCl$_3$/MeOH/H$_2$O 70:30:5) yielding two pure compounds, **2** (3.2 mg) and **7** (2.8 mg) among the 5 fractions obtained (A3.1 to A3.5). The remaining extract (4.0 g) was fractionated by flash chromatography (CHCl$_3$/MeOH/H$_2$O, 60:32:7) to give 4 fractions. The fractions rich in saponins were further separated using MPLC on silica gel 60 (CHCl$_3$/MeOH/H$_2$O 80:20:2, 75:25:3) yielding compound **3** (3.2 mg) and **6** (8.0 mg), which was previously obtained from the leaves extract of *W. florida* "Pink Poppet". The remaining fractions were combined and chromatographed again on silica gel 60 by MPLC (CHCl$_3$/MeOH/H$_2$O 70:30:5), yielding compound **8** (4.4 mg) and **9** (8.6 mg).

3.3.1. 3-O-β-D-xylopyranosyl-(1→4)-[α-L-arabinopyranosyl-(1→3)]-β-D-glucopyranosyl-(1→4)-β-D-xylopyranosyl-(1→3)-α-L-rhamnopyranosyl-(1→2)-β-D-xylopyranosyloleanolic acid (1)

White, amorphous powder. HR-ESI-MS (positive-ion mode) *m/z*: 1315.6029 [M + Na] $^+$ (calcd. for C$_{62}$H$_{100}$NaO$_{28}$, 1315.6299). ^{1}H-NMR (pyridine-d_5, 600 MHz,) and ^{13}C-NMR (pyridine-d_5, 150 MHz): see Tables 1 and 2.

3.3.2. 3-O-α-L-arabinopyranosyloleanolic acid 28-O-β-D-xylopyranosyl-(1→6)-[α-L-rhamnopyranosyl-(1→2)]-β-D-glucopyranosyl ester (2)

White, amorphous powder. HR-ESI-MS (positive-ion mode) *m/z*: 1051.5427 [M + Na] $^+$ (calcd. for C$_{52}$H$_{84}$NaO$_{20}$, 1051.5454). ^{1}H-NMR

(pyridine-d_5, 600 MHz,) and ^{13}C-NMR (pyridine-d_5, 150 MHz): see Tables 1 and 2.

3.3.3. 3-O-β-D-glucopyranosyl-(1→2)-α-L-arabinopyranosyloleanolic acid 28-O-β-D-xylopyranosyl-(1→6)-[α-L-rhamnopyranosyl-(1→2)]-β-D-glucopyranosyl ester (3)

White, amorphous powder. HR-ESI-MS (positive-ion mode) *m/z*: 1213.6004 [M + Na] $^+$ (calcd. for C$_{58}$H$_{94}$NaO$_{25}$, 1213.5982). ^{1}H-NMR (pyridine-d_5, 600 MHz,) and ^{13}C-NMR (pyridine-d_5, 150 MHz): see Tables 1 and 2.

3.4. Acid hydrolysis and GC analysis

The protocol was used according to Hara et al. (1987), and detailed in reference Champy-Tixier et al. (2018).

3.5. Cytotoxicity assay

Compound **1, 3, 4, 6, 7, 9** were tested for cytotoxicity during 48 h against CT26 cells (mouse colon cancer, ATCC® CRL-2638™), B16 (mouse melanoma, B16-F0, ATCC® CRL-6322™) and HepG2 (mouse liver cancer, ATCC® HB-8065™) by MTS method as described previously (Nguyen et al., 2019). The results were expressed as concentrations of compound producing 50 % toxicity (IC$_{50}$ value). Fluorouracil (5-FU) was used as positive control. The experiment was done in quintuplet.

Declaration of Competing Interest

The authors have declared no conflict of interest.

Acknowledgements

Appendix A. Supplementary data

Supplementary material related to this article can be found, in the online version, at doi:https://doi.org/10.1016/j.phytol.2020.04.009.

References

Andriamisaina, N., Mitaine-Offer, A.-C., Pruvot, B., Chluba, J., Miyamoto, T., Tanaka, C., Lacaille-Dubois, M.-A., 2018. Phytochemistry of *Weigela* x "kosteriana variegata" (Caprifoliaceae). Nat. Prod. Comm. 13, 403–406.

Bang, S.-C., Lee, J.-H., Song, G.-Y., Kim, D.-H., Yoon, M.-Y., Ahn, B.-Z., 2005. Antitumor activity of *Pulsatilla koreana* saponins and their structure-activity relationship. Chem. Pharm. Bull. 53, 1451–1454.

Champy-Tixier, A.-S., Mitaine-Offer, A.-C., Real Fernández, F., Miyamoto, T., Tanaka, C., Papini, A.-M., Lacaille-Dubois, M.-A., 2018. Oleanane-type glycosides from the roots of *Weigela florida* "rumba" and evaluation of their antibody recognition. Fitoterapia 128, 198–203.

Hara, S., Okabe, H., Mihashi, K., 1987. Gas-liquid chromatographic separation of Aldose Enantiomers as trimethylsilyl ethers of methyl 2-(Polyhydroxyalkyl)-thiazolidine-4(R)-carboxylates. Chem. Pharm. Bull. 35, 501–506.

Ho Son, K., Young Jung, K., Wook Chang, H., Pyo Kim, H., Sik Kang, S., 1994. Triterpenoid saponins from the aerial parts of *Lonicera japonica*. Phytochemistry 35, 1005–1008.

Nguyen, D.H., Mitaine-Offer, A.-C., Maroso, S., Papini, A.-M., Paululat, T., Bellaye, P.-S., Collin, B., Chambin, O., Lacaille-Dubois, M.-A., 2019. Cytotoxic glycosides from the roots of *Weigela* x "Bristol Ruby". Fitoterapia 137, 104242.

Rezgui, A., Mitaine-Offer, A.-C., Miyamoto, T., Tanaka, C., Delemasure, S., Dutartre, P., Lacaille-Dubois, M.-A., 2016. Oleanolic acid and hederagenin glycosides from *Weigela stelzneri*. Phytochemistry 123, 40–47.

Won, Y.-M., Seong, Z.-K., Kim, J.-L., Kim, H.-S., Song, H.-H., Kim, D.-Y., Kim, J.-H., Oh, S.-R., Cho, H.-W., Cho, J.-H., Lee, H.-K., 2015. Triterpene glycosides with stimulatory activity on melanogenesis from the aerial parts of *Weigela subsessilis*. Arch. Pharm. Res. 38, 1541–1551.

2.4. Phytochemical study of roots of *Cordyline fruticosa* "Fairchild red"

Phytochemical investigation of an aqueous-ethanolic extract of the roots of *Cordyline fruticosa* "Fairchild red" led to the isolation of **11** compounds. Nine of them are previously undescribed steroidal glycosides (**18-26)** in addition to two known compounds (**27, 28**).

2.4.1. Isolation and purification

The dried and powdered of roots of *Cordyline fruticosa* "Fairchild red" (74.2 g) were presented to microwaves three times with the solvent EtOH/H$_2$O (200 W, 60°C, 30 min, 75/35 300 mL each). After evaporation of the solvent under vacuum, 24.9 g of crude of extract was obtained. An aliquot (5.2 g) was submitted by VLC (RP-18 silica gel, H$_2$O, EtOH/H$_2$O 50/50, EtOH) giving 3 fractions (A-C). Fraction C (126.7 mg), rich in saponins, was fractionated by successive MPLC on silica gel 60 (CHCl$_3$/MeOH/H$_2$O 90/10/1, 80/20/2, 75/25/3) resulting 6 pure compounds, **18** (1.8 mg), **19** (3.2 mg), **20** (7.1 mg), **22** (4.4 mg), **23** (4.3 mg) and **24** (4.3 mg). The remaining fractions were combined and chromatographed again on silica gel 60 by MPLC (CHCl$_3$/MeOH/H$_2$O 90/10/1) affording compound **21** (3.9 mg). Another aliquot of the crude extract (11.8 g) was submitted to VLC on RP-18 silica gel in the same conditions as above resulting 3 fractions (D-F). Fraction E (3.2 g) was fractionated by flash chromatography (CHCl$_3$/MeOH/H$_2$O 70/30/5) to give 3 fractions. The fraction rich in saponins E3 (150 mg) was further separated using MPLC on silica gel 60 (CHCl$_3$/MeOH/H$_2$O 80/20/2, 75/25/3) affording compound **25** (7.6 mg), **26** (7.6 mg), **27** (4.5 mg) and **28** (5.4 mg).
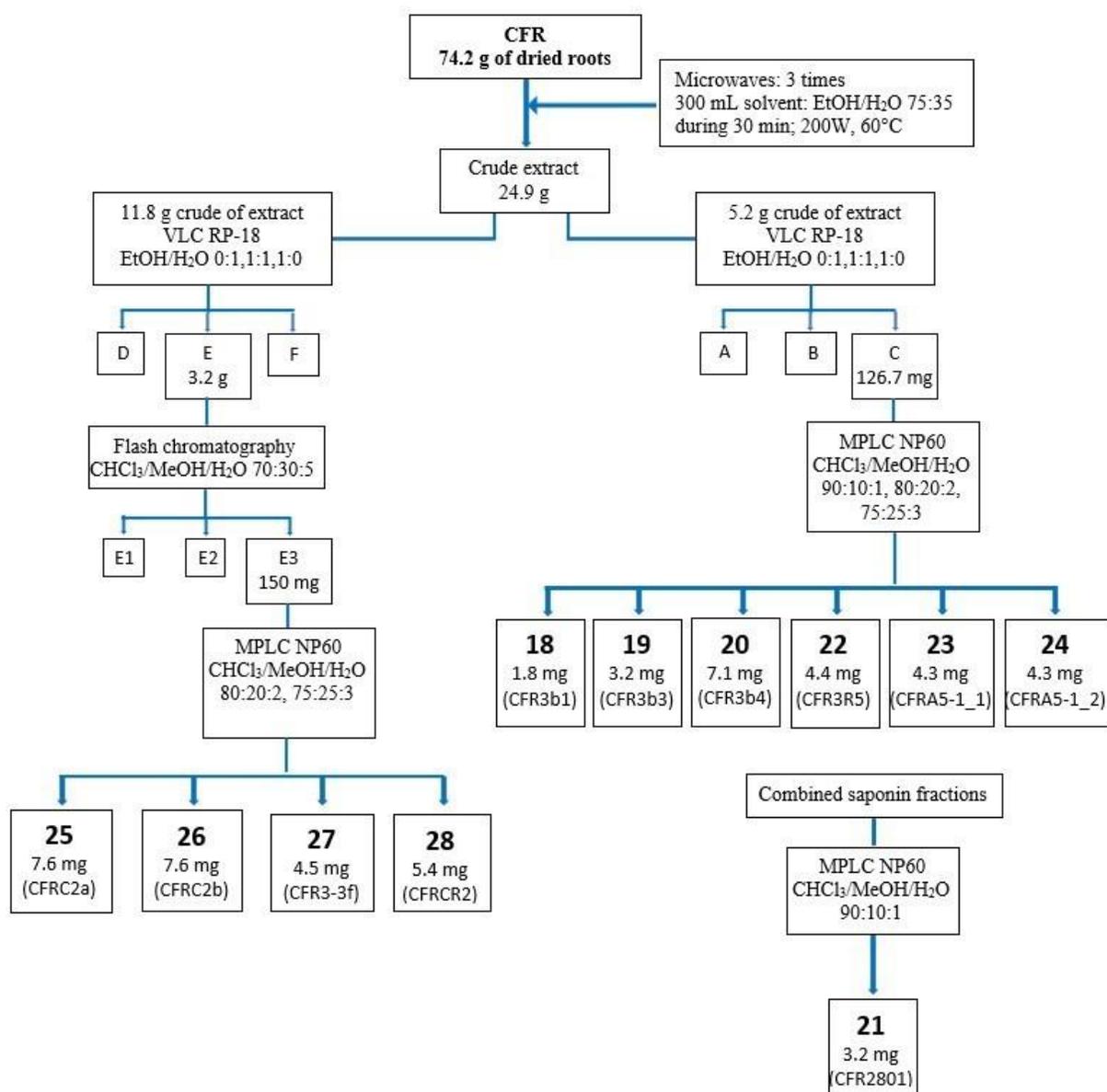
Figure 90. Purification of compounds in roots of *Cordyline fruticosa* "Fairchild red"

2.4.2. Structural determination of isolated saponins

a. Compound 18 (CFR3b1)

Mass spectrometry

The HR-ESIMS (positive-ion mode) spectrum of compound **18** showed a pseudo-molecular ion peak $[M+Na]^+$ at *m/z* 615.3536, indicating a molecular weight of 592 and a molecular formula of $C_{33}H_{52}O_9$.

NMR spectroscopy

Structure of aglycon

The structure of aglycon was identified by analysing spectra NMR ^{1}H, ^{13}C, HSQC and HMBC. The ^{1}H and ^{13}C spectra of the aglycon part of **18** (Table 8) were very characteristic of spirostanol glycoside which showed:

- 2 methyl groups with singlet signal and another one with doublet signal at δ_H 0.83, 1.07 and 1.06 (d, J = 6.4 Hz), respectively.

- 3 oxygen bearing methine proton signals at δ_H 4.00 (dd, J = 11.7, 4.1 Hz, H-1), 3.94 (td, J= 11.7, 4.1 Hz, H-3) and 3.72 (t, J = 11.7 Hz, H-4) (Mimaki et al., 1998b).

- 1 exo-methylene group at δ_H 4.81 and 4.85 (H-27, each 1H, *s*).

The ^{13}C NMR spectrum showed:

- 10 tertiary carbons (CH), 10 secondary carbons (CH_2), 3 primary carbons (CH_3) and 4 quaternary carbons (C).

- 6 carbons of F ring at δ_C 109.7 (C-22), 32.9 (C-23), 28.7 (C-24), 144.0 (C-25), 64.8 (C-26) and 108.7 (C-27) showed a presence of one bearing exo-methylene group at C-25.

In the COSY spectrum, the signal of an oxygen bearing a methine proton at δ_H 4.00 (dd, J = 11.7, 4.1 Hz, H-1) correlated to the δ_H 2.18 (q, J = 11.7 Hz, H-2β) and δ_H 2.93 (dt, J = 11.7, 4.1 Hz, H-2α), with the ROESY correlation between δ_H 4.00 (dd, J = 11.7, 4.1 Hz) and δ_H 1.04 (d, J = 6.4 Hz, H_3-21) and the HMBC correlation between δ_H 1.07 (s, H_3-19) and δ_C 81.2, revealed the location of a hydroxyl group at the C-1 position with a β-orientation. The downfield shift of C-1 δ_C 81.2 suggested a glycosidic linkage. The multiplicity of the H-2β at δ_H 2.18 as a quadruplet (J = 11.7 Hz) suggested a geminal coupling with H-2α and an axial/axial coupling with H-1 and H-3 and hence an α-axial orientation of H-3. This suggestion was confirmed by ROESY correlations at δ_H 4.00 (H-1α)/δ_H 2.93 (H-2α), δ_H 2.93 (H-2α)/δ_H 3.94 (H-3α) and at δ_H 3.94 (H-3α)/δ_H 1.29 (H-5α). Furthermore, the signals at δ_C 74.7 / δ_H 3.72 (t, J = 11.7 Hz) in the HSQC spectrum revealed the presence of an additional hydroxyl group at the 4 position. The H-4, coupled to H-3 (δ_H 3.94, J = 11.7 Hz), was defined in a β-axial orientation through the ROESY correlation at

δ_H 3.72/δ_H 1.07 (s, H$_3$-19). The hydroxyl group was thus assigned as 4α-equatorial. Accordingly, the aglycon of **18** was elucidated as 5α-spirost-25(27)-ene-1β,3β,4α-triol.

Structure of sugar moieties

The monosaccharides were identified by acid hydrolysis and extensive 2D NMR analysis (COSY, TOCY, ROESY, HSQC, HMBC) as α-L-arabinopyranosyl (Ara), α-L-rhamnopyranosyl (Rha), β-D-xylopyranosyl (Xyl), β-D-fucopyranosyl (Fuc) and β-D-glucopyranosyl (Glc). The absolute configurations of the sugars were determined to be D for glucose (Glc), fucose (Fuc) and xylose (Xyl), and L for arabinose (Ara) and rhamnose (Rha), by GC analysis (see Experimental section). The relatively large $^3J_{H-1,H-2}$ values of the Glc, Xyl, and Ara (6.0-8.0 Hz) indicated a ß anomeric orientation for Glc, Fuc and Xyl, and an α anomeric orientation for Ara. The large $^3J_{H-1,C-1}$ values of the Rha (165-168 Hz), confirmed that the anomeric protons were equatorial (α-pyranoid anomeric form).

The sugar part of **18** in the HSQC spectrum corresponding to the osidic chain showed cross-peaks at δ_H/δ_C 4.83 (Fuc H-1)/81.2 (C-1), indicating the presence of one sugar unit which identified as β-D-fucopyranosyl Fuc-1 at δ_H 4.83 (d, J = 7.6 Hz).

The sequence of the oligosaccharide was established by analysing the HMBC, COSY, TOCY and ROESY spectra. The HMBC correlation between δ_H 4.83 (Fuc H-1) and δ_C 81.2 (C-1) and in ROESY correlation at δ_H 4.83 (Fuc H-1) and δ_H 4.00 (dd, J = 11.7, 4.1 Hz, H-1) confirmed the glycosidic linkage of the Fuc at the C-1 position of the aglycon.

Conclusion

All these data above allowed to elucidate **18** as 5α-spirost-25(27)-ene-1β,3β,4α-triol-β-D-fucopyranoside.
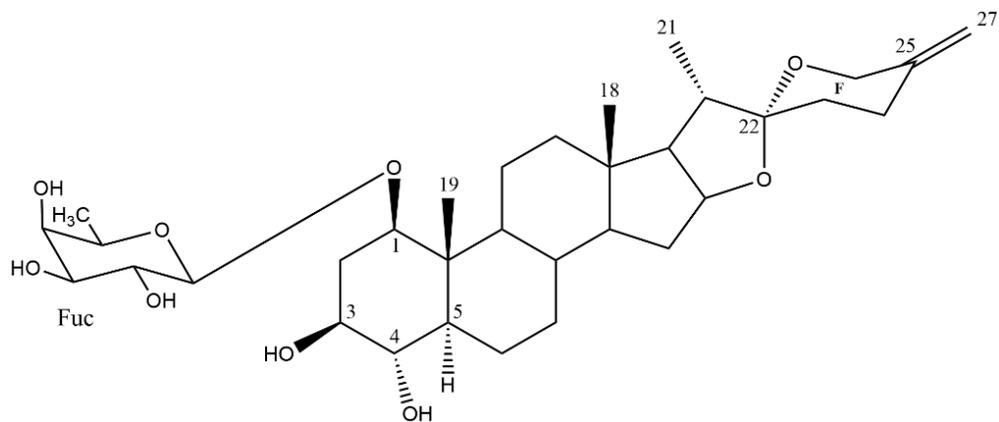
Figure 91. Structure of compound **18**
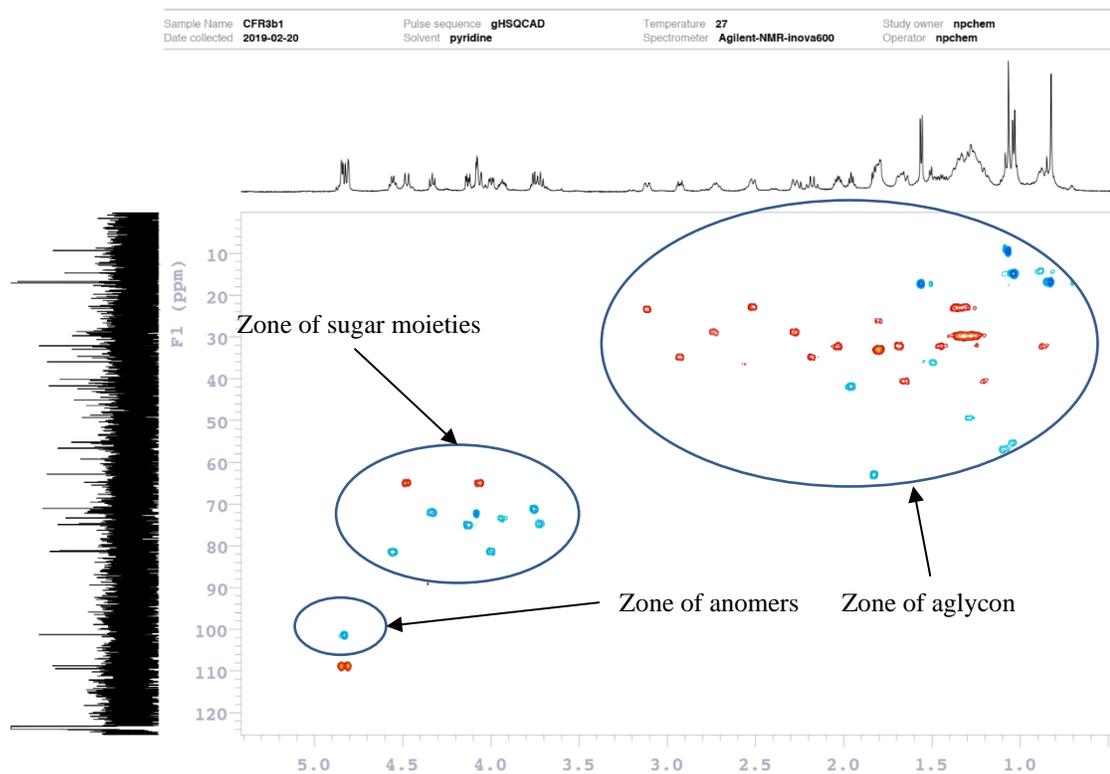
Figure 92. HSQC spectrum of compound **18**
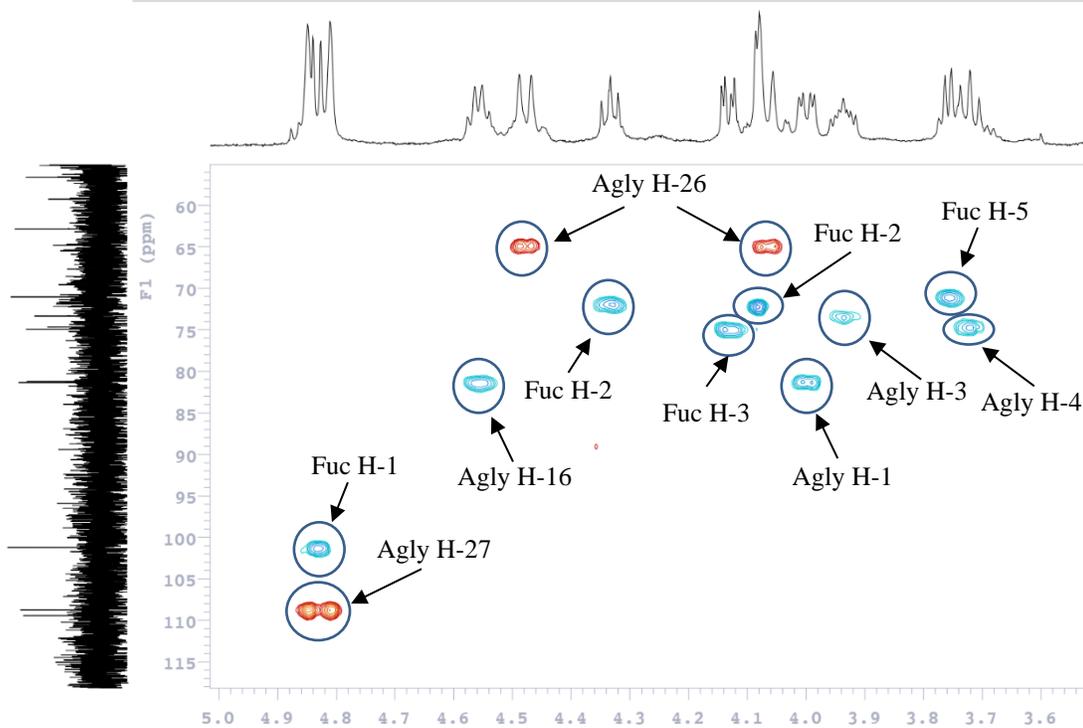
Figure 93. HSQC spectrum of compound **18**
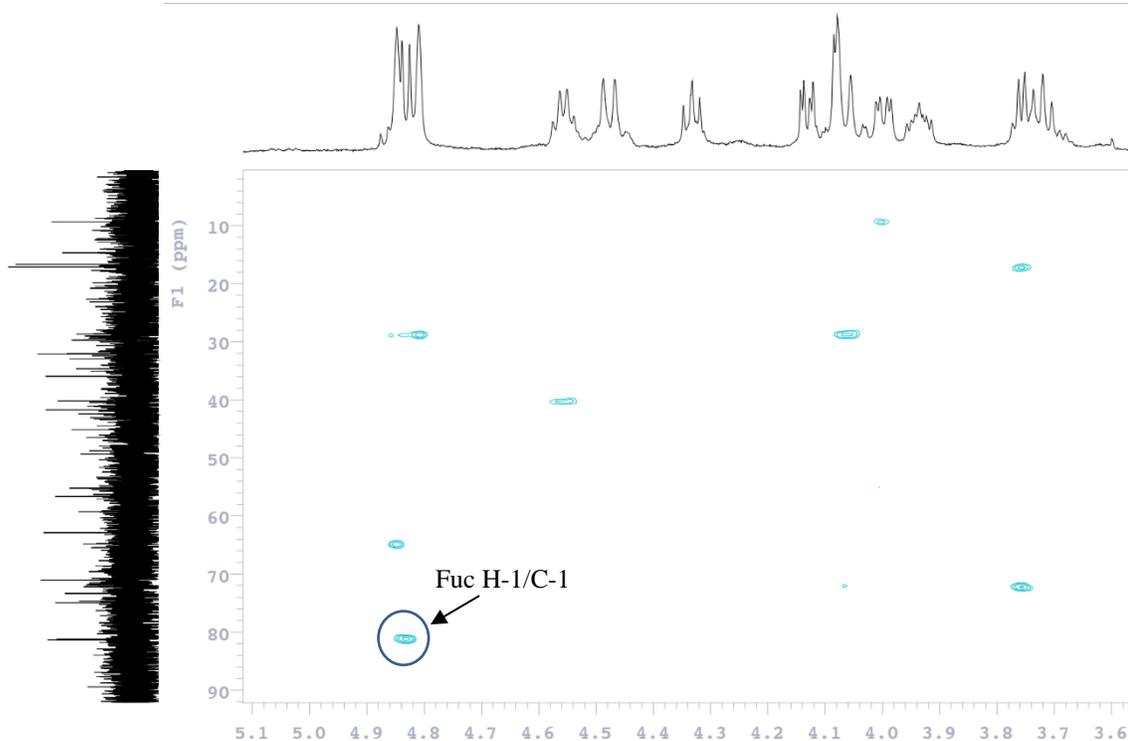
Figure 94. HMBC spectrum of sugar moieties of compound **18**
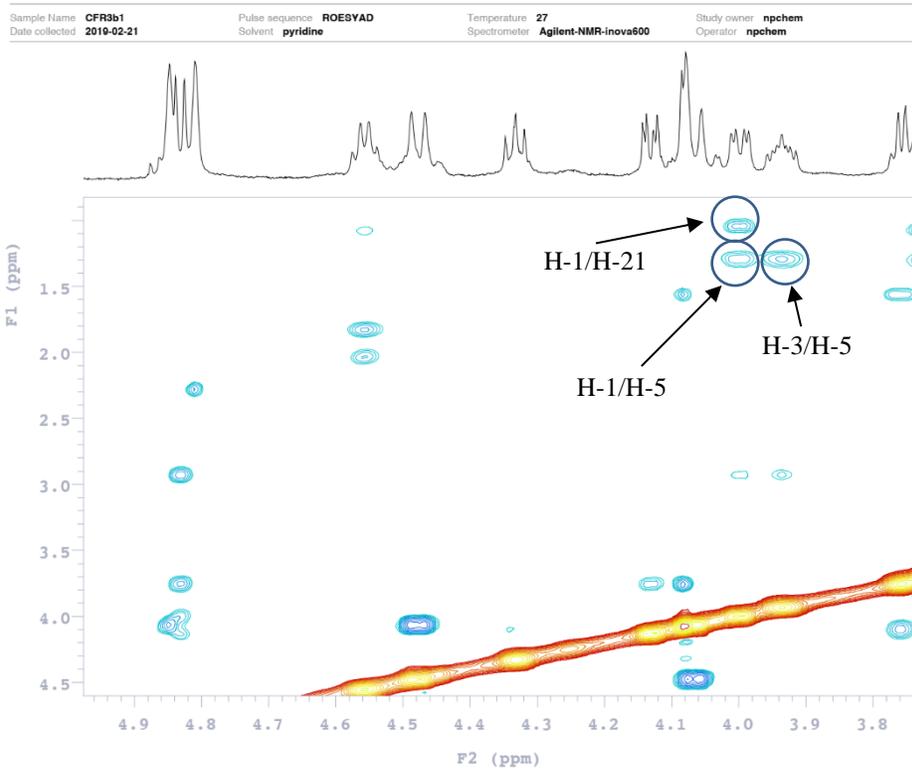
Figure 95. ROESY spectrum of aglycon of compound **18**
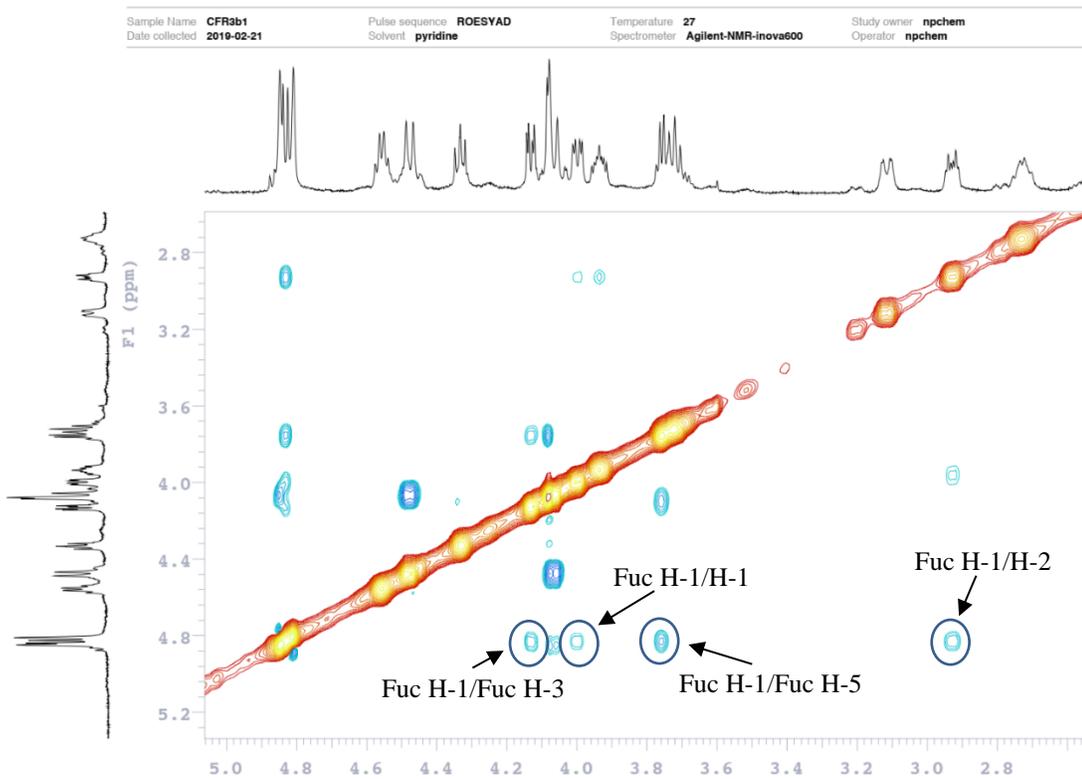
Figure 96. ROESY spectrum of sugar moieties of compound **18**
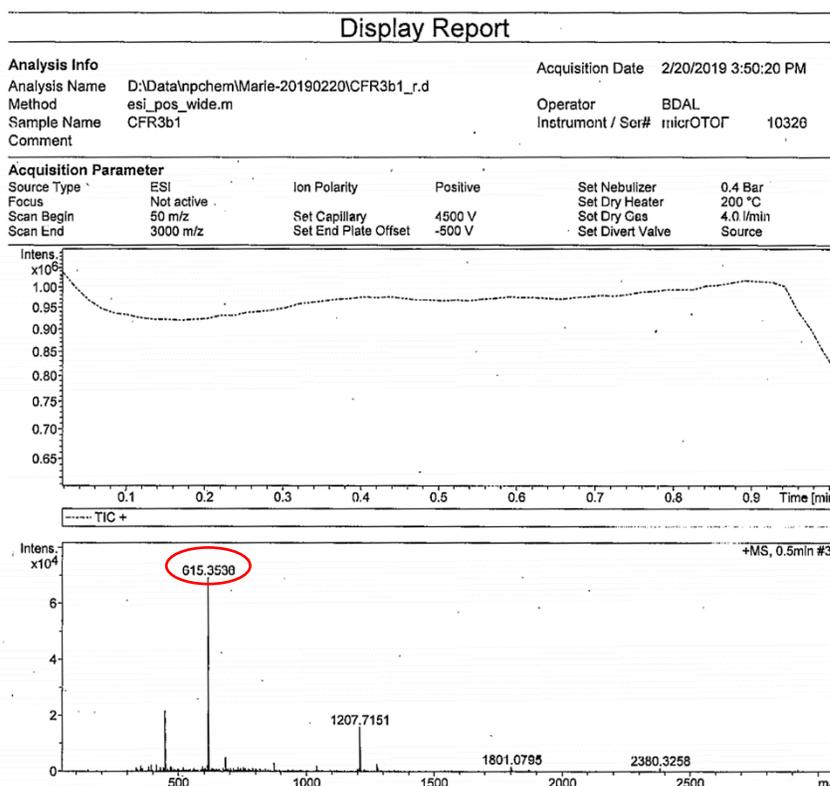
Figure 97. Mass spectrum of compound **18**

b. Compound 19 (CFR3b3)

Mass spectrometry

The HR-ESIMS (positive-ion mode) spectrum of compound **19** showed a pseudo-molecular ion peak [M+Na]$^+$ at *m/z* 601.3369, indicating a molecular weight of 578 and a molecular formula of $C_{33}H_{52}O_9$.

NMR spectroscopy

Structure of aglycon

The analysis of the NMR spectra of compound **19** showed that the aglycon was almost identified to those of compounds **18**. The correlations of HSQC, HMBC and ROESY allowed to identify the genin of compound **19** as spirostanol glycoside which was characterised to compounds **18** (Table 8).

Structure of sugar moieties

110

The molecular weight of compound **19** is lower than **18** 14 amu corresponding to a pentosyl group instead of an hexosyl one. The 2D NMR spectroscopic analyses enabled the full assignments of the resonances of one sugar as β-D-xylopyranosyl (δ_H 5.04, Xyl H-1). The sequence of the oligosaccharide was established by analysing the HMBC and ROESY spectra:

- The HMBC correlation between δ_H 5.04 (Xyl H-1) and δ_C 80.9 (C-1) and a ROESY correlation between δ_H 5.04 (Xyl H-1) and δ_H 4.00 (d, J = 11.7, 4.1 Hz, H-1) proved that Xyl was attached to the C-1 position of the aglycon (Fig.98).

Conclusion

Based on the above evidences, the structure of **19** was characterized as 5α-spirost-(25)27-ene-1β,3β,4α-triol-1-*O*-β-D-xylopyranoside.
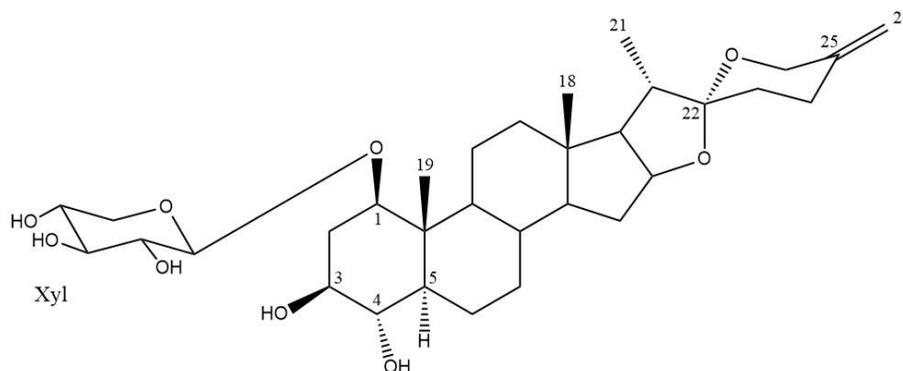
Figure 98. Structure of compound **19**
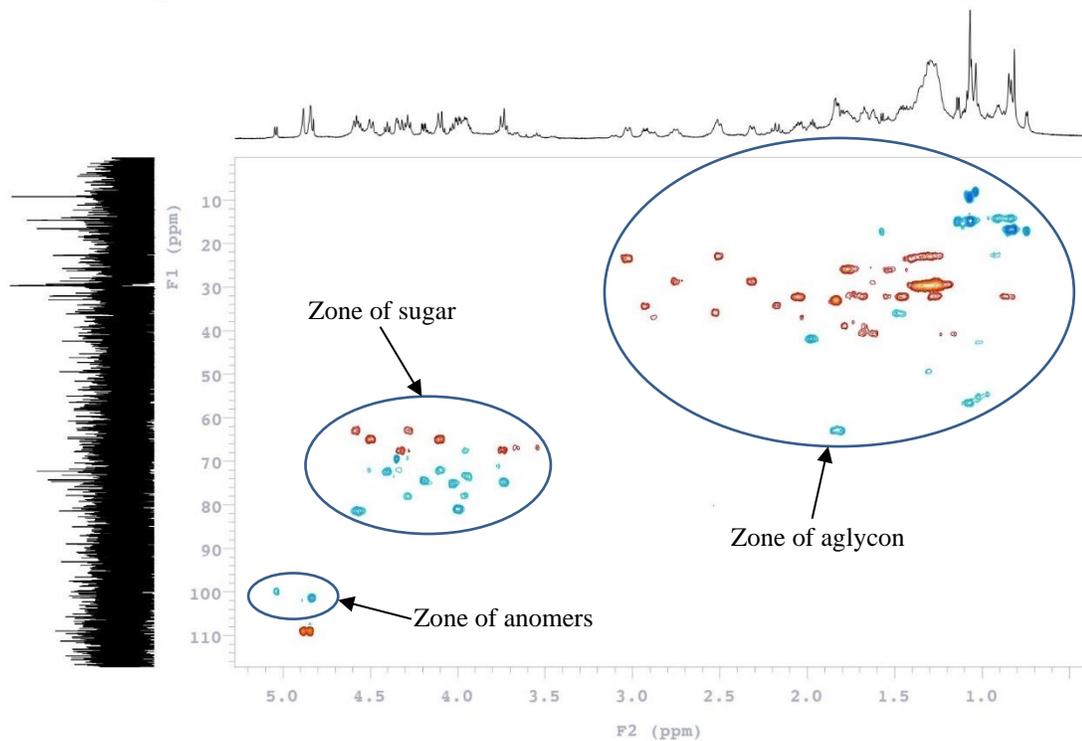
Figure 99. HSQC spectrum of compound **19**
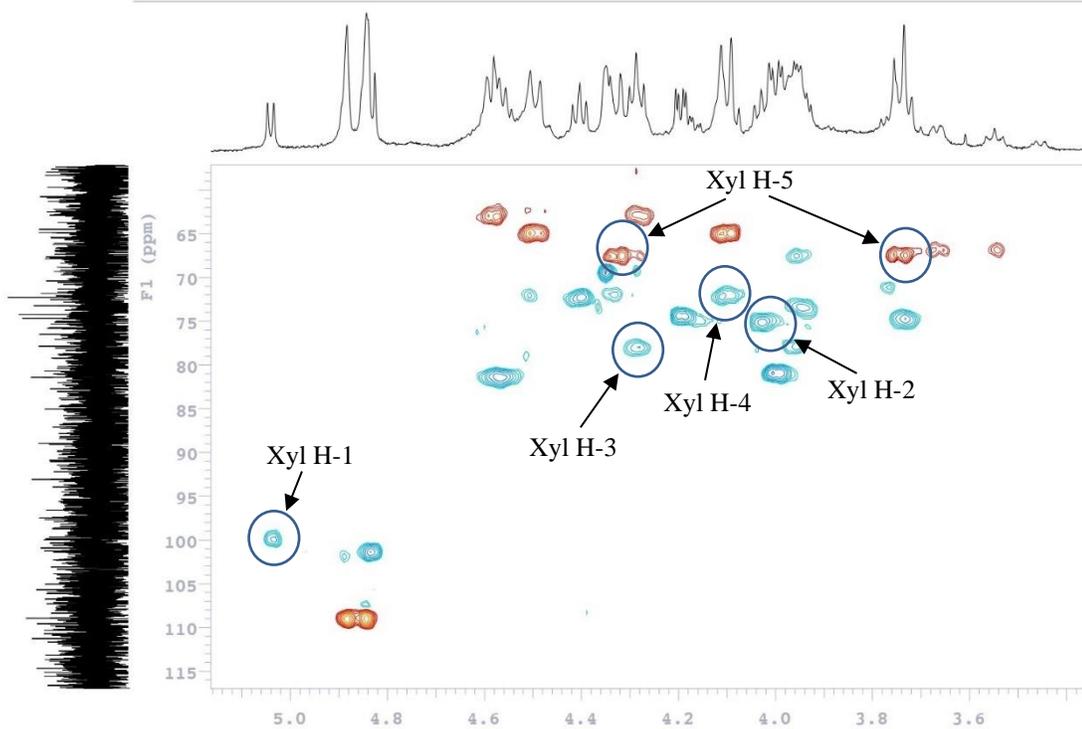
Figure 100. HSQC spectrum of sugar moieties of compound **19**

Xyl H-1/C-1

Figure 101. HMBC spectrum of sugar moieties of compound **19**

Xyl H-1/H-2

Xyl H-1/H-1

Figure 102. ROESY spectrum of sugar moieties of compound **19**

113
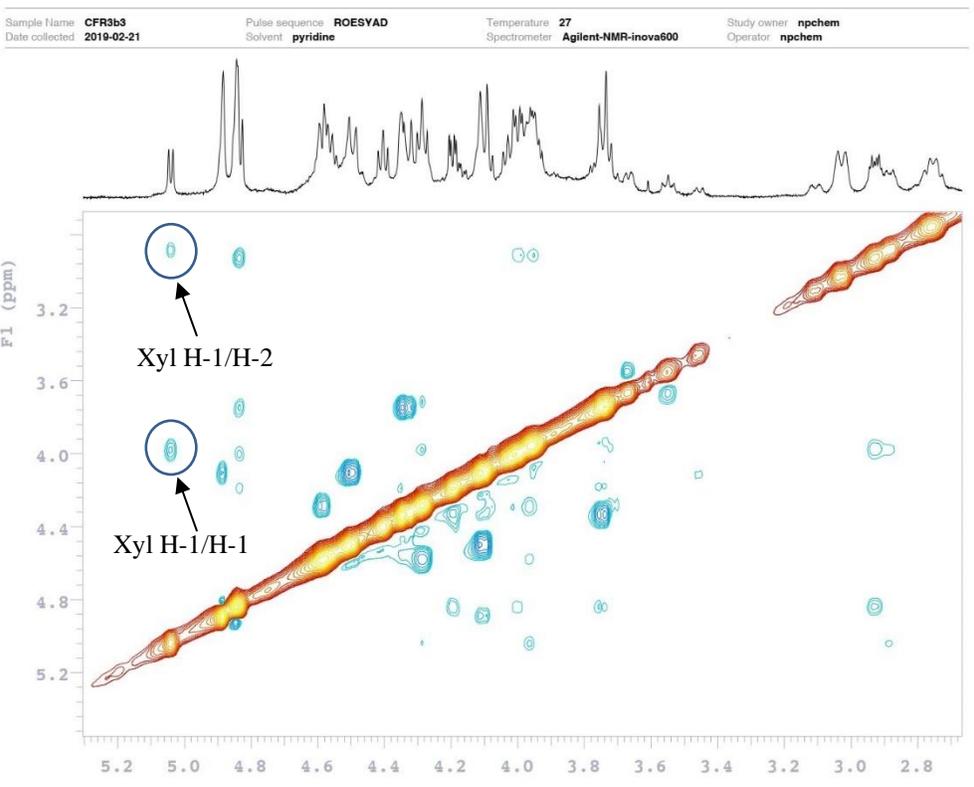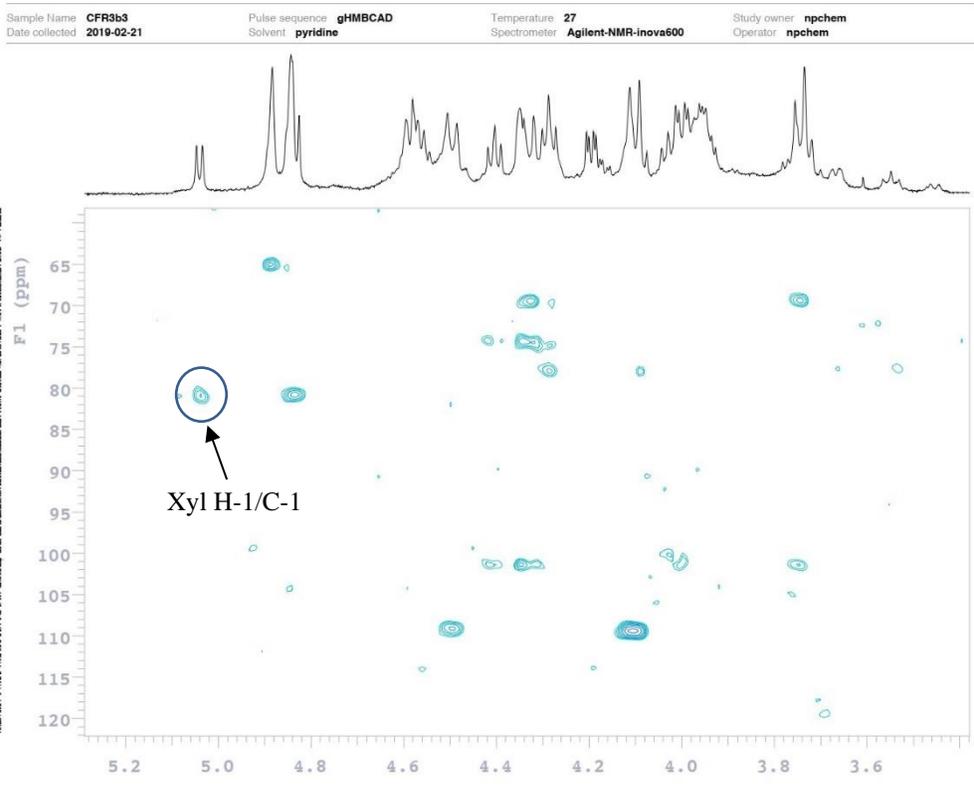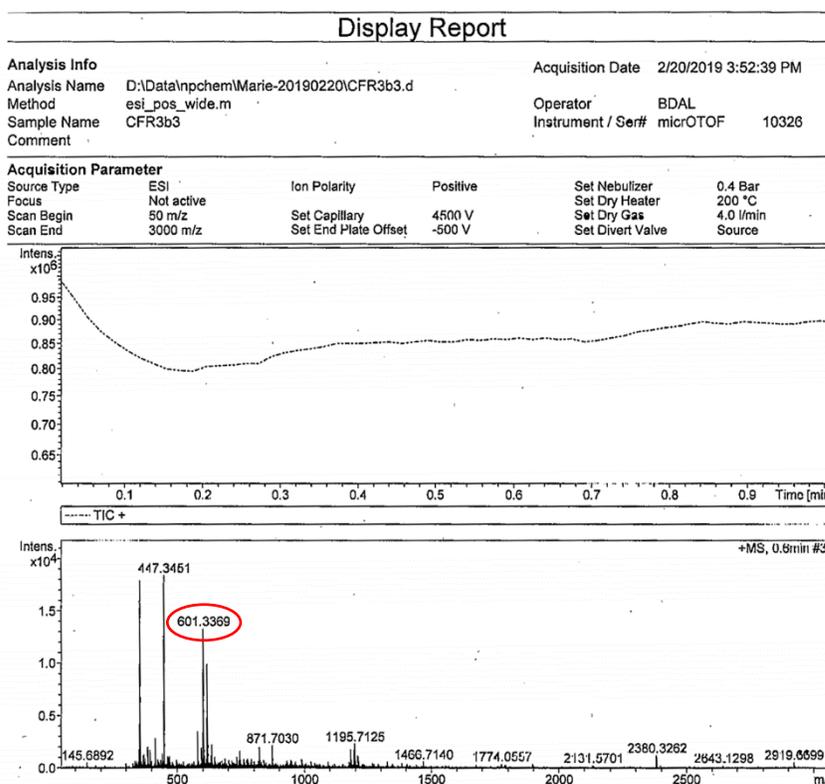
Figure 103. Mass spectrum of compound **19**

c. Compound 20 (CFR3b4)

Mass spectrometry

The HR-ESIMS (positive-ion mode) spectrum of compound **20** showed a pseudo-molecular ion peak [M+Na]$^+$ at *m/z* 745.4171, indicating a molecular weight of 722 and a molecular formula of $C_{39}H_{62}O_{12}$.

NMR spectroscopy

Structure of aglycon

The spectral features of compound **20** in the region of aglycon were quite similar to **18**, excepted the signals due to the A ring carbons. The oxymethine signal at δ_C 74.7 (C-4) in **18** was replaced by a methylene carbon signal at δ_C 39.2, confirmed by the HSQC correlation at δ_C 39.2/δ_H 1.74, 1.77, and the shielded value of C-3 at δ_C 67.7. Accordingly, the aglycon of **20** was characterized as 5α-spirost-25(27)-ene-1β,3β-diol.

Structure of sugar moieties

114

The 2D NMR spectroscopic analyses enabled the full assignments of the resonances of these sugars as:

- 1 β-D-fucopyranosyl Fuc-1 at δ_H 4.71 (d, $J = 7.6$ Hz).

- 1 α-L-rhamnopyranosyl Rha-1 at δ_H 6.35 (br s).

The sequence of the oligosaccharide was established by analysing the HMBC and ROESY spectra:

- The HMBC correlation between δ_H 4.71 (Fuc H-1) and δ_C 83.1 (C-1) and in ROESY at δ_H 4.71 (Fuc H-1) and δ_H 3.80 (dd, $J = 11.7$, 3.5 Hz, H-1), proved that Fuc was linked to the C-1 position of the aglycon (Fig.104).

- The HMBC correlation between δ_H 6.35 (Rha H-1) and δ_C 74.4 (Fuc C-2) and in ROESY at δ_H 6.35 (Rha H-1) and δ_H 4.49 (Fuc H-2) proved that Rha was attached to the Fuc at C-2.

Conclusion

These evidences led to the elucidation of **20** as 5α-spirost-25(27)-ene-1β,3β-diol-1-*O*-α-L-rhamnopyranosyl-(1→2)-β-D-fucopyranoside. The aglycon with a 3α-hydroxyl group was previously isolated by enzymatic hydrolysis from the stems of *Dracaena concinna* (Mimaki et al., 1998b), but this is the first native isolation of 3β-hydroxyl group on the spirostanol glycoside.
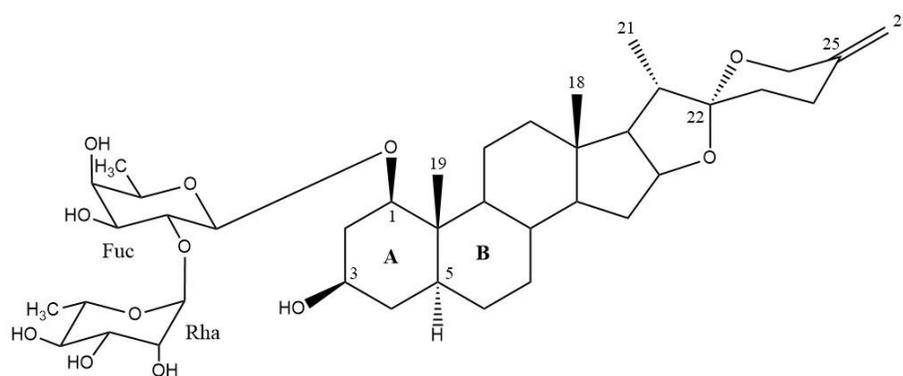
Figure 104. Structure of compound **20**
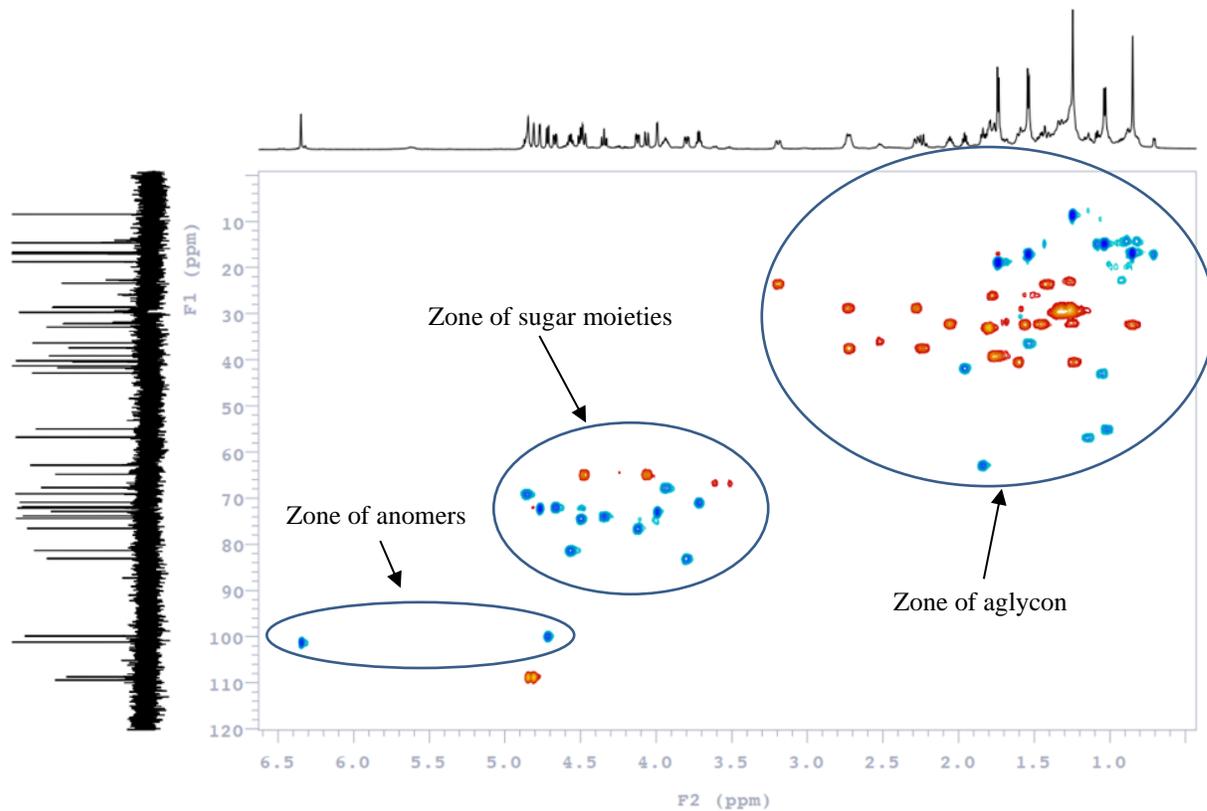
Figure 105. HSQC spectrum of compound **20**
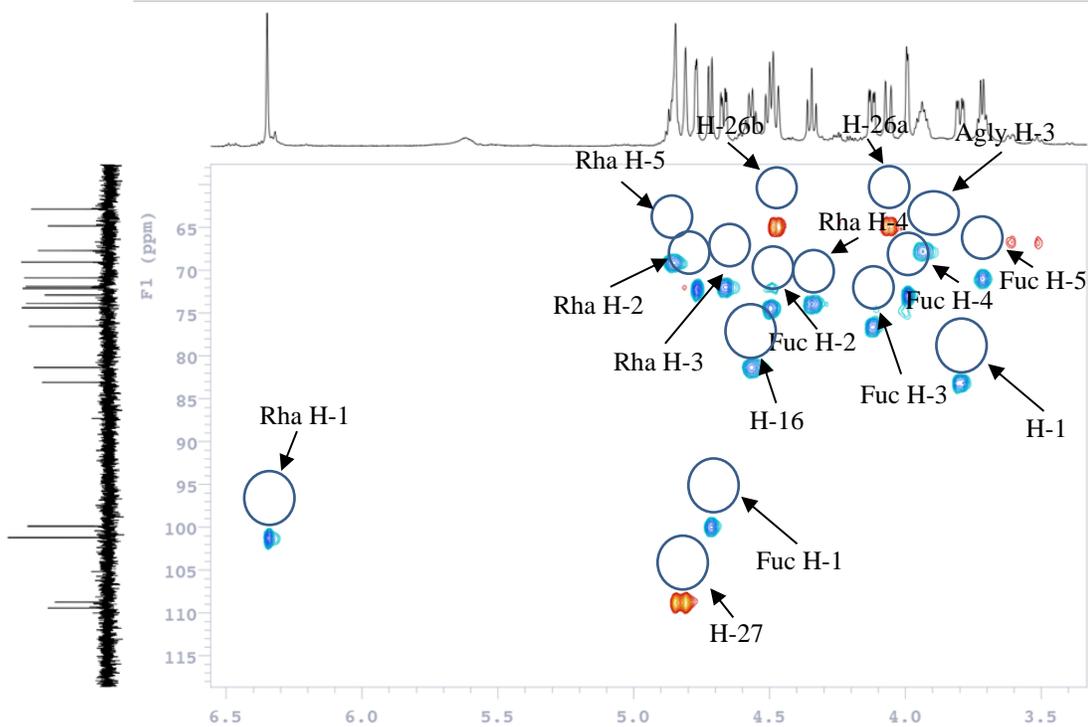
Figure 106. HSQC spectrum of sugar moieties of compound **20**
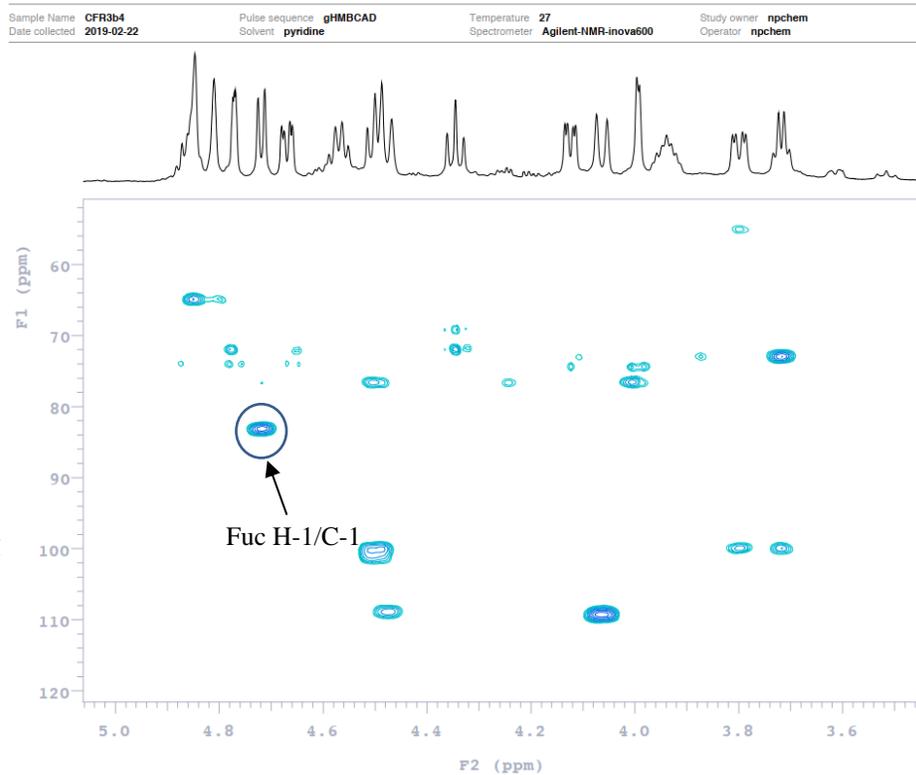
Figure 107. HMBC spectrum of sugar moieties of compound **20**
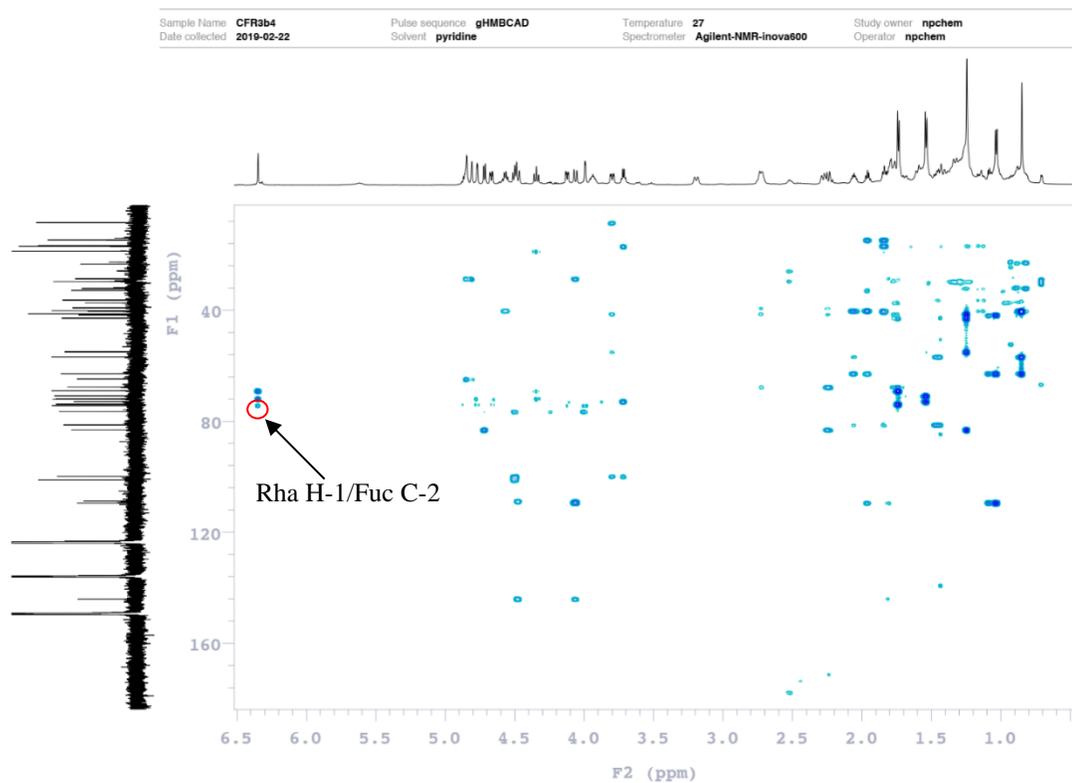
Figure 108. HMBC spectrum of sugar moieties of compound **20**
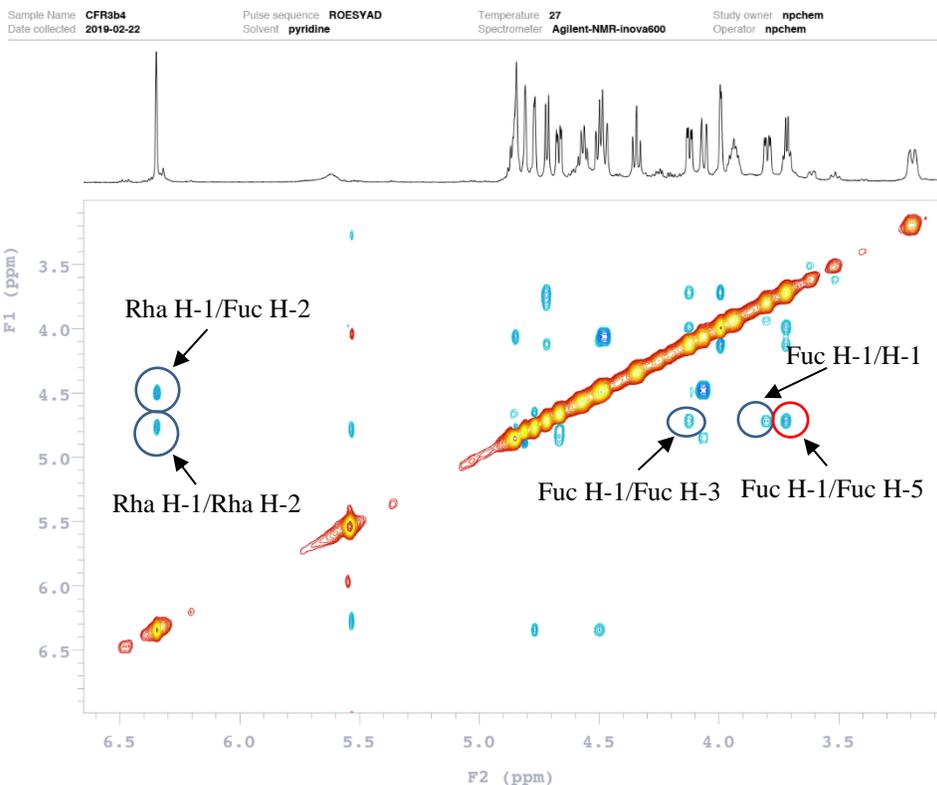
Figure 109. ROESY spectrum of sugar moieties of compound **20**
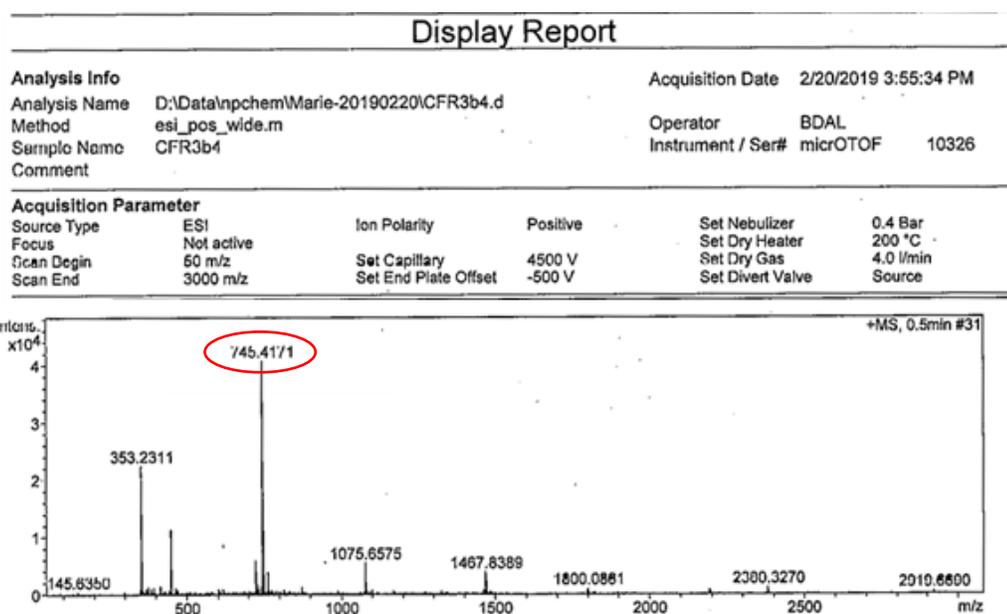
Figure 110. Mass spectrum of compound **20**

d. Compound 21 (CFR2801)

<u>Mass spectrometry</u>

The HR-ESIMS (positive-ion mode) spectrum of compound **21** showed a pseudo-molecular ion peak $[M+Na]^+$ at *m/z* 731.4009, indicating a molecular weight of 708 and a molecular formula of $C_{38}H_{60}O_{12}$.

NMR spectroscopy

Structure of aglycon

The analysis of the NMR spectra of compound **21** showed that the aglycon was the same as compound **20**. The correlations of HSQC, HMBC and ROESY allowed to identify the genin of compound **21** as a spirostanol glycoside which was characterised to compounds **20** (Table 8).

Structure of sugar moieties

The molecular weight of compound **21** differed than **20** by only 14 amu, corresponding to a pentosyl group instead of an hexosyl one. Two cross-peaks were showed in the HSQC indicating the presence of two sugar units, and their structures were established using the 2D NMR spectra:

- 1 α-L-arabinopyranosyl Ara-1 at δ_H 4.73 (d, $J = 7.0$ Hz).

- 1 α-L-rhamnopyranosyl Rha-1 at δ_H 6.32 (br s).

The sequence of the oligosaccharide was established by analysing the HMBC and ROESY spectra:

- The HMBC correlation between δ_H 4.73 (Ara H-1) and δ_C 82.2 (C-1) and in ROESY at δ_H 4.73 (Ara H-1) and δ_H 3.87 (d, $J = 11.7, 3.5$ Hz, H-1) proved that Ara was attached to the C-1 position of the aglycon (**Fig.111**).

- The HMBC correlation between δ_H 6.32 (Rha H-1) and δ_C 75.0 (Ara C-2) and in ROESY at δ_H 6.32 (Rha H-1) and δ_H 4.55 (Ara H-2) proved that Rha was attached to the Ara at C-2.

Conclusion

All the data above allowed to elucidate the structure of **21** as 5α-spirost-25(27)-ene-1β,3β-diol-1-*O*-α-L-rhamnopyranosyl-(1→2)-α-L-arabinopyranoside. As for **20**, the 3α-hydroxyl

derivative was previously isolated by enzymatic hydrolysis from the stems of *Dracaena concinna* (Mimaki et al., 1998b).
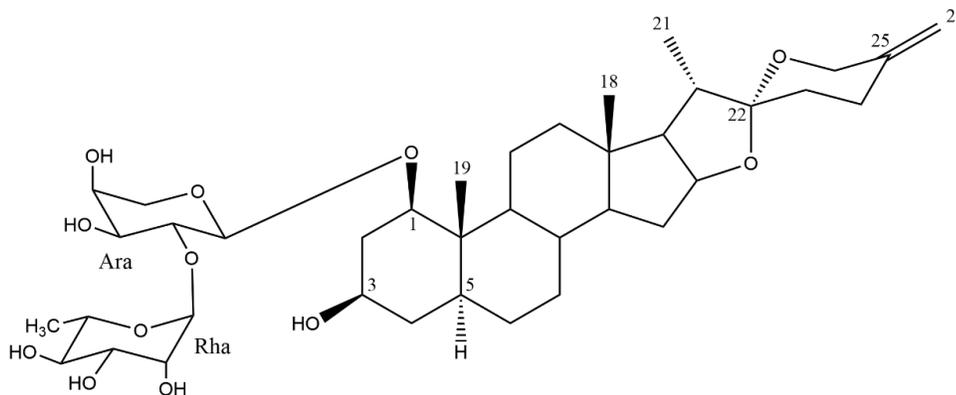
Figure 111. Structure of compound **21**
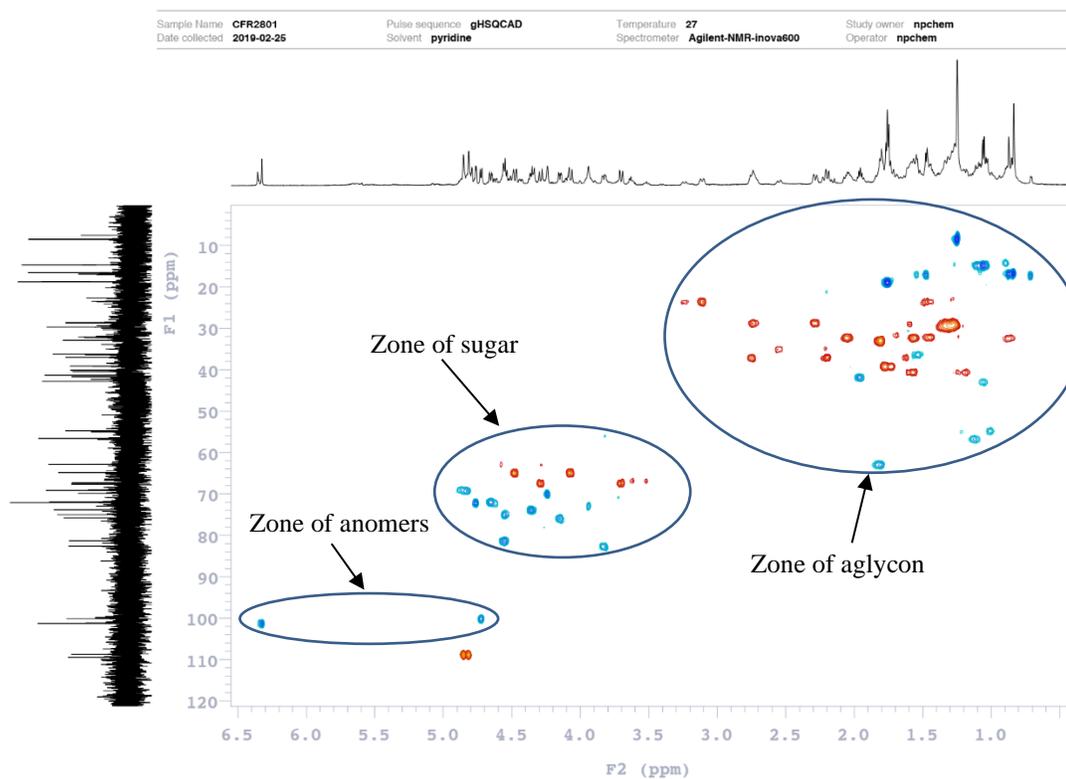
**Figure 112.** HSQC spectrum of compound **21**
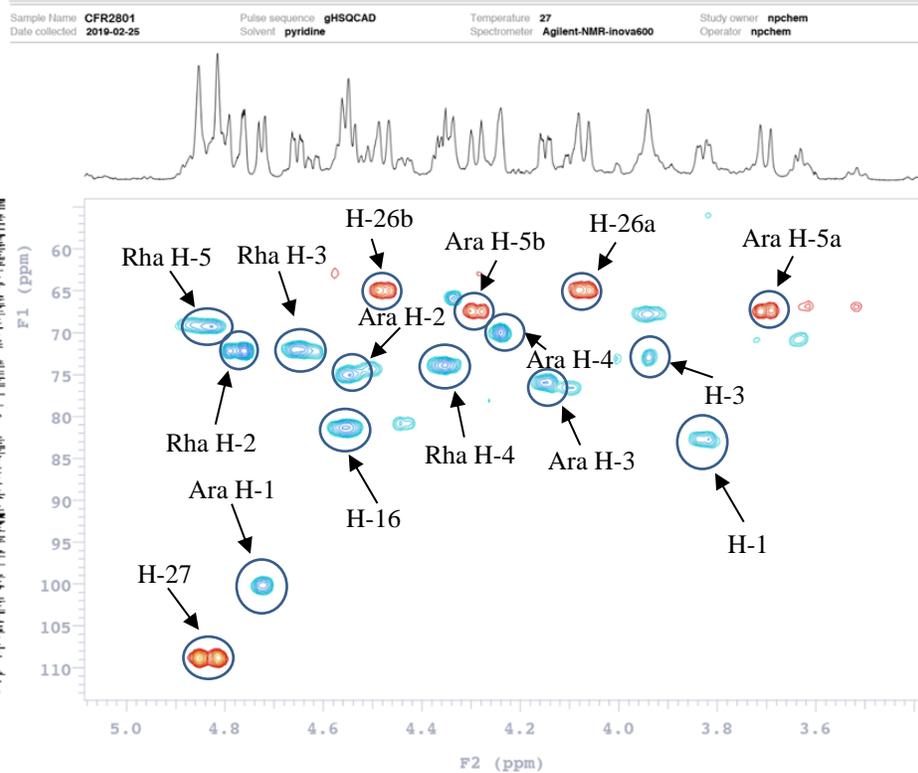
Figure 113. HSQC spectrum of sugar moieties of compound **21**
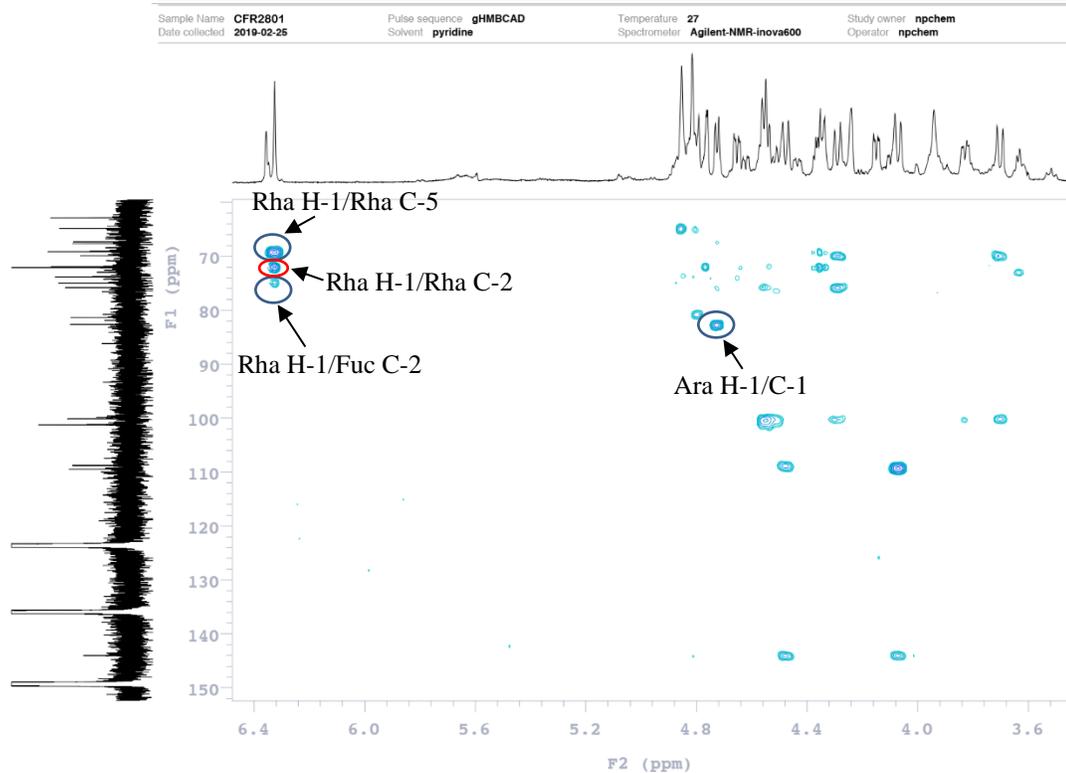
**Figure 114.** HMBC spectrum of sugar moieties of compound **21**
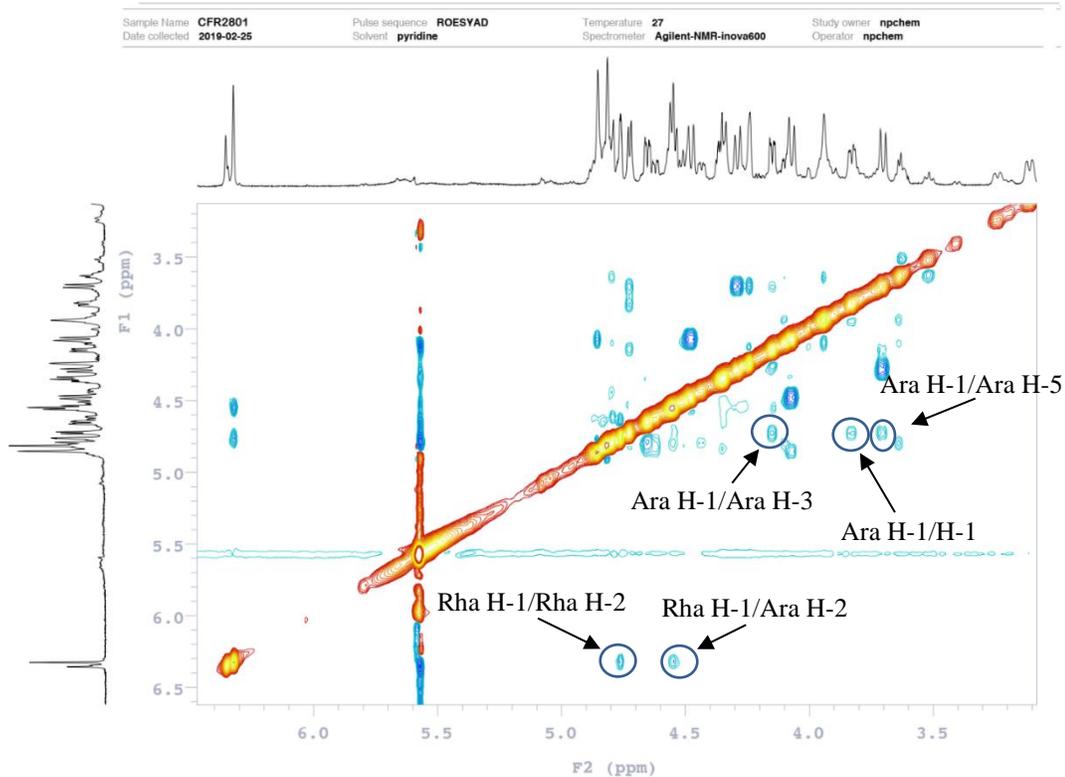
**Figure 115.** ROESY spectrum of sugar moieties of compound **22**
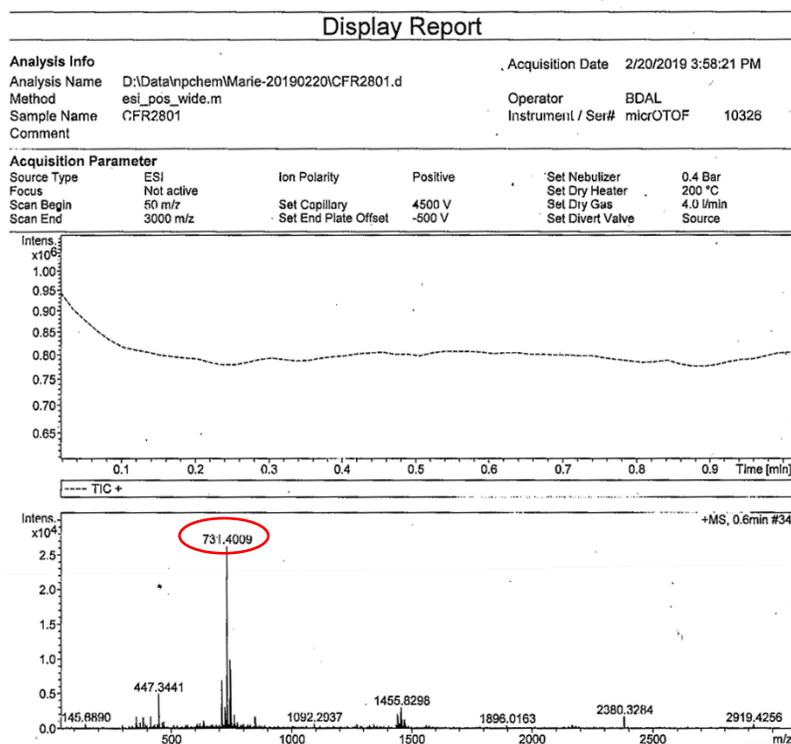
Figure 116. Mass spectrum of compound **22**

e. Compound 22 (CFR3R5)

Mass spectrometry

The HR-ESIMS (positive-ion mode) spectrum of compound **22** showed a pseudo-molecular ion peak [M+Na]$^+$ at *m/z* 761.4122, indicating a molecular weight of 738 and a molecular formula of $C_{39}H_{62}O_{13}$.

NMR spectroscopy

Structure of aglycon

The analysis of the NMR spectra of compound **22** showed that the aglycon was quite similar to compound **18**.

Structure of sugar moieties

The molecular weight of compound **22** differs from **18** by only 146 amu, corresponding to a supplementary pentosyl group. By 2D NMR analyses, two sugar units were identified as:

- 1 β-D-fucopyranosyl Fuc-1 at δ_H 4.72 (d, *J* = 7.6 Hz).

- 1 α-L-rhamnopyranosyl Rha-1 at δ_H 6.40 (br s).

The sequence of the oligosaccharide was established by analysing the HMBC and ROESY spectra:

- The HMBC correlation between δ_H 4.72 (Fuc H-1) and δ_C 82.4 (C-1) and in ROESY at δ_H 4.72 (Fuc H-1) and δ_H 3.94 (dd, *J* = 11.7, 3.5, H-1) revealed the glycosidic linkage of Fuc at the C-1 position of the aglycon. (**Fig.117**).

- The HMBC correlation between δ_H 6.40 (Rha H-1) and δ_C 74.4 (Fuc C-2) and in ROESY at δ_H 6.40 (Rha H-1) and δ_H 4.51 (dd, *J* = 9.4, 7.6 Hz, Fuc H-2) proved the (1→2) linkage between Rha and Fuc.

Conclusion

The structure of **22** was characterized as 5α-spirost-(25)27-ene-1β,3β,4α-triol-1-*O*-α-L-rhamnopyranosyl-(1→2)-β-D-fucopyranoside. The 3α-hydroxyl derivative was previously

isolated by enzymatic hydrolysis from the stems of *Dracaena concinna* (Mimaki et al., 1998b).
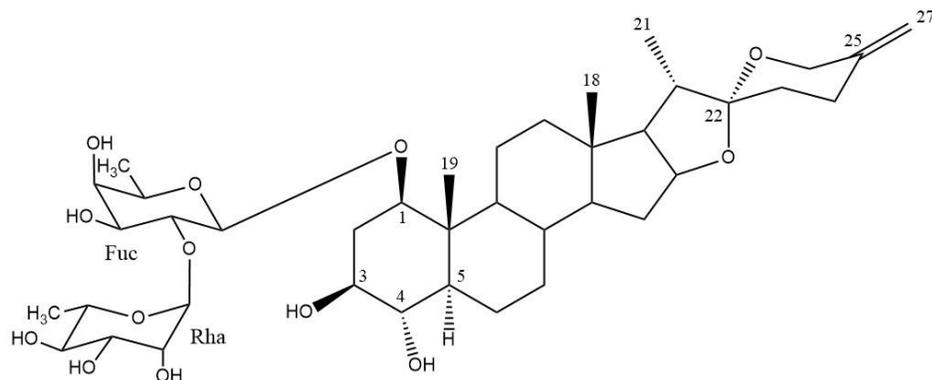
Figure 117. Structure of compound **22**
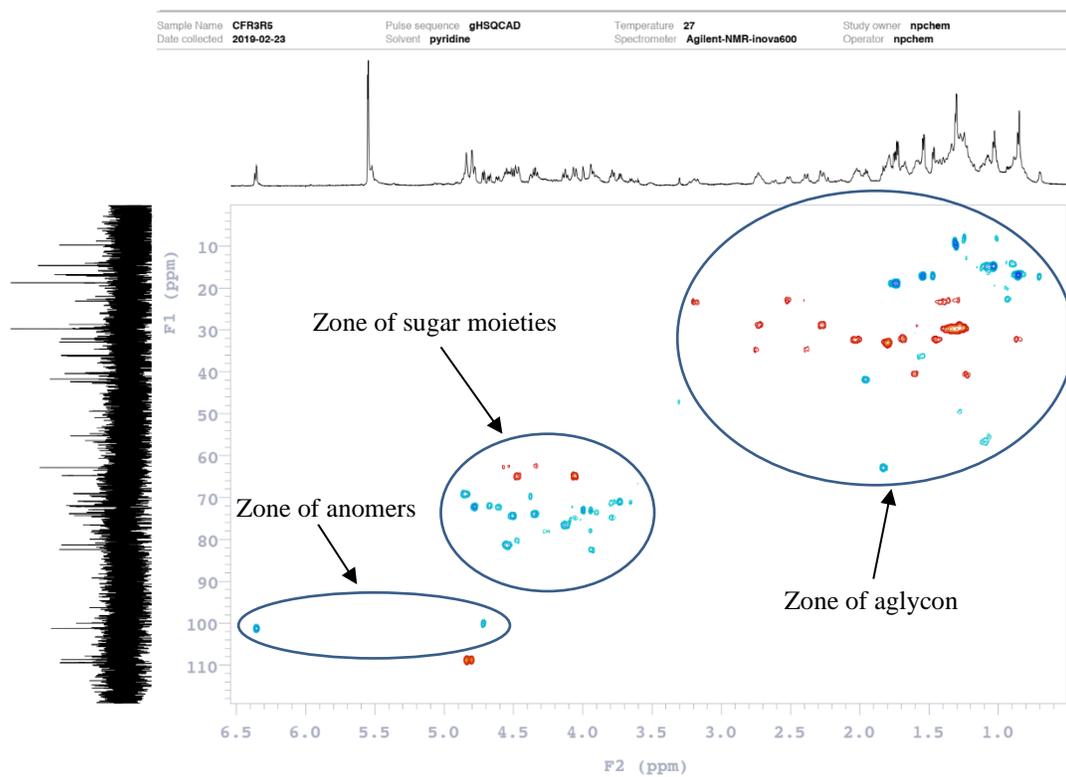
**Figure 118.** HSQC spectrum of compound **22**

124
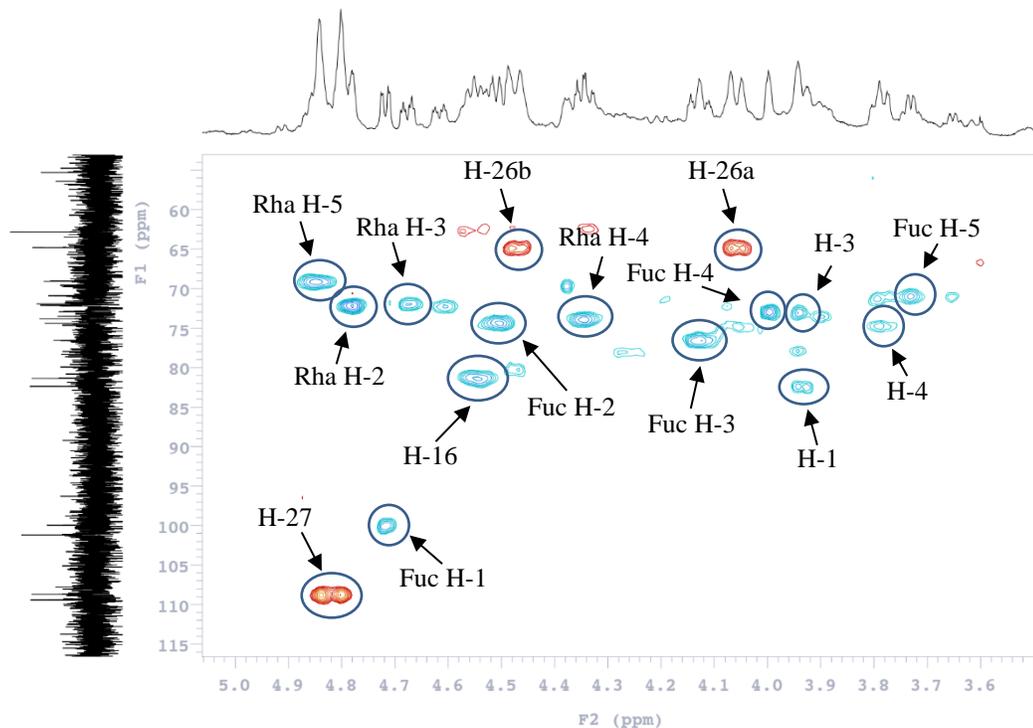
Figure 119. HSQC spectrum of sugar moieties of compound **22**
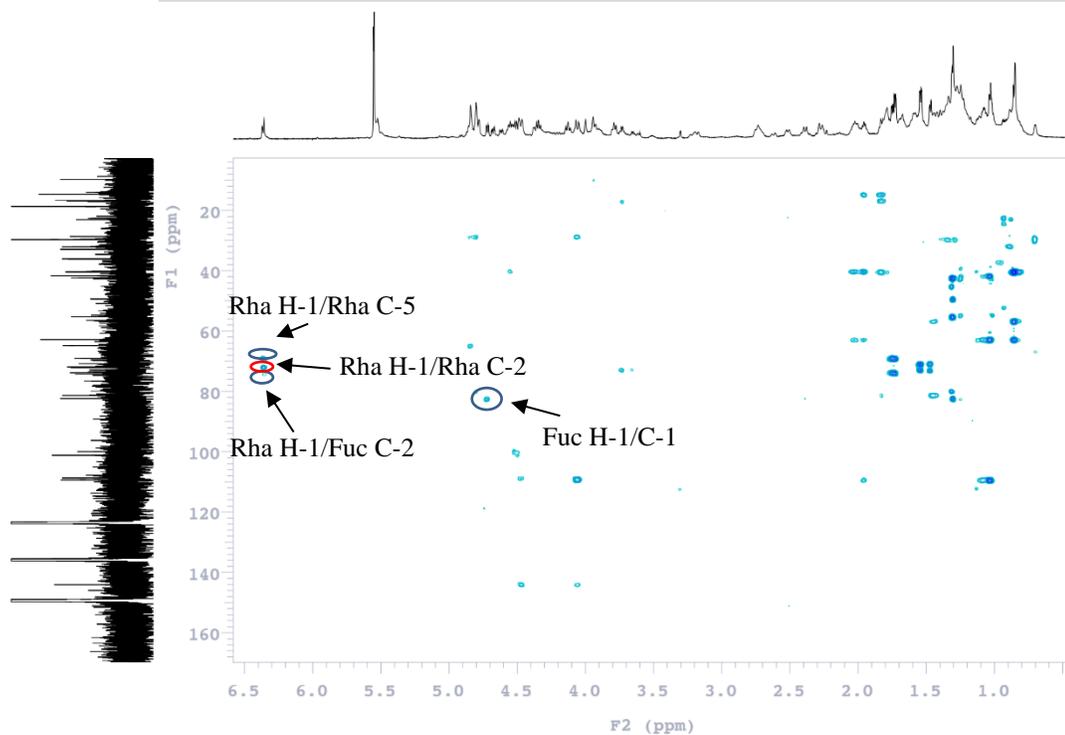
Figure 120. HMBC spectrum of sugar moieties of compound **22**
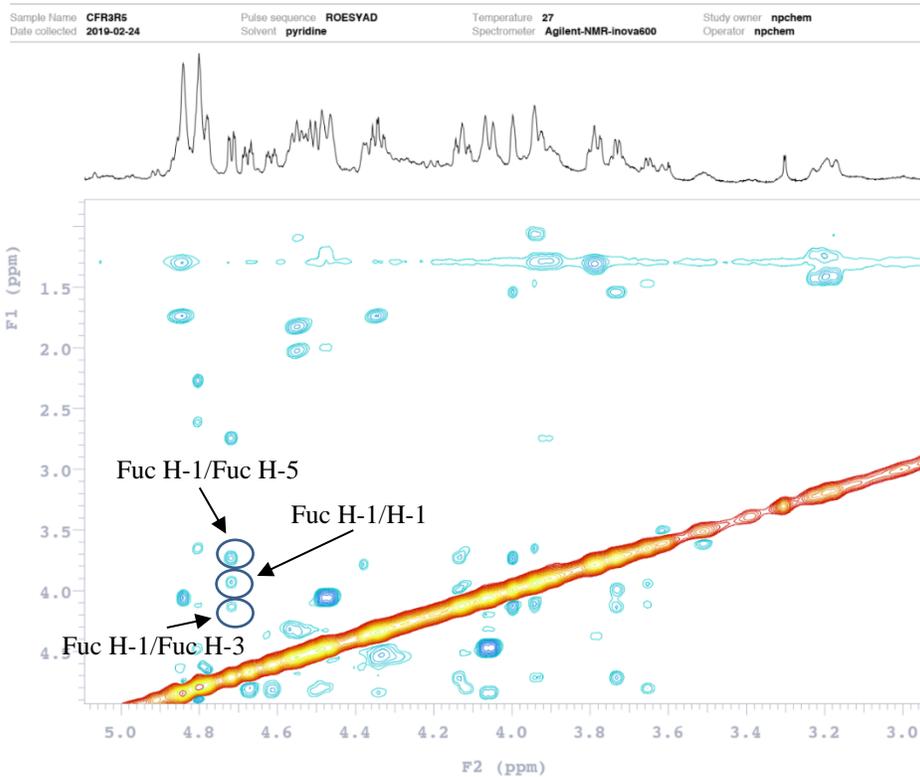
Figure 121. ROESY spectrum of sugar moieties of compound **22**
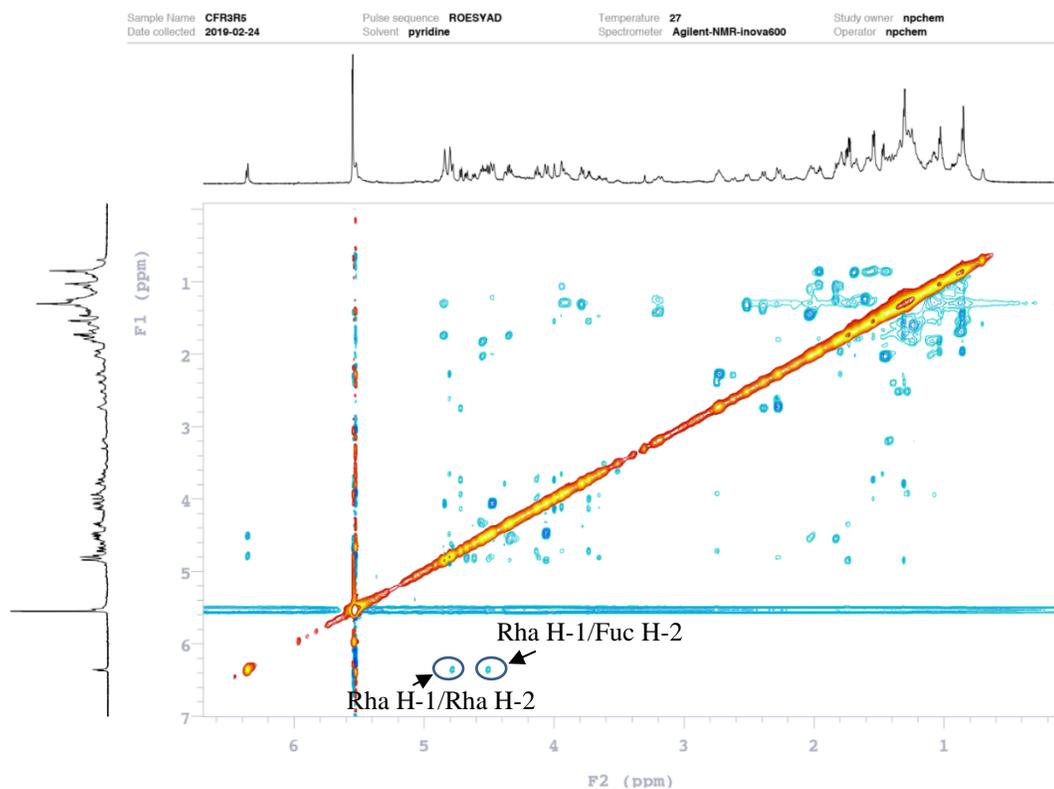
**Figure 122.** ROESY spectrum of sugar moieties of compound **22**
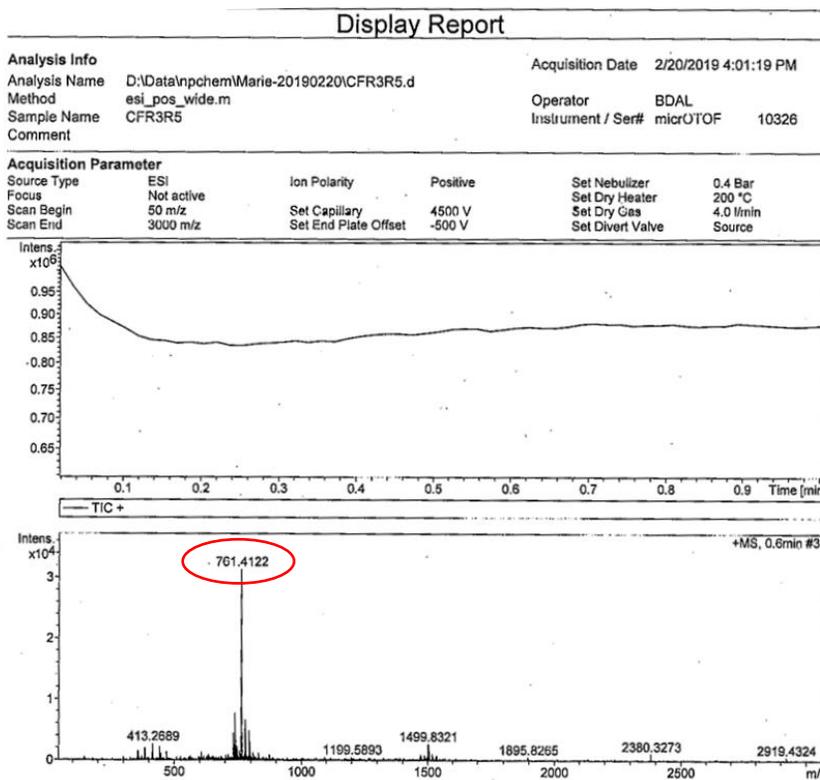
Figure 123. Mass spectrum of compound **22**

f. Compound 23 (CFR5A-1_1)

Mass spectrometry

The HR-ESIMS (positive-ion mode) spectrum of compound **23** showed a pseudo-molecular ion peak [M+2Na]$^+$ at 863.3419 *m/z*, indicating a molecular weight of 818 and a molecular formula of $C_{39}H_{62}O_{16}S$. This was confirmed by the ESIMS (negative-ion mode) spectrum with *m/z* 817.3706 [M–H]$^-$.

NMR spectroscopy

Structure of aglycon

The analysis of HSQC, HMBC and ROESY spectra of compound **23** showed that the aglycon was the same as **22**. (Table 8).

Structure of sugar moieties

The sugar part was shown to be similar to those of compound **22** using the correlations observed in the HMBC, COSY, TOCY and ROESY spectra as :

127

- 1 β-D-fucopyranosyl Fuc-1 at δ_H 4.70 (d, $J = 7.6$ Hz).

- 1 α-L-rhamnopyranosyl Rha-1 at δ_H 6.35 (br s).

The sequence of the oligosaccharide was established by analysing the HMBC and ROESY spectra:

- The HMBC correlation between δ_H 4.70 (Fuc H-1) and δ_C 82.2 (C-1) and in ROESY at δ_H 4.70 (Fuc H-1) and δ_H 3.92 (dd, $J = 11.7, 4.1$ H-1) proved that Fuc was attached to the C-1 position of the aglycon (Fig.124).

- The HMBC correlation between δ_H 6.35 (Rha H-1) and δ_C 75.5 (Fuc C-2) and in ROESY at δ_H 6.35 (Rha H-1) and δ_H 4.52 (dd, $J = 9.4, 7.6$ Hz, Fuc H-2) proved that Rha was attached to the Fuc at C-2.

- The downfield shifts observed in the HSQC spectrum at δ_H/δ_C 5.13 (br s, Fuc H-4)/78.3 (Fuc C-4) revealed that the hydroxy group at Fuc C-4 was substituted. The molecular weight of **23** (*m/z* 818) differs than **22** (*m/z* 738) by 80 amu corresponding to a SO_3H substituent (Fouedjou et al., 2013), which reveals a fucopyranosyl-4-sulfate.

Conclusion

The structure of **23** was characterized as 5α-spirost-(25)27-ene-1β,3β,4α-triol-1-*O*-α-L-rhamnopyranosyl-(1→2)-(4-*O*-sulfo)-β-D-fucopyranoside.
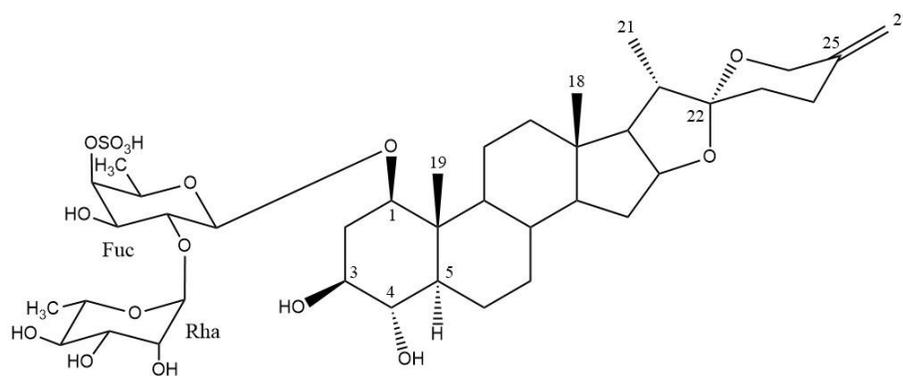
Figure 124. Structure of compound **23**

Zone of sugar moieties

Zone of anomers

Zone of aglycon
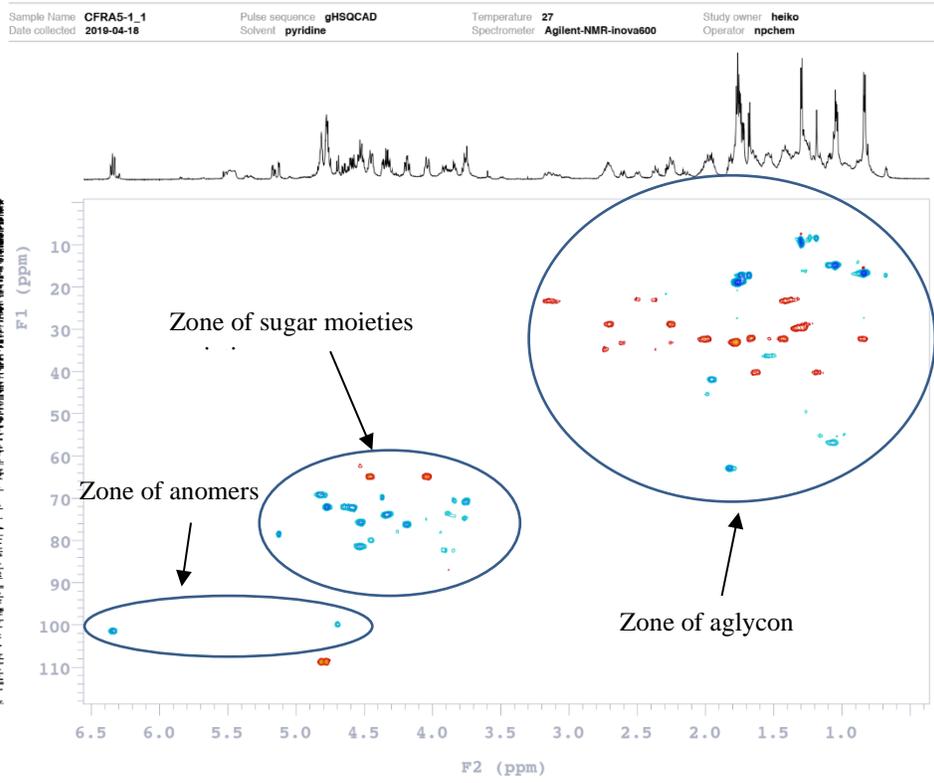
Figure 125. HSQC spectrum of compound **23**

Agly H-26b   Agly H-26a

Rha H-5

Rha H-3   Fuc H-5

Rha H-4

Rha H-2

Fuc H-2

Fuc H-4

Fuc H-3

Rha H-1

Agly H-16   Agly H-1

Agly H-27

Fuc H-1
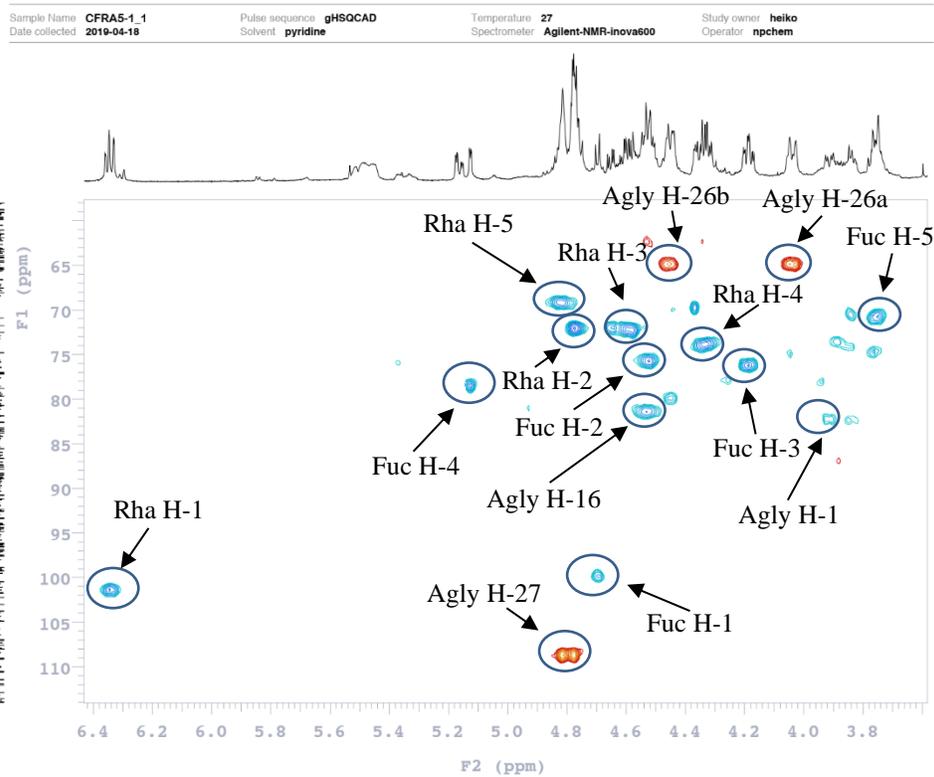
Figure 126. HSQC spectrum of sugar moieties of compound **23**

129
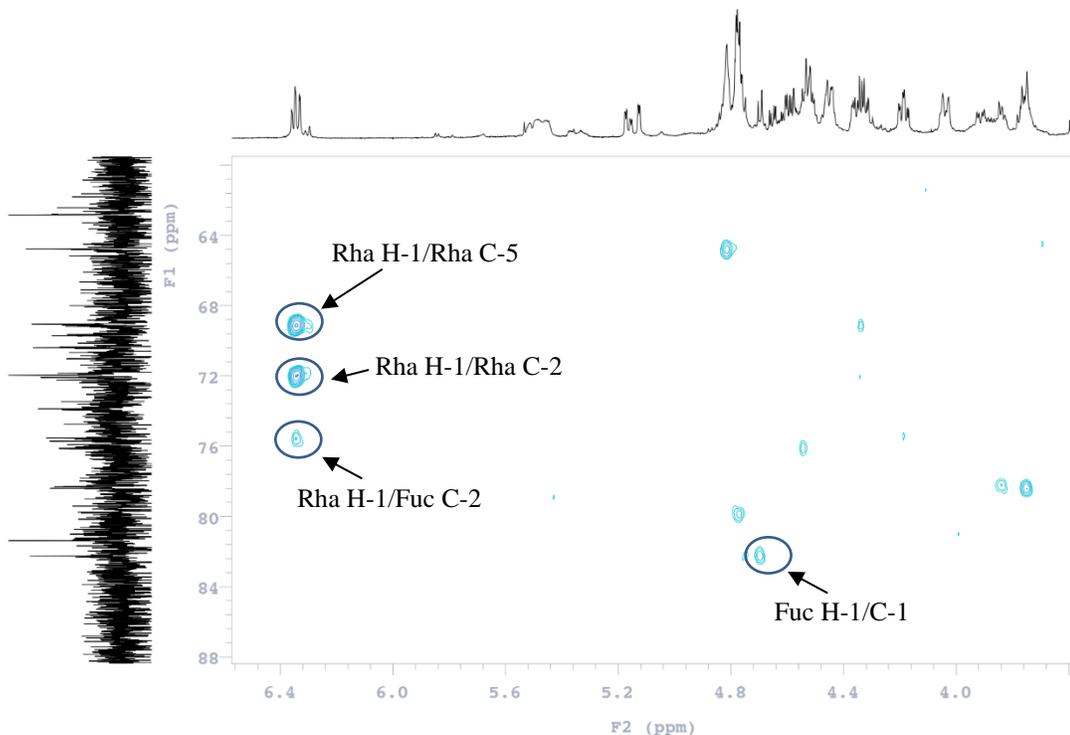
Figure 127. HSQC spectrum of sugar moieties of compound **23**
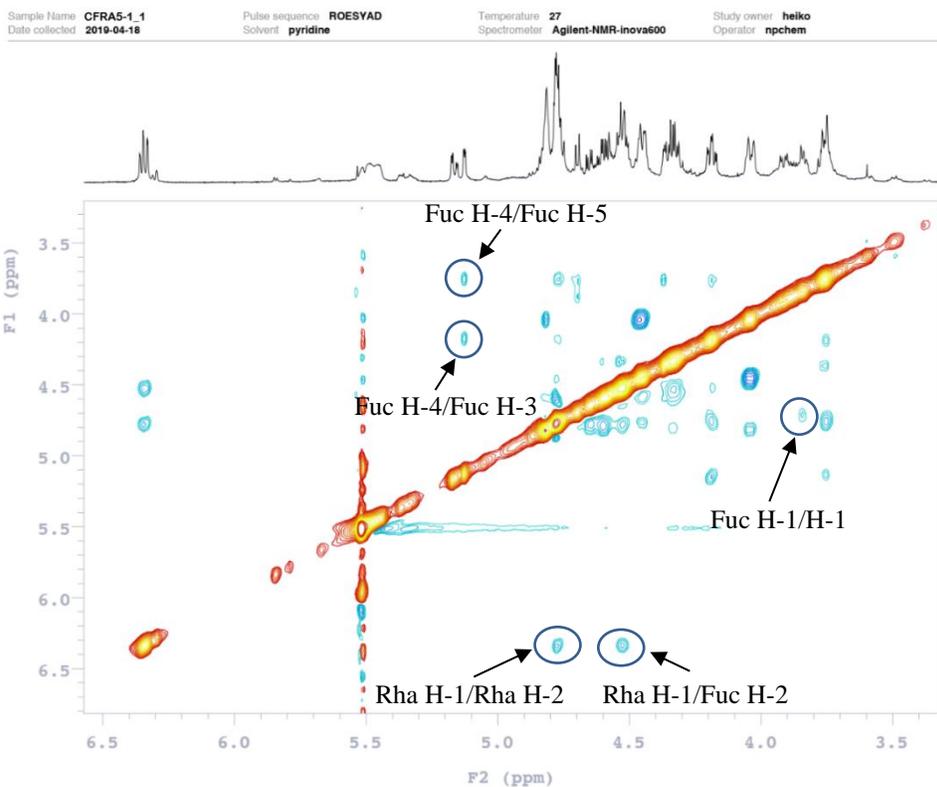
Figure 128. ROESY spectrum of sugar moieties of compound **23**

Mass Spectrum SmartFormula Report

Analysis Info

Analysis Name	D:\Data\npchem\Marie-20190514\CFRA5-1-neg.d		Acquisition Date	5/14/2019 11:15:12 AM
Method	esi_neg_low.m		Operator	BDAL
Sample Name	CFRA5-1		Instrument / Ser#	microTOF 10326
Comment				

Acquisition Parameter

Source Type	ESI	Ion Polarity	Negative	Set Nebulizer	0.4 Bar
Focus	Not active			Set Dry Heater	200 °C
Scan Begin	50 m/z	Set Capillary	3800 V	Set Dry Gas	4.0 l/min
Scan End	1500 m/z	Set End Plate Offset	-500 V	Set Divert Valve	Waste

-MS, 0.9min #56

817.3706

Meas. m/z   #   Formula   Score   m/z   err [mDa]   err [ppm]   mSigma   rdb   e⁻ Conf   N-Rule
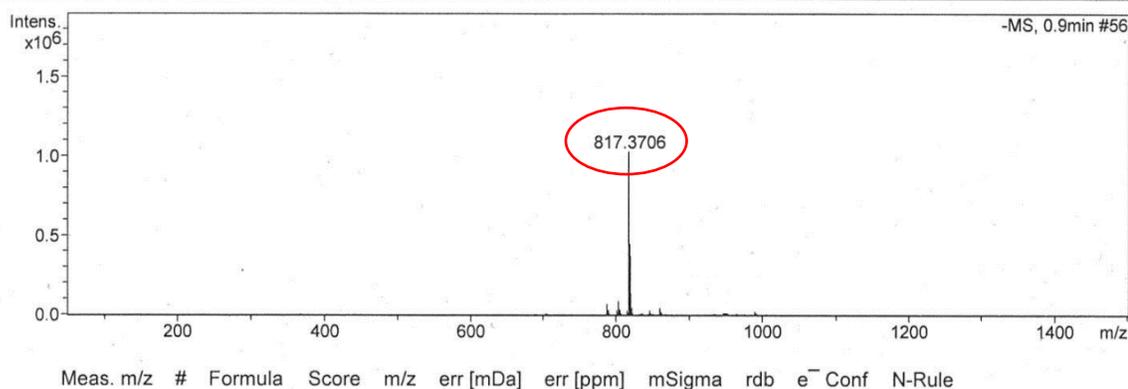
Figure 129. Mass spectrum of compound **23**

g. Compound 24 (CFR5A-1_2)

Mass spectrometry

For compound **24**, the ESIMS (negative-ion mode) spectrum showed a pseudo-molecular ion peak with *m/z* 947.4315 [M–H]⁻ indicating a molecular weight of 948 and a molecular formula of $C_{45}H_{72}O_{19}S$.

NMR spectroscopy

Structure of aglycon

The analysis of the NMR spectra of compound **24** showed that the aglycon was quite similar to those of compounds **23** (Table 8).

Structure of sugar moieties

The molecular weight of compound **24** differs from **23** by only 130 amu, corresponding to a supplementary hexosyl group. The part of the HSQC spectrum corresponding to the osidic chain showed cross-peaks at δ_H/δ_C 4.77 (d, *J* = 7.6 Hz)/99.7, 6.33 (br s)/101.3 and 5.54 (br

131

s)/100.2. After analysing the spectre of HSQC, HMBC, COSY, TOCSY and ROESY, the sugar moieties of compound **24** was identified as:

- 1 β-D-fucopyranosyl Fuc-1 at δ_H 4.70 (d, J = 7.6 Hz).

- 2 α-L-rhamnopyranosyl : Rha I-1 at δ_H 6.33 (br s) and Rha II-1 at δ_H 5.54 (br s)

The sequence of the oligosaccharide was established by analysing the HMBC and ROESY spectra:

- The HMBC correlation between δ_H 4.77 (Fuc H-1) and δ_C 79.8 (Agly C-1) and in ROESY at δ_H 4.77 (Fuc H-1) and δ_H 4.44 (H-1), proved that Fuc was attached to the C-1 position of the aglycon (Fig.130).

- The HMBC correlation between δ_H 6.33 (Rha I H-1) and δ_C 75.5 (Fuc C-2) and in ROESY at δ_H 6.33 (Rha H-1) and δ_H 4.52 (Fuc H-2) proved that Rha I was attached to the Fuc at C-2.

- The HMBC correlation between δ_H 5.54 (Rha II H-1) and δ_C 74.8 (C-3) and in ROESY at δ_H 5.54 (Rha II H-1) and δ_H 3.77 (H-3) proved that Rha I was attached to the C-3 position of the aglycon (Iwagoe et al., 1987; Tschesche et al., 1973)..

- The downfield shifts observed in the HSQC spectrum at δ_H/δ_C 5.16 (br s, Fuc H-4)/78.4 (Fuc C-4) revealed that the hydroxy group at Fuc C-4 was corresponded to a SO_3H substituent (Fouedjou et al., 2013).

Conclusion

The structure of **24** was determined as 5α-spirost-(25)27-ene-1β,3β-diol-1-*O*-α-L-rhamnopyranosyl-(1→2)-(4-*O*-sulfo)-β-D-fucopyranoside 3-*O*-α-L-rhamnopyranosyl ester.

Figure 130. Structure of compound **24**

Figure 131. HSQC spectrum of compound **24**

133

Figure 132. HSQC spectrum of sugar moieties of compound **24**


Figure 133. HMBC spectrum of sugar moieties of compound **24**

**Figure 134.** ROESY spectrum of sugar moieties of compound **24**

Figure 135. Mass spectrum of compound **24**

h. Compound 25 (CFRC2a)

Mass spectrometry

The HR-ESIMS (positive-ion mode) spectrum of compound **25** showed a pseudo-molecular ion peak $[M+Na]^+$ at *m/z* 795.4147, indicating a molecular weight of 772 and a molecular formula of $C_{41}H_{68}O_{17}$.

NMR spectroscopy

Structure of aglycon

The structure of aglycon was identified by analysing spectra NMR ^1H, ^{13}C, HSQC and HMBC. The ^1H and ^{13}C spectra of the aglycon part of **25** (Table 8) were very characteristic of furostanol glycoside which showed:

- 2 tertiary methyl protons at δ_H 0.82 (s, H$_3$-18), 1.06 (s, H$_3$-19) and a secondary methyl group at δ_H 1.05 (d, *J* = 7.0 Hz, H$_3$-21),

- 3 oxygen bearing methine proton signals at δ_H 3.99 (dd, *J* = 11.1, 3.5 Hz, H-1), 3.93 (H-3) and 3.72 (H-4) (Mimaki et al., 1998b).

- Exomethylene protons at δ_H 5.07 and 5.37 (H-27, each 1H, br s).

The ^{13}C NMR spectrum showed:

- 10 tertiary carbons (CH), 10 secondary carbons (CH$_2$), 3 primary carbons (CH$_3$) and 4 quaternary carbons (C).

- 8 characterisitic carbons of a 22-OH furostane-type genin at δ_C 40.5 (C-20), 15.9 (C-21), 110.2 (C-22), 37.5 (C-23), 27.8 (C-24), 146.5 (C-25), 71.9 (C-26) and 111.5 (C-27).

The ROESY correlation between δ_H/δ_H 3.99 (H-1)/1.05 (H$_3$-21) and the HMBC correlation at δ_H 1.06 (s, H$_3$-19)/δ_C 81.3 (C-1) revealed the location of a hydroxyl group at the C-1 position in a β-orientation. The downfield shift to δ_C 81.3 suggested a glycosidic linkage. The multiplicity of the H-2β at δ_H 2.17 as a quadruplet (*J* = 11.1 Hz) suggested an axial/axial coupling with H-1 and H-3 and hence an α-axial orientation of both H-1 and H-3. This was confirmed by ROESY cross-peaks at δ_H 3.99 (H-1)/δ_H 2.92 (H-2α), δ_H 2.92 (H-2α)/δ_H 3.93 (H-3) and at δ_H 3.93 (H-3)/δ_H 1.28 (H-5). The H-4 was defined as β-axial and thus the

hydroxyl group as α-equatorial through the ROESY correlation at δ_H 3.72 (H-4)/δ_H 1.06 (s, H$_3$-19). On the other hand, the configuration of hydroxyl group at C-22 was established to be α from the ROESY correlations between β-H-20 (δ_H 1.96) and H-23a (δ_H 2.29) and H-23b (δ_H 2.22) (Perrone et al., 2009).

Structure of sugar moieties

The ^{1}H NMR spectrum of compound **25** in the sugar region signals of two anomeric protons at δ_H/δ_C 4.83 (d, J = 7.6 Hz)/101.2 and δ_H/δ_C 4.91 (d, J = 7.6 Hz)/103.3 indicating the presence of two sugar units which were identified as:

- 1 β-D-fucopyranosyl Fuc-1 at δ_H 4.83 (d, J = 7.6 Hz).

- 1 β-D-glucopyranosyl Glc-1 at δ_H 4.91 (d, J = 7.6 Hz).

The sequence of the oligosaccharide was established by analysing the HMBC, TOCSY and ROESY spectra:

- The HMBC correlation between δ_H 4.83 (Fuc H-1) and δ_C 81.3 (C-1) and in ROESY at δ_H 4.83 (Fuc H-1) and δ_H 3.99 (dd, J = 11.7, 3.5 Hz, H-1) revealed the glycosidic linkage of Fuc at the C-1 position of the aglycon (Fig.136).

- The HMBC correlation between δ_H 4.91 (Glc H-1) and δ_C 71.9 (C-26) and in ROESY at δ_H 4.91 (Glc H-1)/δ_H 4.40 (br d, J = 12.3 Hz, H-26) proved that Glc was linked to the C-26 position of the aglycon.

Conclusion

All the evidences above revealed the structure of compound **25** was 26-*O*-β-D-glucopyranosyl-5α-furost-(25)27-ene-1β,3β,4α,22α,26-pentol-1-*O*-β-D-fucopyranoside.
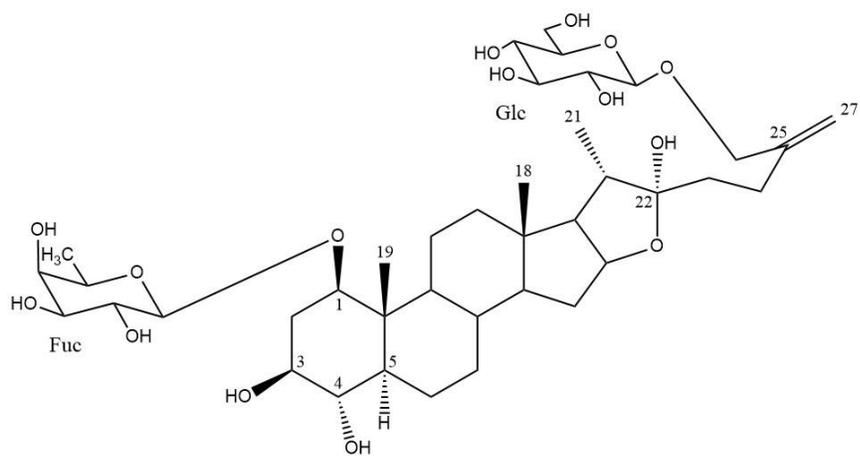
Figure 136. Structure of compound **25**
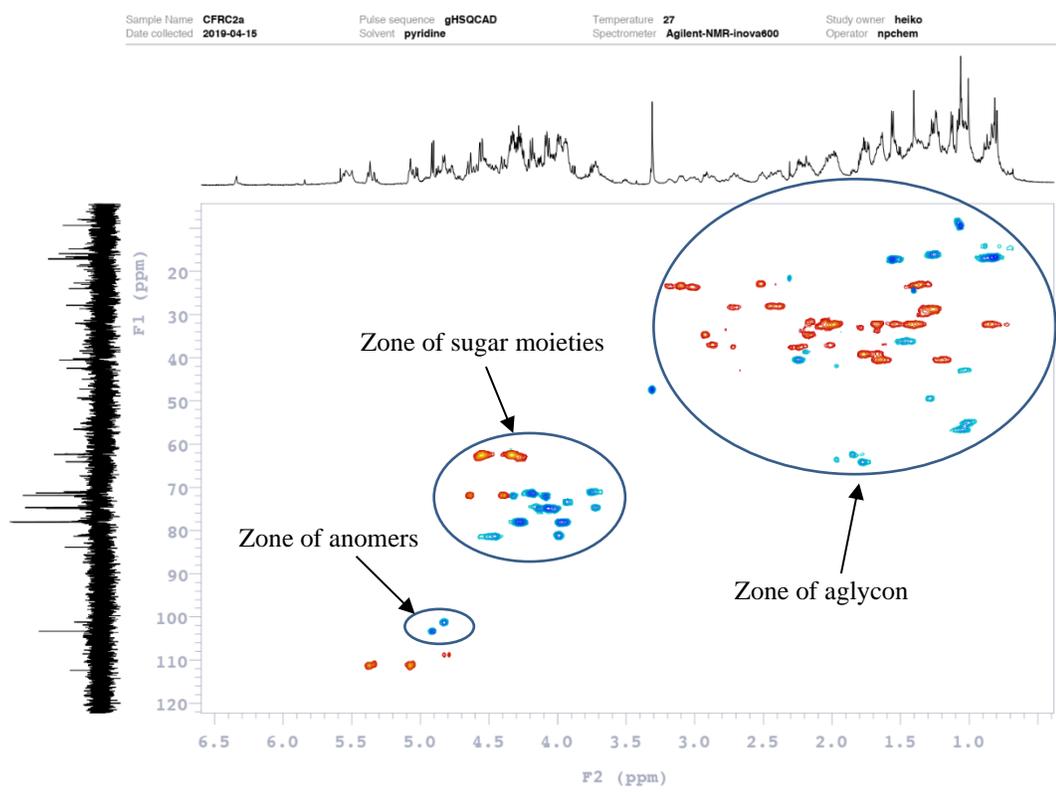
Figure 137. HSQC spectrum of compound **25**

138
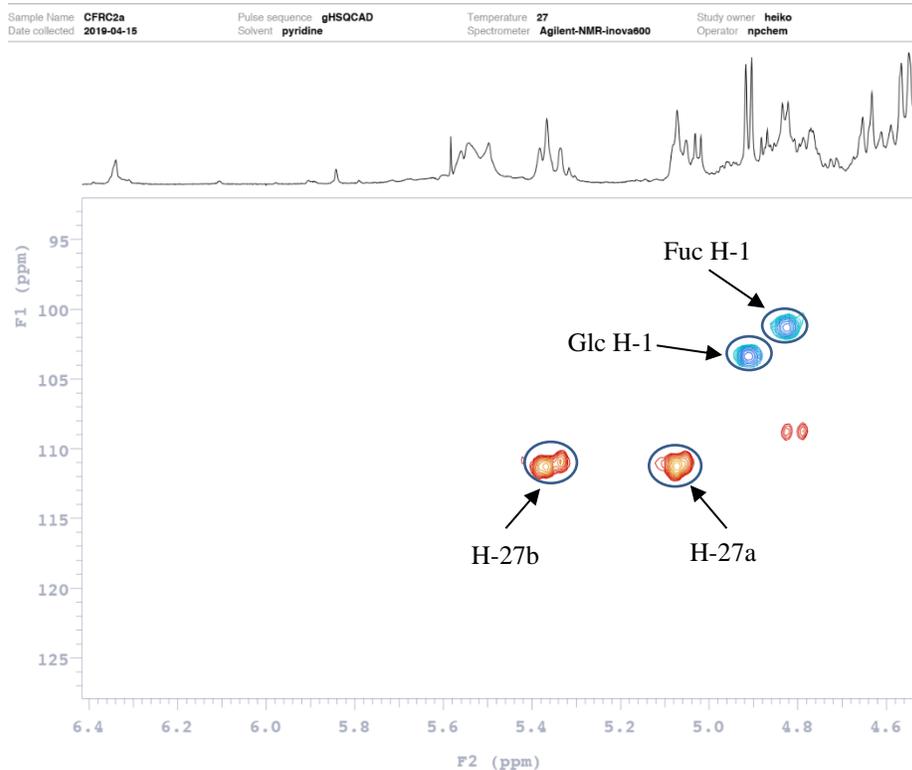
Figure 138. HSQC spectrum of sugar anomers of compound **25**

Figure 139. HSQC spectrum of sugar moieties of compound **25**

Figure 140. HMBC spectrum of sugar moieties of compound **25**

Figure 141. ROESY spectrum of sugar moieties of compound **25**

Figure 142. Mass spectrum of compound **25**

i. Compound 26 (CFRC2b)

The HR-ESIMS (positive-ion mode) spectrum of compound showed a pseudo-molecular ion peak [M+Na]$^+$ at 801.3369 *m/z*, indicating a molecular weight of 786 and a molecular formula of $C_{40}H_{66}O_{15}$. It was apparent from the NMR data (^{1}H, ^{13}C, HSQC, COSY, TOCSY, HMBC, ROESY) of compound **25** and **26** supported by the difference of their molecular weights by only 14 amu corresponding to the presence of a methoxy group instead of a hydroxy group at C-22. This assignment was confirmed by HMBC correlations at δ_H 3.31 (s)/δ_C 112.4 (C-22) and δ_H 1.12 (d, *J* = 6.4 Hz, H-21)/δ_C 112.4 (C-22). The configuration of the OCH$_3$ at the C-22 was identified as an α-orientation by the ROESY correlation at δ_H 3.31 (OCH$_3$)/δ_H 4.46 (q, *J* = 7.0 Hz, H-16). On the basis of these results, the structure of compound **26** was elucidated as 26-*O*-β-D-glucopyranosyl-22α-methoxy-5α-furost-(25)27-ene-1β,3β,4α,26-tetrol-1-*O*-β-D-fucopyranoside.
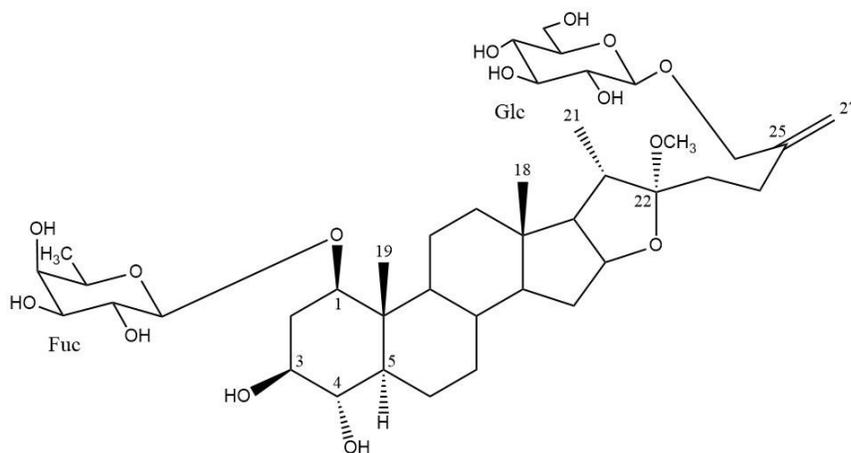
Figure 143. Structure of compound **26**

Figure 144. HSQC spectrum of compound **26**

Figure 145. HSQC spectrum of sugar anomers of compound **26**

Sample Name **CFRC2b**
Date collected **2019-04-16**
Pulse sequence **gHSQCAD**
Solvent **pyridine**
Temperature **27**
Spectrometer **Agilent-NMR-inova600**
Study owner **heiko**
Operator **npchem**

Figure 146. HSQC spectrum of sugar moieties of compound **26**

Sample Name **CFRC2b**
Date collected **2019-04-16**
Pulse sequence **gHMBCAD**
Solvent **pyridine**
Temperature **27**
Spectrometer **Agilent-NMR-inova600**
Study owner **heiko**
Operator **npchem**

Figure 147. HMBC spectrum of sugar moieties of compound **26**

Figure 148. ROESY spectrum of sugar moieties of compound **26**

Figure 149. Mass spectrum of compound **26**

j. Compound 27 (CFR3-3f)

For compound **27**, the HR-ESIMS (positive-ion mode) spectrum showed a pseudo-molecular ion peak [M+Na]$^+$ at *m/z* 891.4748, indicating a molecular weight of 868 and a molecular formula of C$_{45}$H$_{72}$O$_{16}$. By working on literature data, the structure of **27** was identified as 5α-spirost-(25)27-ene-1β,3β-diol-1-*O*-α-L-rhamnopyranosyl-(1→2)-β-D-fucopyranoside 3-*O*-α-L-rhamnopyranosyl ester. This spirostanol glycoside was previously isolated from the roots of *Convallaria majalis* L. (Tschesche et al., 1973).
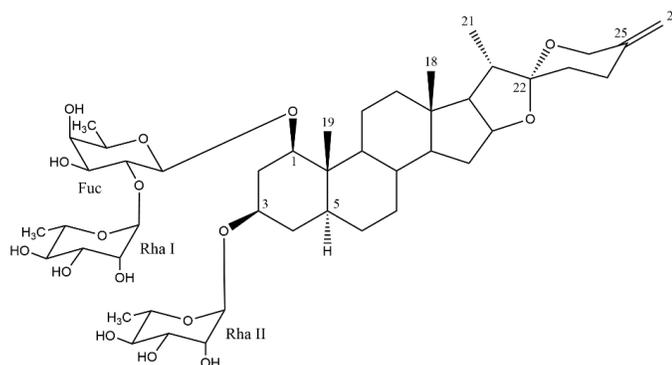

Figure 150. Structure of compound **27**

k. Compound 28 (CFRCR-2)

The HR-ESIMS (positive-ion mode) spectrum of compound **28** showed a pseudo-molecular ion peak [M–H]$^-$ at 801.3732 *m/z*, indicating a molecular weight of 802 and a molecular formula of C$_{39}$H$_{62}$O$_{15}$S. According to literature data, the structure of **28** was identified as 5α-spirost-(25)27-ene-1β,3β-diol-1-*O*-α-L-rhamnopyranosyl-(1→2)-(4-*O*-sulfo)-β-D-fucopyranoside, isolated from the leaves of *Cordyline fruticosa* (L) A. Chev. (Fouedjou et al., 2013).
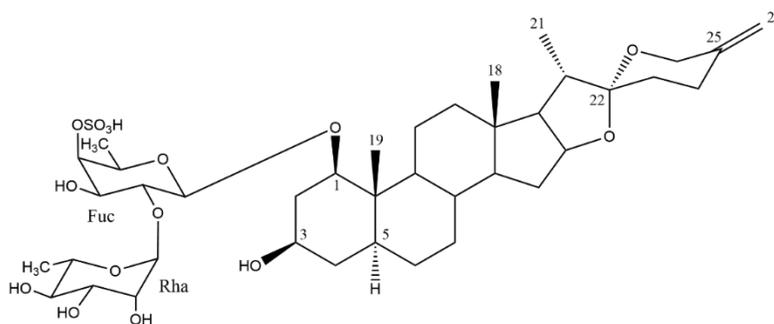
Figure 151. Structure of compound **28**

Table 8. ^{13}C and ^{1}H NMR spectroscopic data of the aglycon moieties of **18-26** in pyridine-d_5 (δ in ppm, J in Hz)

	18 CFR3b1		19 CFR3b3		20 CFR3b4		21 CFR2801		22 CFR3R5		23 CFRA5-1_1		24 CFRA5-1_2		25 CFRC2a		26 CFRC2b	
	δ_C	δ_H	δ_C	δ_H	δ_C	δ_H	δ_C	δ_H	δ_C	δ_H	δ_C	δ_H	δ_C	δ_H	δ_C	δ_H	δ_C	δ_H
1	81.2	4.00 dd (11.7, 4.1)	80.9	4.00 dd (11.7, 4.1)	83.1	3.80 dd (11.7, 3.5)	82.2	3.87 dd (11.7, 3.5)	82.4	3.94 dd (11.7, 3.5)	82.2	3.92 dd (11.7, 4.1)	79.8	4.44 dd (11.7, 4.1)	81.3	3.99 dd (11.1, 3.5)	81.1	4.00 dd (11.1, 3.5)
2	34.6	2.18 q (11.7) 2.93 dt (11.7, 4.1)	34.3	2.18 q (11.7) 2.92 dt (11.7, 4.1)	37.4	2.24 q (11.7) 2.72	35.5	2.16 q (11.7) 2.79	34.6	2.39 q (11.7) 2.75 dt (11.7, 4.1)	34.8	2.36 q (11.7) 2.74	33.1	2.25 q (11.7) 2.60	34.6	2.17 q (11.1) 2.92	34.7	2.17 q (11.1) 2.92
3	73.3	3.94 td (11.7, 4.1)	73.2	3.94 td (11.7, 4.1)	67.7	3.94 tt (8.4, 6.4)	73.0	3.94	72.8	3.94 td (11.7, 4.1)	73.5	3.89	74.8	3.77	73.4	3.93	73.3	3.92
4	74.7	3.72 t (11.7)	74.7	3.73 t (11.7)	39.2	1.74, 1.77	39.0	1.69, 1.75	74.7	3.79	74.7	3.76	39.0	1.69, 1.75	74.7	3.72	74.7	3.71
5	49.3	1.29	49.5	1.30	42.9	1.05	42.5	0.99	49.4	1.28	49.3	1.26	42.5	0.98	49.3	1.28	49.4	1.28
6	29.7	1.26, 1.33	29.7	1.26, 1.33	29.7	1.26, 1.33	29.7	1.28, 1.32	29.7	1.24, 1.34	29.7	1.28, 1.34	29.7	1.28, 1.34	28.8	1.26, 1.32	29.7	1.29, 1.33
7	32.0	0.86, 1.68	32.0	0.86, 1.68	32.2	0.85, 1.56	32.2	0.84, 1.54	32.1	0.85, 1.68	32.1	0.84, 1.66	32.1	0.84, 1.66	32.0	0.84, 1.67	32.1	0.83, 1.67
8	36.0	1.50 m	36.0	1.47 m	36.4	1.54 m	36.2	1.52 m	36.1	1.56 m	36.2	1.52 m	36.2	1.52 m	36.1	1.46 m	35.9	1.48 m
9	55.2	1.04	55.0	1.02	55.0	1.02	54.9	1.01	55.3	1.07	55.3	1.16	55.3	1.16	55.2	1.02	55.2	1.02
10	42.4	–	42.4	–	41.3	–	41.3	–	42.4	–	42.4	–	42.4	–	42.4	–	42.4	–
11	23.2	1.36 3.12 dd (13.2, 3.0)	23.3	1.40 3.03 dd (13.4, 3.0)	23.4	1.41 3.19 dd (13.4, 3.0)	23.6	1.44, 3.14	23.1	1.40 3.18 dd (12.9, 3.0)	23.1	1.42, 3.14	23.1	1.42, 3.14	23.2	1.36, 3.10	23.1	1.36, 3.10
12	40.5	1.20, 1.65	40.8	1.16, 1.62	40.4	1.24, 1.60	40.4	1.20, 1.60	40.4	1.23, 1.60	40.2	1.18, 1.63	40.2	1.18, 1.63	40.5	1.20, 1.64	40.5	1.20, 1.66
13	40.2	–	40.2	–	40.2	–	40.2	–	40.2	–	40.1	–	40.1	–	40.2	–	40.3	–
14	56.6	1.10	56.5	1.07	56.8	1.14	56.7	1.12	56.4	1.10	56.8	1.06	56.8	1.06	56.5	1.05	56.5	1.04
15	32.1	1.44 td (12.7, 5.8) 2.03 td (11.4, 5.8)	32.1	1.46 td (12.3, 5.8) 2.05 td (12.3, 5.8)	32.1	1.46 td (12.6, 5.8) 2.06 td (11.7, 5.8)	32.1	1.44, 2.05	32.2	1.45, 2.02	32.2	1.42, 2.00	32.2	1.42, 2.00	32.0	1.40, 1.98	32.1	1.39, 1.98
16	81.3	4.56 q (7.0)	81.4	4.57 q (7.0)	81.3	4.56 q (7.3)	81.3	4.56 q (7.0)	81.4	4.55 q (7.0)	81.4	4.54 q (7.0)	81.4	4.54 q (7.0)	81.4	4.46 q (7.0)	81.3	4.44 q (7.0)
17	62.9	1.83 dd (7.0, 6.4)	62.9	1.83 overlapped	62.9	1.84 dd (7.3, 6.6)	62.9	1.83	62.8	1.83	62.8	1.82	62.8	1.82	64.0	1.78	64.1	1.76
18	16.7	0.83 s	16.6	0.82 s	17.0	0.85 s	16.8	0.86 s	16.7	0.85 s	16.6	0.84 s	16.6	0.83 s	16.6	0.82 s	16.8	0.81 s
19	9.3	1.07 s	9.2	1.07 s	8.5	1.25 s	8.5	1.20 s	9.7	1.30 s	9.7	1.29 s	8.7	1.30 s	9.3	1.06 s	9.3	1.06 s
20	41.7	1.96 t (6.4)	41.9	1.97 t (6.4)	41.7	1.96 t (6.4)	41.8	1.96 t (6.4)	41.7	1.96 t (6.4)	41.7	1.95 t (7.0)	41.7	1.95 t (7.0)	40.5	1.96 t (7.0)	40.5	2.24 t (6.4)
21	14.7	1.06 d (6.4)	14.7	1.06 d (6.4)	14.7	1.03 d (6.4)	14.7	1.05 d (6.4)	14.7	1.03 d (6.4)	14.7	1.04 d (7.0)	14.7	1.04 d (7.0)	15.9	1.05 d (7.0)	16.0	1.12 d (6.4)
22	109.7	–	109.9	–	109.4	–	109.3	–	109.4	–	109.4	–	109.4	–	110.2	–	112.4	–

Pos.	δC	δH	δC	δH	δC	δH	δC	δH	δC	δH	δC	δH	δC	δH	δC	δH	δC	δH
23	32.9	1.80, 1.81	32.9	1.83, 1.84	32.9	1.80, 1.81	33.0	1.81, 1.82	32.9	1.80, 1.81	32.9	1.77, 1.80	32.9	1.77, 1.80	37.5	2.22, 2.29	31.5	2.05, 2.16
24	28.7	2.28 br d (12.9) 2.73 m	28.6	2.32 br d (12.9) 2.76 m	28.7	2.28 br d (11.7) 2.73 m	28.8	2.28 br d (13.4) 2.74 m	28.7	2.27 br d (13.4) 2.72 m	28.7	2.25, 2.70	28.7	2.25, 2.70	27.8	2.38, 2.44	28.1	2.68, 2.70
25	144.0	–	144.0	–	144.1	–	144.2	–	144.1	–	144.1	–	144.1	–	146.5	–	146.9	–
26	64.8	4.07 br d (12.3) 4.48 br d (12.3)	64.9	4.10 br d (12.3) 4.49 br d (12.3)	64.8	4.06 br d (12.3) 4.48 br d (12.3)	65.0	4.08 br d (12.3) 4.47 br d (12.3)	64.8	4.06 br d (12.3) 4.48 br d (12.3)	64.8	4.04 br d (12.3) 4.45 br d (12.3)	64.8	4.04 br d (12.3) 4.45 br d (12.3)	71.9	4.40 br d (12.3) 4.63 br d (12.3)	71.8	4.37 br d (12.3) 4.62 br d (12.3)
27	108.7	4.81 br s 4.85 br s	108.9	4.84 br s 4.88 br s	108.7	4.81 br s 4.85 br s	108.8	4.82 br s 4.85 br s	108.7	4.80 br s 4.84 br s	108.6	4.78 br s 4.82 br s	108.6	4.78 br s 4.82 br s	111.5	5.07 br s 5.37 br s	111.4	5.04 br s 5.32 br s
OMe																	47.3	3.31 s

Overlapped proton signals are reported without designated multiplicity.

Table 9. ^{13}C and ^{1}H NMR spectroscopic data of the sugar moieties of **18-26** in pyridine-d_5 (δ in ppm, J in Hz)

	18 CFR3b1		19 CFR3b3		20 CFR3b4		21 CFR2801		22 CFR3R5		23 CFRA5-1_1		24 CFRA5-1_2		25 CFR2a		26 CFR2b	
	δ_C	δ_H	δ_C	δ_H	δ_C	δ_H	δ_C	δ_H	δ_C	δ_H	δ_C	δ_H	δ_C	δ_H	δ_C	δ_H	δ_C	δ_H
Fuc-1	101.2	4.83 d (7.6)			99.9	4.71 d (7.6)			100.0	4.72 d (7.6)	99.7	4.70 d (7.6)	99.7	4.77 d (7.6)	101.2	4.83 d (7.6)	101.2	4.82 d (7.6)
2	72.0	4.33 dd (9.4, 7.6)			74.4	4.49 dd (9.4, 7.6)			74.4	4.51 dd (9.4, 7.6)	75.5	4.52 dd (9.4, 7.6)	75.5	4.52 dd (9.4, 7.6)	72.0	4.33 dd (9.4, 7.6)	71.9	4.32 dd (9.4, 7.6)
3	74.9	4.13 dd (9.4, 3.5)			76.5	4.12 dd (9.4, 2.9)			76.5	4.13 dd (9.4, 2.9)	76.2	4.18	76.2	4.20	74.9	4.14 dd (9.4, 2.9)	74.9	4.12 dd (9.4, 2.9)
4	72.2	4.08 br d (3.5)			72.9	4.00 br d (2.9)			72.9	4.00 br d (2.9)	78.3	5.13 br s	78.4	5.16 br s	72.2	4.08 br d (2.9)	72.1	4.07 br d (2.9)
5	71.0	3.76 br q (6.4)			70.9	3.72 br q (6.4)			70.9	3.73 br q (6.4)	70.4	3.75	70.3	3.85	71.1	3.76 br q (6.4)	71.0	3.75 br q (6.4)
6	17.1	1.56 d (6.4)			17.0	1.54 d (6.4)			17.0	1.54 d (6.4)	17.1	1.68 d (6.4)	17.2	1.74 d (6.4)	17.1	1.56 d (6.4)	17.1	1.56 d (6.4)
Xyl-1			100.0	5.04 d (7.0)														
2			75.1	4.03 dd (7.0, 8.2)														
3			77.9	4.29 overlapped														
4			72.3	4.10														
5			67.5	3.75 t (11.1), 4.32 dd (11.1, 4.6)														
Ara-1							100.1	4.73 d (7.0)										
2							75.0	4.55										
3							75.8	4.15										
4							69.9	4.24										
5							67.3	3.70 dd (12.6, 0.5), 4.29										
Rha I-1					101.2	6.35 br s	101.3	6.32 br s	101.2	6.40 br s	101.3	6.35 br s	101.3	6.33 br s				
2					72.1	4.76 br s	72.1	4.78 br s	72.1	4.78 br s	72.1	4.78 br s	72.1	4.78 br s				
3					71.9	4.65 dd (9.4, 3.5)	71.9	4.67 dd (9.4, 2.9)	71.9	4.67 dd (9.4, 2.9)	72.1	4.60 dd (9.4, 3.5)	72.1	4.60 dd (9.4, 3.5)				

Position			C	H	C	H	C	H	C	H	C	H	C	H	C	H
4			73.8	4.36 dd (9.9, 9.4)	73.8	4.35 dd (9.9, 9.4)	73.8	4.35 dd (9.9, 9.4)	73.9	4.34 dd (9.9, 9.4)	73.9	4.34 dd (9.9, 9.4)				
5			69.2	4.84 dq (9.9, 6.4)	69.1	4.85 dq (9.9, 5.9)	69.1	4.85 dq (9.9, 5.9)	69.0	4.82 dq (9.9, 5.9)	69.0	4.82 dq (9.9, 5.9)				
6			18.8	1.75 d (6.4)	18.7	1.74 d (5.9)	18.7	1.74 d (5.9)	18.8	1.76 d (5.9)	18.8	1.76 d (5.9)				
Rha II-1											100.2	5.54 br s				
2											72.4	4.58 br s				
3											72.0	4.65 dd (9.4, 3.5)				
4											73.8	4.34 dd (9.9, 9.4)				
5											69.8	4.37 dq (9.9, 5.9)				
6											18.2	1.72 d (5.9)				
Glc-1													103.3	4.91 d (7.6)	103.4	4.87 d (7.6)
2													74.9	4.07	74.7	4.06
3													78.0	4.27	78.1	4.26
4													71.3	4.18	71.4	4.19
5													78.1	3.96	78.0	3.95
6													62.4	4.33 dd (12.3, 5.6) 4.55	62.4	4.33 dd (12.3, 5.6) 4.54

Overlapped proton signals are reported without designated multiplicity. Nd: Not determined

2.5. Phytochemical study of aerial parts of *Cordyline fruticosa* "Fairchild Red"

Phytochemical investigation on aqueous-ethanolic extract of the aerial parts of *Cordyline fruticosa* "Fairchild Red" led to the isolation of **4** previously undescribed steroidal glycosides (**29-32**).

2.5.1. Isolation and purification

The dried and powdered aerial parts of *Cordyline fruticosa* "Fairchild Red" (103.9 g) were submitted to microwaves three times with the solvent EtOH/H_2O (200 W, 60°C, 30 min, 75/35, 300 mL each). After filtration and evaporation, 15.3 g of the crude extract were obtained. An aliquot of the extract (7.5 g) was submitted to VLC (RP-18 silica gel, H_2O, EtOH/H_2O 50/50, EtOH) to give 3 fractions (A-C). Fraction B (1.9 g), rich in saponins, was fractionated by flash chromatography ($CHCl_3$/MeOH/H_2O 70/30/5) to give 2 fractions. The fraction rich in saponins was further separated using MPLC on silica gel 60 (15-40 µm, $CHCl_3$/MeOH/H_2O 80/20/2, 75/25/3) yielding compound **29** (14.0 mg) and **30** (6.3 mg). The remaining fractions were combined and chromatographed on successive MPLC on silica gel RP-18 (MeOH/H_2O 40/60→49/51) yielding compounds **31** (6.1 mg) and **32** (17.6 mg).
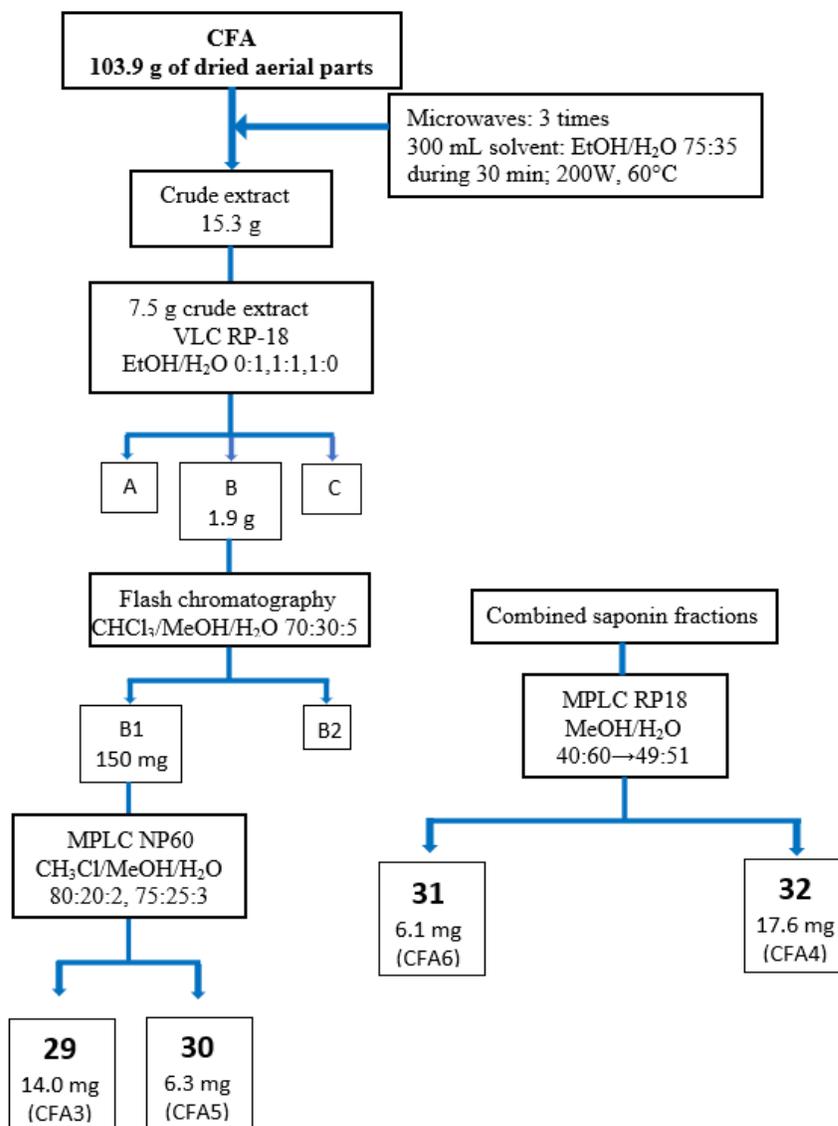
Figure 152. Purification of compounds in aerial parts of *C. fruticosa* "Fairchild Red"

2.5.2. Structural determination of isolated saponins

a. Compound 29 (CFA3)

Mass spectrometry

The HR-ESIMS (positive-ion mode) spectrum of compound **29** showed a pseudo-molecular ion peak [M+Na]$^+$ at *m/z* 795.4171, indicating a molecular weight of 772 and a molecular formula of $C_{39}H_{64}O_{15}$.

NMR spectroscopy

Structure of aglycon

The aglycon signals of **29** were quite superimposable to those of **25** with the exceptions of the signals due to the A ring carbons. The oxymethine signal at δ_C 74.7 (C-4) in **25** was replaced by a methylene carbon signal at δ_C 36.9, confirmed by the HSQC correlation at δ_C 36.9/δ_H 1.57, 1.63, and the shielded value of C-3 at δ_C 66.0. Based on these observations, the aglycon of **29** was characterized as 5α-furost-(25)27-ene-1β,3β,22α,26-tetrol.

Structure of sugar moieties

The monosaccharides were identified by acid hydrolysis and extensive 2D NMR analysis (COSY, TOCY, ROESY, HSQC, HMBC) as α-L-rhamnopyranosyl (Rha), β-D-fucopyranosyl (Fuc) and β-D-glucopyranosyl (Glc). The absolute configurations of the sugars were determined to be D for glucose (Glc) and fucose (Fuc), and L rhamnose (Rha), by GC analysis (see Section 1.3.4). The relatively large $^3J_{H-1,H-2}$ values of the Glc and Fuc (6.0-8.0 Hz) indicated a ß anomeric orientation for Glc and Fuc. The large $^3J_{H-1,C-1}$ values of the Rha (165-168 Hz), confirmed that the anomeric protons were equatorial (α-pyranoid anomeric form).

The HSQC spectrum of compound **29** in the sugar region indicates signals of two anomeric protons of two sugar units which were identified, using COSY, TOCSY, HMBC and ROESY spectra as:

- 2 β-D-glucopyranosyl: Glc I-1 at δ_H/δ_C 5.03 (d, J = 8.2 Hz)/100.1 and Glc II-1 at δ_H/δ_C 4.96 (d, J = 7.6 Hz)/104.6.

The sequence of the oligosaccharide was established by analysing the HMBC and ROESY spectra:

- The HMBC correlation between δ_H 5.03 (Glc I H-1) and δ_C 81.1 (C-1) and in ROESY at δ_H 5.03 (Glc I H-1) and δ_H 3.99 (dd, J = 11.7, 3.5 Hz, H-1) proved that Glc I was attached to the C-1 position of the aglycon (Fig.160).

- The HMBC correlation between δ_H 4.96 (Glc II H-1) and δ_C 73.9 (C-26) proved that Glc II was attached to the C-26 position of the aglycon.

Conclusion

All the evidences above revealed the structure of compound **29** was 26-*O*-β-D-glucopyranosyl-5α-furost-(25)27-ene-1β,3β,22α,26-tetrol-1-*O*-β-D-glucopyranoside.
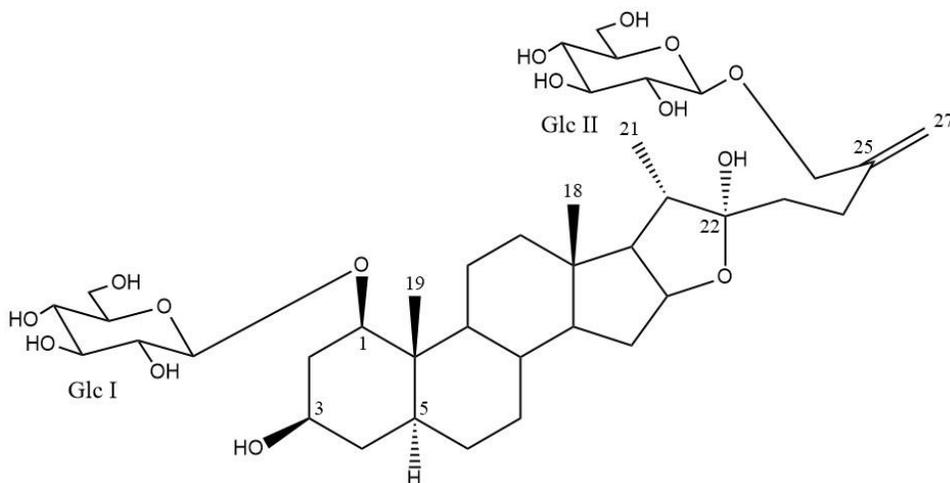
Figure 153. Structure of compound **29**
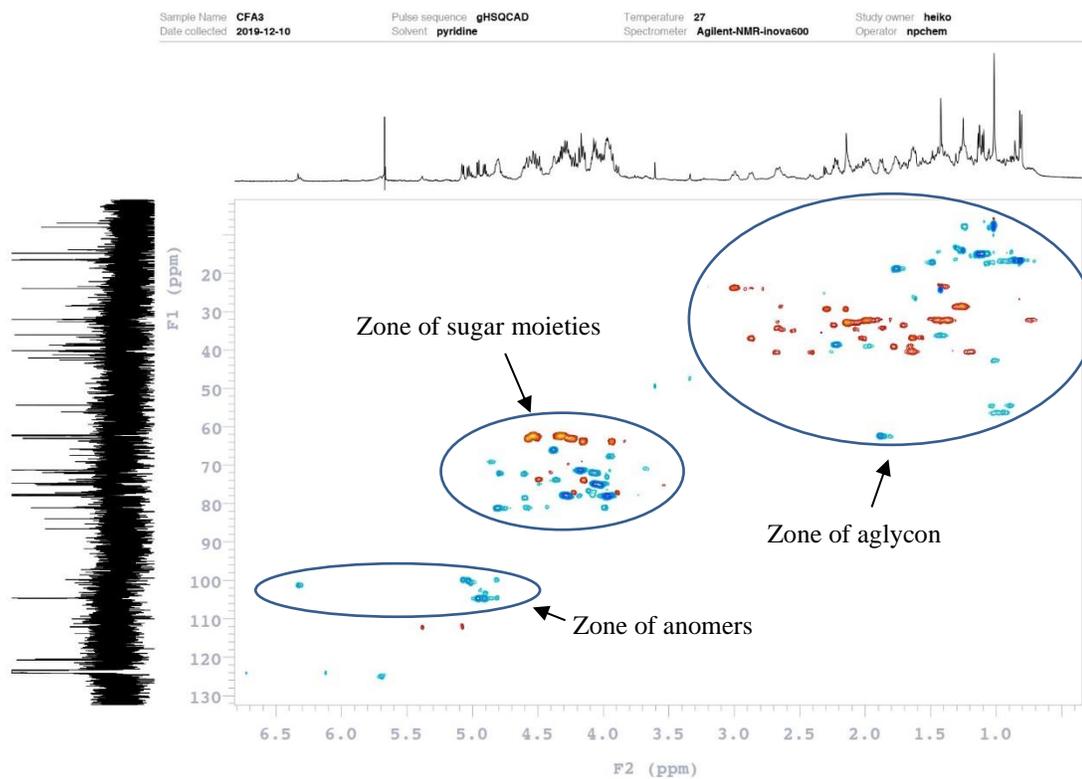
Figure 154. HSQC spectrum of compound **29**
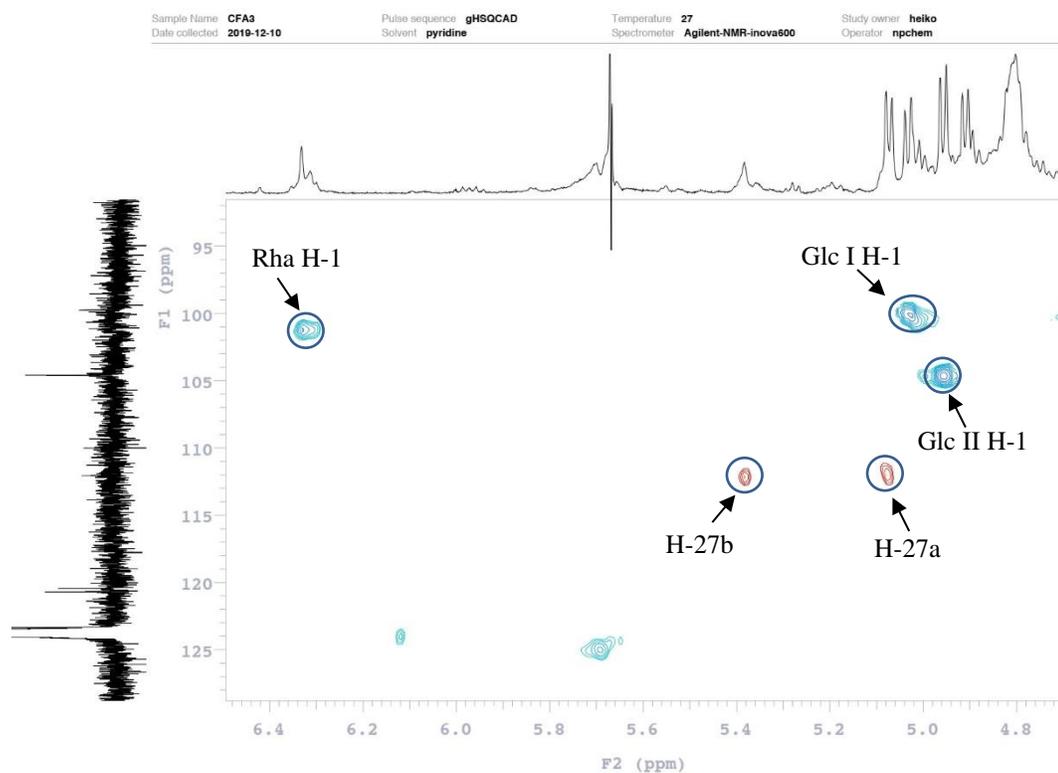
Figure 155. HSQC spectrum of sugar anomers of compound **29**
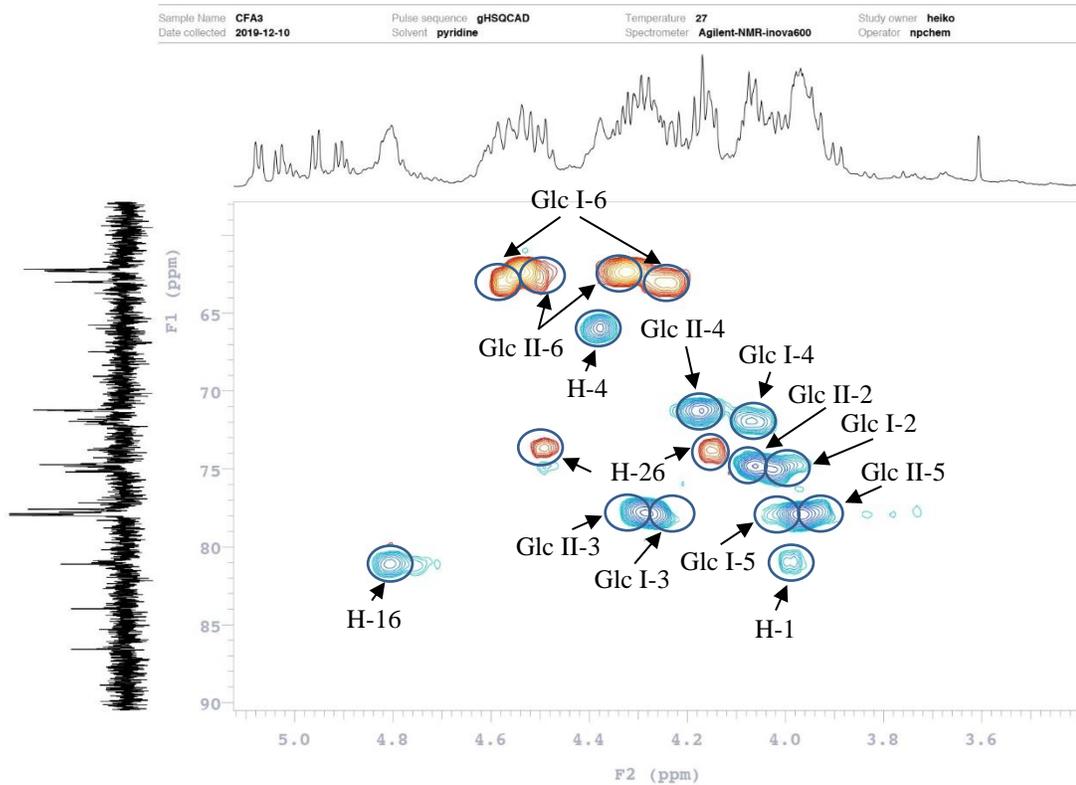
Figure 156. HSQC spectrum of sugar moieties of compound **29**
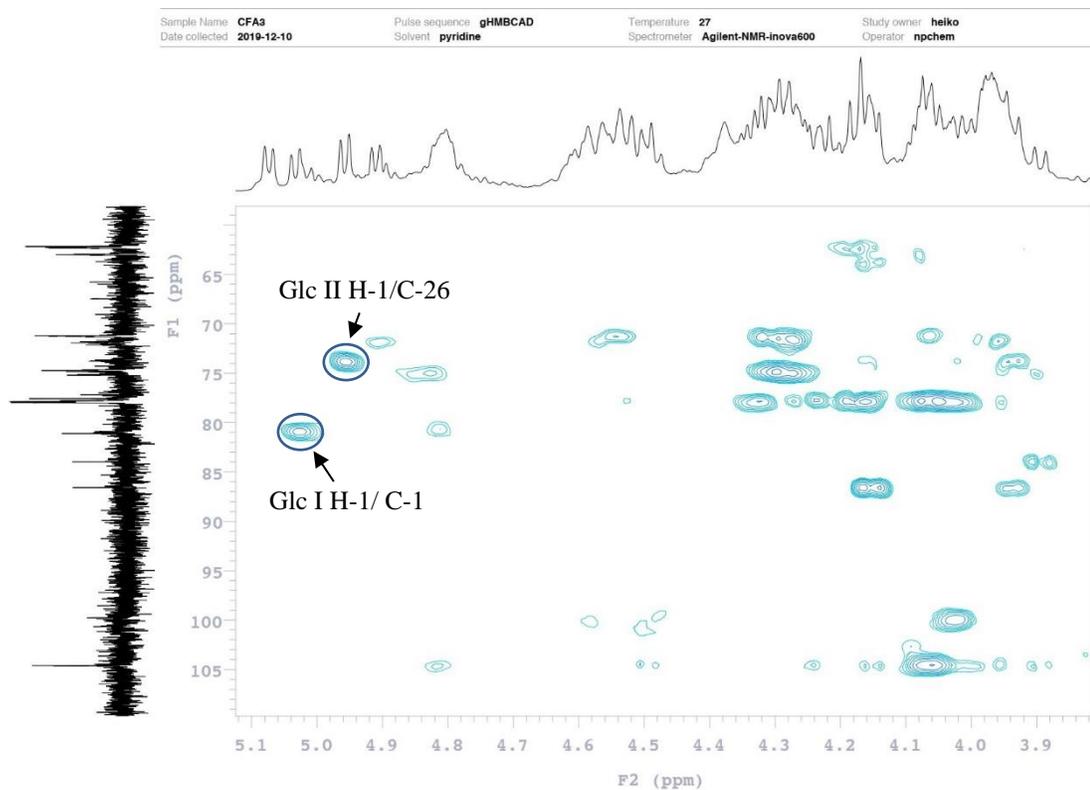
Figure 157. HMBC spectrum of sugar moieties of compound **29**
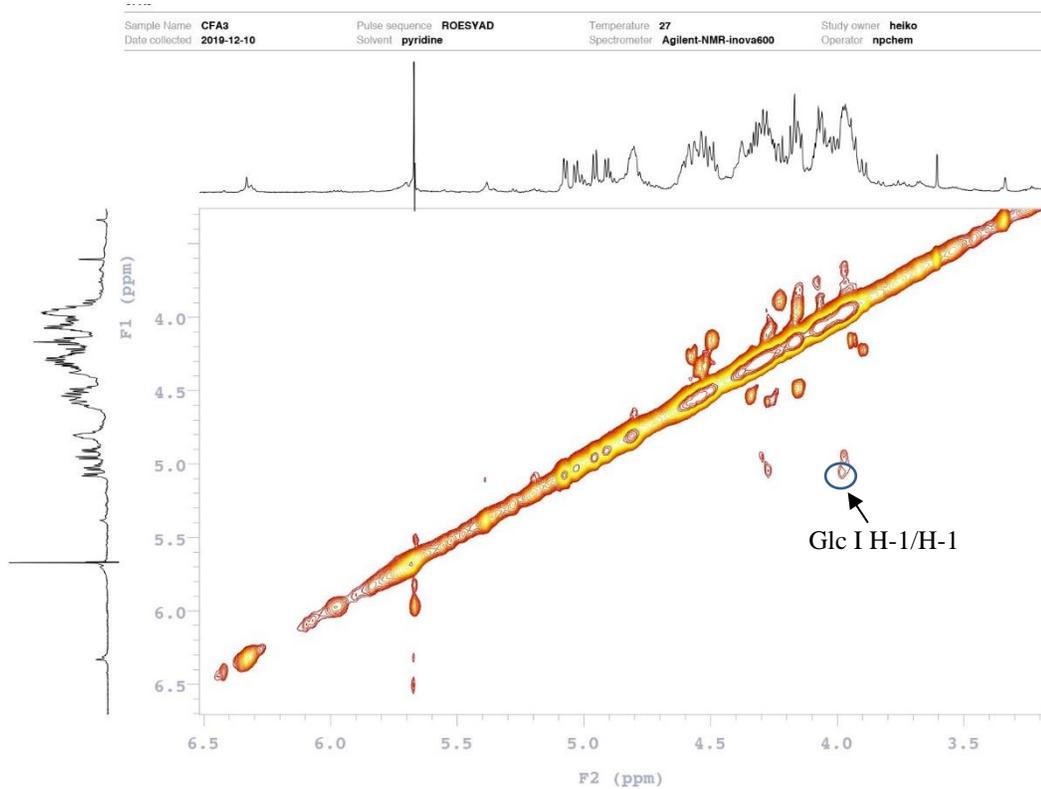
Figure 158. ROESY spectrum of sugar moieties of compound **29**
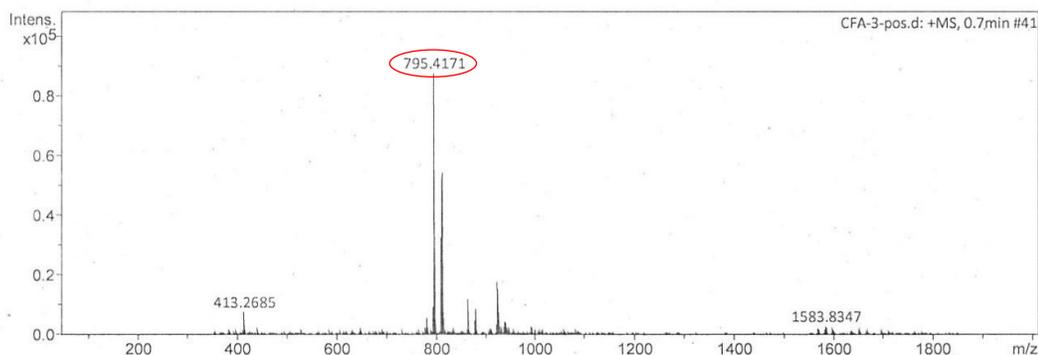
Figure 159. Mass spectrum of compound **29**

b. Compound 30 (CFA5)

Mass spectrometry

The HR-ESIMS (positive-ion mode) spectrum of compound **30** showed a pseudo-molecular ion peak [M+Na]$^+$ at *m/z* 941.4797, indicating a molecular weight of 918 and a molecular formula of $C_{45}H_{74}O_{19}$.

NMR spectroscopy

The molecular weight of compound **30** differs from **29** by only 146 amu, corresponding to a supplementary pentosyl group. The part of the HSQC spectrum corresponding to the anomeric signals showed cross-peaks at δ_H/δ_C 5.02 (d, *J* = 7.6 Hz)/100.0, δ_H/δ_C 6.35 (br s)/101.2 and δ_H/δ_C 4.86 (d, *J* = 7.6 Hz)/103.4. After analysing the HSQC, HMBC, COSY, TOCSY and ROESY spectra, the sugar moieties of compound **30** was identified as:

- 1 α-L-rhamnopyranosyl Rha-1 at δ_H 6.35 (br s).

- 2 β-D-glucopyranosyl Glc I-1 at δ_H 5.02 (d, *J* = 7.6 Hz) and Glc II-1 at δ_H 4.86 (d, *J* = 7.6 Hz).

The sequence of the oligosaccharide was established by analysing the HMBC and ROESY spectra:

157

- The HMBC correlation between δ_H 5.02 (Glc I H-1) and δ_C 80.9 (C-1) and in ROESY at δ_H 5.02 (Glc I H-1) and δ_H 3.98 (H-1) proved that Glc I was attached to the C-1 position of the aglycon (Fig.153).

- The HMBC correlation between δ_H 6.35 (Rha H-1) and δ_C 74.4 (Glc I C-2) and in ROESY at δ_H/δ_H 6.35 (Rha H-1)/4.50 (Glc I H-2) proved that Rha was attached to the C-2 position of the Glc I.

- The HMBC correlation between δ_H 4.86 (Glc II H-1) and δ_C 71.9 (C-26) and the ROESY correlation between 4.86 (Glc II H-1)/δ_H 4.61 (H-26) proved that Glc II was attached to the C-26 position of the aglycon.

Conclusion

All the evidences above revealed the structure of compound **30** was 26-*O*-β-D-glucopyranosyl-5α-furost-(25)27-ene-1β,3β,22α,26-tetrol-1-*O*-α-L-rhamnopyranosyl-(1→2)-β-D-glucopyranoside.
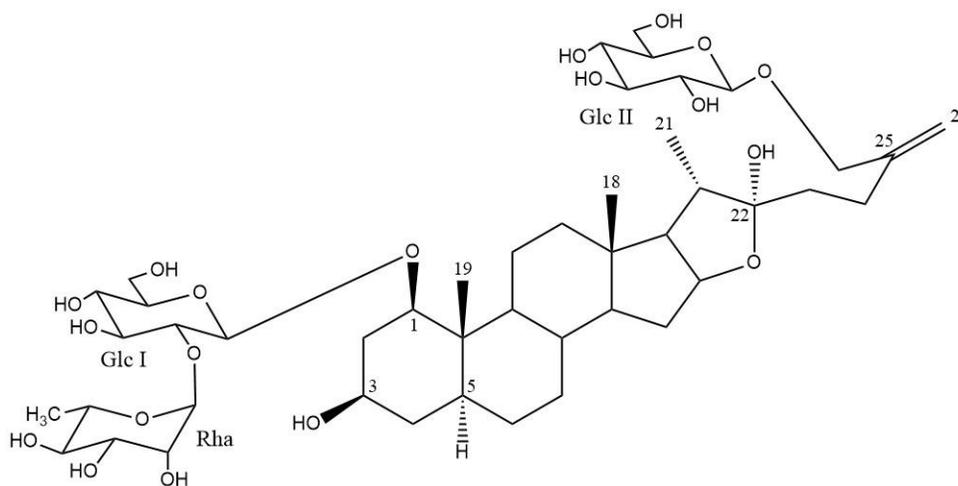
Figure 160. Structure of compound **30**
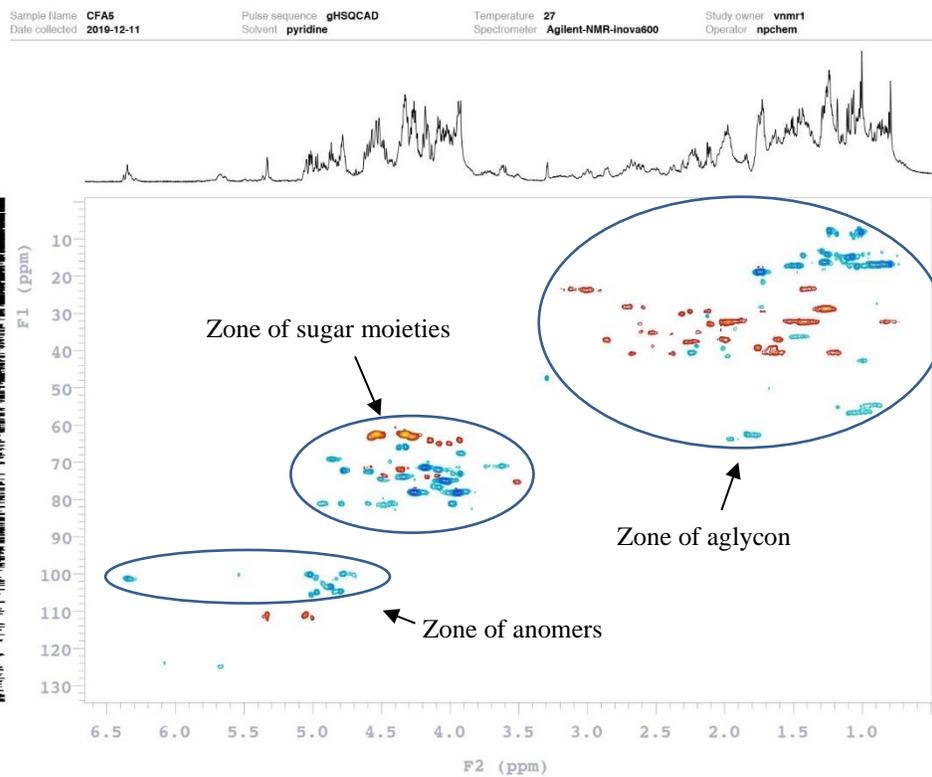
Figure 161. HSQC spectrum of compound **30**
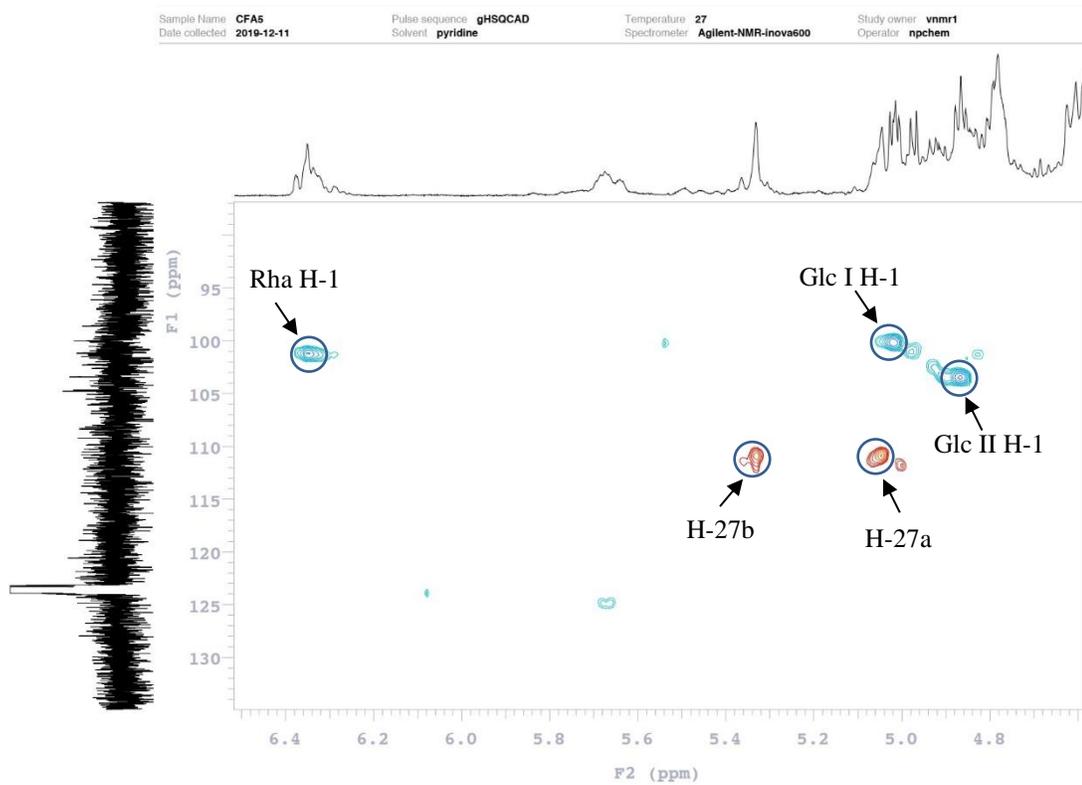
Figure 162. HSQC spectrum of sugar anomers of compound **30**
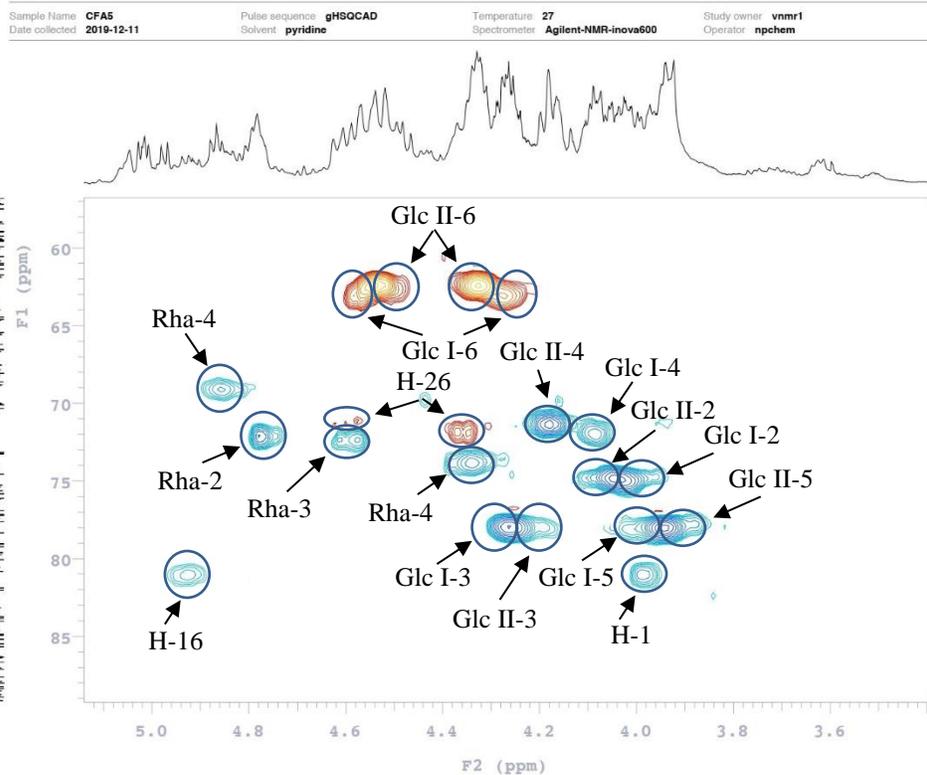
Figure 163. HSQC spectrum of sugar moieties of compound **30**
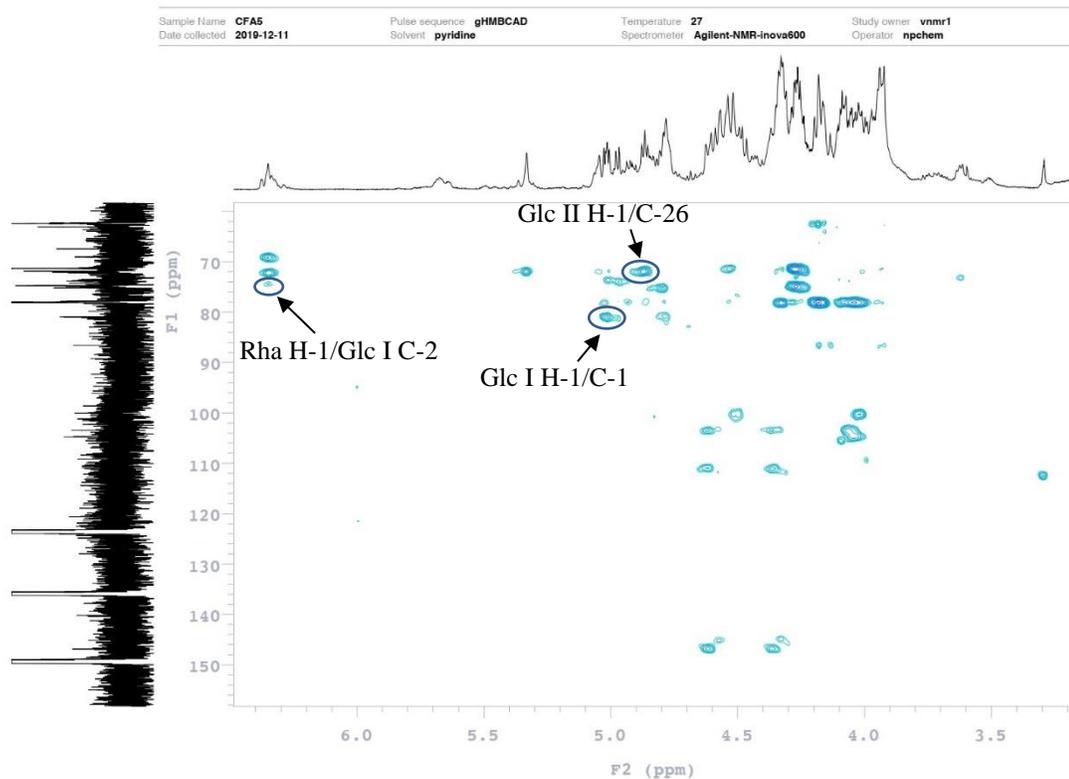
Figure 164. HMBC spectrum of sugar moieties of compound **30**
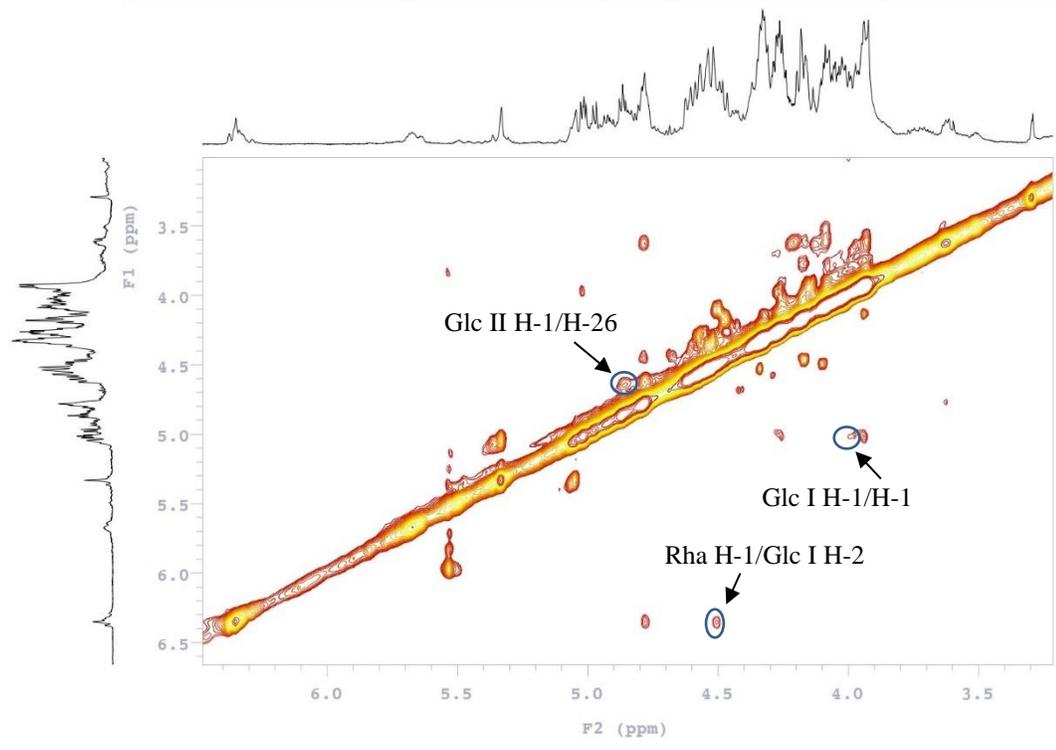
Figure 165. ROESY spectrum of sugar moieties of compound **30**
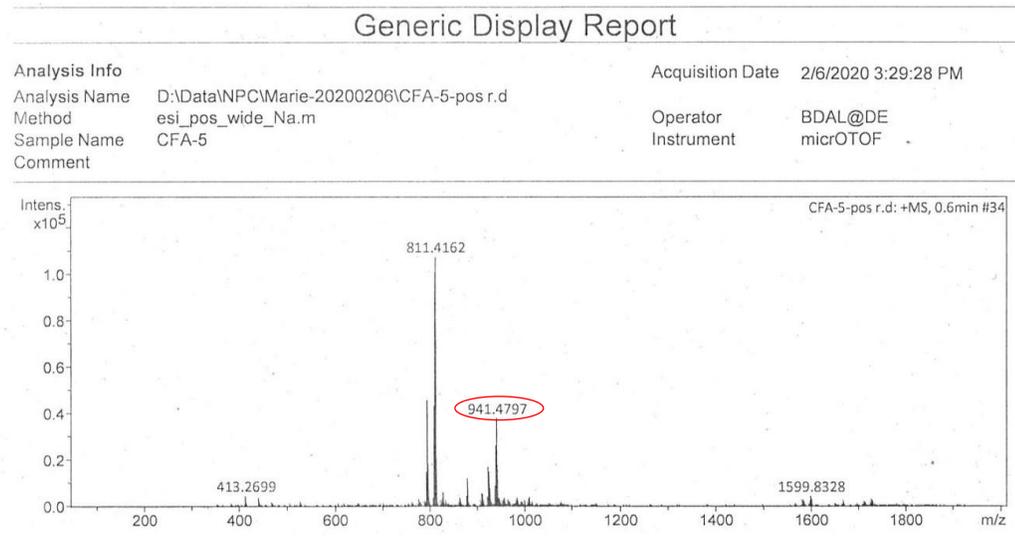
Figure 166. Mass spectrum of compound **30**

c. Compound 31 (CFA6)

Mass spectrometry

The HR-ESIMS (positive-ion mode) spectrum of compound **31** showed a pseudo-molecular ion peak $[M+Na]^+$ at *m/z* 925.4814, indicating a molecular weight of 902 and a molecular formula of $C_{45}H_{74}O_{18}$.

NMR spectroscopy

Structure of aglycon

The analysis of the NMR spectra of compound **31** showed that the aglycon was similar to compound **30** (Table 10).

Structure of sugar moieties

The ^1H NMR spectrum of compound **31,** in the sugar region signals, showed signals of three anomeric protons at δ_H/δ_C 4.82 (d, *J* = 7.6 Hz)/99.7, δ_H/δ_C 6.33 (br s)/101.1 and δ_H/δ_C 4.89 (d, *J* = 7.6 Hz)/103.3, indicating the presence of three sugar units:

- 1 β-D-fucopyranosyl Fuc-1 at δ_H 4.82 (d, *J* = 7.6 Hz).

- 1 α-L-rhamnopyranosyl Rha-1 at δ_H 6.33 (br s).

- 1 β-D-glucopyranosyl Glc-1 at δ_H 4.89 (d, *J* = 7.6 Hz).

The sequence of the oligosaccharide was established by analysing the HMBC and ROESY spectra:

- The HMBC correlation between δ_H 4.82 (Fuc H-1) and δ_C 80.6 (C-1) and in the ROESY spectrum at δ_H 4.82 (Fuc H-1) and δ_H 4.44 (dd, *J* = 11.7, 3.5 Hz, H-1) proved that Fuc was attached to the C-1 position of the aglycon.

- The HMBC correlation between δ_H 6.33 (Rha H-1) and δ_C 74.3 (Fuc C-2) and in ROESY at δ_H 6.33 (Rha H-1) and δ_H 4.50 (Fuc H-2) proved that Rha was attached to the C-2 position of the Fuc.

- The HMBC correlation between δ_H 4.89 (Glc H-1) and δ_C 72.0 (C-26) and the ROESY correlation between 4.89 (Glc H-1)/δ_H 4.65 (H-26) proved that Glc was attached to the C-26 position of the aglycon.

Conclusion

All the evidences above revealed the structure of compound **31** as 26-*O*-β-D-glucopyranosyl-5α-furost-(25)27-ene-1β,3β,22α,26-tetrol-1-*O*-α-L-rhamnopyranosyl-(1→2)-β-D-fucopyranoside.
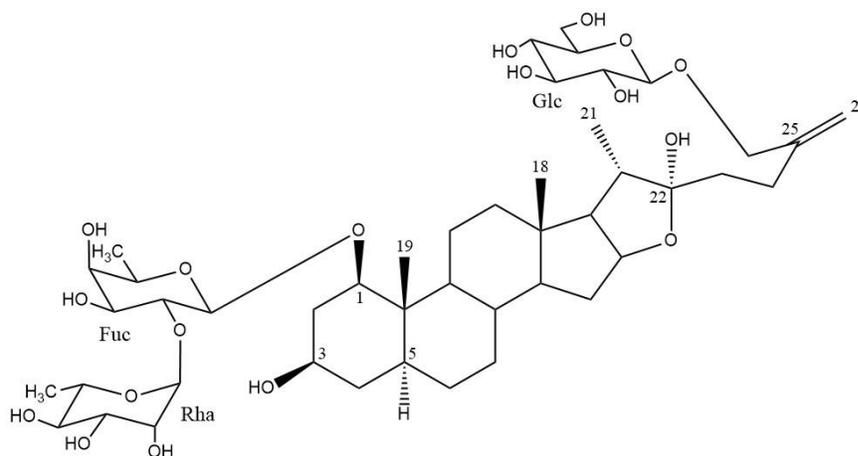
Figure 167. Structure of compound **31**
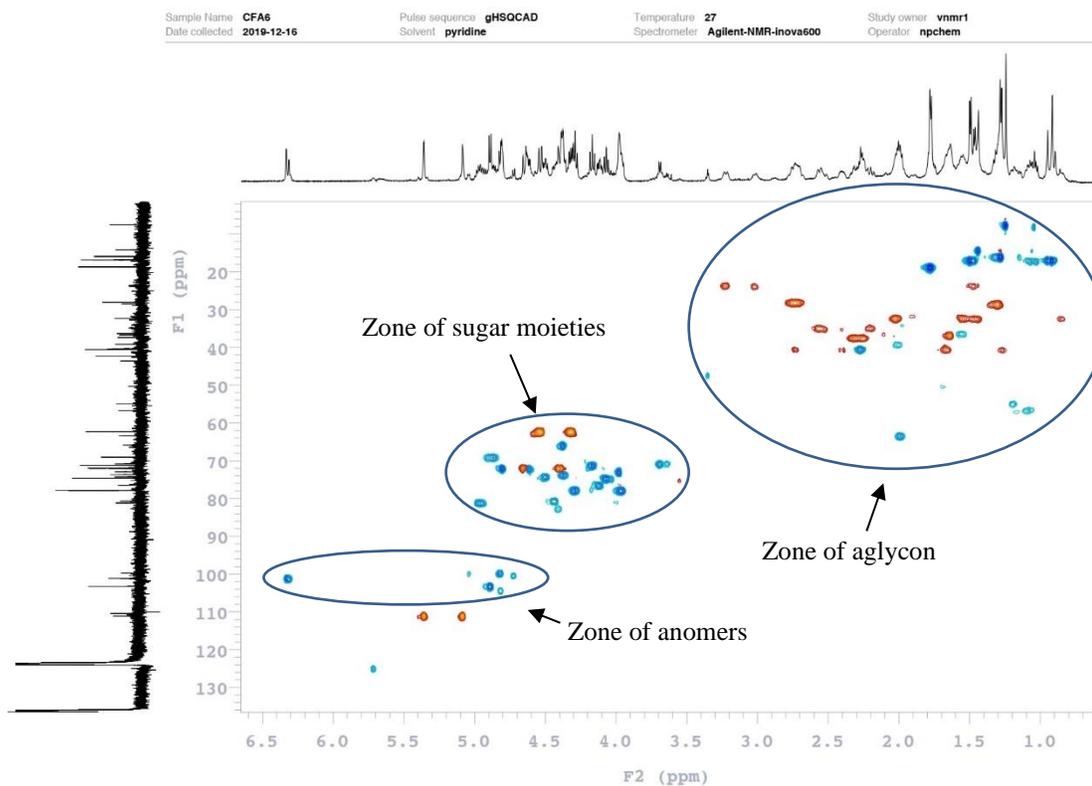
Figure 168. HSQC spectrum of compound **31**

163
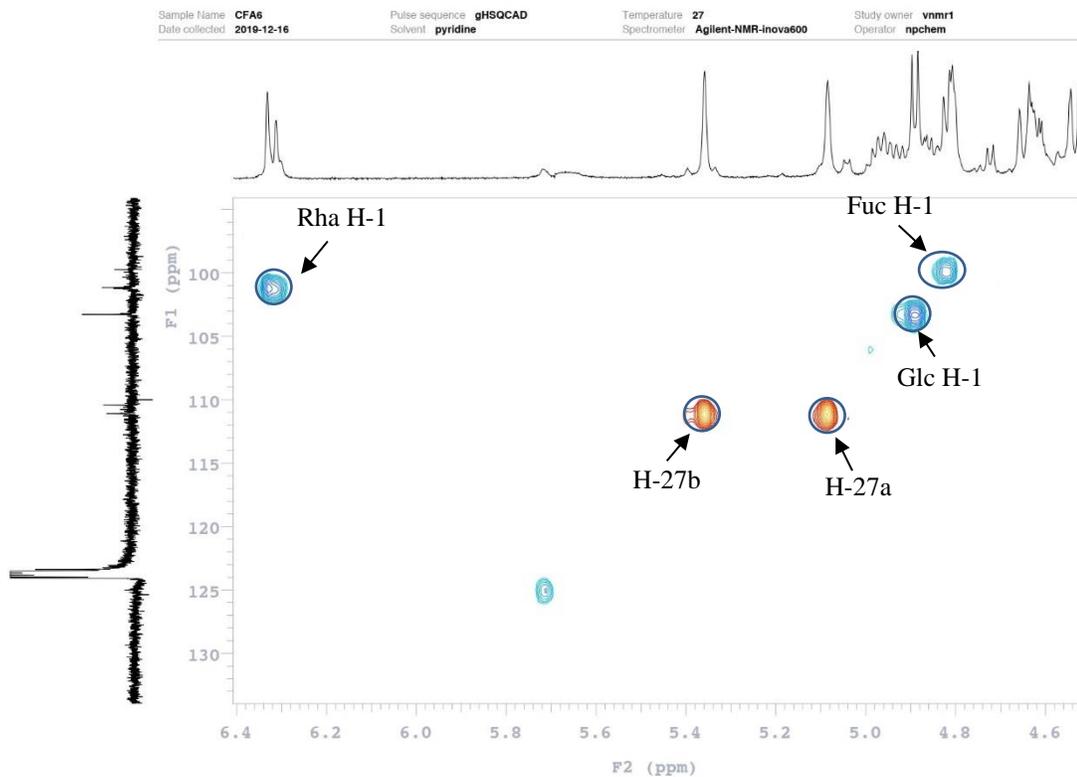
Figure 169. HSQC spectrum of sugar anomers of compound **31**
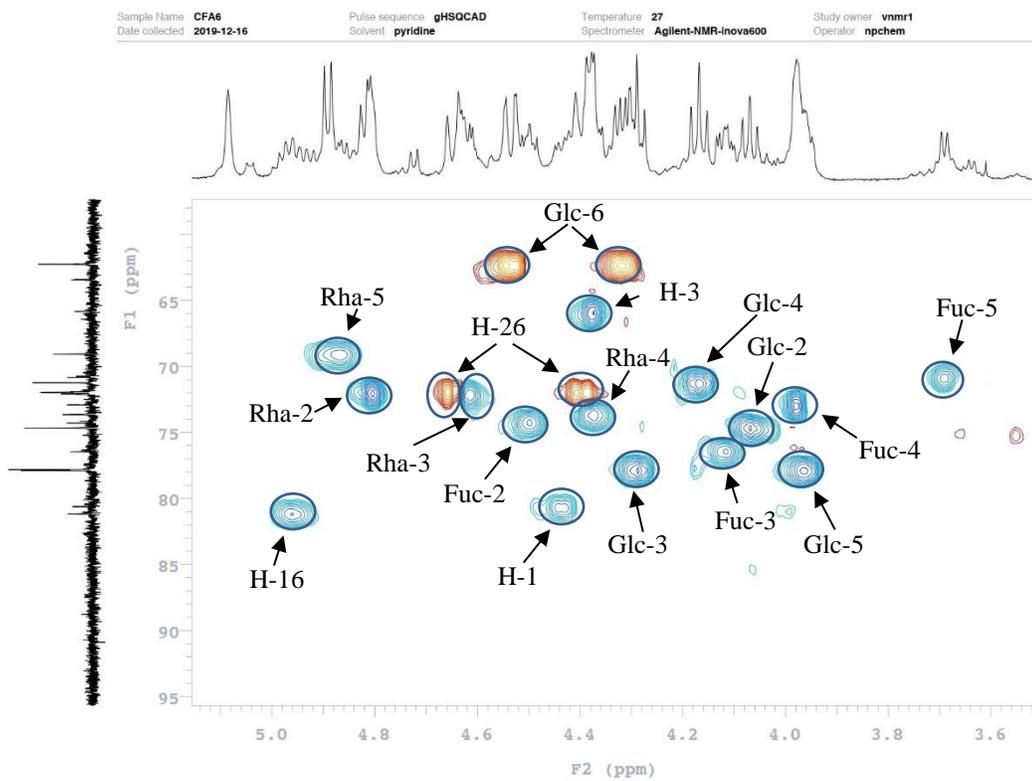
Figure 170. HSQC spectrum of sugar moieties of compound **31**
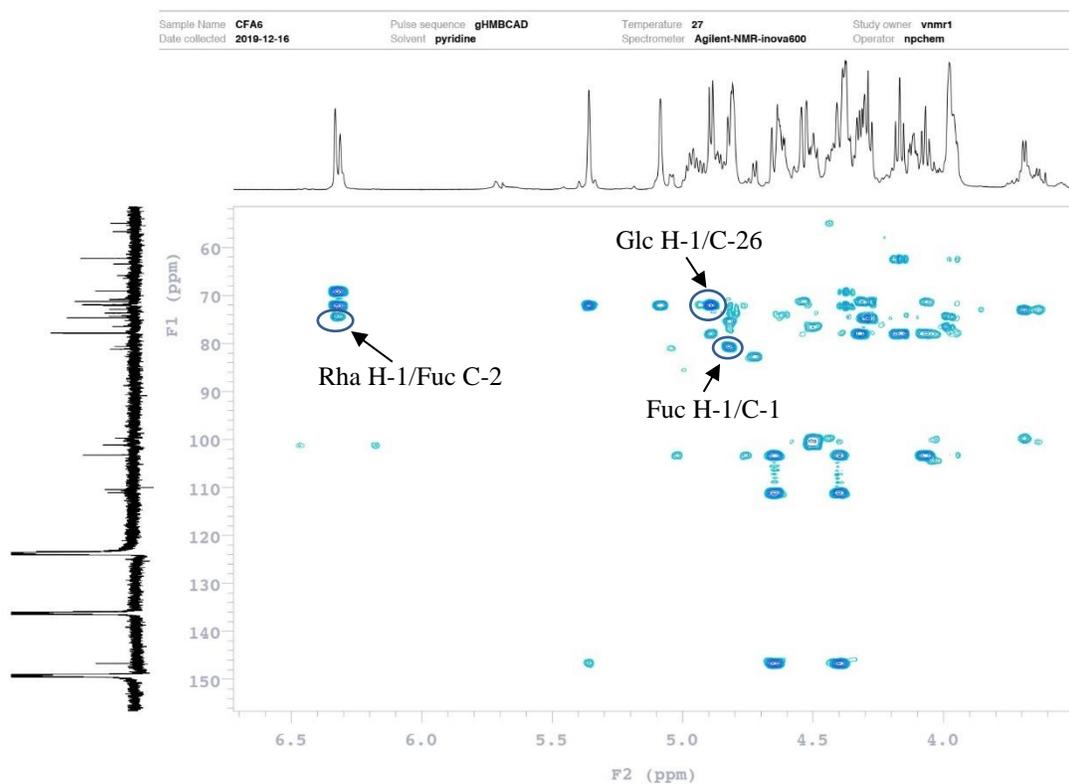
Figure 171. HMBC spectrum of compound **31**
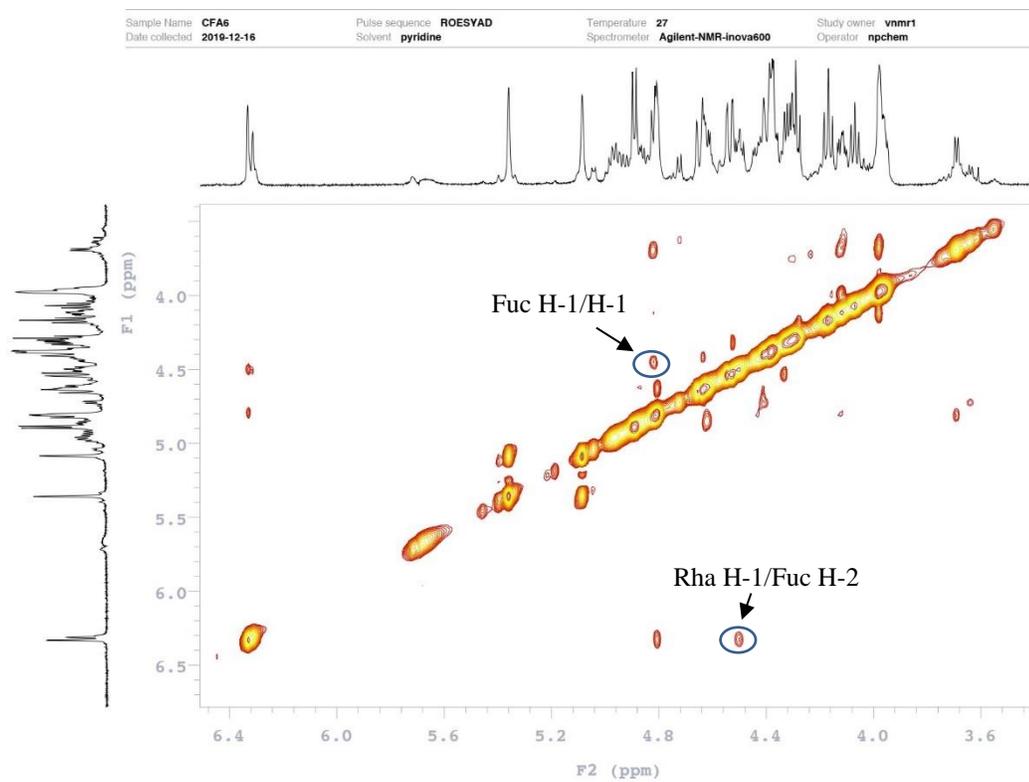
Figure 172. ROESY spectrum of compound **31**

Generic Display Report

Analysis Info		Acquisition Date	2/6/2020 3:33:26 PM
Analysis Name	D:\Data\NPC\Marie-20200206\CFA-6-pos.d		
Method	esi_pos_wide_Na.m	Operator	BDAL@DE
Sample Name	CFA-6	Instrument	micrOTOF
Comment			
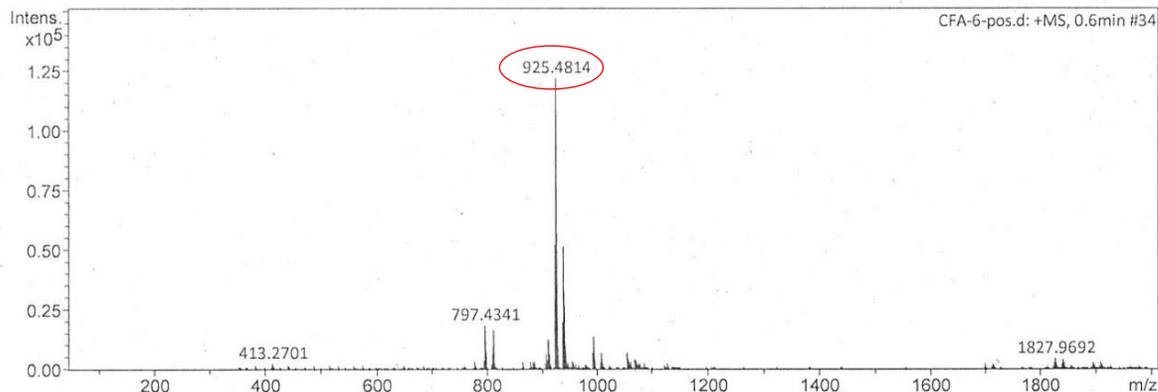
Figure 173. Mass spectrum of compound **31**

d. Compound 32 (CFA4)

The HR-ESIMS (positive-ion mode) spectrum of compound **32** showed a pseudo-molecular ion peak [M+Na]$^+$ at 939.4938 *m/z*, indicating a molecular weight of 916 and a molecular formula of $C_{46}H_{76}O_{18}$. It was apparent from the NMR data (^{1}H, ^{13}C, HSQC, COSY, TOCSY, HMBC, ROESY) that signals of compounds **31** and **32** were almost superimposable. The difference of their molecular weights by only 14 amu corresponds to the presence of a complementary methoxy group instead of a hydroxy group at C-22. This assignment was confirmed by HMBC correlations at δ_H 3.29 (s)/δ_C 112.4 (C-22) and δ_H 1.11 (d, *J* = 6.4 Hz, H-21)/δ_C 112.4 (C-22). The configuration of 22-OCH$_3$ was determined as an α-orientation by the ROESY correlation at δ_H 3.29 (s)/δ_H 1.11 (d, *J* = 6.4 Hz, H-21) and δ_H 3.29 (s)/δ_H 2.02 (H-5). On the basis of these results, the structure of compound **32** was elucidated as 26-*O*-β-D-glucopyranosyl-22α-methoxy-5α-furost-(25)27-ene-1β,3β,26-triol-1-*O*-α-L-rhamnopyranosyl-(1→2)-β-D-fucopyranoside.

166
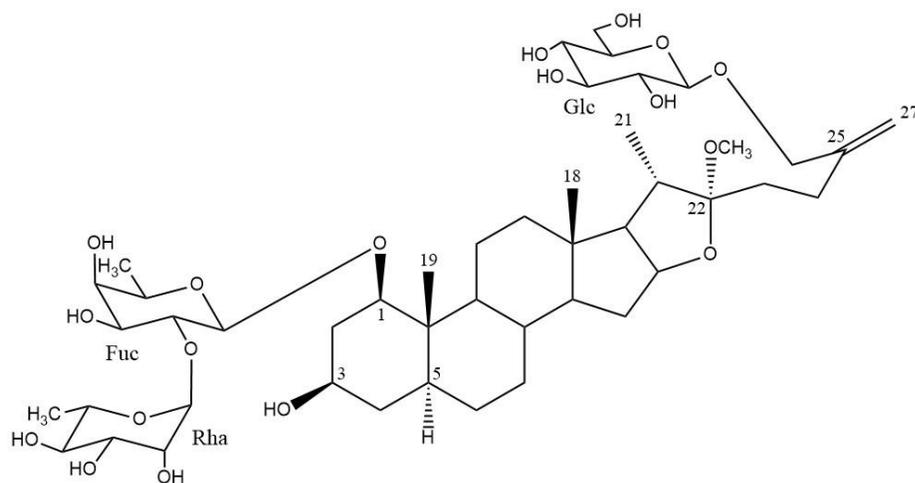
Figure 174. Structure of compound **32**
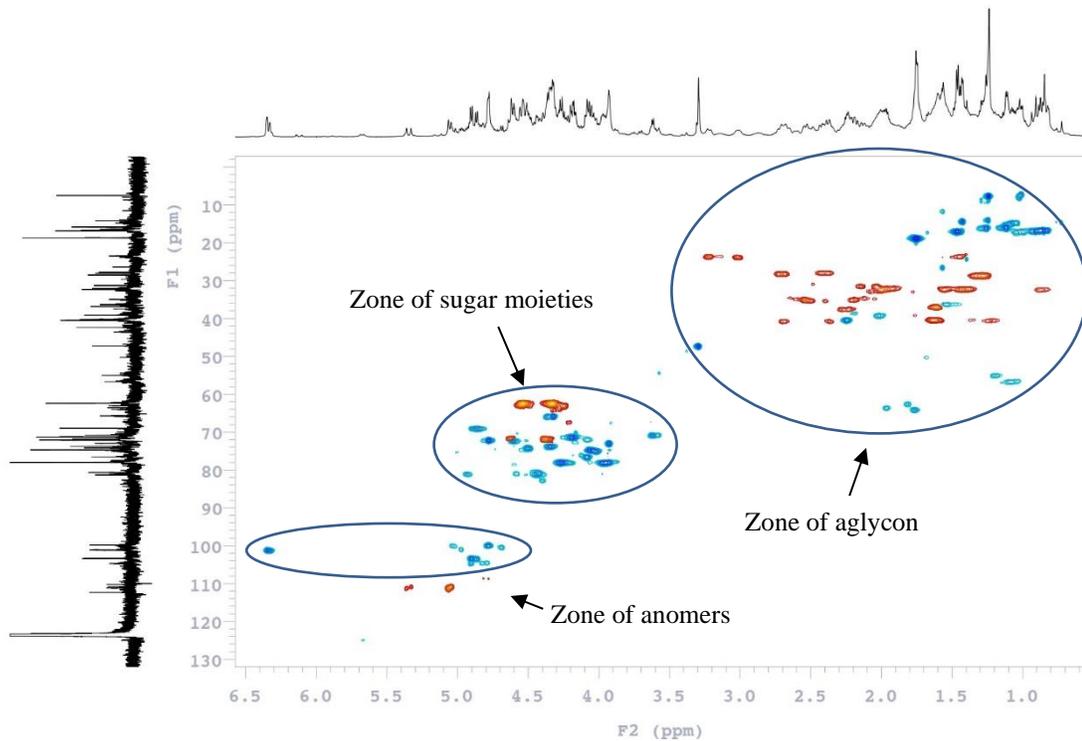
Figure 175. HSQC spectrum of compound **32**

167
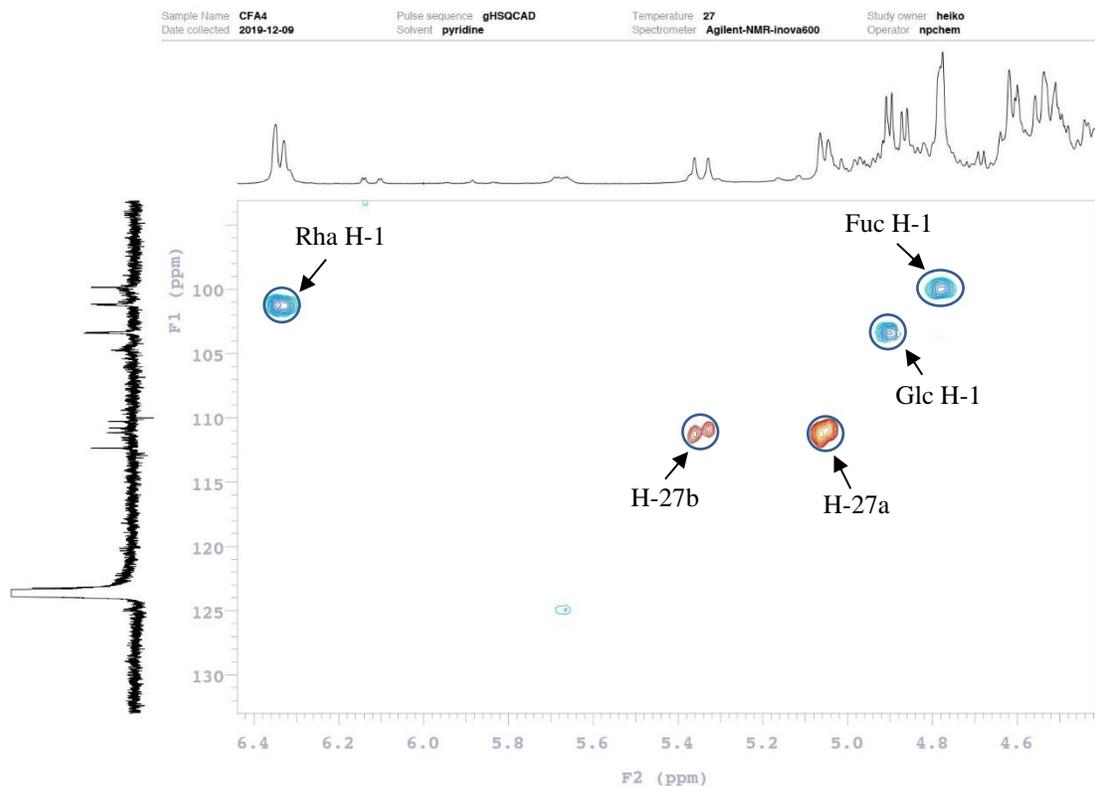
Figure 176. HSQC spectrum of sugar anomers of compound **32**
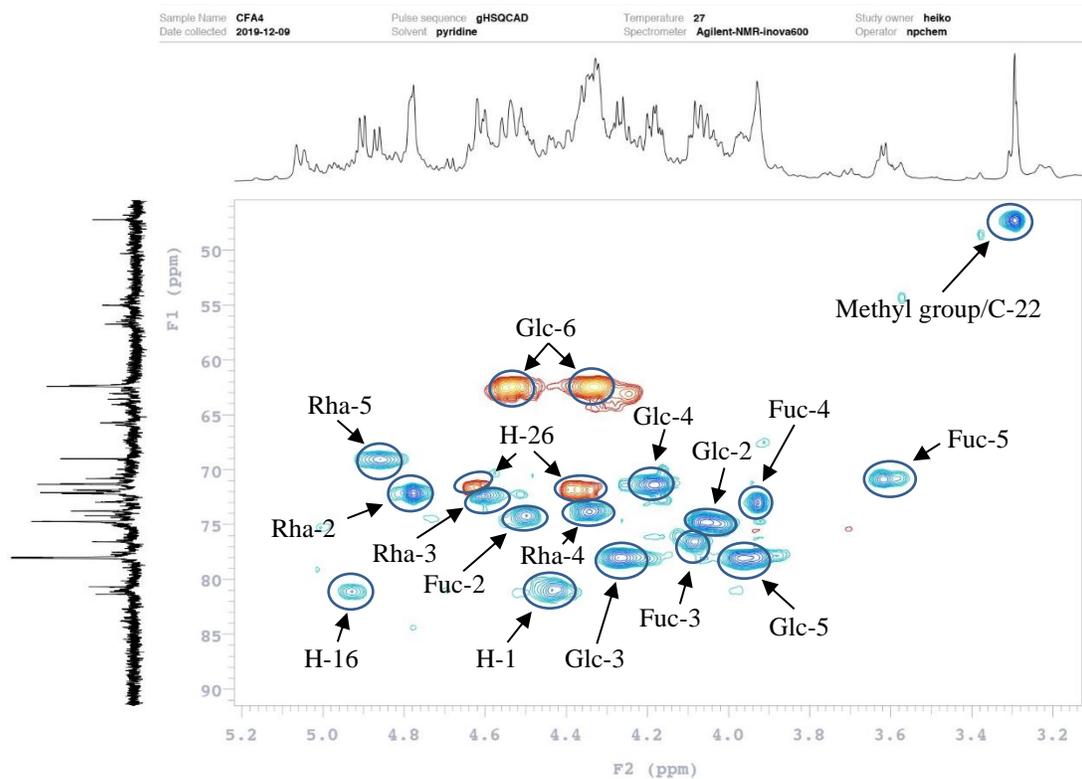
**Figure 177.** HSQC spectrum of sugar moieties of compound **32**
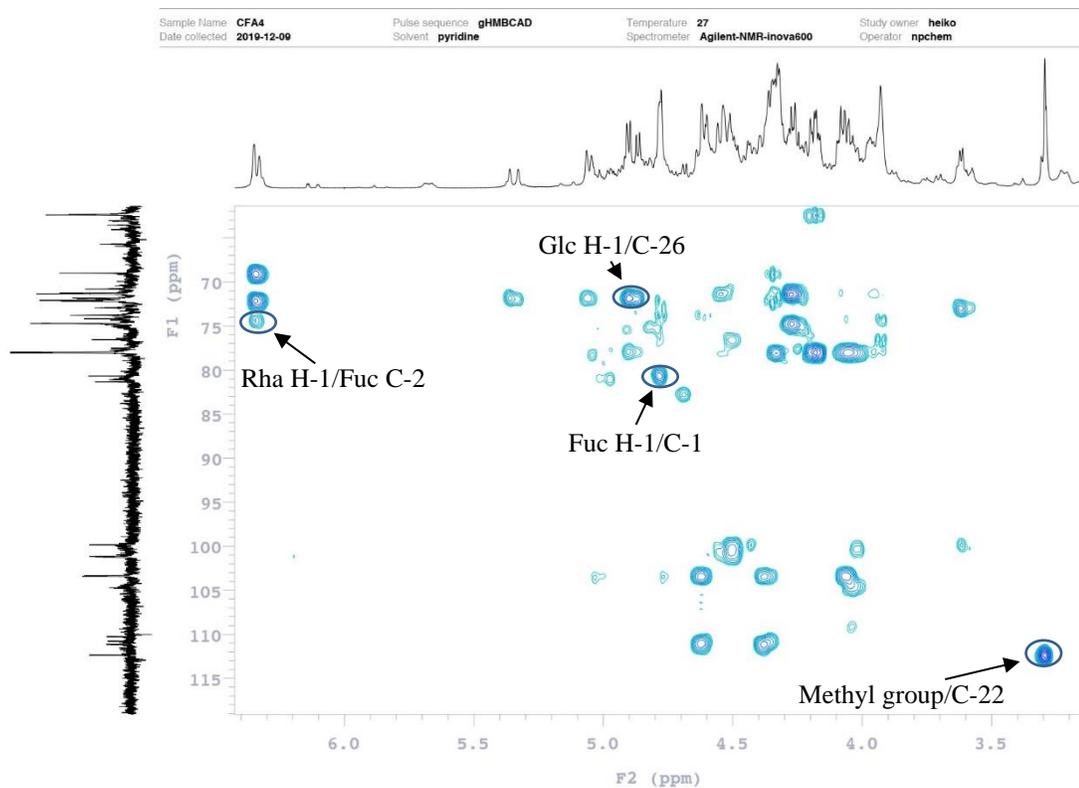
Figure 178. HMBC spectrum of sugar moieties of compound **32**
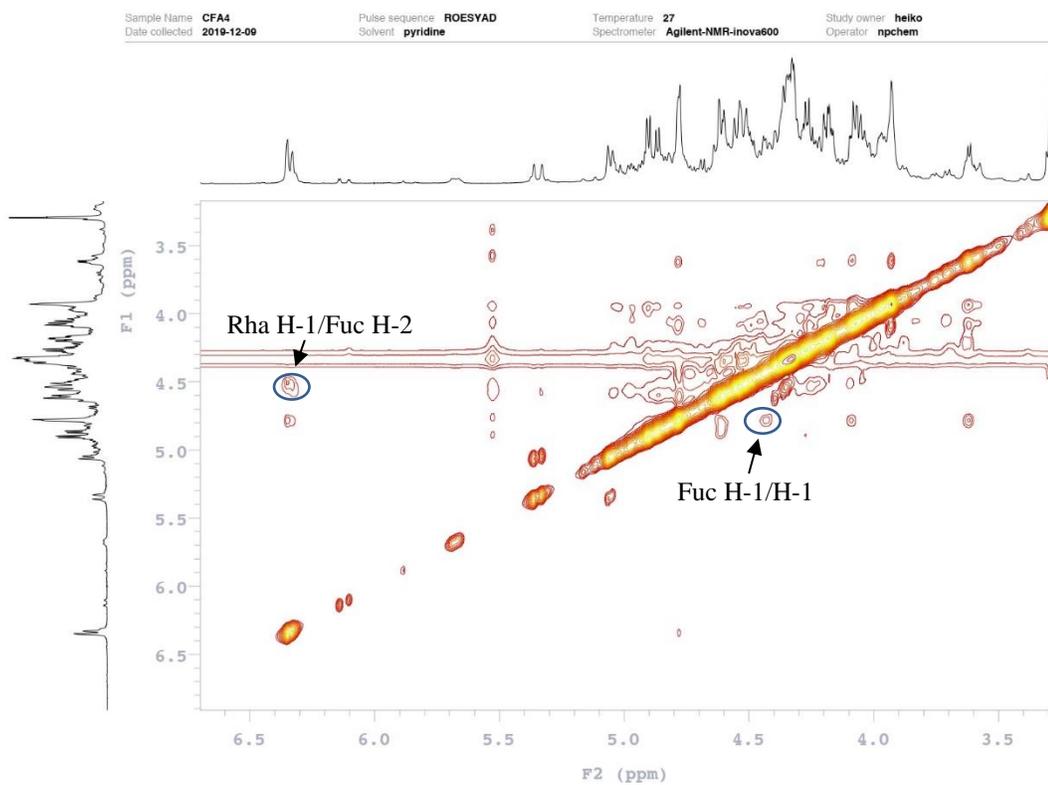
**Figure 179.** ROESY spectrum of sugar moieties of compound **32**

Figure 180. Mass spectrum of compound **32**

Table 10. ^{13}C and ^1H NMR spectroscopic data of the aglycon moieties of **29-32** in pyridine-d_5 (δ in ppm, J in Hz)

	29 CFA3		30 CFA5		31 CFA6		32 CFA4	
	δ_C	δ_H	δ_C	δ_H	δ_C	δ_H	δ_C	δ_H
1	81.1	3.99 dd (11.7, 3.5)	80.9	3.98	80.6	4.44 dd (11.7, 3.5)	80.7	4.43
2	34.2	2.02, 2.87	37.0	1.99 q (11.7), 2.86	34.8	2.20, 2.56	35.0	2.19, 2.53
3	66.0	4.38	65.7	4.34	65.8	4.37	65.7	4.32
4	36.9	1.57, 1.63	37.1	1.60, 1.63	37.0	1.64, 1.66	36.9	1.60, 1.64
5	39.0	1.98	39.1	2.01	39.2	2.00	39.2	2.02
6	28.5	1.26,1.30	28.5	1.24, 1.28	28.5	1.28, 1.32	28.5	1.26, 1.32
7	32.0	0.74, 1.44	32.1	0.82, 1.53	32.2	0.85, 1.54	32.0	0.86, 1.55
8	36.1	1.42	36.1	1.46	36.3	1.58	36.3	1.52
9	54.4	0.90	55.1	1.18	55.0	1.19	55.0	1.20
10	42.1	–	42.6	–	42.3	–	42.3	–
11	23.8	1.40, 3.00	23.8	1.38, 3.00	23.9	1.47, 3.22	23.5	1.44, 3.20
12	40.3	1.20, 1.64	40.3	1.20, 1.64	40.5	1.27, 1.67	40.6	1.22, 1.63
13	40.2	–	40.2	–	40.4	–	40.2	–
14	56.1	0.96	56.5	1.05	56.7	1.08	56.7	1.08
15	32.1	1.36, 1.99	32.0	1.42, 1.98	32.3	1.45, 2.02	32.1	1.41, 1.98
16	81.1	4.81	81.1	4.92 q (8.2)	81.2	4.98 q (7.0)	81.3	4.93 q (7.0)
17	62.3	1.88	62.4	1.84	63.5	1.99	64.1	1.76
18	16.6	0.81 s	16.5	0.79 s	16.8	0.92 s	16.9	0.85 s
19	8.0	1.02 s	8.0	1.24 s	7.5	1.24 s	7.52	1.24 s
20	38.8	2.21 t (6.4)	41.2	1.98 t (6.4)	40.6	2.27	40.5	2.24
21	14.8	1.13 d (6.4)	14.8	1.08 d (6.4)	15.9	1.28 d (6.4)	15.9	1.11 d (6.4)
22	120.5	–	109.3	–	110.4	–	112.4	–
23	40.4	2.42, 2.68	37.5	2.20, 2.26	37.4	2.24, 2.32	31.3	2.04, 2.14
24	29.1	2.15, 2.29	28.5	2.59, 2.70	28.0	2.70, 2.76	28.1	2.68, 2.72
25	148.8	–	148.9	–	146.7	–	146.4	–
26	73.9	4.15, 4.49	71.9	4.36 br d (12.3), 4.61 br d (12.3)	72.0	4.40 br d (12.3), 4.65 br d (12.3)	71.8	4.36 br d (12.3), 4.62 br d (12.3)
27	112.0	5.08 br s 5.38 br s	110.9	5.05 br s, 5.33 br s	111.1	5.08 br s, 5.36 br s	111.1	5.05 br s 5.34 br s
OMe							47.2	3.29 s

Overlapped proton signals are reported without designated multiplicity.

Table 11. ^{13}C and ^1H NMR spectroscopic data of the sugar moieties of **29-32**

in pyridine-d_5 (δ in ppm, J in Hz)

	29 CFA3		30 CFA5		31 CFA6		32 CFA4	
	δ_C	δ_H	δ_C	δ_H	δ_C	δ_H	δ_C	δ_H
Fuc-1					99.7	4.82 d (7.6)	99.8	4.78 d (7.6)
2					74.3	4.50 dd (9.4, 7.6)	74.2	4.50 dd (9.4, 7.6)
3					76.5	4.12	76.6	4.10 dd (9.4, 2.9)
4					72.9	3.98	72.9	3.93 br d (2.9)
5					70.8	3.69 br q (6.4)	70.8	3.62 br q (6.4)
6					16.9	1.49 d (6.4)	16.9	1.46 d (6.4)
Rha I-1			101.2	6.35 br s	101.1	6.33 br s	101.2	6.35 br s
2			72.1	4.78 br s	72.0	4.80 br s	72.1	4.78 br s
3			72.3	4.60 dd (9.4, 2.9)	72.1	4.61 dd (9.4, 2.9)	72.2	4.60 dd (9.4, 3.5)
4			73.8	4.34 dd (9.4, 9.4)	73.7	4.37 dd (9.4, 9.4)	73.8	4.35 dd (9.4, 9.4)
5			69.0	4.86 dq (9.4, 5.9)	69.1	4.87 dq (9.4, 5.9)	69.0	4.83 dq (9.4, 5.9)
6			18.7	1.73 d (5.9)	18.7	1.77 d (5.9)	18.7	1.75 d (5.9)
Glc I-1	100.1	5.03 d (8.2)	100.0	5.02 d (7.6)	103.3	4.89 d (7.6)	103.4	4.90 d (7.6)
2	75.1	4.03	74.4	4.50	74.7	4.07	74.7	4.05
3	77.9	4.28	78.1	4.27	77.8	4.29	78.0	4.26
4	72.0	4.08	72.0	4.10	71.2	4.17	72.2	4.18
5	78.0	3.98	78.1	3.94	77.9	3.96	78.0	3.96
6	63.0	4.26 dd (12.3, 5.6), 4.54	63.1	4.28 dd (11.7, 5.8), 4.57	62.3	4.30 dd (11.7, 5.8), 4.54	62.4	4.33, 4.54
Glc II-1	104.6	4.96 d (7.6)	103.4	4.86 d (7.6)				
2	75.2	4.08	74.7	4.05				
3	78.0	4.30	78.0	4.26				
4	71.2	4.17	71.3	4.18				
5	78.1	3.97	78.0	3.96				
6	62.3	4.32 dd (12.3, 5.8), 4.57	62.4	4.35 dd (12.3, 5.8), 4.54				

Overlapped proton signals are reported without designated multiplicity. Nd: Not determined

2.6. Phytochemical study of roots of *Dracaena braunii*

Phytochemical investigation on aqueous-ethanolic extract of the roots of *Dracaena braunii* led to the isolation of **3** steroidal glycosides (**33-35**). All of them have been previously described in litterature.

2.6.1. Isolation and purification

The dried and powdered of roots of *Dracaena braunii* (6.2 g) were extracted by microwaves two times with the solvent $EtOH/H_2O$ (200 W, 60°C, 30 min, 75/35, 250 mL each). After filtration and evaporation, 1.2 g crude of extract was collected and further fractionated by VLC (RP-18 silica gel, H_2O, $EtOH/H_2O$ 50/50, EtOH) giving 3 fractions (A-C). Fraction B (330 mg), rich in saponins, was chromatographed on successive MPLC on silica gel 60 ($CHCl_3/MeOH/H_2O$ 80/20/2, 75/25/3) resulting 2 pure compounds, **33** (3.9 mg) and **35** (4.8 mg). The remaining fractions were combined and chromatographed again on silica gel 60 by MPLC ($CHCl_3/MeOH/H_2O$ 75/25/3) to give 5 fractions. Fraction rich in saponin was further purified by MPLC on silica gel RP-18 (gradient of $MeOH/H_2O$ 30/70→60/40) yielding compound **34** (15.9 mg).
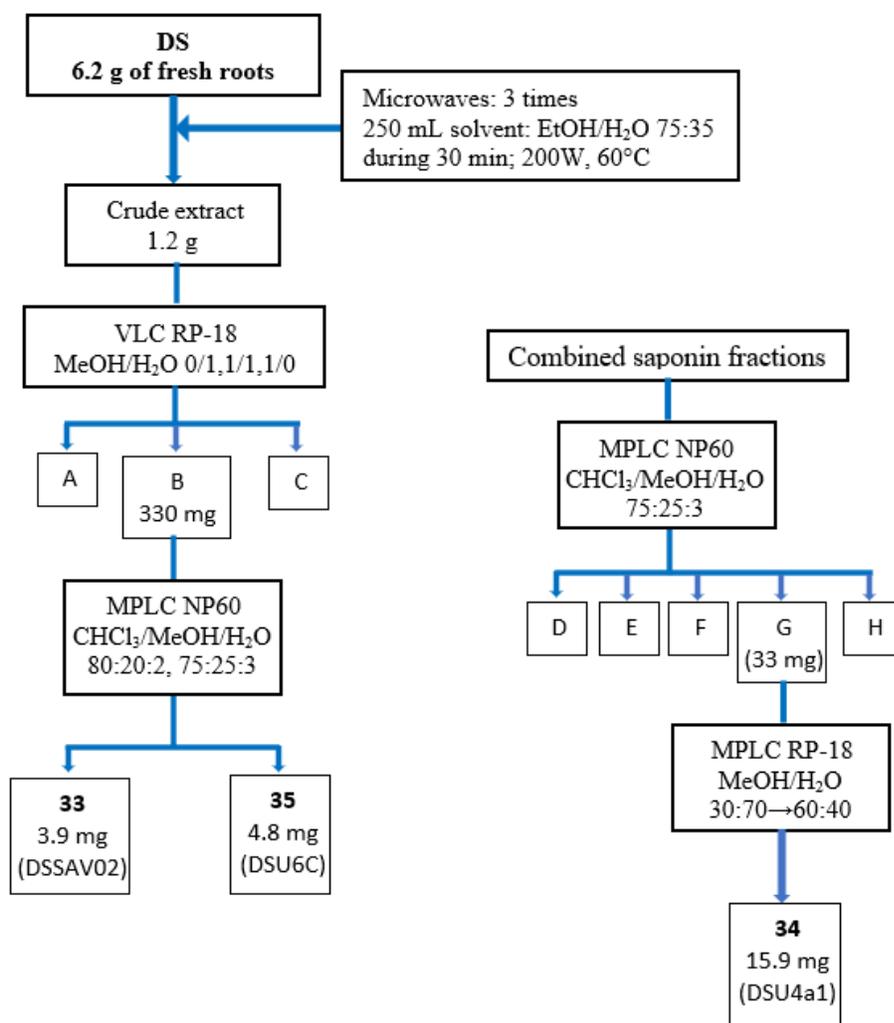
Figure 181. Purification of compounds in roots of *Dracaena braunii*

2.6.2. Structural determination of isolated saponins

a. Compound 33 (DSSAV02)

For compound **33**, the HR-ESIMS (positive-ion mode) spectrum showed a pseudo-molecular ion peak [M+Na]$^+$ at *m/z* 1165.5099, indicating a molecular weight of 1142 and a molecular formula of $C_{55}H_{82}O_{25}$. According to literature data, the structure of **33** was identified as (23*S*,24*S*)-3β,23-dihydroxy-1β-[*O*-(2,3,4-tri-*O*-acetyl-α-L-rhamnopyranosyl-(1→2)-*O*-[β-D-xylopyranosyl-(1→3)]-α-L-arabinopyranosyl)oxy]spirost-5,25(27)-dien-24-yl β-D-fucopyranoside. This spirostanol glycoside has been isolated from the whole plant *Sansevieria trisfasciata* (Mimaki et al., 1996).
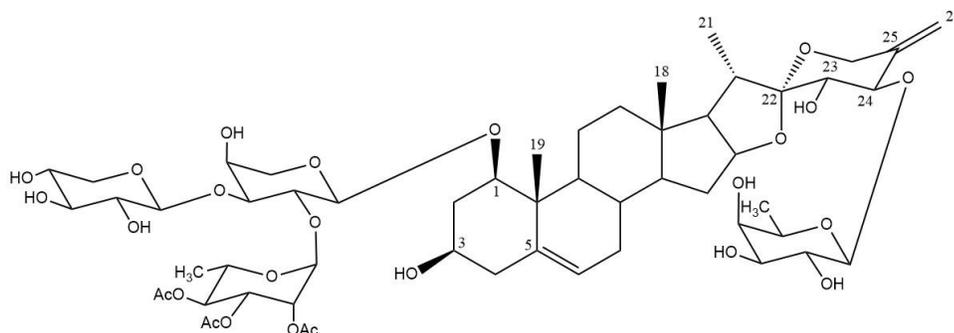
Figure 182. Structure of compound **33**

b. Compound 34 (DSU4a1)

The HR-ESIMS (positive-ion mode) spectrum of compound **34** showed a pseudo-molecular ion peak [M+Na]$^+$ at *m/z* 909.4581, indicating a molecular weight of 886 and a molecular formula of $C_{44}H_{70}O_{18}$. Comparing the NMR data with literature, the structure of **34** was identified as 26-*O*-β-D-glucopyranosyl-furosta-5,25(27)-diene-1β,3β,22α,26-tetrol-1-*O*-α-L-rhamnopyranosyl-(1→2)-α-L-arabinopyranoside (Deglucoruscoside). This spirostanol glycoside was previously isolated from rhizomes of *Ruscus aculeatus* L (Bombardelli et al., 1972).
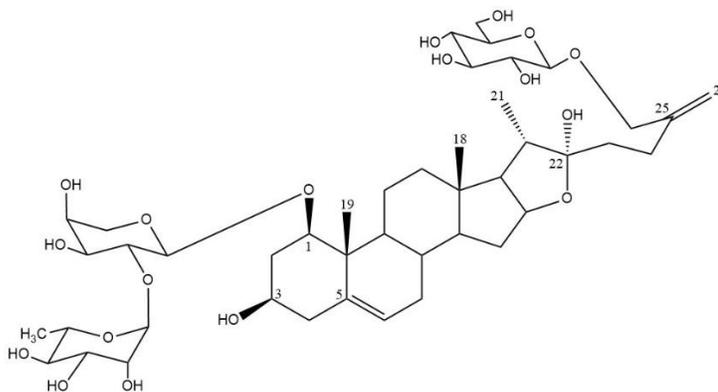
Figure 183. Structure of compound **34**

c. Compound 35 (DSU6C)

The HR-ESIMS (positive-ion mode) spectrum of compound **35** showed a pseudo-molecular ion peak [M+Na]$^+$ at *m/z* 1041.5007, indicating a molecular weight of 1018 and a molecular formula of $C_{44}H_{70}O_{18}$. By working on literature data, the structure of **35** was identified as 26-*O*-β-D-glucopyranosyl-furosta-5,25(27)-diene-1β,3β,22α,26-tetrol-1-*O*-{α-L-

rhamnopyranosyl-(1→2)-*O*-[β-D-xylopyranosyl-(1→3)]-α-L-arabinopyranoside}.   This

spirostanol glycoside was found in the leaves of *Ruscus colchicus* (Perrone et al., 2009).
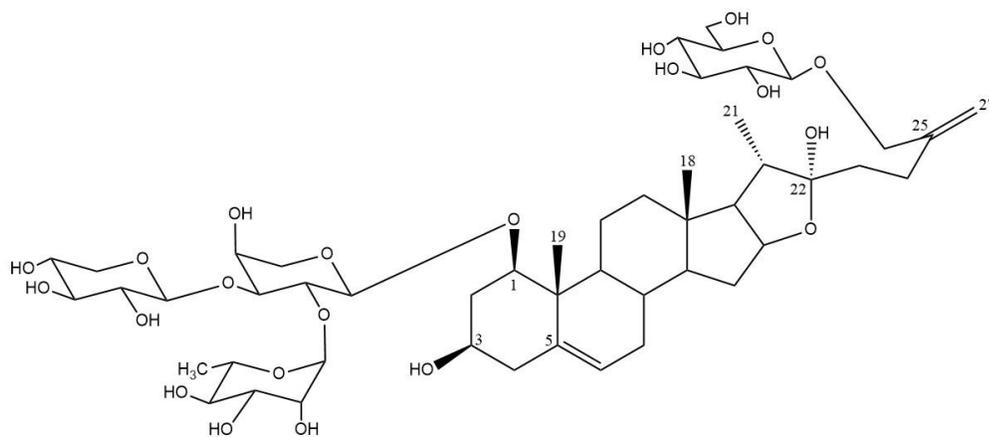
Figure 184. Structure of compound **35**

CHAPTER 3

BIOLOGICAL STUDY

1. Introduction

Cytotoxic activities have been described for a number of saponins, and many articles dealing with this subject continue to appear in the scientific literature each year. One of the first studies was reported in 1960 by Fries et al., in which saponins isolated from sea cucumber showed interesting antitumor activity. Since then, numerous publications have appeared on the cytotoxic and antitumor properties of this phytochemical class (Hostettmann and Terreaux, 2000; Lacaille-Dubois and Wagner, 2000; Lacaille-Dubois and Wagner, 1996; Pettit et al., 1991; Rao and Sung, 1995). Saponin could therefore act as potential anticancer agents by inhibiting carcinogenesis or by direct antiproliferative and/or cytotoxic effects against cancer cells (Lacaille-Dubois and Wagner, 2000; Lacaille-Dubois and Wagner, 1996; Pettit et al., 1991). Most of these studies are performed *in vitro*, and only 10% of them have reached the preclinical stage. It is interesting to note that most of the compounds were tested in mice, and that only 24% of the studies were performed on human cancer cell lines, the main ones are: HeLa (epithelial uteri), MCF-7, MDA-MB43 (mammary adenocarcinoma), HepG2 (liver carcinoma), HL-60 (promyelocytic acute leukemia), Caco-2, HT-29, HCT116 and SW480 (colon) (Thakur et al., 2011). Herein, we report the biological activity of saponins isolated from *Dracaena*, *Cordyline* and *Weigela* genus and discuss the structure/activity relashionships.

1.1. Bioactivities of steroidal saponins from the *Dracaena* and *Cordyline* genus

1.1.1. Cytotoxicity and antitumor activity

Steroidal saponins isolated from the *Dracaena* genus shown cytotoxicities and antitumor activities:

- Mimaki et al. (1999) isolated nine steroidal saponins including five new ones from *Dracaena draco*. Cytostatic activity of the isolated saponins on human promyelocytic leukemia HL-60 cells was evaluated. Two of those showed relatively potent cytostatic activity (IC_{50} = 1.3 and 2.6 µg/mL) compared with etoposide used as a positive control (IC_{50} = 0.3 µg/mL).

- Another cytotoxicity test on human promyelocytic leukemia HL-60 cells was performed on nine steroidal saponins from *Dracaena surculosa* (Yokosuka et al., 2000). Three known

of them exhibited weak cytotoxic activity (IC_{50} = 5.2, 4.2 and 8.7 µg/mL) whereas IC_{50} of etoposide used as a positive control was at 0.22 µg/mL.

- Nine new compounds including three spirostanol sapogenins, five furostanol saponins, one pregnan glycoside along with another eight known steroidal saponins were characterised from *Dracaena angustifolia* by Tran et al. (2001). All compounds were then tested for their antiproliferative activity against murine colon 26-L5 carcinoma, human HT-1080 fibrosarcoma and B-16 BL6 melanoma cells. Three of them showed potent antiproliferative activity against HT-1080 fibrosarcoma cells (IC_{50} 0.2, 0.3 and 0.6 µM) and another one showed significant activity against colon 26-L5 carcinoma and B-16 BL6 melanoma cells with IC_{50} 5.3 and 4.2 µM, respectively, in comparison with doxorubicin (IC_{50} = 0.2 µM).

- One spirostanol saponin isolated from *Dracaena draco* by González et al. (2003) showed potent cytotoxic activity measured on human promyelocytic leukemia HL-60 cells with IC_{50} = 2.0 ± 0.9 µM.

- Cytotoxic activity of three spirostanol saponins isolated from *Dracaena deisteliana* and *dracaena arborea* were evaluated against the HT-29 and HCT 116 human colon cancer cell lines (Kougan et al., 2010). One of those compounds, spiroconazole A, exhibited weak cytotoxic activities with IC_{50} values of 1.67 and 2.04 µM against HT-29 and HCT 116 cells, respectively, compared with paclitaxel used as positive control (IC_{50} = 3.21 and 1.40 nM against HCT 116 and HT-29, respectively).

- Three new steroidal saponins along with two known ones were characterised from *Dracaena marginata* (Rezgui et al., 2013). Three of them were chosen for cytotoxicity bioassay against colorectal SW480 human cancer cell line and mammary EMT6 mouse cancer cell line which one showed moderate cytotoxicity with IC_{50} values of 14.3 µM against SW480 and 8.6 µM against EMT6 in comparison with doxorubicin used as positive control (IC_{50} = 1.47 (SW480) and 9.21 µM (EMT6)).

- Shen et al. (2014) have isolated thirteen steroidal saponins from *Dracaena cambodiana* and evaluated their cytotoxicities on three human cancer cell lines K562, BEL-7402 and SGC-7901. Three of them showed significant cytotoxicities with IC_{50} = 1.27, 5.09, 4.77 µM against K562, IC_{50} = 4.72, 1.13, 6.44 µM against BEL-7402 and IC_{50} = 2.88, 3.39, 5.61

µM against SGC-7901 compared with paclitaxel used as positive control (IC_{50} = 5.98, 3.75, 1.88 µM, respectively).

- A potent cytotoxicity against HL-60 cells were showed on steroidal saponins isolated from *Dracaena thalioides* (Tang et al., 2014) with IC_{50} values range from 0.38 to 17.3 µM in comparison with cisplatin (IC_{50} = 1.40 µM) and etoposide (IC_{50} = 0.38 µM) used as positive controls.

- Fouedjou et al. (2013) have isolated three new steroidal saponins from the leaves of *Cordyline fruticosa* and evaluated their cytotoxic activity against three tumor cell lines MDA-MB 231, HCT 116 and A375. Two of those compounds showed moderate cytotoxic activity compared with cisplatin used as positive control.

- Another cytotoxicity test on steroidal saponins isolated from the aerial parts of *Cordyline fruticosa* L. var. *strawberries* on three tumor cell lines MDA-MB 231, HCT 116 and A375, revealed a weak cytotoxic activity in comparison with cisplatin used as positive control (Ponou et al., 2019).

1.1.2. Other bioactivities

- Six new steroidal saponins along with eight known ones were isolated from fresh stems of *Dracaena angustifolia* by Min et al. (2010) and later tested on antifugal activity. Two of those compounds were active against *Cryptococcus neoformans* with IC_{50} = 9.5 and 20.0 µg/mL, respectively, compared with Amphotericin B used as positive control (IC_{50} = 2.5 µg/mL).

- Another study on *Dracaena angustifolia* were performed by Huang et al. (2013) about an anti-inflammatory activity against formyl-L-methionyl-L-leucyl-L-phenylalanine (fMLP)-induced superoxide anion production. One steroidal saponin exhibited significant activity against superoxide generation (IC_{50} = 18.55 ± 0.23 µM) and elastase (IC_{50} = 1.74 ± 0.25 µM) in comparison with phosphatidylinositol-3-kinase used as positive control for inhibition of superoxide generation (IC_{50} = 2.00 ± 0.59 µM) and elastase release (IC_{50} = 4.94 ± 1.69 µM).

- Three new saponins isolated from *Cordyline fruticosa* were evaluated for their antimicrobial activity against *Staphylococcus aureus, Escherichia coli, Pseudomonas aeruginosa, Enterococcus faecalis,* and *Candida albicans*. One of those compounds showed a moderate activity against *Enterococcus faecalis* (Fouedjou et al., 2013).

1.2. Bioactivities of triterpenoid saponins from the *Weigela* genus

- Four triterpenoid saponins were isolated from the aerial parts of *Weigela subsessilis* by Won et al. (2015) and later evaluated for their cytotoxic activity against murine B16F0 melanoma cell lines. Two of those compounds showed good stimulatory effects on melanogenesis without decreasing the cell viability.

- The major triterpenoid saponins isolated from *Weigela stelzneri* by Rezgui et al. (2016) was evaluated for their cytotoxic activity against colorectal SW480 human cancer cell line and mammary EMT6 mouse cancer cell line. Two of those compounds exhibited a potent cytotoxic activity with $IC_{50} = 0.97 \pm 0.03$, 3.84 ± 0.43 µM against SW480 and $IC_{50} = 1.26 \pm 0.01$, 3.22 ± 0.02 µM against EMT6 in comparison with etoposide and methotrexate used as positive control ($IC_{50} = 20$ µM in all of cases).

- Four triterpenoid saponins were isolated from *Weigela* x "kosteriana variegata" by Andriamisaina et al. (2018) and tested later for their toxicological properties in an *in vivo* zebrafish assay. The results show that the most active compounds were toxic to the larvae in the range of 1 µM.

- Champy-Tixier et al. (2018) isolated three triterpenoid saponins from the roots of *Weigela florida* "rumba" (Bunge) A. DC. Two of those compounds were further evaluated as antigens in enzyme-linked immunosorbent assay (ELISA) to recognize IgM antibodies in multiple sclerosis (MS) patients' sera.

1.3. Correlation between the structure and cytotoxicity of saponins

There are close relationships between the chemical structure of saponins and their biological activities. Observations from numerous studies confirm that the structure of the aglycon and the sugar moiety influences to biological activity of saponins (Chwalek et al.,

2006; Mimaki et al., 2001). Herein, those correlations were summered due to the previously reported cytotoxicity.

1.3.1. In case of steroidal saponins

- Although the introduction of a hydroxyl group at C-17α position of the aglycon slightly reduced their cytotoxicities, an hydroxyl group at C-27 position led to a considerable decrease in the cytotoxic activity. Furthermore, the attachment of an α-L-Rha group at C-2 position of the glycosidic moiety led to the exhibition of a potent activity (Mimaki et al., 2001).

- Tran et al. (2001) suggested that the presence of Fuc and Xyl linked at C-24 position of the aglycon of spirostanol saponins seemed to be important for the cytotoxic activity against HT-1080 fibrosarcoma cells. Furthermore, without the Fuc, Xyl and acetyl groups, a spirostanol saponin showed a significant activity against colon 26-L5 carcinoma and B-16 BL6 melanoma cell lines.

- Steroidal saponins with a glycosyl group linked at C-1 position of the aglycon showed no activity with the exceptions of those possessing some acyl groups at the glycosyl moiety. It could be assumed that the presence of a certain degree of lipophilicity in the sugar moiety is essential for exhibiting the cytotoxic activity (Mimaki et al., 2001). This suggestion was confirmed by Rezgui et al., 2013.

- The presence of an acetyl group at Glc C-6 position of glycosidic moiety may considerably decreased the cytotoxicity against HT-29 cells and had no effect against HCT116 cells (Kougan et al., 2010). Tang et al. (2014) assumed that the presence of an acetyl group at C-4 of the α-L-Rha exhibited less cytotoxicity than the one without the acetyl group.

- Furostanol saponins hardly exhibited specific properties of saponins, but the furostanol glycosides bearing α-L-Rha-(1→2)-β-D-Glc or an α-L-Rha-(1→2)-[α-L-Rha-(1→4)]-β-D-Glc at C-3 position of the aglycon were found to be cytotoxic to HL-60 cells (Mimaki et al., 2001).

1.3.2. In case of triterpenoid saponins

- The presence of an α-L-Rha-(1→2)-α-L-Ara or α-L-Rha-(1→2)-α-L-Xyl sequence at the C-3 position of the aglycon is a structural requirement essential for potent cytotoxic activity of oleanane saponins (Bang et al., 2005; Gauthier et al., 2009a). Moreover, trisaccharides with a third sugar linked at C-4 position of Ara or C-3 position of Rha exhibited stronger cytotoxicities than disaccharides. But, a change in the sugar moiety influences cytotoxic activity (Rezgui et al., 2016).

- The cytotoxicity of the lupane-type saponins were much weaker than those of oleananes, when an α-L-Rha-(1→2)-α-L-Ara sequence was present in a branched sugar moiety at C-3 of the aglycon (Gauthier et al., 2009b).

- The existence of a free COOH at C-28 is important for antitumor activity, conformed with some reports (Chwalek et al., 2006; Rezgui et al., 2016), but was contradictory to Gauthier et al. (2009a) who showed that some bidesmosidic betulinic acid saponins glycosylated at C-28 were highly cytotoxic.

- Comparison of activities exerted by saponins derived from oleanolic acid and hederagenin made the authors postulate that the hydroxyl group at C-23 has a negative effect on cytotoxicity (Barthomeuf et al., 2002; Park et al., 2001). It could be explained by the attribution to the electron donating effect of two lone-paired electrons of hydroxyl group toward C-3 of the aglycon (Bang et al., 2005).

- A very interesting observation comes from *in vivo* experiments, as no direct correlation was seen with *in vitro* cytotoxicity: Oleanolic acid derivatives showed much stronger cytotoxicities *in vitro* than those of hederagenin, and had an inferior *in vivo* antitumor activity. This may be due to the differences in bioavailability of these structures, so the presence of a hydroxyl at C-23 seems to be more effective for *in vivo* antitumor activity (Sobolewska et al., 2020).

1.4. Cytotoxic mechanism of saponins

Saponins are potential cytotoxic agents, with different mechanisms of action. Their cytotoxic effects may be due to either apoptosis inducement or nonapoptotic cell death

stimulation. There is a number of well-known processes which lead to the same effect with different mechanisms of action. The most important mechanisms are summarized in Table 12 (Podolak et al., 2010).

Table 10. Mechanisms of cytotoxic activity of saponins

Process	Mode of action
Apoptosis intrinsic pathway	- Cytochrome C release - Mitochondria membrane depolimerization - GADD153/CHOP transcription factor expression increase - Caspase 3 and 9 activation - PARP-1 cleavage - MAPK cascade activation - p-STAT-3 decrease - Bcl-2, c-myc, surviving downregulation - VEGF downregulation - p53 stimulation - NF-κB inhibition - JAKs dephosphorylation - Protein phosphatase-1 activation - Intracellular Ca^{2+} homeostasis disruption
Apoptosis extrinsic pathway	- Fas enhancement - Fas ligand enhancement
Apoptosis non-specified	- Telomerase activity inhibition
Cell cycle arrest	- CDK6 downregulation - Cyclin D3 downregulation - Cyclin D1 downregulation - p27kip upregulation - CDK2 inhibition
Autophagy	- Microtubule-associated protein light chain-3 increase - Autophagic vacuoles number - increase - AMPK-TSC2 regulation - Cellular ATP decrease

	- AMPK activation
Angiogenesis inhibition	- Thrombospondin-1 expression increase
	- PKC expression decrease
	- ERK activation
	- P38MAPK activation
	- Endothelial cell proliferation inhibition
	- Tube-formation inhibition
Cytoskeleton disintegration	- Microtubule disassembly
	- Tubulin polymerization inhibition
	- Actin filaments disruption
	- Intracellular ATP decrease
	- Nucleus morphology changes
Metastasis inhibition	- Cell motility and migration inhibition
	- Cell adhesion inhibition
	- MMP-2, MMP-9 downregulation
	- TIMP-2 upregulation

2. Materials and methods

2.1. The principle of MTS colorimetric assay

MTS tetrazolium compound is reduced by viable cells, leading to generate a soluble colored formazan in cell culture media. NAD(P)H-dependent dehydrogenase enzymes in metabolically active cells has an important role in this conversion. The absorbance can be measured at 490-500 nm. The assay can be used to measure of cell proliferation and analyse of pharmaceutical compounds. Comparing to the routine MTT assay, this colorimetric one can be performed by adding the reagent directly into the cell culture media, with out washing or solubilization step and can be carried out in a 96-well microtiter plate (Abcam Cambrige, 2019).
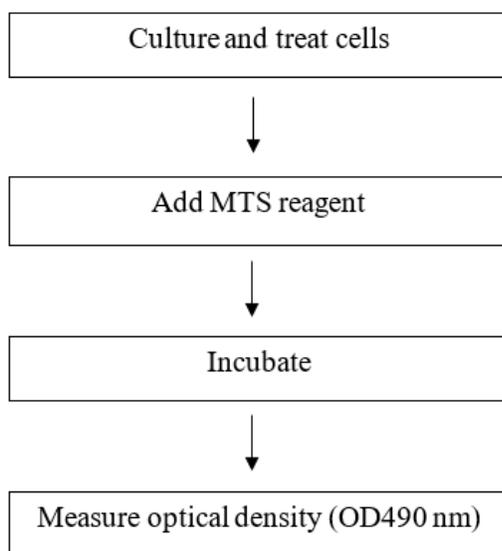
Figure 185. MTS assay summary

2.2. Experiment protocol

Cells were purchased from ATCC (USA); Fetal Bovine Serum (FBS) was from Dutscher. RPMI 1640 medium was from Corning. MTS colorimetric assay was from Abcam. Microplate reader was from Spark®, Tecan.

This experiment protocol was carried out according to the manufacturer's instruction (Abcam Cambridge). Cells were seeded at the density of 5×10^3 cells in 96 well plates (Falcon), cultivated for 48 h before treatments in RPMI 1640 medium (Corning) with 10% FBS (Dutcher). Cells were then treated with the isolated compounds at the concentrations from 1 to 50 µM, for 36h in RPMI1640 medium without FBS (200µl per well). Viability was measured using MTS colorimetric assay (Abcam) following the manufacturer recommendations. Briefly, 20 µl of MTS reagent was added into each well and optical density at 490 nm was read using a microplate reader (Spark®, Tecan) after 1h incubation at 37°C, 5% CO_2, in the dark. The results were expressed as concentrations of compound producing 50% toxicity (IC_{50} value). Fluorouracil (5-FU) was used as positive control and exhibited IC_{50} values of 11.7 µM. The experiments were repeated five times (Abcam Cambrige, 2019).

3. Results of cytotoxic study on isolated and selected saponins

The cytotoxic tests were done in Centre Georges-François Leclerc, ICMUB UMR CNRS 6302. The results were expressed as concentrations of compound producing 50% toxicity (IC50 value).

3.1. Cytotoxic study on the saponins isolated from *Weigela* x "Bristol Ruby"

Since saponins isolated from *Weigela stelzneri* exhibited significant cytotoxic activities on SW480 human cell lines and EMT-6 mouse cell lines (Rezgui et al., 2016), we have investigated the cytotoxicity of the compounds **1-3, 6, 7** by using MTS colorimetric assay on the mouse colon cancer cell line CT26 with different concentrations from 1 to 50 µM.

Table 11. IC50 of compounds **1-3**, **6** and **7** against colon cancer cells (CT-26)

Compounds	IC$_{50}$ (µM)
1	1.97
2	1.22
3	1.48
6	1.09
7	1.87
5-FU	11.7

5-FU was used as positive control.
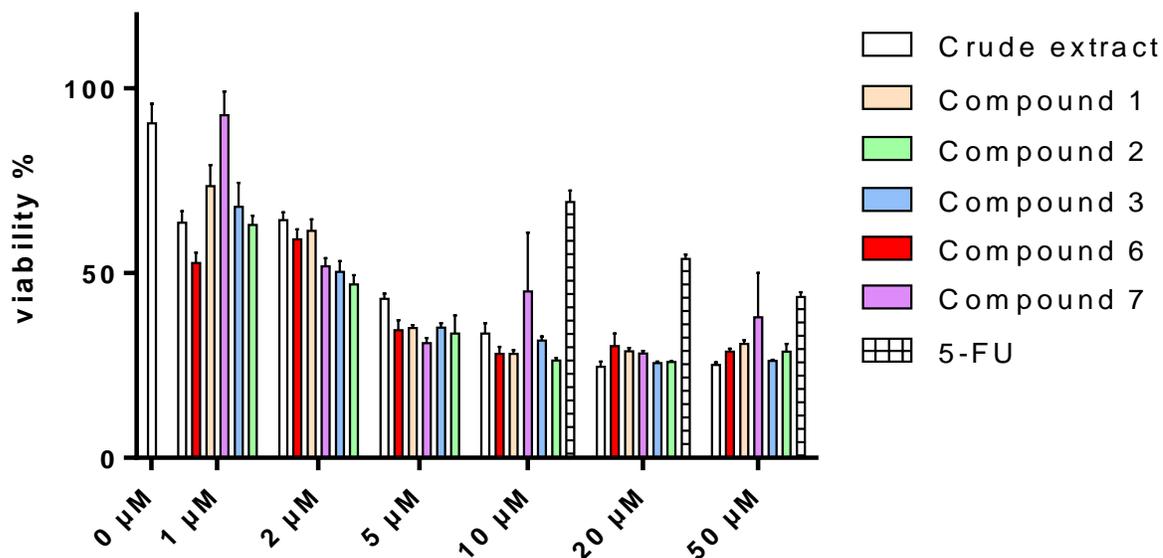
Figure 186. Evaluation of the cytotoxic activity of compounds **1-3**, **6** and **7** against colon cancer cells (CT-26)**,** in concentrations ranging from 1 to 50 µM. Fluorouracil (5-FU) was used as positive control.

Compounds **1**-**3**, **6** and **7**, monodesmosidic and bidesmosidic saponins, were tested to evaluate their cytotoxic activity against a mouse colon cancer cell line (CT26), in concentrations ranging from 1 to 50 µM (Fig. 186). All the tested glycosides showed potent cytotoxicities, with IC_{50} from 1.09 to 1.97 µM, comparing to 5-FU with an IC_{50} of 11.7 µM (Table 11). First of all, to propose clear structure / activity relationships, oleanolic acid is important for the cytotoxicity. In the literature, a substitution for example by a primary alcoholic function at C-23, as hederagenin, seems to decrease the activity (Bang et al., 2005; Rezgui et al., 2016). For the osidic part, the presence of the common sequences α-L-rhamnopyranosyl-(1→2)-β-D-xylopyranosyloleanolic or α-L-rhamnopyranosyl-(1→2)-arabinopyranosyloleanolic acid, have a role in the cytotoxicity (Bang et al., 2005; Rezgui et al., 2016), but in our study, we can propose more precisely the key sequence β-D-xylopyranosyl-(1→3)-α-L-rhamnopyranosyl-(1→2)-β-D-xylopyranosyloleanolic acid or β-D-xylopyranosyl-(1→3)-α-L-rhamnopyranosyl-(1→2)-arabinopyranosyloleanolic acid. Moreover, a linear oligosaccharide chain linked at the C-3 position in **1** and **7**, instead of a branched one in **2**, **3** and **6**, seems to weakly decrease the activity. Compound **6** shows the

more potent activity, even if its structure contains a linear oligosaccharide chain and an esterification at the position 28, two structural.
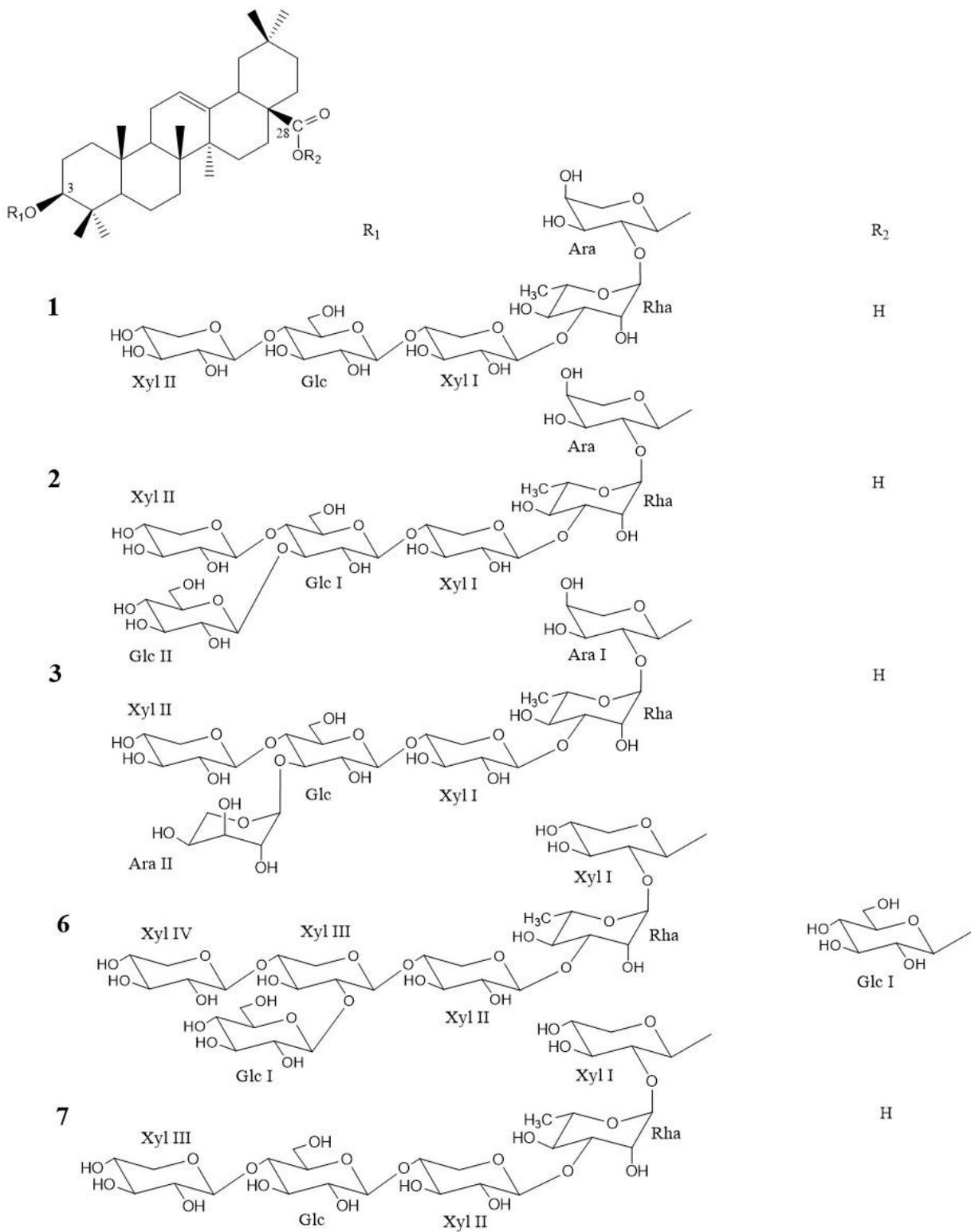
Figure 187. Structure compounds **1-3, 6** and **7**

3.2. Cytotoxic study on the saponins isolated from *Weigela florida* "Pink Poppet" and *Weigela florida* "Jean's Gold"

The cytotoxicities of the isolated compounds **8, 10, 11, 13, 15, 17** against mouse colon cancer (CT26 cells), mouse melanoma (B16 cells) and human liver cancer (HepG2 cells) were evaluated by MTS assay, in concentrations ranging from 1 to 50 μM (Fig. 188). The results of their cytotoxicities were shown in Table 12.

Table 12. Cytotoxic activity of compounds **8, 10, 11, 13, 15, 17**

against three mouse cancer cell lines

Compounds	IC_{50} (μM)		
	CT26	B16	HepG2
8	2.45	2.35	2.77
10	2.19	2.32	2.83
11	–	–	–
13	–	–	–
15	–	–	–
17	–	–	–

"–": no data is available due to low toxicity.
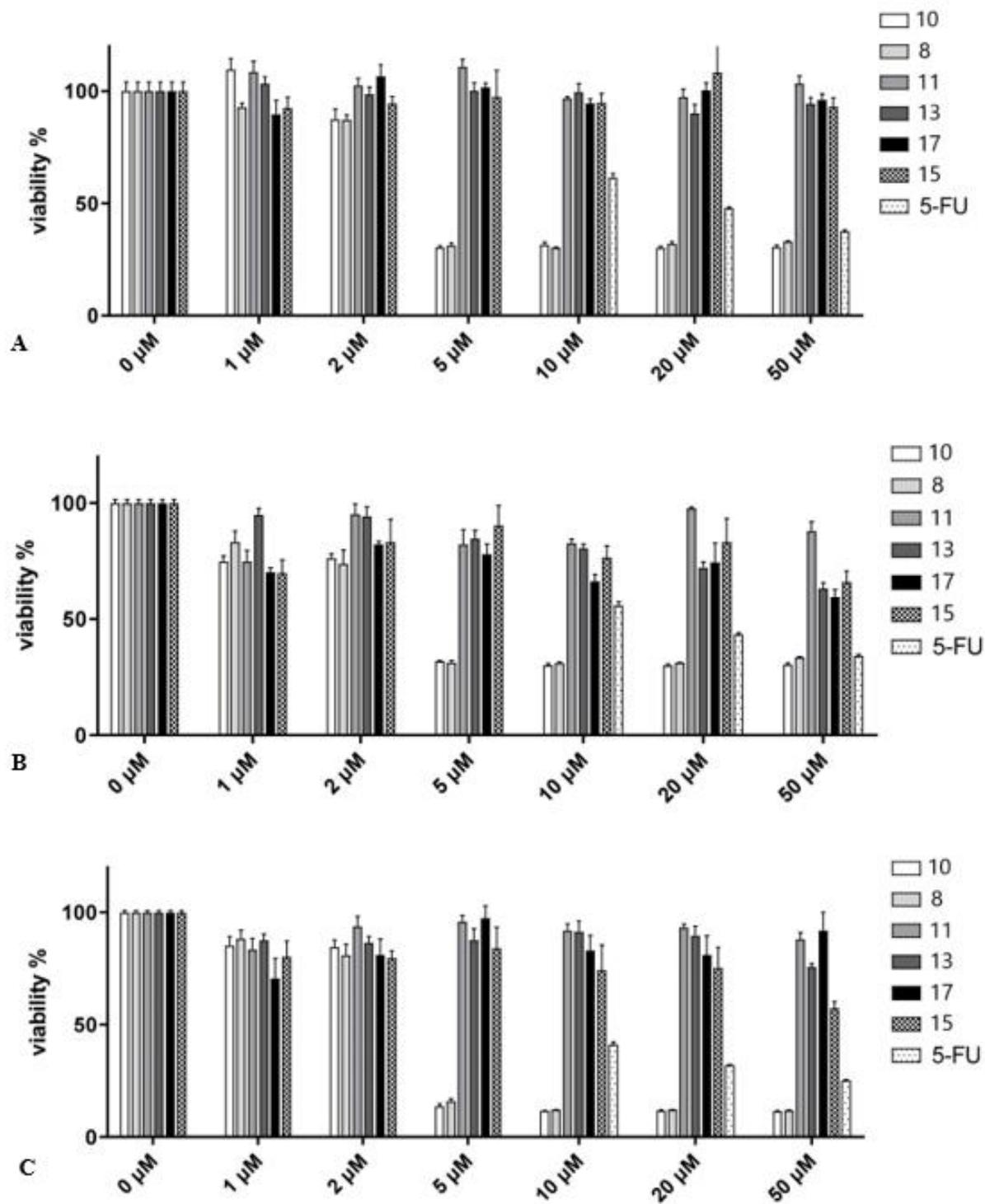
Figure 188. Evaluation of the cytotoxic activity of compounds **8, 10, 11, 13, 15, 17** against CT26 (**A**), B16 (**B**) and HepG2 (**C**), in concentrations ranging from 1 to 50 µM.
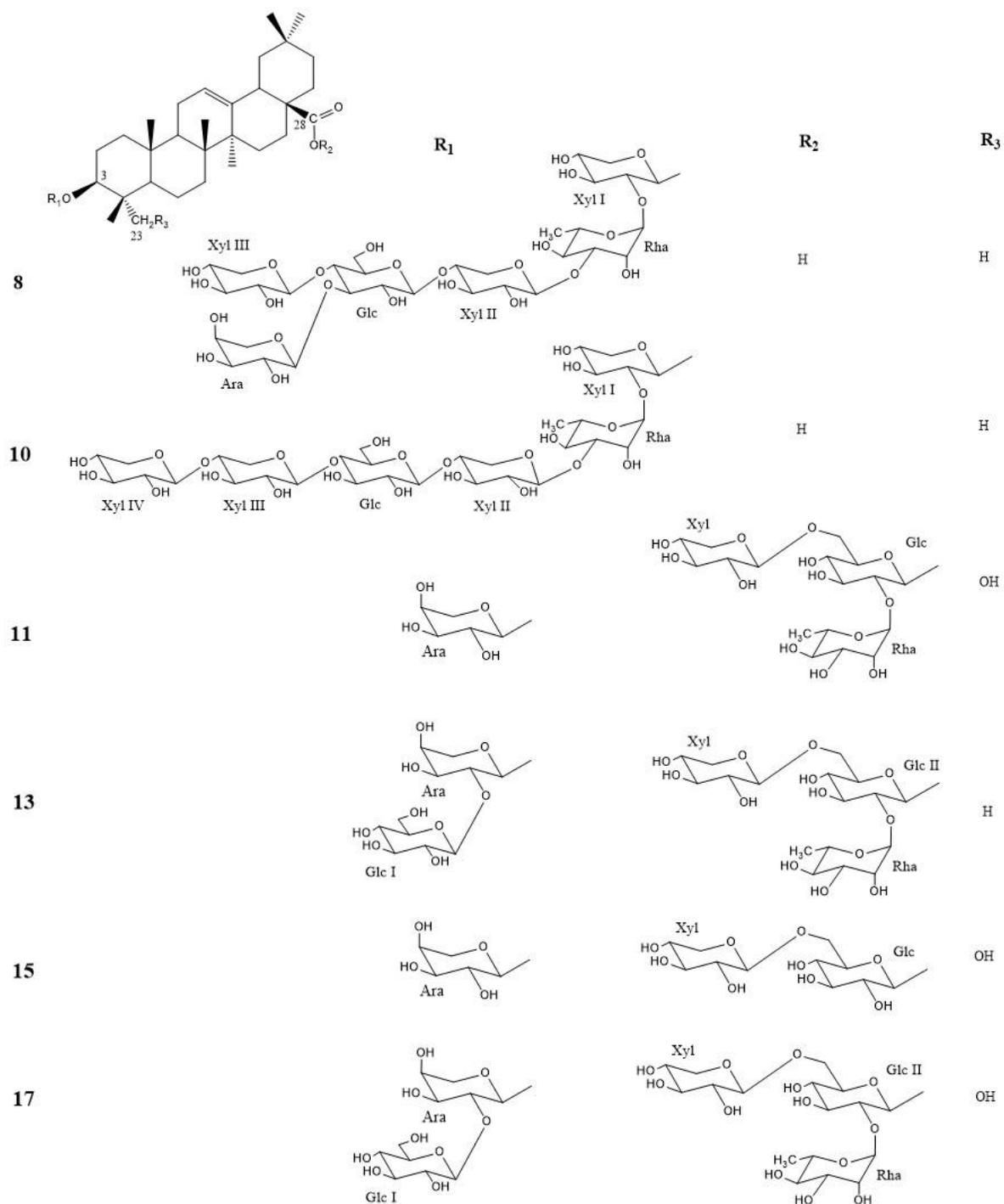
Figure 189. Structure compounds **8, 10, 11, 13, 15** and **17**

The bidesmosidic oleanolic derivative **13** along to those hederagenin **11**, **15**, **17** were inactive cell lines. The appearance of the ester group at C-28 and/or the primary alcohol function at C-23 led to a negative effect which was previously described by (Bang et al., 2005) and confirmed by Rezgui et al., 2016. On the other hand, two monodesmosidic

oleanolic acid glycosides **8, 10** exhibited a good cytotoxic activity on both cell lines, with IC50 (µM) at 2.35 (B16), 2.45 (CT26), 2.78 (HepG2) for **8**, and 2.32 (B16), 2.19 (CT26), 2.83 (HepG2) for **10** (Table 12), according to the presence of sequence β-D-xylopyranosyl-(1→3)-α-L-rhamnopyranosyl-(1→2)-β-D-xylopyranosyloleanolic acid which was previously described in *W*. x "Bristol Ruby".

Conclusion and perspectives

Vietnam flora is one of the richest biodiversity on earth, with an abundant vegetation and its high rate of endemism. However, there are still very few studies that value this particularity of the country. The present thesis included a study of the chemical constituents of one species harvested in Vietnam and three others provided by a company located in France, belonging to two different plant families. These plants were *Weigela* x *"Bristol Ruby"*, *Weigela florida* "Pink poppet" and *Weigela florida "Jean's gold"* (Caprifoliaceae), *Cordyline fruticosa "Fairchild red"* and *Dracaena braunii* (Asparagaceae). The choice of species was based, following a thorough literature search, on the saponin content of certain species of the same genus.

The phytochemical study allowed the isolation of 35 natural compounds using several chromatographic techniques (Flash chromatography, Vacuum liquid chromatography, Column chromatography, Medium pressure liquid chromatography). Their characterization was carried out using spectroscopic techniques (Mass spectroscopy and Nuclear Magnetic Resonance). The isolated molecules of the Caprifoliaceae family are triterpenoid saponins while the others of the Asparagaceae family are steroidal saponins. These compounds are distributed as follows:

From the family Caprifoliaceae:

- *Weigela* x "Bristol ruby": 7 oleanane-type triterpenoid saponins were isolated including 6 previously undescribed in addition to 1 known.
- *Weigela florida* "Pink poppet": 3 oleanane-type and 1 hederagenin-type triterpenoid saponins were isolated including 1 previously undescribed in addition to 3 knowns.
- *Weigela florida* "Jean's gold": 2 oleanane-type and 4 hederagenin-type triterpenoid saponins were isolated including 2 previously undescribed in addition to 4 knowns.

From the family Asparagaceae:

- *Cordyline fruticosa* "Fairchild red": 9 spirostane-type and 6 furostane-type steroidal saponins were isolated including 13 previously undescribed in addition to 2 knowns.
- *Dracaena braunii*: Three known compounds were purified from the roots.

Preliminary biological tests were based on their structural diversity including the nature of the aglycones and sugars, the type of inter-glycosidic bond and the type of saccharide sequence. Five saponins extracted from *Weigela* x "Bristol ruby" were using to evaluate their cytotoxic activity against CT26 cell lines. Six other isolated from two other *Weigela* species, *Weigela florida* "Pink poppet" and *Weigela florida* "Jean's gold", were tested for their cytotoxicity against not only CT26 cell lines, but also two other cancer cell lines B16 and HepG2 in comparison with 5-FU used as positive control. In both cases, the presence of the sequence β-D-xylopyranosyl-(1→3)-α-L-rhamnopyranosyl-(1→2)-β-D-xylopyranosyloleanolic acid or β-D-xylopyranosyl-(1→3)-α-L-rhamnopyranosyl-(1→2)-arabinopyranosyloleanolic acid played an important role in cytotoxic activity. In contrary, the cytotoxic activity of hederagenin-type triterpenoid saponins were inactive *in vitro*, but those saponins exhibited an inferior *in vivo* antitumor activity due to literature. Thus, it will interresting to evaluate the *in vivo* cytotoxic activity of this type saponins in the further study.

Moreover, this work opens new perspectives:

Diosgenin, a genin of the saponin dioscin which was firstly extracted from the rhizome of *Dioscorea tokoro* Makino (Honda, 1904) and also successfully purified from the roots of *Dracaena braunii*, possess interesting potentials. This compound exhibits good anticancer activities including liver cancer (Cruz et al., 2018), colon carcinoma (Raju and Bird, 2007), hepatocellular carcinoma (Chen et al., 2018), breast cancer (He et al., 2014), prostate cancer (Hamid et al., 2017), gastric cancer (Dong et al., 2018). The anticancer mechanism of diosgenin is related to the modulation of multiple cell signaling that plays a significant role in proliferation, differentiation, migration, apoptosis, oncogenesis, and angiogenesis (Raju and Rao, 2012). But, like others natural plant compounds, diosgenin has less toxicity than chemical drugs, and its bioactivities can be limited because of low water solubility and poor absorption. In order to overcome limitations and enhance therapeutic efficacy of diosgenin, a new method is required to not only enhances its positive bioavailability but also decreases its negative characteristics. This perspective will focus on diosgenin encapsulation.

BIBLIOGRAPHY

1. Abcam Cambrige, 2019. MTS Assay Kit (Cell Proliferation) (Colorimetric) (ab197010). https://www.abcam.com/mts-assay-kit-cell-proliferation-colorimetric-ab197010.html (accessed 9.2.20).

2. Agrawal, P.K., Jain, D.C., Gupta, R.K., Thakur, R.S., 1985. Carbon-13 NMR spectroscopy of steroidal sapogenins and steroidal saponins. Phytochemistry 24, 2479–2496. https://doi.org/https://doi.org/10.1016/S0031-9422(00)80653-6

3. Agrawal, P.K., Jain, D.C., Pathak, A.K., 1995. NMR spectroscopy of steroidal sapogenins and steroidal saponins: An update. Magn. Reson. Chem. 33, 923–953. https://doi.org/10.1002/mrc.1260331202

4. Andriamisaina, N., Mitaine-Offer, A.-C., Pruvot, B., Chluba, J., Miyamoto, T., Tanaka, C., Lacaille-Dubois, M.-A., 2018. Phytochemistry of *Weigela* x "kosteriana variegata" (Caprifoliaceae), Natural Product Communications.

5. Bang, S.-C., Lee, J.-H., Song, G.-Y., Kim, D.-H., Yoon, M.-Y., Ahn, B.-Z., 2005. Antitumor activity of Pulsatilla koreana saponins and their structure-activity relationship. Chem. Pharm. Bull. (Tokyo). 53, 1451–1454.

6. Barthomeuf, C., Debiton, E., Mshvildadze, V., Kemertelidze, E., Balansard, G., 2002. In vitro activity of hederacolchisid A1 compared with other saponins from *Hedera colchica* against proliferation of human carcinoma and melanoma cells. Planta Med. 68, 672–675.

7. Blunden, G., Sitton, D., Beach, S.J., Turner, C.H., 1984. Australigenin, a New Steroidal Sapogenin from *Cordyline australis* Fruits. J. Nat. Prod. 47, 266–269. https://doi.org/10.1021/np50032a005

8. Bombardelli, E., Bonati, A., Gabetta, B., Mustich, G., 1972. Glycosides from rhizomes of *Ruscus aculeatus* L. II. Fitoterapia.

9. Borges, R.M., Valença, S.S., Lopes, A.A., Barbi, N. dos S., da Silva, A.J.R., 2013. Saponins from the roots of *Chiococca alba* and their in vitro anti-inflammatory activity. Phytochem. Lett. 6, 96–100.
    https://doi.org/http://dx.doi.org/10.1016/j.phytol.2012.11.006

10. Boutaghane, N., Voutquenne-Nazabadioko, L., Harakat, D., Simon, A., Kabouche, Z., 2013. Triterpene saponins of *Genista ulicina* Spach. Phytochemistry 93, 176–181. https://doi.org/http://dx.doi.org/10.1016/j.phytochem.2013.03.020

11. Britanica, 1999. Britanica. https://www.britannica.com/plant/Dipsacales (accessed 11.2.19).

12. Bruneton, J., 2016. Pharmacognosie, phytochimie, plantes médicinales. Lavoisier Publishing, Paris.

13. C Keller, A., Ma, J., Kavalier, A., He, K., Brillantes, A.-M., Kennelly, E., 2011. Saponins from the traditional medicinal plant *Momordica charantia* stimulate insulin secretion in vitro, Phytomedicine : international journal of phytotherapy and phytopharmacology. https://doi.org/10.1016/j.phymed.2011.06.019

14. C Mitaine-Offer, A., Abderrazak, M., Hanquet, B., Birlirakis, N., A Lacaille-Dubois, M., 2001. Two Triterpene Saponins from *Achyranthes bidentata*, Chemical & pharmaceutical bulletin. https://doi.org/10.1248/cpb.49.1492

15. Cech, N., Enke, C., 2001. Practical Implications of Some Recent Studies in Electrospray Ionization Fundamentals, Mass spectrometry reviews. https://doi.org/10.1002/mas.10008

16. Chaieb, I., 2010. Saponins as Insecticides: A Review, Tunisian Journal of Plant Protection.

17. Champy-Tixier, A.-S., Mitaine-Offer, A.-C., Real Fernández, F., Miyamoto, T., Tanaka, C., Papini, A.-M., Lacaille-Dubois, M.-A., 2018. Oleanane-type glycosides from the roots of *Weigela florida* "rumba" and evaluation of their antibody recognition. Fitoterapia 128, 198–203. https://doi.org/https://doi.org/10.1016/j.fitote.2018.04.017

18. Chan, K.W., Iqbal, S., Khong, N.M.H., Ooi, D.-J., Ismail, M., 2014. Antioxidant activity of phenolics–saponins rich fraction prepared from defatted kenaf seed meal. LWT - Food Sci. Technol. 56, 181–186. https://doi.org/http://dx.doi.org/10.1016/j.lwt.2013.10.028

19. Chen, Z., Xu, J., Wu, Y., Lei, S., Liu, H., Meng, Q., Xia, Z., 2018. Diosgenin inhibited the expression of TAZ in hepatocellular carcinoma. Biochem. Biophys. Res.

Commun. 503, 1181–1185. https://doi.org/10.1016/J.BBRC.2018.07.022

20. Christenhusz, M., Byng, J., 2016. The number of known plant species in the world and its annual increase, Phytotaxa. https://doi.org/10.11646/phytotaxa.261.3.1

21. Chwalek, M., Lalun, N., Bobichon, H., Plé, K., Voutquenne-Nazabadioko, L., 2006. Structure–activity relationships of some hederagenin diglycosides: Haemolysis, cytotoxicity and apoptosis induction. Biochim. Biophys. Acta - Gen. Subj. 1760, 1418–1427. https://doi.org/https://doi.org/10.1016/j.bbagen.2006.05.004

22. Cruz, M. de F.S.J., Pereira, G.M., Ribeiro, M.G., da Silva, A.M., Tinoco, L.W., da Silva, B.P., Parente, J.P., 2016. Ingasaponin, a complex triterpenoid saponin with immunological adjuvant activity from *Inga laurina*. Carbohydr. Res. 420, 23–31. https://doi.org/https://doi.org/10.1016/j.carres.2015.11.008

23. Cruz, M.S., Navoni, J.A., da Costa Xavier, L.A., Madalena Rocha Silva Teles, M., Barbosa-Filho, J.M., Almeida-Lima, J., de Oliveira Rocha, H.A., do Amaral, V.S., 2018. Diosgenin induces genotoxic and mutagenic effects on HepG2 cells. Food Chem. Toxicol. 120, 98–103. https://doi.org/10.1016/J.FCT.2018.07.011

24. Dong, R., Guo, J., Zhang, Z., Zhou, Y., Hua, Y., 2018. Polyphyllin I inhibits gastric cancer cell proliferation by downregulating the expression of fibroblast activation protein alpha (FAP) and hepatocyte growth factor (HGF) in cancer-associated fibroblasts. Biochem. Biophys. Res. Commun. 497, 1129–1134. https://doi.org/10.1016/J.BBRC.2018.02.193

25. Elyashberg, M., 2015. Identification and structure elucidation by NMR spectroscopy, TrAC Trends in Analytical Chemistry. https://doi.org/10.1016/j.trac.2015.02.014

26. Fang, Y.-S., Cai, L., Li, Y., Wang, J.-P., Xiao, H., Ding, Z.-T., 2015. Spirostanol steroids from the roots of *Allium tuberosum*. Steroids 100, 1–4. https://doi.org/http://dx.doi.org/10.1016/j.steroids.2015.03.015

27. Finegardening, 2019. *Cordyline*. https://www.finegardening.com/genus/cordyline (accessed 2.16.19).

28. Fouedjou, R., Teponno, R., Quassinti, L., Bramucci, M., Petrelli, D., Vitali, L., Fiorini, D., Tapondjou, A., Barboni, L., 2013. Steroidal saponins from the leaves of *Cordyline fruticosa* (L.) A. Chev. and their cytotoxic and antimicrobial activity,

Phytochemistry Letters. https://doi.org/10.1016/j.phytol.2013.10.001

29. Fries, S.L., Standaert, F.G., Whitcomb, E.R., Nigrelli, R.F., Chanley, J.D., Sobotka, H., 1960. Some pharmacologic properties of holothurin a, a glycosidic mixture from the sea cucurmber*. Ann. N. Y. Acad. Sci. 90, 893–901. https://doi.org/10.1111/j.1749-6632.1960.tb26432.x

30. Fu, Q., Qiu, L., Yuan, H.-M., Du, Y.-F., Cheng, X.-L., Tang, T.-T., Wang, P., Xu, L., Liang, J.-M., Yang, L.-F., Zou, L., Xu, S.-Y., 2017. Triterpenoid saponins from *Clematis chinensis* and their inhibitory activities on NO production. Phytochem. Lett. 21, 206–210. https://doi.org/http://dx.doi.org/10.1016/j.phytol.2017.07.004

31. Gardenia, 2019. https://www.gardenia.net/plant/*Weigela-florida*-Bristol-Ruby (accessed 2.12.19).

32. Gauthier, C., Legault, J., Girard-Lalancette, K., Mshvildadze, V., Pichette, A., 2009a. Haemolytic activity, cytotoxicity and membrane cell permeabilization of semi-synthetic and natural lupane- and oleanane-type saponins. Bioorg. Med. Chem. 17, 2002–2008. https://doi.org/https://doi.org/10.1016/j.bmc.2009.01.022

33. Gauthier, C., Legault, J., Piochon, M., Lavoie, S., Tremblay, S., Pichette, A., 2009b. Synthesis, cytotoxicity, and haemolytic activity of chacotrioside lupane-type neosaponins and their germanicane-type rearrangement products. Bioorg. Med. Chem. Lett. 19, 2310–2314. https://doi.org/https://doi.org/10.1016/j.bmcl.2009.02.076

34. González, A.G., Hernández, J.C., León, F., Padrón, J.I., Estévez, F., Quintana, J., Bermejo, J., 2003. Steroidal Saponins from the Bark of *Dracaena draco* and Their Cytotoxic Activities. J. Nat. Prod. 66, 793–798. https://doi.org/10.1021/np020517j

35. Hamid, A.A., Kaushal, T., Ashraf, R., Singh, A., Chand Gupta, A., Prakash, O., Sarkar, J., Chanda, D., Bawankule, D.U., Khan, F., Shanker, K., Aiyelaagbe, O.O., Negi, A.S., 2017. (22β,25R)-3β-Hydroxy-spirost-5-en-7-iminoxy-heptanoic acid exhibits anti-prostate cancer activity through caspase pathway. Steroids 119, 43–52. https://doi.org/10.1016/J.Steroids.2017.01.001

36. Hara, S., Okabe, H., Mihashi, K., 1987. Gas-Liquid Chromatographic Separation of Aldose Enantiomers as Trimethylsilyl Ethers of Methyl 2- (Polyhydroxyalkyl) -

thiazolidine-4 (R) -carboxylates. Chem. Pharm. Bull. (Tokyo). 35, 501–506. https://doi.org/10.1248/cpb.35.501

37. He, Z., Chen, H., Li, G., Zhu, H., Gao, Y., Zhang, L., Sun, J., 2014. Diosgenin inhibits the migration of human breast cancer MDA-MB-231 cells by suppressing Vav2 activity. Phytomedicine 21, 871–876. https://doi.org/10.1016/J.Phymed.2014.02.002

38. Herlt, A., Mander, L., Pongoh, E., J Rumampuk, R., Tarigan, P., 2002. Two Major Saponins from Seeds of *Barringtonia asiatica* : Putative Antifeedants toward Epilachna sp. Larvae, Journal of natural products. https://doi.org/10.1021/np000600b

39. Hernández, J.C., León, F., Estévez, F., Quintana, J., Bermejo, J., 2006. A Homo-Isoflavonoid and a Cytotoxic Saponin from *Dracaena draco*. Chem. Biodivers. 3, 62–68. https://doi.org/10.1002/cbdv.200690008

40. Ho, B., 2006. *Cordyline obtecta*.http://www.cpbr.gov.au/gnp/interns-2006/cordyline-obtecta.html (accessed 2.16.19).

41. Ho, C.S., Lam, C.W.K., Chan, M.H.M., Cheung, R.C.K., Law, L.K., Lit, L.C.W., Ng, K.F., Suen, M.W.M., Tai, H.L., 2003. Electrospray Ionisation Mass Spectrometry: Principles and Clinical Applications. Clin. Biochem. Rev. 24, 3–12.

42. Ho Son, K., Young Jung, K., Wook Chang, H., Pyo Kim, H., Sik Kang, S., 1994. Triterpenoid saponins from the aerial parts of *Lonicera japonica*. Phytochemistry 35, 1005–1008. https://doi.org/https://doi.org/10.1016/S0031-9422(00)90656-3

43. Hoffmann, E., Stroobant, V., 2007. Mass Spectrometry: Principles and Applications.

44. Honda, J., 1904. Untersuchungen über die Saponinsubstanzen der *Dioscorea Tokoro* Makino. Arch. für Exp. Pathol. und Pharmakologie 51, 211–226.

45. Hostettmann, K., Terreaux, C., 2000. Medium pressure liquid chromatography A2 - Wilson, Ian D. BT - Encyclopedia of Separation Science. Academic Press, Oxford, pp. 3296–3303. https://doi.org/https://doi.org/10.1016/B0-12-226770-2/01891-3

46. Hostettmann, K., Wolfender, J.L., 2000. Natural products | Liquid Chromatography, in: Wilson, I.D.B.T.-E. of S.S. (Ed.),. Academic Press, Oxford, pp. 3424–3434. https://doi.org/https://doi.org/10.1016/B0-12-226770-2/01651-3

47. Huang, H.-C., Lin, M.-K., Hwang, S.-Y., Hwang, T.-L., Kuo, Yao-Haur, Chang, C.-I., Ou, C.-Y., Kuo, Yueh-Hsiung, 2013. Two anti-inflammatory steroidal saponins

from *Dracaena angustifolia* Roxb. Molecules 18, 8752–8763.
https://doi.org/10.3390/molecules18088752

48.   Huber, H., 1977. The Treatment of the Monocotyledons in an Evolutionary System of Classification, in: Kubitzki, K. (Ed.), Flowering Plants: Evolution and Classification of Higher Categories Symposium, Hamburg, September 8--12, 1976. Springer Vienna, Vienna, pp. 285–298. https://doi.org/10.1007/978-3-7091-7076-2_18

49.   Ishii, H., Kitagawa, I., Matsushita, K., Shirakawa, K., Tori, K., Tozyo, T., Yoshikawa, M., Yoshimura, Y., 1981. The configuration and conformation of the arabinose moiety in platycodins, saponins isolated from *Platycodon grandiflorum*, and mi-saponins from *Madhuca longifolia* based on Carbon-13 and Hydrogen-1 NMR spectroscopic evidence: the total structures of the saponins,, Tetrahedron Letters. https://doi.org/10.1016/S0040-4039(01)90369-7

50.   Iwagoe, K., Konishi, T., Kiyosawa, S., 1987. Studies on the Constituents of the Aerial Parts of *Reineckia carnea* Kunth, Yakugaku Zasshi. https://doi.org/10.1248/yakushi1947.107.2_140

51.   J Just, M., Recio, M., Giner, R., J Cuéllar, M., Máñez, S., Bilia, A.R., Rios, J.-L., 1998. Anti-Inflammatory Activity of Unusual Lupane Saponins from *Bupleurum fruticescens*, Planta medica. https://doi.org/10.1055/s-2006-957469

52.   Jardiland, 2019. https://www.jardiland.com/weigelia-jean-s-gold-9005006.html (accessed 2.12.19).

53.   Jewers, K., M.B. Burbage, M., Blunden, G., Griffin, W.J., 1974. Brisbagenin and brisbenone, two new spirostanes from *Cordyline* species. Steroids 24, 203–208. https://doi.org/https://doi.org/10.1016/0039-128X(74)90103-2

54.   Jun, T., Feng-E, W., Ming-Hua, Q., Rui-Lin, N., 1993. Triterpenoid saponins from *Pterocephalus hookeri*. Phytochemistry 32, 1535–1538. https://doi.org/https://doi.org/10.1016/0031-9422(93)85174-P

55.   Kougan, G.B., Miyamoto, T., Tanaka, C., Paululat, T., Mirjolet, J.-F., Duchamp, O., Sondengam, B.L., Lacaille-Dubois, M.-A., 2010. Steroidal Saponins from Two Species of *Dracaena*. J. Nat. Prod. 73, 1266–1270.

https://doi.org/10.1021/np100153m

56. Krikorian, A.D., 1986. The Families of the Monocotyledons: Structure, Evolution, and Taxonomy. R. M. T. Dahlgren , H. T. Clifford , P. F. Yeo . Q. Rev. Biol. 61, 108–109. https://doi.org/10.1086/414792

57. Lacaille-Dubois, M.A., Wagner, H., 2000. Bioactive saponins from plants: An update, in: Atta-ur-Rahman, B.T.-S. in N.P.C. (Ed.), Bioactive Natural Products (Part B). Elsevier, pp. 633–687. https://doi.org/10.1016/S1572-5995(00)80015-0

58. Lacaille-Dubois, M.A., Wagner, H., 1996. A review of the biological and pharmacological activities of saponins. Phytomedicine 2, 363–386. https://doi.org/http://dx.doi.org/10.1016/S0944-7113(96)80081-X

59. Lamarck, J.B. de, 1808. Encyclopédie méthodique: Botanique.

60. List, T.P., http://www.theplantlist.org/browse/A/Caprifoliaceae/Weigela/(accessed 2.12.19).

61. Looking at plant, 2014. *Cordyline fruticosa* "Fairchild Red". https://looking-at-plants.com/plants_a_-_z/cordyline_fruticosa_'fairchild_red' (accessed 2.17.19).

62. Majinda, R.R.T., 2012. Extraction and isolation of saponins. Methods Mol. Biol. 864, 415–426. https://doi.org/10.1007/978-1-61779-624-1_16

63. Marrero, A., 1998. A new species of the wild dragon tree, *Dracaena* (Dracaenaceae) from Gran Canaria and its taxonomic and biogeographic implications, Botanical Journal of the Linnean Society. https://doi.org/10.1006/bojl.1998.0193

64. Massiot, G., Lavaud, C., 1995. Structural elucidation of saponins, in: Atta-ur-Rahman, B.T.-S. in N.P.C. (Ed.), Structure and Chemistry (Part C). Elsevier, pp. 187–224. https://doi.org/https://doi.org/10.1016/S1572-5995(06)80132-8

65. Milgate, J., Roberts, D.C.K., 1995. The nutritional & biological significance of saponins. Nutr. Res. 15, 1223–1249. https://doi.org/http://dx.doi.org/10.1016/0271-5317(95)00081-S

66. Mimaki, Y., Inoue, T., Kuroda, M., Sashida, Y., 1996. Steroidal saponins from *Sansevieria trifasciata*. Phytochemistry 43, 1325–1331. https://doi.org/10.1016/S0031-9422(96)00397-4

67. Mimaki, Y., Kuroda, M., Ide, A., Kameyama, A., Yokosuka, A., Sashida, Y., 1999.

Steroidal saponins from the aerial parts of *Dracaena draco* and their cytostatic activity on HL-60 cells. Phytochemistry 50, 805–813. https://doi.org/https://doi.org/10.1016/S0031-9422(98)00614-1

68. Mimaki, Y., Kuroda, M., Takaashi, Y., Sashida, Y., 1998a. Steroidal saponins from the leaves of *Cordyline stricta*. Phytochemistry 47, 79–85. https://doi.org/https://doi.org/10.1016/S0031-9422(97)00545-1

69. Mimaki, Y., Kuroda, M., Takaashi, Y., Sashida, Y., 1998b. Steroidal saponins from the stems of *Dracaena concinna*. Phytochemistry 47, 1351–1356. https://doi.org/10.1016/S0031-9422(97)00717-6

70. Mimaki, Y., Takaashi, Y., Kuroda, M., Sashida, Y., 1997. Steroidal glucosides from leaves of *Cordyline stricta*. Phytochemistry 45, 1229–1234. https://doi.org/https://doi.org/10.1016/S0031-9422(97)00109-X

71. Mimaki, Y., Yokosuka, A., Kuroda, M., Sashida, Y., 2001. Cytotoxic activities and structure-cytotoxic relationships of steroidal saponins. Biol. Pharm. Bull. 24, 1286–1289.

72. Min, X., Ying-Jun, Z., Xing-Cong, L., Jacob, M.R., Chong-Ren, Y., 2010. Steroidal Saponins from Fresh Stems of *Dracaena angustifolia*. J. Nat. Prod. 73, 1524–1528. https://doi.org/10.1021/np100351p

73. Missouri Botanical Garden, 2019a. No Title [WWW Document]. URL http://www.missouribotanicalgarden.org/PlantFinder/PlantFinderDetails.aspx?taxonid=257689&isprofile=0& (accessed 2.12.19).

74. Missouri Botanical Garden, 2019b. No Title [WWW Document]. URL http://www.mobot.org/mobot/research/apweb/orders/asparagalesweb.htm (accessed 2.12.19).

75. Missouri Botanical Garden, n.d. No Title [WWW Document]. URL http://www.mobot.org/mobot/research/apweb/orders/dipsacalesweb.htm (accessed 2.2.19).

76. Moghimipour, E., Handali, S., 2015. Saponin: Properties, Methods of Evaluation and Applications, Annual Research & Review in Biology. https://doi.org/10.9734/ARRB/2015/11674

77. Morrissey, J., Osbourn, A., 1999. Fungal Resistance to Plant Antibiotics as a Mechanism of Pathogenesis, Microbiology and molecular biology reviews : MMBR.

78. Moses, T., Papadopoulou, K.K., Osbourn, A., 2014. Metabolic and functional diversity of saponins, biosynthetic intermediates and semi-synthetic derivatives. Crit. Rev. Biochem. Mol. Biol. 49, 439–462. https://doi.org/10.3109/10409238.2014.953628

79. Mostafa, A., Sudisha, J., El-Sayed, M., Ito, S., Ikeda, T., Yamauchi, N., Shigyo, M., 2013. Aginoside saponin, a potent antifungal compound, and secondary metabolite analyses from *Allium nigrum* L. Phytochem. Lett. 6, 274–280. https://doi.org/http://dx.doi.org/10.1016/j.phytol.2013.03.001

80. Mostafa, A.E., El-Hela, A.A., Mohammad, A.-E.I., Cutler, S.J., Ross, S.A., 2016. New triterpenoidal saponins from *Koelreuteria paniculata*. Phytochem. Lett. 17, 213–218. https://doi.org/http://dx.doi.org/10.1016/j.phytol.2016.07.008

81. Murayama, T., Kasahara, A., Shiono, Y., Ikeda, M., 2003. Structure Elucidation of a Triterpene Glycoside Isolated from *Weigela hortensis*. Nat. Med. 57, 181–184.

82. Murphy, B., D'Aux, R.C.D., 1975. The use of Sephadex LH-20 column chromatography to separate unconjugated steroids, Journal of steroid biochemistry. https://doi.org/10.1016/0022-4731(75)90138-7

83. Naidu, A.S., 2000. Natural Food Antimicrobial Systems, Catechins. https://doi.org/10.1201/9781420039368

84. Nguyen, D.H., Mitaine-Offer, A.-C., Maroso, S., Papini, A.-M., Paululat, T., Bellaye, P.-S., Collin, B., Chambin, O., Lacaille-Dubois, M.-A., 2019. Cytotoxic glycosides from the roots of *Weigela* x "Bristol Ruby." Fitoterapia 137, 104242. https://doi.org/10.1016/J.FITOTE.2019.104242

85. Oleszek, W., Bialy, Z., 2006. Chromatographic determination of plant saponins—An update (2002–2005). J. Chromatogr. A 1112, 78–91. https://doi.org/http://dx.doi.org/10.1016/j.chroma.2006.01.037

86. P. Munafo Jr, J., Gianfagna, T., 2014. Chemistry and biological activity of steroidal glycosides from the *Lilium* genus, Nat. Prod. Rep. https://doi.org/10.1039/C4NP00063C

87. Park, H.-J., Kwon, S.-H., Lee, J.-H., Lee, K.-H., Miyamoto, K., Lee, K.-T., 2001. Kalopanaxsaponin A is a basic saponin structure for the anti-tumor activity of hederagenin monodesmosides. Planta Med. 67, 118–121.

88. Perrone, A., Muzashvili, T., Napolitano, A., Skhirtladze, A., Kemertelidze, E., Pizza, C., Piacente, S., 2009. Steroidal glycosides from the leaves of *Ruscus colchicus*: Isolation and structural elucidation based on a preliminary liquid chromatography-electrospray ionization tandem mass spectrometry profiling, Phytochemistry. https://doi.org/10.1016/j.phytochem.2009.08.016

89. Pertuit, D., Larshini, M., Brahim, M.A., Markouk, M., Mitaine-Offer, A.-C., Paululat, T., Delemasure, S., Dutartre, P., Lacaille-Dubois, M.-A., 2017. Triterpenoid saponins from the roots of *Spergularia marginata*. Phytochemistry 139, 81–87. https://doi.org/http://dx.doi.org/10.1016/j.phytochem.2017.03.007

90. Pettit, G.R., Doubek, D.L., Herald, D.L., Numata, A., Takahasi, C., Fujiki, R., Miyamoto, T., 1991. Isolation and Structure of Cytostatic Steroidal Saponins from the African Medicinal Plant Balanites aegyptica. J. Nat. Prod. 54, 1491–1502. https://doi.org/10.1021/np50078a002

91. PlantsRescue, 2019. *Dracaena sanderiana* [WWW Document]. URL www.plantsrescue.com/tag/dracaena-braunii/%0D (accessed 2.16.19).

92. Podolak, I., Galanty, A., Sobolewska, D., 2010. Saponins as cytotoxic agents: a review. Phytochem. Rev. 9, 425–474. https://doi.org/10.1007/s11101-010-9183-z

93. Ponou, B.K., Teponno, R.B., Tapondjou, A.L., Lacaille-Dubois, M.-A., Quassinti, L., Bramucci, M., Barboni, L., 2019. Steroidal saponins from the aerial parts of *Cordyline fruticosa* L. var. strawberries. Fitoterapia 134, 454–458. https://doi.org/https://doi.org/10.1016/j.fitote.2019.03.019

94. Raju, J., Bird, R.P., 2007. Diosgenin, a naturally occurring furostanol saponin suppresses 3-hydroxy-3-methylglutaryl CoA reductase expression and induces apoptosis in HCT-116 human colon carcinoma cells. Cancer Lett. 255, 194–204. https://doi.org/10.1016/J.CANLET.2007.04.011

95. Raju, J., Rao, C., 2012. Diosgenin, a Steroid Saponin Constituent of Yams and Fenugreek: Emerging Evidence for Applications in Medicine, in: Bioactive

Compounds in Phytomedicine. https://doi.org/10.5772/26700

96. Rao, A. V, Sung, M.-K., 1995. Saponins as Anticarcinogens. J. Nutr. 125, 717S-724S. https://doi.org/10.1093/jn/125.3_Suppl.717S

97. Reich, E., Maire-Widmer, V., 2019. Thin-layer chromatography | Overview☆, in: Worsfold, P., Poole, C., Townshend, A., Miró, M.B.T.-E. of A.S. (Third E. (Eds.), . Academic Press, Oxford, pp. 84–92. https://doi.org/https://doi.org/10.1016/B978-0-12-409547-2.00540-0

98. Reynolds, W.F., Enríquez, R.G., 2002. Choosing the Best Pulse Sequences, Acquisition Parameters, Postacquisition Processing Strategies, and Probes for Natural Product Structure Elucidation by NMR Spectroscopy. J. Nat. Prod. 65, 221–244. https://doi.org/10.1021/np010444o

99. Rezgui, A., Mitaine-Offer, A.-C., Miyamoto, T., Tanaka, C., Delemasure, S., Dutartre, P., Lacaille-Dubois, M.-A., 2016. Oleanolic acid and hederagenin glycosides from *Weigela stelzneri*. Phytochemistry 123, 40–47. https://doi.org/https://doi.org/10.1016/j.phytochem.2015.12.016

100. Rezgui, A., Mitaine-Offer, A.-C., Pertuit, D., Miyamoto, T., Tanaka, C., Delemasure, S., Dutartre, P., Lacaille-Dubois, M.-A., 2013. Steroidal Saponins from *Dracaena marginata*. Nat. Prod. Commun. 8, 1934578X1300800205. https://doi.org/10.1177/1934578X1300800205

101. Sennikov, A.N., Soltis, D.E., Mabberley, D.J., Byng, J.W., Fay, M.F., Christenhusz, M.J.M., Chase, M.W., Stevens, P.F., Soltis, P.S., Judd, W.S., Group, T.A.P., 2016. An update of the Angiosperm Phylogeny Group classification for the orders and families of flowering plants: APG IV. Bot. J. Linn. Soc. 181, 1–20. https://doi.org/10.1111/boj.12385

102. Sheffield Botanical Garden [WWW Document], n.d. URL http://www.sbg.org.uk/portfolio-items/the-genus-weigela-caprifoliaceae/ (accessed 2.12.19).

103. Shen, H.-Y., Zuo, W.-J., Wang, H., Zhao, Y.-X., Guo, Z.-K., Luo, Y., Li, X.-N., Dai, H.-F., Mei, W.-L., 2014. Steroidal saponins from dragon's blood of *Dracaena cambodiana*. Fitoterapia 94, 94–101.

https://doi.org/https://doi.org/10.1016/j.fitote.2014.01.020

104. Silva, B.P. da, Parente, J.P., 2013. A new complex triterpenoid saponin from *Calliandra pulcherrima* with haemolytic activity and adjuvant effect. Phytochem. Lett. 6, 633–639. https://doi.org/http://dx.doi.org/10.1016/j.phytol.2013.08.009

105. Sobolewska, D., Galanty, A., Grabowska, K., Makowska-Wąs, J., Wróbel-Biedrawa, D., Podolak, I., 2020. Saponins as cytotoxic agents: an update (2010–2018). Part I— steroidal saponins. Phytochem. Rev. 19, 139–189. https://doi.org/10.1007/s11101-020-09661-0

106. Sparg, S.G., Light, M.E., van Staden, J., 2004. Biological activities and distribution of plant saponins. J. Ethnopharmacol. 94, 219–243. https://doi.org/https://doi.org/10.1016/j.jep.2004.05.016

107. Sticher, O., 2008. Natural product isolation. Nat. Prod. Rep. 25, 517–554. https://doi.org/10.1039/B700306B

108. Tang, L., Wang, Z., Wu, H., Yokosuka, A., Mimaki, Y., 2014. Steroidal glycosides from the underground parts of *Dracaena thalioides* and their cytotoxic activity. Phytochemistry 107, 102–110. https://doi.org/https://doi.org/10.1016/j.phytochem.2014.07.021

109. Thakur, M., Melzig, M., Fuchs, H., Weng, A., 2011. Chemistry and pharmacology of saponins: Special focus on cytotoxic properties, Botanics: Targets and Therapy. https://doi.org/10.2147/BTAT.S17261

110. The Angiosperm Phylogeny Group, 2009. Angiosperm Phylogeny Group III (APG III). An update of The Angiosperm Phylogeny Group classification for the orders and families of flowering plants: APG III. Botanical Journal of the Linnean Society. Bot. J. Linn. Soc. 161, 105–121. https://doi.org/10.1111/j.1095-8339.2009.00996.x

111. Tran, Q. Le, Tezuka, Y., Banskota, A.H., Tran, Q.K., Saiki, I., Kadota, S., 2001. New Spirostanol Steroids and Steroidal Saponins from Roots and Rhizomes of *Dracaena angustifolia* and Their Antiproliferative Activity. J. Nat. Prod. 64, 1127–1132. https://doi.org/10.1021/np0100385

112. Tschesche, R., Hermann, K.-H., Langlais, R., Tjoa, B.T., Wulff, G., 1973. Steroidsaponine mit mehr als einer Zuckerkette, VII. Convallamarosid, ein

trisdesmosidisches 22-Hydroxyfurostanol-Glycosid aus den Wurzeln von *Convallaria majalis* L. Chem. Ber. 106, 3010–3019. https://doi.org/10.1002/cber.19731060932

113. Tsukamoto, T., Ueno, Y., 1936. Glucosides of *Dioscorea tokoro* Makino. I. Dioscin, dioscoreasapotoxin and diosgenin. Yakugaku Zasshi 56, 802(in German 135–40).

114. Van, L., Jin Lee, G., Kim Long Vu, H., Won Kwon, S., Khoi Nguyen, N., Hill Park, J., Nguyen, D., 2015. Ginseng Saponins in Different Parts of *Panax vietnamensis*, ChemicaL & Pharmaceutical bulletin. https://doi.org/10.1248/cpb.c15-00369

115. W. Chase, M., L. REVEAL, J., Fay, M., 2009. A subfamilial classification for the expanded asparagalean families Amaryllidaceae, Asparagaceae and Xanthorrhoeaceae, Botanical Journal of the Linnean Society. https://doi.org/10.1111/j.1095-8339.2009.00999.x

116. Watson, L., A., Dallwitz, M.J., 1992. The families of Flowering Plants: descriptions, illustrations, identification, and information retrieval. [WWW Document]. URL https://www.delta-intkey.com/angio/www/caprifol.htm (accessed 2.11.19).

117. Wen, Y.-S., Ni, W., Qin, X.-J., Yan, H., Chen, C.-X., Hua, Y., Cheng, Y.-C., He, L., Liu, H.-Y., 2015. Steroidal saponins with cytotoxic activity from the rhizomes of *Paris polyphylla* var. yunnanensis. Phytochem. Lett. 12, 31–34. https://doi.org/http://dx.doi.org/10.1016/j.phytol.2015.02.011

118. Willamette Botany, 2001. Asparagaceae [WWW Document]. URL https://willamettebotany.org/asparagaceae/ (accessed 8.31.20).

119. Won, Y.-M., Seong, Z.-K., Kim, J.-L., Kim, H.-S., Song, H.-H., Kim, D.-Y., Kim, J.-H., Oh, S.-R., Cho, H.-W., Cho, J.-H., Lee, H.-K., 2015. Triterpene glycosides with stimulatory activity on melanogenesis from the aerial parts of *Weigela subsessilis*. Arch. Pharm. Res. 38, 1541–1551. https://doi.org/10.1007/s12272-014-0524-0

120. Xiang, L., Wang, Y., Yi, X., He, X., 2016. Antiproliferative and anti-inflammatory furostanol saponins from the rhizomes of *Tupistra chinensis*. Steroids 116, 28–37. https://doi.org/http://dx.doi.org/10.1016/j.steroids.2016.10.005

121. Yang, M.-H., Blunden, G., Patel, A., Crabb, T.A., Brain, K., Griffin, W.J., 1990. Two furostane sapogenins from *Cordyline rubra*. Phytochemistry 29, 1332–1334.

https://doi.org/https://doi.org/10.1016/0031-9422(90)85458-R

122. Yendo, A.C.A., de Costa, F., Cibulski, S.P., Teixeira, T.F., Colling, L.C., Mastrogiovanni, M., Soulé, S., Roehe, P.M., Gosmann, G., Ferreira, F.A., Fett-Neto, A.G., 2016. A rabies vaccine adjuvanted with saponins from leaves of the soap tree (*Quillaja brasiliensis*) induces specific immune responses and protects against lethal challenge. Vaccine 34, 2305–2311.
    https://doi.org/http://dx.doi.org/10.1016/j.vaccine.2016.03.070

123. Yokosuka, A., Mimaki, Y., Sashida, Y., 2002. Four New 3,5-Cyclosteroidal Saponins from *Dracaena surculosa*. Chem. Pharm. Bull. 50, 992–995.
    https://doi.org/10.1248/cpb.50.992

124. Yokosuka, A., Mimaki, Y., Sashida, Y., 2000. Steroidal Saponins from *Dracaena surculosa*. J. Nat. Prod. 63, 1239–1243. https://doi.org/10.1021/np000145j

125. Zhang, Y., Liu, C., Qi, Y., Li, S., Wang, J., 2013. Application of accelerated solvent extraction coupled with counter-current chromatography to extraction and online isolation of saponins with a broad range of polarity from *Panax notoginseng*. Sep. Purif. Technol. 106, 82–89.
    https://doi.org/http://dx.doi.org/10.1016/j.seppur.2012.12.031

126. Zhao, D., Yan, D., Huang, M., Sun, Y., 2012. Efficient protocol for isolation and purification of different soyasaponins from soy hypocotyls, Journal of Separation Science. https://doi.org/10.1002/jssc.201200531

127. Zonneveld, B, S.A.Z., 2019. World Checklist of Cordyline [WWW Document]. Facil. by R. Bot. Gard. Kew. Publ. Internet. URL https://wcsp.science.kew.org/qsearch.do (accessed 2.16.19).

MICROENCAPSULATION PART

VALORISATION OF CURCUMIN POWDER

CONTENT

LIST OF FIGURES

LIST OF TABLES

INTRODUCTION

Curcumin (CAS Registry Number 458-37-7), the principal curcuminoid found in turmeric, is generally considered as its most active constituent (Sharma et al., 2005). Other major curcuminoids present in turmeric are: demethoxycurcumin (curcumin II, n° CAS 22608-11-3), bisdemethoxycurcumin (curcumin III, n° CAS 33171-05-0), and the recently identified cyclocurcumin, n° CAS 153127-42-5 (Kiuchi et al., 1993). More and more evidences point out towards curcumin having potential health benefits including antioxidant, anti-inflammatory, antimicrobial, anti-amyloid and antitumor properties (Aggarwal et al., 2006; Chattopadhyay et al., 2004).

In acidic and neutral conditions (pH 3-7), the major constituents present are curcumin molecules in bis-keto form where curcumin acts as a proton donor (pKa 8.1), inducing a crucial role in the antioxidant activity (Wang et al., 1997). *In vitro*, curcumin can significantly inhibit the generation of reactive oxygen species (ROS) like superoxide anions, H_2O_2 and nitrite radical generation by activated macrophages, which play an important inflammatory activity (Joe and Lokesh, 1994). Curcumin also lowers the production of ROS *in vivo* (Chattopadhyay et al., 2004). So curcumin can play interesting application to develop health benefits product in food and pharmaceutical industries (Aditya et al., 2015; Rafiee et al., 2019; Shin et al., 2016).

Due to its hydrophobic nature (logP = 3.07 according SciFinder, with values of logD = 3.07 for pH ≤ 6, and logD still at a high value, 1.93, at pH = 9), curcumin is nearly insoluble in water at acidic or neutral pH. The compound is, however, soluble in alkali (logD = 0.63 at pH = 10). The use of curcumin is thereby limited due to its low water solubility, high decomposition rate in alkaline media and photodegradation in organic solvents (Tønnesen et al., 2002). Numerous studies related to absorption, distribution, metabolism and excretion of curcumin have revealed poor absorption and rapid metabolism of curcumin that severely decreases its bioavailability (Garcea et al., 2004; Holder et al., 1978; Ravindranath & Chandrasekhara, 1980; Ringman et al., 2012; Vareed et al., 2008; Wahlström & Blennow, 1978; Yang et al., 2007).

Microencapsulation is widely used in food and pharmaceutical industries as an alternative technology for enhancing entrapment, protection, controlled release and functionalization of bioactive substances. A variety of microencapsulation techniques were used to improve the solubility and bioavailability curcumin, such as spray drying (Lucas et al., 2020), solvent evaporation (Xiao et al., 2015), coacervation (Ang et al., 2019), supercritical fluid (Ribas et al., 2019), inclusion complexation (Mangolim et al., 2014) and ionotropic gelation (Nguyen et al., 2014). The main advantage of encapsulation is that curcumin will be protected from oxidation, and its solubility increased improving therefore its bioavailability and making controlled release in gastrointestinal tract achievable (Anand et al., 2007).

Polymers are often used as carriers due to their non-toxicity and safe history of human consumption, thus ionotropic gelation is a common method used to entrap drug with hydrophilic polymer. This method is based on polyelectrolytes ability to crosslink in the presence of counter ions to form hydrogel beads (Pillay and Fassihi, 1999). Pectins gather a family of oligosaccharides and polysaccharides that have common features but are diverse in their fine structures (Willats et al., 2006). The degree of esterification (DE) and degree of amidation (DA), both expressed as a percentage of carboxyl groups (esterified or amidated), are important means to classify pectins (Chambin et al., 2006). Interestingly, complexes are formed due to the combination of low methoxyl pectin (DE < 50%) and divalent cations (calcium ions) caused by reducing the solubility and inducing non-covalent associations of carbohydrate chains (Sriamornsak and Nunthanid, 1998). Therefore, calcium pectinate has been investigated as an insoluble hydrophilic coating for sustained-release delivery by an interfacial complexation process (Günter and Popeyko, 2016).

A surfactant (surface active agent) is an amphiphilic molecule including a hydrophobic tail and a hydrophilic head in structure (Santos et al., 2013). The main problems of curcumin come from its poor solubility in water and lowly pharmacokinetic profile, which could be significantly improved by using surfactants. They are employed to increase solubility, protect curcumin against gastrointestinal degradation, enhance colloidal stability and oral bioavailability from the preparation (Araiza-Calahorra et al., 2018; Cheng et al., 2018; Nguyen et al., 2014). As FDA proved surfactants, Kolliphor® HS 15 and TPGS® are the

non-ionic ones widely used as solubilizer, emulsifier and absorption enhancer (Nguyen et al., 2014; Seo et al., 2012; Zhang et al., 2012). Furthermore, TPGS® is reported to possess antioxidant properties releasing free α-tocopherol which then localizers in the cell membrane and protects the membrane from lipid peroxidation and damage (Yan et al., 2007).

Proteins and surfactants can be used individually to positively impact drug delivery. In some cases, proteins are analogous to surfactants forming self- assembled stable structures. Due to this ability, β-Lactoglobulin (BLG), a major whey protein in bovine milk, has shown to increase solubility and especially, antioxidant activity of curcumin (Li et al., 2013; Sneharani et al., 2010).

The purpose of this study was to improve the solubility and bioavailability of curcumin without affecting its antioxidant activity and simultaneously achieve controlled release in gastrointestinal tract by encapsulation with ionotropic gelation method thanks to the combination of pectin with various surfactants.

CHAPTER 1

LITERATURE REVIEW

1. Turmeric and its active ingredients

Turmeric, the powdered rhizome of the plant *Curcuma longa*, has been anciently used in the Indian subcontinent as food preservative, dye due to its distinctive yellow colour, and as a spice (Aggarwal et al., 2006). It has been used for centuries in the Ayurvedic system of medicine as a blood purifier, an anti-inflammatory, would healing, scars lightening, in cosmetics, cure for jaundice, digestive enhancer, appetite suppressant, treating stomach and liver problems (Steinhauser, 2015). Turmeric has been used in home remedies for the treatment of skin diseases and softening of rough skins in the shape of bath soap and creams in India (Aggarwal et al., 2007).

Turmeric mainly consists of carbohydrates, proteins, some fat and minerals. The essential oil obtained by steam distillation of rhizomes has a-phellandrene (1%), sabinene (0.6%), cineol (1%), borneol (0.5%), zingiberene (25%) and sesquiterpines (53%) (Anamika, 2012).

2. Chemical profile of curcumin

Isolated in 1910 for the first time, curcumin was obtained in an orange-yellow crystalline powder and identified as [1,7-bis-(4-hydroxy-3-methoxyphenyl)-1,6-heptadiene-3,5-dion and shown to be diferuloylmethane (Aggarwal et al., 2003). The chemical structure of curcumin consists of two para-hydroxyl groups responsible for antioxidant activity, two keto groups and two double bonds responsible for anti-inflammatory, anticancer and antimutagenic activity, two methoxy groups and an active methylene group (Pandey et al., 2011).

Chemically, curcumin exhibits keto-enol tautomerism in acidic and neutral aqueous solutions and in the cell membrane (Wang et al., 1997) (Fig.190). In acidic and neutral conditions (pH = 3 - 7), curcumin acts as an extraordinarily potent H-atom donor (Jovanovic et al., 1999). In the keto form of curcumin, the heptadienone linkage between the two methoxyphenol rings contains a highly activated carbon atom, and the C-H carbon bonds on this carbon are very weak due to delocalisation of the unpaired electron on the adjacent

oxygens (Sharma et al., 2005). However, in situations (pH > 8) where the enolate form is dominant, curcumin acts instead as an electron donor (Jovanovic et al., 1999).
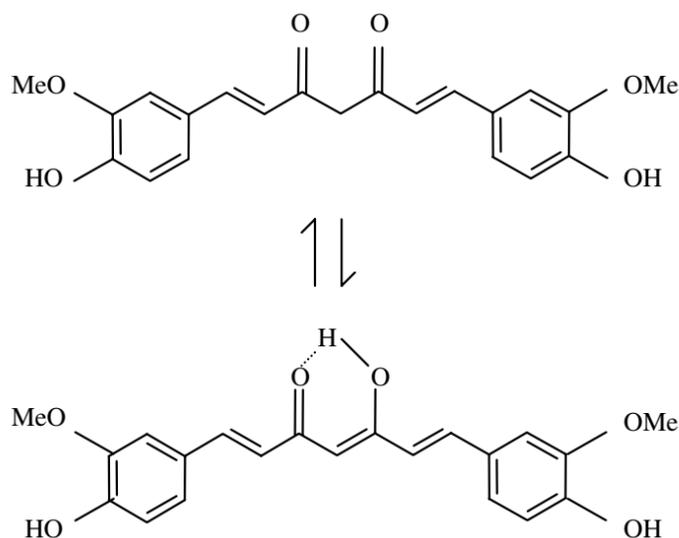
Figure 190. Tautomerism of curcumin under aqueous solutions (Sharma et al., 2005)

Curcumin is relatively insoluble in water due to its hydrophobic nature, but soluble in acetone, ethanol and dimethylsulphoxide. The use of curcumin is thereby limited by its low water solubility, high decomposition rate in alkaline media and photodegradation in organic solvents (Tønnesen et al., 2002).

Curcumin is unstable at basic pH, and degrades within 30 min to trans-6-(40-hydroxy-30-methoxyphenyl)-2,4-dioxo-5-hexanal, ferulic acid, feruloylmethane and vanillin (Lin et al., 2000). This degradation is blocked by the presence of foetal calf serum or human blood, or addition of antioxidants such as ascorbic acid, N-acetylcysteine or glutathione in culture media or phosphate buffer above pH 7 (Wang et al., 1997). Tønnesen et al. (2002) reported the complex kinetics of pH-dependent degradation of curcumin in aqueous solution offering the suggestion of its potential antimicrobial activity by photosensitisation.

Numerous studies related to absorption, distribution, metabolism and excretion of curcumin have revealed poor absorption and rapid metabolism of curcumin that severely decreases its bioavailability (Garcea et al., 2004; Holder et al., 1978; Ravindranath & Chandrasekhara, 1980; Ringman et al., 2012; Vareed et al., 2008; Wahlström & Blennow, 1978; Yang et al., 2007).

Uptake and distribution of curcumin in body tissues is obviously important for its biological activity. Ravindranath et al. (1980) showed that after oral administration of 400 mg of curcumin to rats, only traces of unchanged drug were found in the liver and kidney. At 30 min, 90% of curcumin was found in the stomach and small intestine, but only 1% was present at 24 h (Ravindranath et al., 1981).

3. Pharmacological activity of curcumin

Curcumin, the principal curcuminoid found in turmeric, is generally considered as its most active constituent (Sharma et al., 2005). More and more evidences point out towards curcumin having potential health benefits including antioxidant, anti-inflammatory, antimicrobial, anti-amyloid and antitumor properties (Aggarwal et al., 2006; Chattopadhyay et al., 2004) evidencing the beneficial properties of curcumin to the organism (Fig. 191).
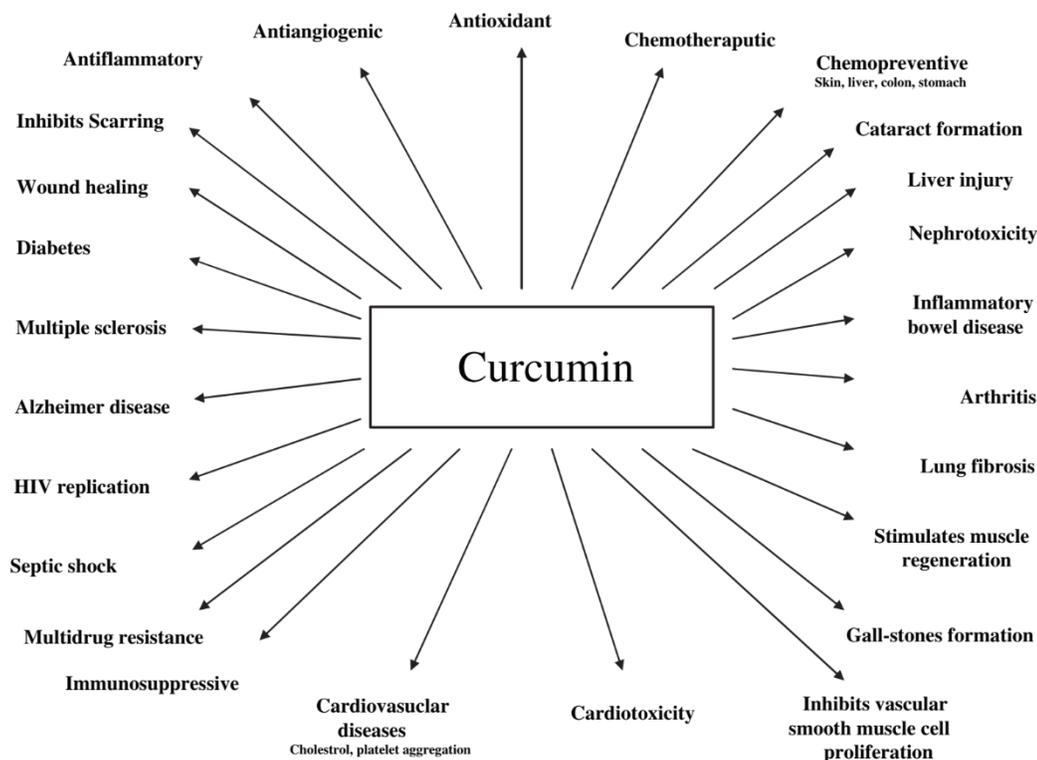
Figure 191. Pharmacological activity of curcumin (Aggarwal et al., 2006)

4. Encapsulation in food industry

Encapsulation may be defined as a process to entrap one substance (active agent) within another substance (wall material). The encapsulated substance can be called the core, fill, active, internal or payload phase, while the substance encapsulating was often called the coating, membrane, shell, capsule, carrier material, external phase, or matrix (Fang & Bhandari, 2010; Wandrey et al., 2010).

In the food industry, encapsulation process can be applied for a variety of reasons. Encapsulation is a useful tool to improve delivery of bioactive molecules and living cells into foods (de Vos et al., 2010; Wandrey et al., 2010). Encapsulation aims to preserve stability of the bioactive compounds during processing and storage and to prevent undesirable interactions with food matrix. Another benefit of encapsulation is less evaporation and degradation of volatile actives, such as aroma. Furthermore, encapsulation is used to mask unpleasant feelings during eating, such as bitter taste and astringency of polyphenols. This technology may provide barriers between sensitive bioactive materials and the environment, and thus, to allow taste and aroma differentiation, mask bad tasting or smelling, stabilize food ingredients or increase their bioavailability (Nedovic et al., 2011).

4.1. Some methods of microencapsulation

Microencapsulation is widely used in food and pharmaceutical industries as an alternative technology for enhancing entrapment, protection, controlled release and functionalization of bioactive substances. In the literature, a variety of microencapsulation techniques were used to improve solubility and bioavailability of active gradients, such as spray drying, solvent evaporation, coacervation, supercritical fluid, inclusion complexation and ionotropic gelation. Although a variety of alternative microencapsulation techniques is available, no single method is suitable for encapsulating different types of core material. Ultimately, the best method will depend upon the type of core material, the required particle size, the permeability of the shell wall, and the different properties of the microcapsule.

To this day, various curcumin encapsulation techniques are divided into 3 basic groups: chemical, physical and physicochemical methods. Each method has its own advantages as

well as disadvantages, so they are listed and described basically according to their principles in Table 13:

Table 13. Some methods of curcumin encapsulation

Method	Characteristics	Advantages	Disadvantages	Ref.
Physical methods				
Spray drying	Transformation of a fluid into a dry powder by atomization in a hot drying gas stream that is generally air.	Rapid, continuous, reproducible, single-step, and scalable without major modifications	- Product lost during manufacture (walls of drying chamber). - High temperature can change the structure of materials.	Gómez-Estaca et al., 2015; Paradkar et al., 2004, Blanco-García et al., 2017
Extrusion (ionic gelation)	Extrusion methods consists of dropping droplets of an aqueous solution of polymer and active into a gelling bath.	High flexibility.	Short-range product, high cost.	Gangurde and Amin, 2015; Nguyen et al., 2014
Physicochemical methods				
Coacervation	Spontaneous phase separation and involves	High encapsulation efficiency,	Very expensive,	Aziz et al., 2007; Chirio et al., 2011;

	reaction between two oppositely charged polymers to yield a polymer rich and polymer poor region.	simple and solvent-free process, controlled release possibility.	complexity of technique.	Shahgholian and Rajabzadeh, 2016
Chemical methods				
Polymerization	A polymerization reaction occurs between two very reactive monomers at the interface of two immiscible solvents.	Low viscosity, easy heat removal, use directly.	Hard to control core size, instability.	Aditya et al., 2015; Duan et al., 2012

4.1.1. Spray drying

Spray drying is one of the oldest and the most widely used encapsulation technique in the food industrial sector. It is a flexible, continuous, but more important an economical operation. It produces particles of good quality, which size is less than 40 µm (Zuidam and Nedovic, 2010). This feature is desired from the standpoint of sensorial and textural characteristics of final products. Although spray-dryers are widespread in the food industry, there are several disadvantages of this technique such complexity of the equipment, non-uniform conditions in the drying chamber and it is not always easy to control particle size. The principle of spray drying is dissolve the core in a dispersion of carrier material. The misture is then subsequently atomized in heated air leading to an evaporation of water. The powdered particles are then separated after they fall to the bottom of the drier (Fig.192). About 80-90% of encapsulates are spray-dried ones, rest of them are mostly prepared by spray-chilling, freeze-drying, melt extrusion and melt injection (Nedovic et al., 2011).
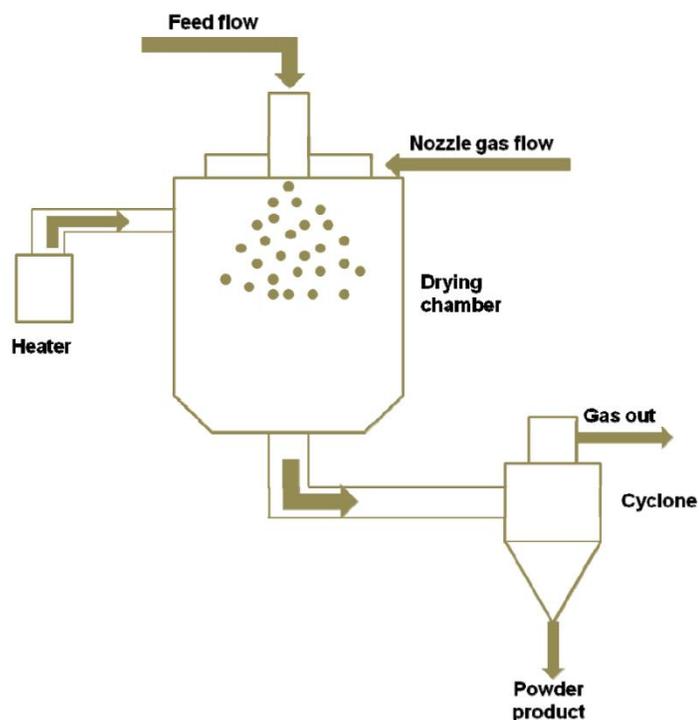
Figure 192. Schematic presentation of the spray drying method

(Munin and Edwards-Lévy, 2011)

4.1.2. Emulsification-solvent removal methods

These processes are based on evaporation or extraction of the internal phase of an emulsion giving rise to the precipitation of the polymer coating, first dissolved into this phase, in the form of particles (Fig.193). In this method, the active compound is dissolved or dispersed in the polymer solution. The mixture is then emulsified by ultrasounds or homogenizer in a large amount of water containing surfactants to obtain an oil-in-water emulsion. After removal of solvent, particles are washed and collected by filtration or centrifugation, the dried or freeze-dried. The two-step technique calls for initial emulsification of polymer solution in a volatile organic solvent, followed by internal phase solvent evaporation or extraction that results in hardening and precipitation of microparticles. Solvent evaporation is generally performed at atmospheric pressure (or sometimes under reduced pressure) to promote evaporation of the volatile solvent. The solvent extraction process, however, involves quenching in excess water or relevant quench medium, allowing for solvent diffusion through oil droplets (Alam et al., 2013).

220
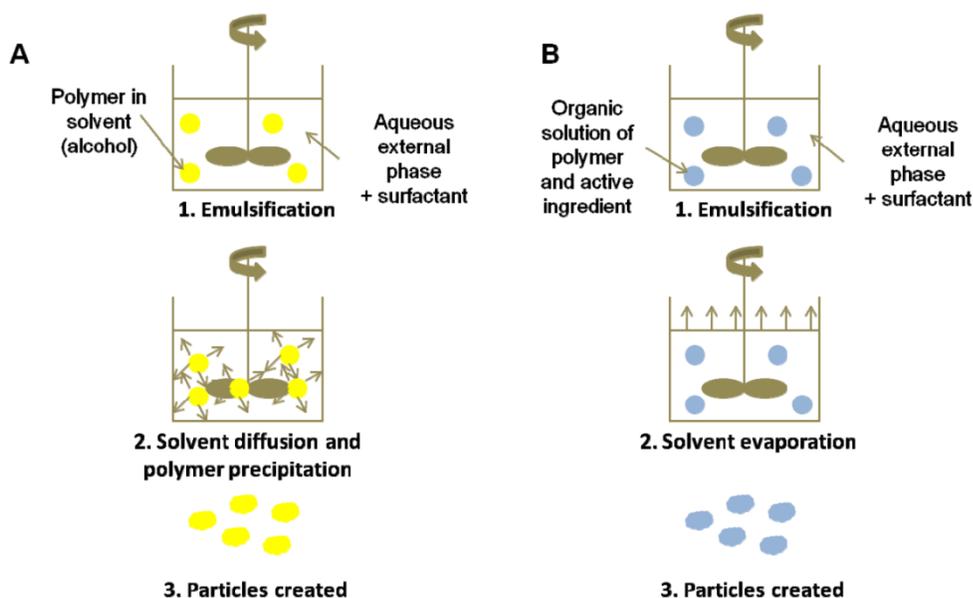
Figure 193. Schematic presentation of the emulsification-solvent removal methods (Munin and Edwards-Lévy, 2011)

4.1.3. Coacervation

This method is based on the ability of cationic and anionic water-soluble polymers to interact in water to form a liquid, neutral, polymer-rich phase called coacervate. The complex coacervation process is the separation of an aqueous polymeric solution into two miscible liquid phases: a dense coacervate phase and a dilute equilibrium phase. The dense coacervate phase wraps as a uniform layer around dispersed core materials. The core material, which can be oily droplets, is dispersed into the aqueous solution of the two polymers. The coating in liquid form is removed from a polymer solution, coats the material to be encapsulated, solidified and collected by centrifugation or filtration (Fig.194). Drying can be accomplished by spray or fluidized bed drying (Gibbs et al., 1999). This is an immobilization rather than an encapsulation technology and is therefore mostly proposed and applied for bioactive food molecules rather than for bioactive living cells. The technique is applied for flavours, oils but also for some water-soluble bioactive molecules (de Vos et al., 2010).

221
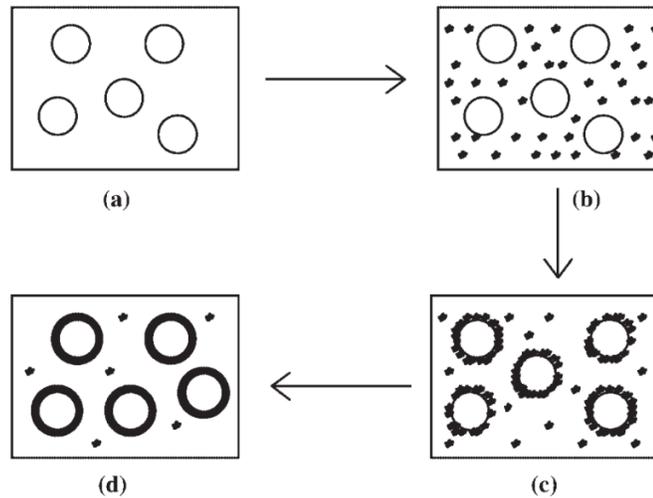
Figure 194. Schematic representation of the coacervation process. (a) Core material dispersion in solution of shell polymer; (b) separation of coacervation from solution; (c) coating of core material by microdroplets of coacervate; (d) coalescence of coacervate to form continuous shell around core particles (Van Parys, 2006).

4.1.4. Fluid bed coating

A modified spray dry methodology that enlarges the field of application is the fluid bed coating methodology. In this technology, the bioactive food components are suspended in air and the matrix molecules are sprayed onto the bioactive components and form a capsule (Fig.195). The choice for matrix molecules is broader than for traditional spray drying. It may be fats, proteins, carbohydrates but also emulsifiers. It may even be applied to give spray dried products or a sensitive core of for example oils as a second coating. It is also useful for applying an additional layer of molecules for targeted release in the gut. In principle the core is always solid (de Vos et al., 2010).
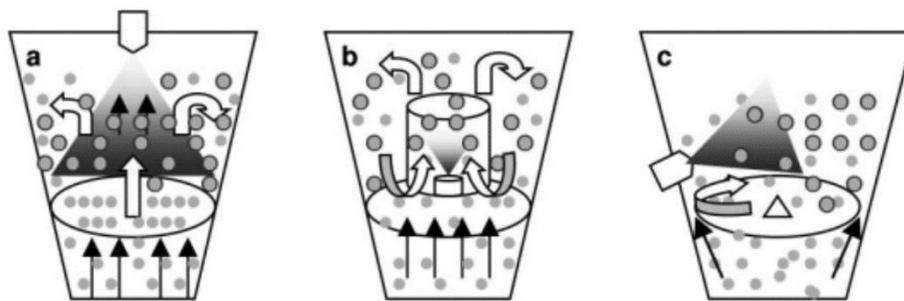
Figure 195. Schematic presentation of the fluid bed coater.
(a) Top spray; (b) bottom spray; (c) tangential spray (Van Parys, 2006)

4.1.5. Inclusion complexation

Inclusion complexation consists of entrapment of active compound by a polymer through physicochemical interactions. In this technique, β-cyclodextrin is used since the centre is hydrophobic while the outer surface is hydrophilic due to its seven glucose units linked 1 to 4 (Fig.196). In the centre of the cyclodextrin, water molecules are replaced by less polar molecules. The complex then precipitates out of solution. Only water can serve as the suspension medium. The precipitate is recovered and dried by conventional means. Binding by the cyclodextrin can occur up to 200 °C. The moisture and temperature conditions of the mouth, however, allow release of the bound material (Gibbs et al., 1999).
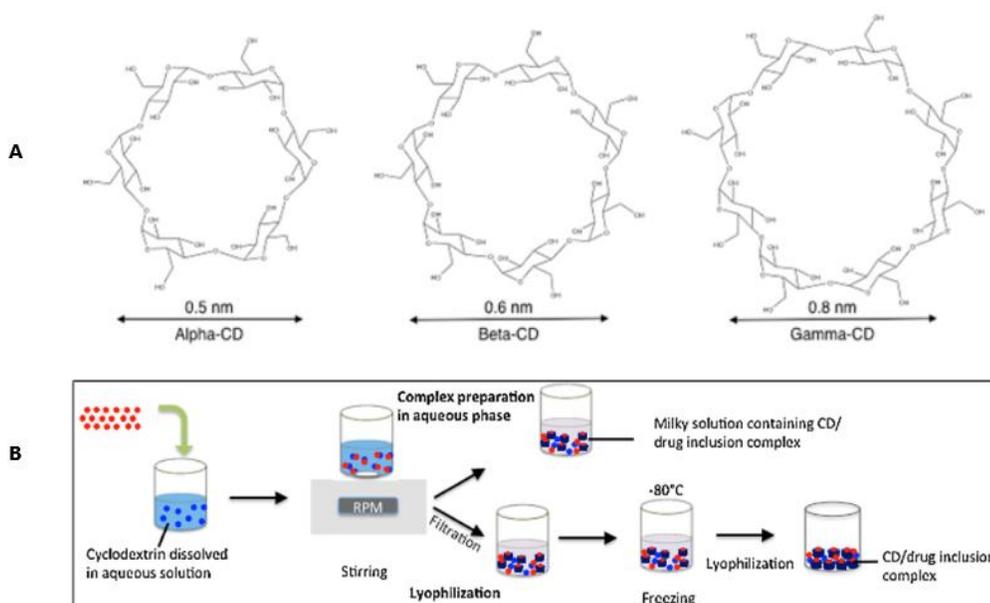
Figure 196. (A) Types of cyclodextrins; (B) Schematic presentation of inclusion complexation (Gharib et al., 2015)

4.1.6. Ionotropic gelation

Ionotropic gelation is defined as the capability of polyelectrolytes to crosslink in the presence of counter ions. The natural polyelectrolytes have a property of coating on the drug core and acts as release rate retardants contains certain anions on their chemical structure. These anions forms meshwork structure by combining with the polyvalent cations and induce gelation by binding mainly to the anion blocks. The hydrogel beads are produced by dropping a drug-loaded polymeric solution into the aqueous solution of

polyvalent cations (Fig.197). The cations diffuse into the drug-loaded polymeric drops, forming a three-dimensional lattice of ionically crossed linked moiety. Biomolecules can also be loaded into these hydrogel beads under mild conditions to retain their three-dimensional structure.
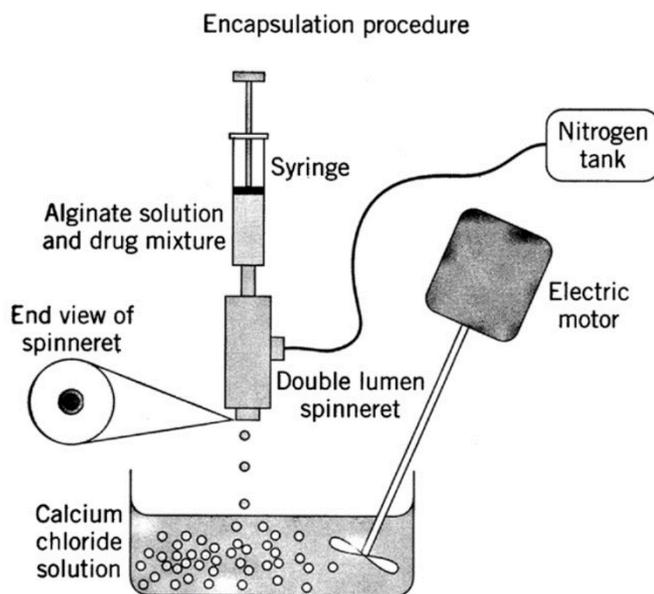
Figure 197. Schematic presentation of the ionotropic gelation method

(Suri et al., 2013)

4.2. Carriers

Most of the polysaccharide based targeted delivery systems protect the bioactive food components from the deleterious conditions in the stomach and upper part of the small bowel. The degradation of the polysaccharide matrix molecules mainly depends on the hydrolysis of the glycosidic linkages between the molecules and subsequent release of the bioactive components (de Vos et al., 2010).

4.2.1. Chitosan

Chitosan, a partially deacetylated product of chitin, is a copolymer consisting of β-(1→4)-2-acetamido-D-glucose and β-(1→4)-2-amino-D-glucose units (Fig.198), with the latter usually exceeding 80% (Yoon et al., 2000). This biopolymer is a glucosaminoglycan and is composed of two common sugars, glucosamine and N-acetylglucosamine, the proportion of which depends on the alkaline treatment (Bakshi et al., 2019). Chitosan, despite its

crystallinity, is insoluble in water at pH > 7; however, it is soluble in dilute acids owing to the presence of a protonated amino groups in acidic conditions (pH < 6.0). Furthermore, the presence of reactive functional groups such as amino, primary, and secondary hydroxyl groups makes chitosan particularly amenable to structural modification to yield materials of different mechanical and physical properties. Owing to this simplicity of modification, negligible toxicity and biodegradability, mucoadhesive property, chitosan and its derivatives are being extensively used by pharmaceutical industries (Yadav and Karthikeyan, 2019).
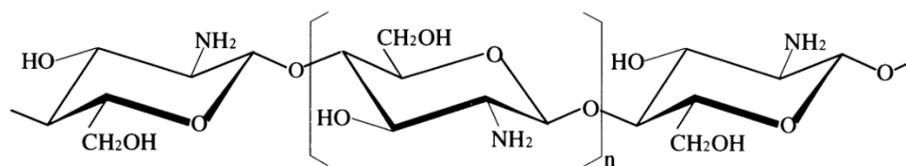
Figure 198. Chemical structure of chitosan (Okuyama et al., 2000)

4.2.2. Alginate

One of the most commonly applied polysaccharides is alginate. Alginates are linear polymers with 1-4 linked-β-D-mannuronic acid (M) and α-L-guluronic acid (G) residues arranged as blocks of either type of unit or as a random distribution of each type (Fig.199). They can be obtained in different G/M ratios which provides different degrees of mechanical stability. Alginates are compatible with almost all method of encapsulations but often combine alginates with spray drying and extrusion. Depending on the chemical characteristics of the capsule, alginate-based capsules are generally applied to facilitate the release of bioactive components in the ileum or colon (Yadav & Karthikeyan, 2019).
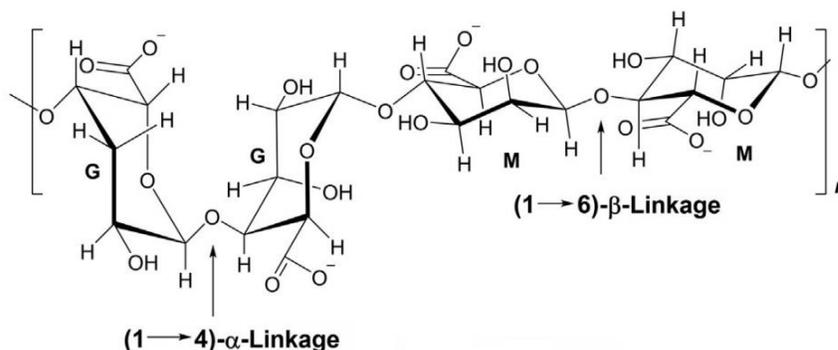
Figure 199. Chemical structure of alginate (Yadav and Karthikeyan, 2019)

4.2.3. Dextran

Dextran is bacterial derived sugars that are rapidly degraded by dextranases which are abundantly present in Bacteroides. Dextran is polysaccharides with a linear polymer backbone, with mainly 1,6-α-D-glucopyranosidic linkages (Fig.200). Dextran produces relatively low-viscosity solutions, which distinguishes it from other high molecular weight polysaccharides. The intrinsic viscosity is affected by the nature and pH of solvent, degree of branching, number of intermolecular bonds and temperature. Furthermore, dextrans can be chemically modified with a variety of reagents making it a valuable carrier system with for conjugation with drug molecules (Dhaneshwar et al., 2006).
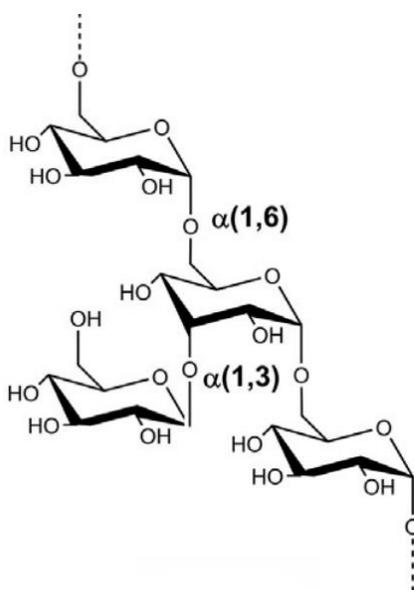
Figure 200. Chemical structure of dextran (Yadav & Karthikeyan, 2019)

4.2.4. Pectin

Pectin is plant derived molecules which are mostly linear polymers of mainly α-(1-4)-linked D-galacturonic acid residues and 1,2-linked L-rhamnose residues (Fig.201A). These polysaccharides are advantageous for targeted delivery because they remain intact in the stomach and the small intestine. The application of pectin as unmodified molecule is limited due to its high solubility in water. Pectin is capable of forming gels by different mechanisms regardless of their degree of methylation:

- Highly methylated pectin (HM) is capable of forming a gel under the conditions of low water activity, typically held by high concentrations of sugar and at acidic pH (between 2.2 and 2.8). The gelling mechanism in this case corresponds to the formation of hydrophobic interactions between the methyl groups and of hydrogen bonds between the carboxylic groups of the non-esterified galaturonic acid residues and the secondary alcohols (Bakshi et al., 2019).

- Low methylated pectin (LM) is capable of forming a gel in the presence of multivalent cations and more particularly with Ca^{2+} (Fig.201B). This gelling mechanism is based on the interactions between cations and deprotonated carboxylic groups of galacturonic acids. This association forms an "egg box" type gel due to Van der Waals bonds, hydrogen bonds and electrostatic bonds. The ability of LM pectin to associate with calcium depends on the degree of methylation but also on the distribution of non-esterified galacturonic acids. After enzymatic de-esterification of pectin, the formation of bonds with calcium is higher than after chemical de-esterification (Daas et al., 1999; Fraeye et al., 2010; Grant et al., 1973).
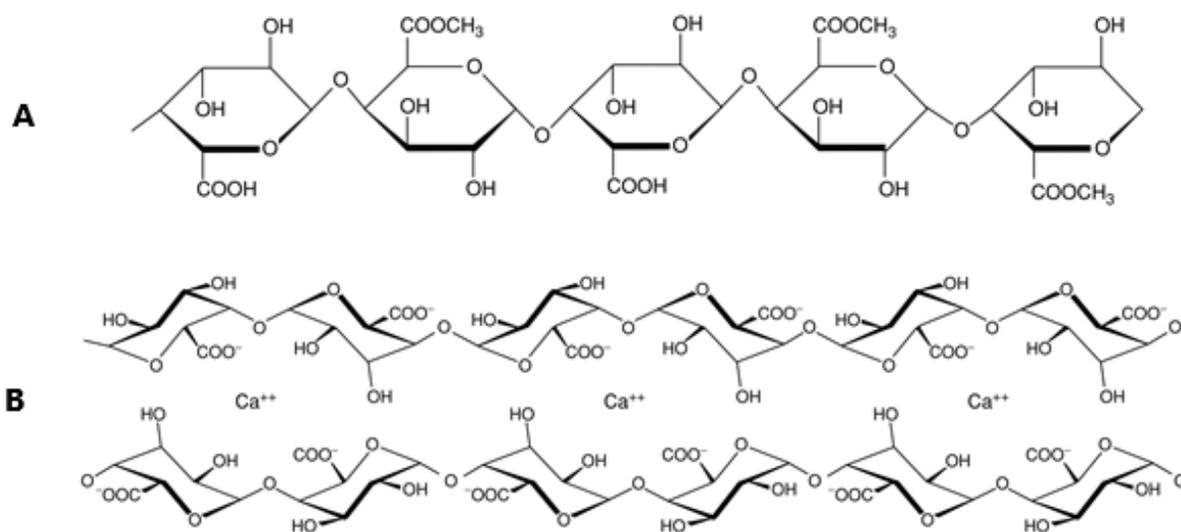
Figure 201. Chemical structure of pectin (A) and eggbox model showing calcium-induced junction zones (B) (Flutto, 2003)

4.3. Surfactants

Surfactants are very exotic molecules due to their amphiphilic behaviour. This means that a surfactant molecule contains both a hydrophobic part (lipophilic) and a hydrophilic part

(lipophobic). The non-polar hydrophobic part is typically referred to tail (composed by one or more hydrocarbon chains, although fluorocarbon and dimethylsiloxane chains can be used) and the polar hydrophilic part is referred to head group which might be either charged or uncharged.

Surfactants exist in many different forms in nature, classified according to the chemical nature of their polar head group. Surfactants with a negatively charged head group are referred to anionic, whereas cationic surfactants contain a positively charged head group. Among of those, nonionic surfactants are the most common type of surface active agent used in preparing vesicles due to the superior benefits they impart with respect to stability, compatibility and toxicity compared to their anionic, amphoteric or cationic counterparts (Santos et al., 2013). Nonionic surfactants consist of both polar and non-polar segments and possess high interfacial activity. The formation of bilayer vesicles instead of micelles is dependent on the hydrophilic-lipophilic balance (HLB) of the surfactant, the chemical structure of components and the critical packing parameter. The chain length and size of the hydrophilic head group of the nonionic surfactant along with the HLB value of a surfactant plays a key role in entrapment efficiency by controlling drug entrapment of the vesicle it forms. Therefore, surfactant systems play an important role in modern drug delivery since they allow, for instance, the control of drug uptake and release rate and minimization of drug degradation and toxicity. An effective synergism between surfactant systems and drugs is nowadays recognized as a key issue to assure therapeutic efficiency (Santos et al., 2013).

CHAPTER 2

EXPERIMENTAL PART

1. Materials

Curcumin (purity > 65%) was obtained from Sigma-Aldrich, Germany. Amidated low-methoxyl pectin (Unipectine® 305 C, DA = 20-24%, DE = 20-28%, pKa = 3.5), used as a polymer carrier, was purchased from Cargill, France. Kolliphor® HS 15 (Macrogol 15 Hydroxystearate, melting point: 30 °C, hydrophilic-lipophilic balance ≈ 14-16) and TPGS® (Vitamin E Polyethylene Glycol Succinate, hydrophilic-lipophilic balance ≈ 13.2, melting point: 37-41 °C) were supplied by BASF, Germany. BiPro® beta-lactoglobulin (BiPro® BLG) was obtained from Davisco, Switzerland. Ethanol (EtOH) 96% (v/v), hydrochloric acid (HCl) 1M and sodium hydroxide (NaOH) 1 M were obtained from VRW International, France. Calcium chloride dihydrate (purity > 99 %) and potassium phosphate dibasic (KH_2PO_4) 0.1 M, 2,2-Diphenyl-1-picrylhydrazyl (DPPH, CAS number = 1898-66-4) were obtained from Sigma-Aldrich (Germany). All the reagents were analytical grade.

2. Physicochemical parameters

2.1. Solubility study

The solubility of curcumin in different surfactants was measured spectrophotometrically at 426 nm. The method was conducted according to Nguyen et al. (2014). 1 g of each surfactant (5%, w/v) was weighed and dissolved in 20 mL of deionized water. Surfactants used were Kolliphor® HS 15, TPGS® and BiPro® BLG. An excess amount of curcumin (20 mg) was added and dispersed in these solutions. They were then stirred for 15 minutes at high rate (500 rpm), sonicated for 15 minutes (37 Hz) and stirred for another 15 minutes. After storing 12 hours in the dark, 2 mL of centrifuged (5000 rpm, 5 minutes) supernatant was taken and dissolved in 2 mL of EtOH 96 % (v/v). The mixture was finally diluted with EtOH 96% (v/v) before measuring the absorbance at 426 nm. Blank was deionized water in EtOH 96 % (v/v). All experiments were done in triplicate.

To calculate concentration of solubilized curcumin, equation from calibration curve was used. Calibration curve was obtained by dissolving curcumin powder in EtOH 96%.

Calibration curve equation: $y = 0.1869x + 0.0077$ ($R^2 = 0.999$) (Fig.209)

y – absorbance measured at 426 nm

x – curcumin concentration in mg/L

2.2. Short term stability study

20 mg of curcumin powder was dissolved in 20 mL of deionized water (pH = 6.8) containing 5 g/L of Kolliphor® HS 15. Curcumin concentration in solution was measured spectrophotometrically (426 nm) at t_0 and after at different time intervals in duration of 24 days. Stability was determined at three different environmental conditions: darkness at 25 ºC, darkness at 37 ºC and daylight at 25 ºC. Blank was deionized water containing 5 g/L Kolliphor® HS 15 concentration. All experiments were done in triplicate.

All calculations were made according to equation from calibration curve obtained using dissolved curcumin in phosphate buffer pH 7.4 containing 5 g/L of Kolliphor® HS 15 concentration.

Calibration curve equation: y = 0.1268x – 0.0255 (R^2 = 0.9998) (Fig.208)

y – absorbance measured at 426 nm

x – curcumin concentration in mg/L

Percentage of degradation was determined by Eq.(1):

$$PD\ (\%) = \frac{C_{max} - C_{24}}{C_{max}} \times 100 \qquad (1)$$

where *PD* is percentage of degradation of curcumin, C_{max} is maximum concentration of curcumin solubilised and C_{24} is concentration of curcumin after 24 days.

2.3. Encapsulation of curcumin by ionotropic gelation in pectin beads with different surfactants

Curcumin was encapsulated by ionotropic gelation according to a method of Chambin et al. (2006). 1.6 g of amidated low-methoxyl pectin was weighed and dissolved in 20 mL of deionized water (pH = 6.8), stirred at high speed (700 rpm) for 2 hours at room temperature. Depending on the type of beads, surfactant was dissolved in 20 mL of deionized water (Table 14). The surfactant levels used were selected making sure the viscosity of the pectinate solution kept visually unchanged, and still permitted to prepare beads. 500 mg of

curcumin were then added to the surfactant solution and stirred for 15 minutes. After homogenization, curcumin mixture was transferred to pectin solution and dispersed by stirring for another 15 minutes and sonication for 5 minutes to disintegrate possible aggregates of undissolved curcumin. Dispersion was pumped and poured dropwise into calcium chloride solution (10%, w/v) using IPC Ismatec pump at 8 rpm with a 1.5 mm needle in diameter. Beads were left to cured for 5 minutes and then filtered and washed twice with 200 mL of deionized water to remove calcium chloride excess from the beads surface. They were oven dried for 48 hours at 37 ^{o}C.

Table 14. Type of beads and mass of surfactant used for production

Beads	Surfactant	Mass of surfactant (g)
Curcumin beads	-	-
BiPro® BLG beads	BiPro® beta-lactoglobulin (77.9 % of BLG)	3
Kolliphor® beads	Kolliphor® HS 15	10
TPGS® beads	Vitamin E Polyethylene Glycol Succinate	4

2.4. Encapsulation efficiency (EE) and encapsulation yield (EY)

100 ± 1 mg of each type of dried beads was added after washing to 200 mL of extraction medium (phosphate buffer pH 7.4 with 5 g/L of Kolliphor® HS 15) and stirred at 500 rpm for 48 hours. During those 48 hours, extraction medium with beads was sonicated three times (10 minutes, 37 Hz). After 48 hours, 5 mL of extraction medium was taken and added to 2 mL of melted Kolliphor® HS 15 and vortexed for 5 minutes. 1 mL of solution was then diluted with 19 mL of deionized water in volumetric flask of 20 mL. Concentration of extracted curcumin was determined spectrophotometrically at 426 nm. All experiments were done in triplicate.

All calculations are made according to equation from calibration curve made using dissolved curcumin in PBS 7.4 containing 5 g/L of Kolliphor® HS 15 concentration (Fig.208).

Encapsulation efficiency (EE) and encapsulation yield (EY) were calculated according to Eq.(2):

$$EE\ (\%) = \frac{M_{ex}}{M_0} \times 100 \quad ; \quad EY\ (\%) = \frac{M_{ex}}{M_{db}} \times 100 \qquad (2)$$

where M_{ex} is mass of curcumin encapsulated, M_o is starting mass of curcumin used for encapsulation and M_{db} is mass of dried beads.

3. Morphologic description of beads by scanning electron microscopy

Morphology of dried pectinate beads and curcumin powder were studied using scanning electron microscopy (SEM) to determine the size, surface and internal structure. The samples were fixed on metal stub double-sided sticky tape and fractured with a scalpel (Swann Morton, England B.S.). Subsequently, the samples were coated with a thin gold layer (100–150 Å) under vacuum using an ion sputter coater (POLARON Thermo VG Scientific, East Grinstead, Sussex, UK) and examined using a SEM FEI La B6 (Eindhoven, Netherlands), at an accelerating voltage of 5 kV with an electron detector for low vacuum conditions.

4. Dissolution studies in simulated intestinal medium

Curcumin release from the beads was tracked during 7 hours in conditions of human intestine (pH 7.4 and 37 ºC). Dissolution studies were not conducted in gastric conditions since no significant release of curcumin at pH 1.2 had been previously reported by Nguyen et al. (2014). 400 ± 1 mg of dry beads was added to 1 L of dissolution medium (PBS 7.4 and PBS 7.4 containing 5 g/L Kolliphor® HS 15) which was firstly tempered to 37 ºC in SOTAX AT7 dissolution apparatus (stirring rate 50 rpm). Release of curcumin was measured at certain time intervals during 7 hours: 1, 10, 20, 30, 60, 90, 120, 150, 180, 210, 240, 270, 330 and 420 minutes. Curcumin concentration was determined spectrophotometrically at 426 nm. All experiments were performed in triplicate.

All calculations are made according to equation from calibration curve made using dissolved curcumin in PBS 7.4 containing 5 g/L of Kolliphor® HS 15 concentration (Fig.209).

Percentage of release of curcumin during time:

$$PR\ (\%) = \frac{Mt}{Mc}\ x\ 100$$

PR – percentage of release of curcumin during time (%)

Mt – mass of curcumin released in certain time (mg)

Mc – mass of curcumin encapsulated in 400 mg of dry beads (mg)

Mathematical modeling of curcumin release from beads was applied according to Korsmeyer-Peppas model (Eq.(3)) to determine the release behaviour:

$$\frac{M_t}{M_\infty} = k \times t^n \qquad (3)$$

where M_t/M_∞ is absolute cumulative amounts of drug released at time t and infinity, k is constant incorporating structural and geometrical characteristics of the device and n is exponent indicative of the mechanism of drug release (Siepmann and Siepmann, 2008).

5. Differential Scanning Calorimetry (DSC) study

DSC analysis was applied to study the physical forms of encapsulated curcumin within the different beads. DSC analyzer (Q20, TA Instruments, USA) was calibrated with Indium for temperature and enthalpy (Tm= 156.6 °C, ΔHf = 28.71 J/g). A quantity of each type of beads was weighed and placed in a sealed aluminum pan. Scans were recorded between 20 °C and 190 °C at heating rate of 10 °C/min under nitrogen (flow rate of 20 mL/min). All experiments were performed in triplicate.

Percentage of crystalline curcumin in beads was calculated according to Eq.(4):

$$P_{CC} = \frac{\Delta H_C}{\Delta H_f} * 100 \qquad (4)$$

where P_{CC} is percentage of crystalline curcumin in bead (%), ΔH_C is enthalpy of crystallization of curcumin in bead and ΔH_f is the enthalpy of melting for a fully crystalline curcumin powder.

6. DPPH radical scavenging assay

6.1. DPPH method applied on curcumin powder

Bulk solution was prepared by dissolving 36.8 mg of curcumin in 100 mL of EtOH 96 % (v/v). The solution was diluted to different concentrations (1.0, 1.25, 1.5, 1.75, 2.0, 2.5, 3.0, 3.5 x 10-5 M) with EtOH 96 % (v/v). 5 mL of DPPH in EtOH 96 % solution (concentration 0.0678 g/L w/v, meaning $1.7*10^{-4}$ M) were added to 5 mL of each curcumin solution at different concentrations. DPPH radical has a deep purple color in solution, and becomes colorless or pale yellow when neutralized. This property permits visual monitoring of the reaction, and the number of initial radicals can be counted from the change in the optical absorption at 515 nm (Alger, 1997). Absorbance was measured at 515 nm for 2 hours at different time intervals. Blank was ethanol and control was DPPH solution in EtOH 96 %.

6.2. DPPH method applied on extraction and dissolution medium samples

During experiments with extraction of curcumin from the beads, after 48 hours of extraction, 1 mL of extraction medium was taken and diluted with 4 mL of EtOH 96 %. 5 mL of DPPH solution was then added and measured spectrophotometrically at 515 nm for 2 hours at different time intervals.

During dissolution kinetics studies, after 330 minutes of dissolution, 1 mL of dissolution medium is taken and diluted with 4 mL of EtOH 96%. 5 mL of DPPH solution was then added and measured spectrophotometrically at 515 nm for 2 hours in different time intervals.

Concentrations of extraction and dissolution medium were shown before adding of DPPH solution in Table 15 and measured spectrophotometrically at 426 nm. Blank in both cases was 1 mL of dissolution or extraction medium without curcumin in 9 mL of EtOH 96%. Control was 1 mL of dissolution or extraction medium without curcumin diluted with 4 mL of EtOH 96% and 5 mL of DPPH in EtOH 96% solution.

Table 15. Concentration of extraction and dissolution medium before adding DPPH solution

Beads	Extraction medium concentration (mg/L)	Dissolution medium concentration (mg/L)
Curcumin beads	47.3 ± 5.1	48.4 ± 3.5
Kolliphor® beads	27.9 ± 3.0	22.6 ± 0.5
BiPro® BLG beads	51.8 ± 3.1	41.0 ± 2.0
TPGS® beads	38.6 ± 0.3	28.7 ± 2.2

Antioxidant activity of curcumin was expressed as percentage of radical scavenging which represented difference between control and sample after 2 hours (Eq. (5)):

$$PI\ (\%) = \frac{A_{co} - A_{At}}{A_{co}} \times 100 \qquad (5)$$

where PI was percentage of radical scavenging (inhibition), A_{co} was absorbance (515 nm) of control at $t = 0$ min and A_{At} was absorbance (515 nm) of curcumin at $t = 2$ h (Ak and Gülçin, 2008).

CHAPTER 3

RESULTS AND DISCUSSION

1. Physicochemical parameters

1.1. Solubility studies

Solubility study was performed to determine which of the surfactants is the most effective to disperse curcumin (Table 16). Kolliphor® HS 15 and TPGS® proved to be more effective than BiPro® BLG to solubilize curcumin. Those surfactants are non-ionic solubilizers, possessing the favourable hydrophilic-lipophilic balance (HLB $\approx$ 13-16) and are currently used for manufacturing aqueous parenteral preparations with vitamins and other lipophilic compounds (Reintjes, 2011). The water solubility of curcumin was highly increased with these surfactants. Our experimental value for solubility in deionized water (1.12 mg/L) was higher than the one reported by Tønnesen, 2002 and higher than that reported by Carvalho et al., 2015 (1.34 mg/L). The slightly different values between Kolliphor® HS 15 (562.7 ± 1.1 mg/L) and TPGS® (601.9 ± 3.0 mg/L) (Nguyen et al., 2014; Song et al., 2016) could be explained by the specificity of their interaction with curcumin (Seo et al., 2012). Solubility of curcumin in EtOH 99.5 % has been seen as 6700 times higher than in water (Carvalho et al., 2015), however, ethanol is not an appropriate solvent for pectin-curcumin microparticles because of precipitation due to the interaction between ethanol and pectin.

Table 16. Solubility of curcumin in deionized water with different mediums

Surfactant and solvents	Curcumin concentration (mg/L)
Deionized water[a]	0.011
PBS 7.4	82.3 ± 6.2
Ethanol (99.5 %)[b]	8895.9 ± 737.2
BiPro® BLG	15.7 ± 1.4
Kolliphor® HS 15	562.7 ± 1.1
TPGS®	601.9 ± 3.0

a. Tønnesen, 2002

b. Carvalho et al., 2015

Otherwise, curcumin in PBS 7.4 solution was solubilized much more than in water (82.3 ± 6.2 mg/L). The pH dependence of curcumin solubility has been described by Song et al., 2016 as constant at pH 1.2 and 4.5, higher 25.1 times at pH 6.8 and at pH 7.4.

The 2nd lowest solubility of curcumin was in the BiPro® BLG solution (15.7 ± 1.4 mg/L). However, it was 1427 times higher than in water. BLG was used as stabilizer in order to improve curcumin's bioavailability due to its stability in acidic pH and the presence of specific receptors in small intestine. Furthermore, BLG has previously been selected to deliver curcumin to cancer cells and improve antioxidant activity by different authors (Aditya et al., 2015; Li et al., 2013).

1.2. Short term stability study

To measure its stability over time in those conditions, short term stability was experimented by monitoring curcumin in deionized water (pH = 6.8) and 5 g/L Kolliphor® HS 15 in different environmental conditions. The percentage of curcumin degradation was measured at various time points in a period of 24 days.
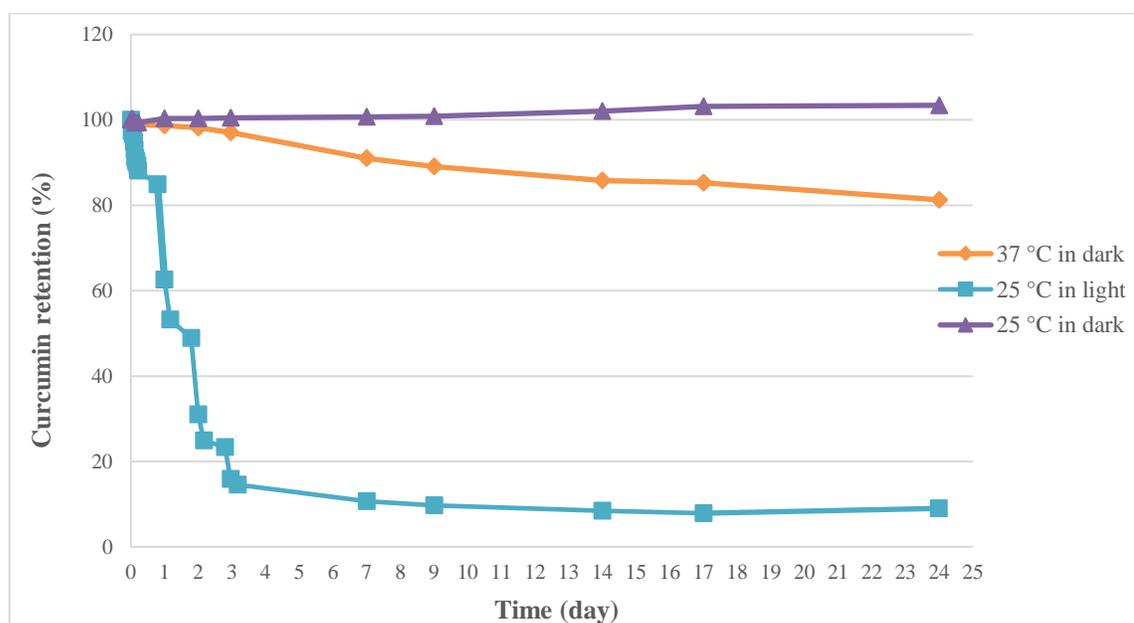
	Darkness 25 °C	Darkness 37 °C	Light 25 °C
Percentage of curcumin degradation (%)	0 ± 2.11	19 ± 6.69	91 ± 1.96

Figure 202. Stability of curcumin in deionized water (pH = 6.8) containing 5 g/L Kolliphor® HS 15 in duration of 24 days in different environmental conditions

The degradation of curcumin was started quickly in daylight at 25 °C, while curcumin was almost stable in darkness (37 °C) and degraded slowly in darkness at 25 °C (Fig.202). The solubility of curcumin was expectedly affected by a temperature increase of, showing its highest value at 37 °C. Although temperature was beneficial to solubility, it negatively affected stability. Those degradations continued over time: curcumin dramatically degraded after 72 h exposure to daylight at 25 °C. The kinetics of curcumin degradation were monitored over 24 days. The highest degradation (up to 91 ± 2%) occurred at 25 °C in daylight. On the contrary, curcumin was stable at 25 °C in darkness and only slightly degraded at 37 °C in darkness (19 ± 6%). This can be explained by the strong absorbency of curcumin in the visible wavelength range, making it prone to degradation and modification in daylight. It thus confirmed the need for microencapsulation studies (Paramera et al., 2011). All samples were protected from daylight during all the following experiments.

2. Encapsulation efficiency (EE) and encapsulation yield (EY)

EE and EY can be considered as two important parameters to evaluate the curcumin loading in the polymeric matrixes. The results were presented in Table 17.

Firstly, EE was estimated as a percentage of curcumin entrapped in pectin beads in comparison to the curcumin amount initially used for the bead preparation. Since curcumin is hydrophobic, the EE for all types of beads was very high (>75%) showing the interest of pectinate gel as a potential carrier in pharmaceutical and food industries (Chambin et al., 2006). Curcumin beads have the highest EE due to no surfactant use. Kolliphor® beads, on the other side, have the lowest EE because of the increased curcumin solubility which induced a higher curcumin diffusion to calcium chloride solution during production process. Results for EE were in correlation with those obtained by Nguyen et al., 2014. In case of TPGS® bead, a high EE was achieved surprisingly, not affected by its high solubility (601.9 mg/L). This result was interesting in comparison with Kolliphor® beads. This could be explained by the property of TPGS® which is an amphiphilic copolymer used for preparation of micelles (CMC = 0.02% w/v) (Keshari et al., 2019). Owing this ability, the

loaded curcumin TPGS micelles were formed and so dissolved curcumin could not diffuse out of the matrix into the CaCl$_2$ solution.

Commercial BiPro® BLG was used for production of beads due to its efficacy in increasing curcumin solubility. The percentage of encapsulation was high (90.5%) because of a lower solubility limiting the diffusion out the capsules during the microcapsules production process.

On the other hand, EY is an indicator of curcumin share in the total mass of particles. This parameter is proportional to encapsulation efficiency (Table 17). Therefore, both Kolliphor® and TPGS® beads showed lower EY (6.3% and 9.0%) than other beads due to their ability to solubilize curcumin during production.

Table 17. Encapsulation efficiency and encapsulation yield of beads

Beads	EE (%)	EY (%)
Curcumin beads	91.7 ± 4.1	16.2 ± 0.7
BiPro® BLG beads	90.5 ± 2.1	13.5 ± 0.3
Kolliphor® beads	76.7 ± 5.5	6.3 ± 0.2
TPGS® beads	90.7 ± 1.4	9.0 ± 0.2

3. Morphologic description of beads by scanning electron microscopy

The size, morphology, surface topology and internal structure of curcumin powder and pectinate beads were carried out in the pictures obtained by SEM (Fig.203). Pectinate beads formed instantaneously when the dispersion was dripped onto the CaCl$_2$ solution. After drying in oven, their size ranged from 2-3mm. Both types of beads were almost regular ovoid in shape, but the Kolliphor® and TPGS® beads (Fig. 203 C and D) exhibited a rounder shape and a smooth surface than the other ones which displayed a rough surface. All beads were characterised by a dense inner structure. Interestingly, curcumin crystals were only found and observed in BiPro® BLG beads (observation of 10 beads) as a result of the lowest solubility in BLG based capsules.
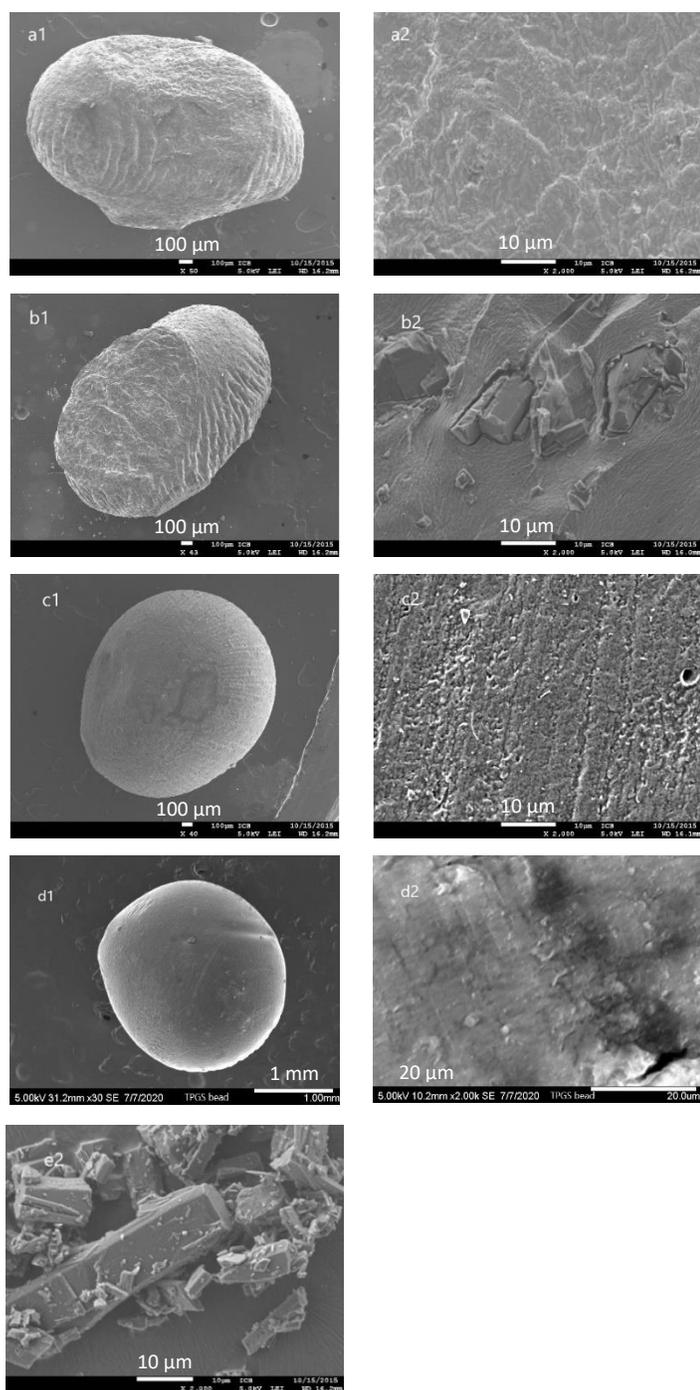
Figure 203. SEM micrographs of pectinate beads and curcumin powder with views of surface (1) and internal beads (2) from Curcumin beads (a), BiPro® BLG beads (b), Kolliphor® beads (c), TPGS® beads (d) and Curcumin powder (e).

4. Dissolution study in simulated intestinal medium

Results of release in simulated intestinal medium are used to understand the behavior of nutraceuticals released in the intestinal tract. It is important in the formulation system

design that bioactive compounds are readily released from the encapsulation material because its availability and efficiency can be modified by restricted release. A simulated release study of curcumin from beads was followed through 7 hours in conditions simulating intestinal tract temperature and pH of and the release pattern was shown in Fig.204 and 205.
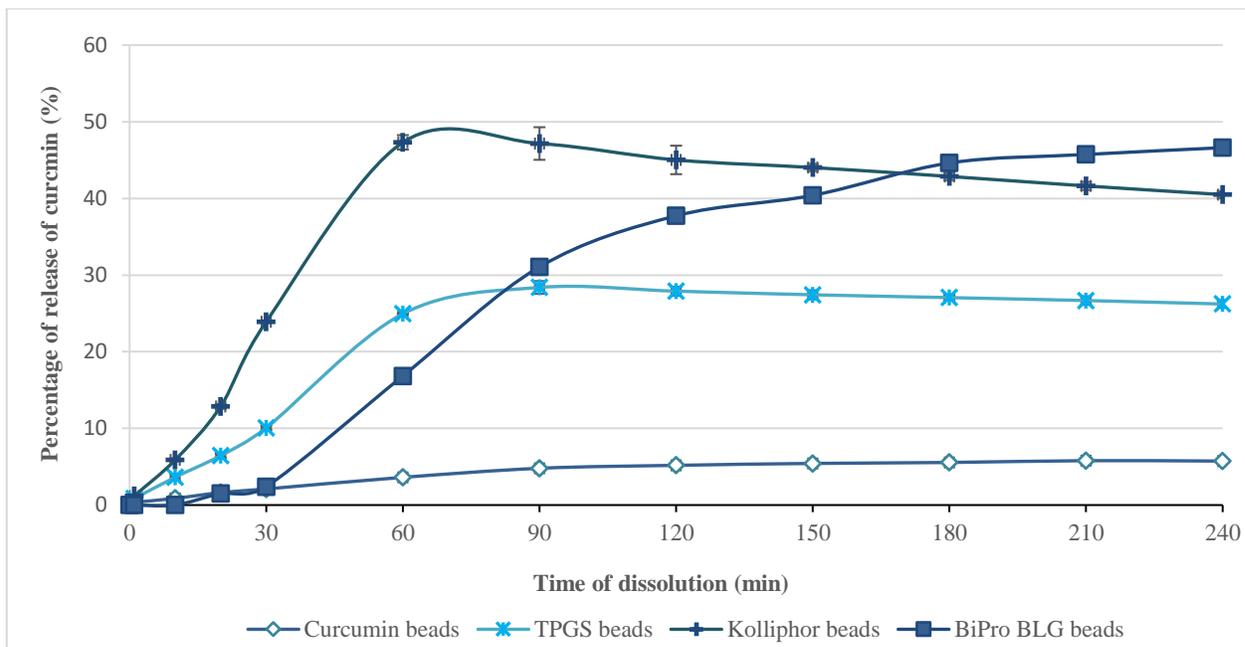
Figure 204. Curcumin release from a pectinate matrix of different types of beads during 4 hours in PBS 7.4 medium

As shown in Fig.204, the release of curcumin reached only a low extent ($< 5\%$) after the first 30 minutes of dissolution for Curcumin and Bipro[®] BLG beads, but it was significantly higher from Kolliphor[®] (25%) and TPGS[®] (10%) beads due to solubilization of the drug by micellization. The maximum release amount was reached after nearly 60 minutes for Kolliphor[®] beads, 90 minutes for TPGS beads, 4 hours for BiPro[®] BLG and Curcumin beads. It is obvious that the dissolution of curcumin that was encapsulated with surfactants (Kolliphor[®] HS 15 and TPGS[®]) was relatively rapid, contrary to BiPro[®] BLG beads whereas the release was gradual but continuous and lasted for several hours, probably due to the barrier properties of the outer protein layer of the wall. Interestingly, in case of Kolliphor[®] beads, above 45% dissolution rate was observed within 60 minutes, but further decreased to 40 % after 4 hours. The decrease of percentage release of curcumin with the

increase of time interval could be explained by the precipitation of the drug that existed in supersaturated state in buffer. This result was confirmed by Seo et al. 2012 where precipitated drug was visually observed at the end of dissolution test and the degradation of curcumin may be was low due to the protection against light in dissolution test.
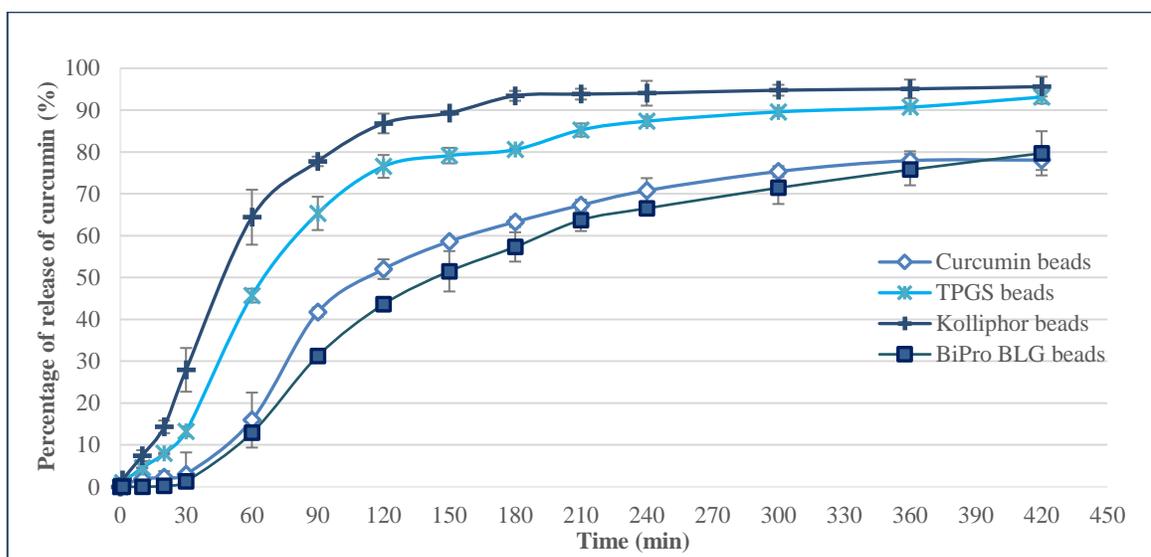
Figure 205. Curcumin release from a pectinate matrix of different types of beads during 7 hours in PBS 7.4 containing 5 g/L Kolliphor® HS 15

As the aqueous solubility of curcumin is very low, 5 g/L Kolliphor® HS 15 was added to PBS 7.4 medium for another dissolution study based on the results of solubility test. Figure 205 shows the dissolution of curcumin from a pectinate matrix of different types of beads.

The release from Kolliphor® HS 15 beads started immediately after the start of dissolution experiment. A significant release of curcumin was observed after 30 minutes of dissolution, with a steep slope of release for 180 minutes. At that point, 93% of release was achieved. When the beads got in contact with the dissolution medium, surface curcumin rapidly dissolved resulting in an increase of curcumin release and reduced lag time (Nguyen et al., 2014).

Curcumin beads, on the contrary, showed a profile with a lag time. During the first 30 minutes, there was no significant release of curcumin and it took 7 hours to reach a release of only 80 %. This result could be explained by the low water solubility of curcumin in

absence of surfactant. TPGS® beads showed an interesting release of curcumin: slower than Kolliphor® beads after first 30 minutes but not different after 7 hours of dissolution.

BiPro® BLG beads showed a release profile similar to curcumin beads without any surfactant. Conclusively, the presence of surfactants in formulation played a very important role in curcumin release from beads (Cheng et al., 2018; Nguyen et al., 2014; Sookkasem et al., 2015). This effect seems to be linked to the increase of curcumin solubility and so could drive the choice of surfactants to modulate curcumin release.

Table 18. Mathematical modeling of release kinetics of curcumin from pectin beads

	Korsmeyer-Peppas			
	R^2	n	k_p	Release mechanism
Curcumin beads	0.93	1.04	0.23	Supercase II transport
Kolliphor® beads	0.95	0.72	0.45	Anomalous transport
TPGS® beads	0.95	0.84	0.97	Anomalous transport
BiPro® BLG beads	0.86	1.83	0.003	Supercase II transport

To determine the mechanism of curcumin release from the particles, mathematical modeling of using the Korsmeyer-Peppas model (Eq. 3) was applied the release profile. A satisfactory linearity ($R^2 = 0.86 - 0.95$) was obtained for all profiles. Depending on geometry of drug delivery system, the indicator of release profile, n, has different values. For spheric polymeric delivery system, n has been defined: as 0.43 for Fickian diffusion, $0.43 < n < 0.85$ for anomalous transport and $n = 0.85$ for polymer swelling (Siepmann & Siepmann, 2008). For the Kolliphor® and TPGS® beads, the calculated n values were found equal to 0.72 and 0.84, respectively, indicating a release mechanism following an anomalous transport mode. In case of BiPro® BLG and Curcumin beads, their release exponents n were higher than 1 indicating the supercase II transport of release mechanism. In all cases, the Fickian curcumin release rate was non-Fickian and depended on the chemical reaction with dissolution medium (*i.e.* pectin depolymerisation), physical mass transfer process of curcumin (*i.e.* diffusion) and its physical state (Nguyen et al., 2014). The swelling of the different beads was also observed during the dissolution experiment. This stage was firstly shown for the curcumin release from the beads by visual observation.

The glassy pectin polymer of dried beads swelled by contact with the release medium due to water diffusion into the system. The increase of water content led to an increased mobility of curcumin and polymer chains. Kolliphor® and TPGS® beads showed a faster water uptake than the other ones as a result of their morphological characteristics. Indeed BiPro® BLG and Curcumin beads displayed a slow water uptake. The swelling contributed to the diffusion of encapsulated curcumin into the release medium.

5. Differential scanning calorimetry (DSC) study

The effect of surfactant on the thermal characteristics and crystanillinity of curcumin was then experimented except for BiPro® BLG beads due to its low improvement of curcumin solubility. Curcumin showed a melting peak at 173.46 °C which was in accordance with previously published results (Nguyen et al., 2014). Pectin powder exhibited a transition at 80.56 °C which was not visible for the pectin-based beads except those with TPGS® beads. Kolliphor® HS 15 showed a melting peak at 32.63 °C also visible for Kolliphor® beads. Similarly, TPGS® exhibited a melting peak at 40.06 °C also detected for TPGS® bead at lower temperature (32.62°C) (Fig.206A).
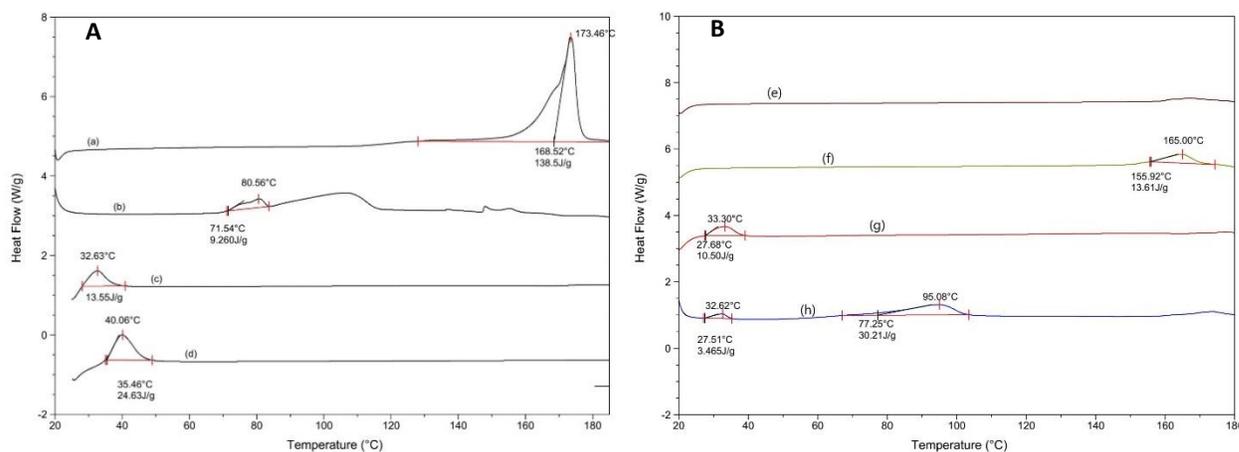
Figure 206. DSC thermograms of curcumin (a), pectin (b), Kolliphor® HS 15 (c), TPGS® (d), Blank bead (e), Curcumin bead (f), Kolliphor® bead (g), TPGS® bead (h).

Bead	The percentage of crystalline curcumin in beads (%)
Curcumin bead	60.1 ± 6.3
Kolliphor® bead	0
TPGS® bead	17.3 ± 8.3

The lower melting point of curcumin was due to its interaction with the pectinate matrix (Nguyen et al., 2014). For Curcumin beads, 60.1% of curcumin was in crystalline state. In case of TPGS beads, 17.3 % of curcumin was still crystalline, while the melting peak of curcumin disappeared in Kolliphor® beads, confirmed a better dissolution of curcumin in the presence of surfactants. As a result, curcumin in these beads is expected to be mainly in the amorphous state following the encapsulation process. These results were in good agreement with those of Seo et al., 2012 and Song et al., 2016 which explained by the dissolution of curcumin in the melted Kolliphor® HS 15 and TPGS® when thermal ananlysis was carried out.

6. DPPH radical scavenging assay

DPPH assay has been widely used to evaluate the free radical scavenging effectiveness of various antioxidant substances (Floegel et al., 2011). The method is based on the reduction of DPPH in alcoholic solution in the presence of a hydrogen-donating antioxidant inducing the formation of the yellow colored non-radical form (DPPH-H) in the reaction (Ak & Gülçin, 2008). A significant decrease was reported in the concentration of DPPH radical due to the scavenging ability of curcumin (Tapal & Tiku, 2012).

A
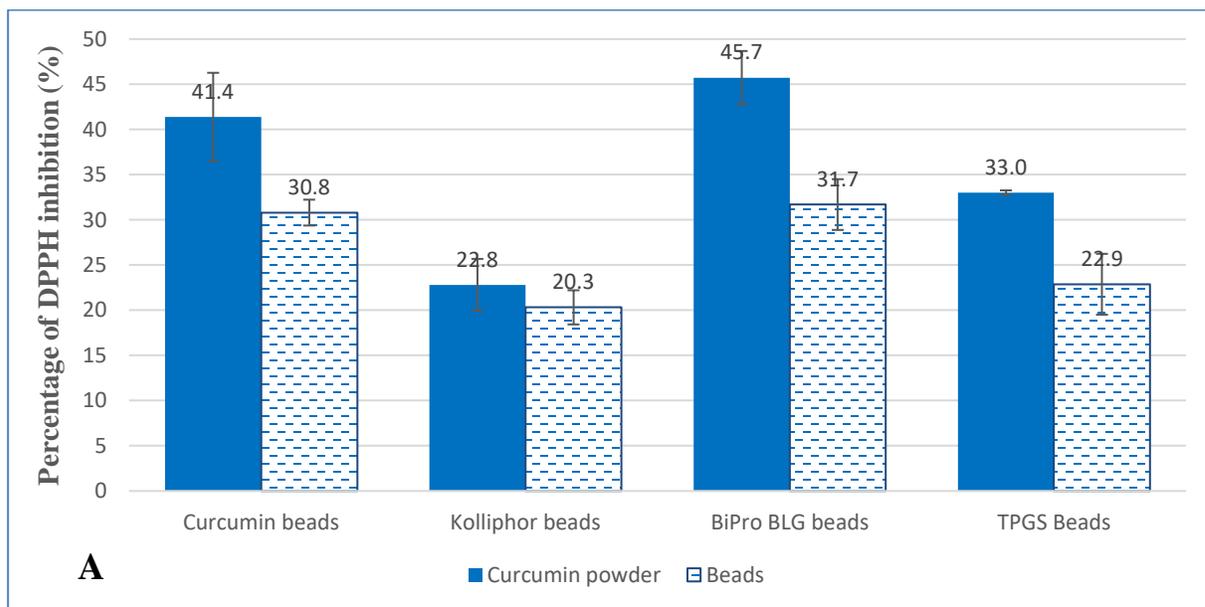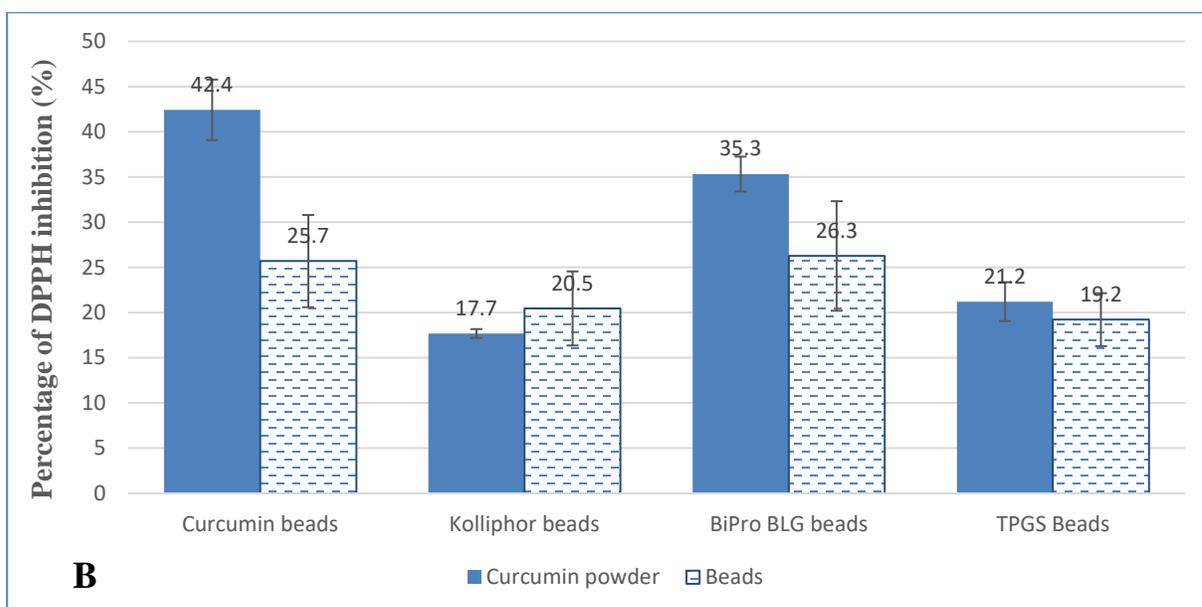
Figure 207. DPPH radical scavenging activity of curcumin powder and curcumin from pectinate beads after 48 hours of extraction (A) and 330 minutes of dissolution (B).

DPPH method was applied for curcumin powder and encapsulated curcumin in order to investigate the effect of i) encapsulation-drying processes and ii) the release and dissolution on the anti-oxidant properties. All DPPH experiments were carried out with an aliquot of medium obtained after extraction or dissolution (mimicking intestinal fluids) to avoid turbidity due to the presence of beads. Figure 4 outlines the percentage of DPPH radical scavenging activity of curcumin from pectinate beads after encapsulation compared with curcumin powder. The antioxidant activity was lower (around 10% decrease) for all kinds of pectinate beads when compared to curcumin powder. Exception was Kolliphor® beads where percentage of inhibition did not seem to change with encapsulation. According to Ak & Gülçin, 2008, stability of curcumin can be improved in emulsions, so it could be assumed that Kolliphor® HS 15 also increased curcumin stability during production of Kolliphor® beads. Since for all other beads percentage of inhibition reduced, oxidation probably occurred during manufacturing process even if protection against light was set.

After 330 minutes of dissolution experiment, the percentage of inhibition seemed unchanged in Kolliphor® and TPGS® beads indicating the efficacy of curcumin to donate its hydrogen atom to radicals with these surfactants (Fig.207B). In case of TPGS® beads, it could be explained by its antioxidant properties (Yan et al., 2007). The other beads showed

248

a decreasing percentage of inhibition around 9-17%. It could be explained by the lower curcumin solubility. Curcumin beads and BiPro® BLG beads leading to a dispersion of crystalline curcumin which could not take part in the radical scavenging process.

CONCLUSION AND PERSPECTIVES

Low bioavailability followed by virtually insoluble in water, poor absorption with crystalline state are one of the main reasons why curcumin has been unsuccessful to use in therapeutic in spite of its pharmacological properties. This barrier can be solved by encapsulation in "egg-box" matrix with surfactants and pectin. But, the most problem in spite of using surfactant in encapsulation is how to find not only the good surfactant but also the right ratio between materials used to encapsulate curcumin successfully. In this study, curcumin was successfully encapsulated by inotropic gelation with different surfactants: Kolliphor® HS 15, TPGS® and BiPro® BLG. It was interesting to show that Kolliphor® HS 15 and TPGS® increased significantly solubility of curcumin in comparison to water or PBS medium. Since solubility of curcumin was higher with Kolliphor®, these beads had the lowest EE and EY due to a higher amount of curcumin loss during encapsulation process. Curcumin, BiPro® BLG and TPGS® beads have EE and EY above 90%, with no significant curcumin loss during production. Curcumin was in the crystalline state in the powder form, but it was transformed to amorphous state during the manufacturing process of Kolliphor® and TPGS® beads. According to these characteristics, curcumin release from Kolliphor® and TPGS® beads was faster and stronger than from the other beads in intestinal model medium. Mathematical models have shown that the type of curcumin release from the pectin matrix particles is Supercase II transport in case of BiPro® BLG and Curcumin beads possessed a smaller and more compact structure leading to a slow water uptake. To the Kolliphor® and TPGS® beads, their release mechanism followed the anomalous transport which showed a faster water uptake than the other ones relating to their morphological characteristics. The antioxidant activity of curcumin was decreased in a few extend (10%) after encapsulation with surfactants except for Kolliphor® beads which protected better curcumin. During dissolution experiment, Kolliphor® HS 15 and TPGS® allowed to maintain antioxidant properties of curcumin. Therefore, the use of surfactant encapsulation formulations played important roles through not only enhancing drug solubility and encapsulation efficiency, but also affecting physical state, release kinetics and protection for antioxidant capacity of

curcumin. So, the choice of surfactant is essential to obtain the properties and functionalities of pectinate curcumin beads. Kolliphor® HS 15 seemed to be the more promising surfactant for both curcumin protection during manufacturing process and release.

BIBLIOGRAPHY

1. Aditya, N.P., Yang, H., Kim, S., Ko, S., 2015. Fabrication of amorphous curcumin nanosuspensions using β-lactoglobulin to enhance solubility, stability, and bioavailability. Colloids Surfaces B Biointerfaces 127, 114–121. https://doi.org/https://doi.org/10.1016/j.colsurfb.2015.01.027

2. Aggarwal, B.B., Bhatt, I.D., Ichikawa, H., Ahn, K.S., Sethi, G., Sandur, S.K., Natarajan, C., Seeram, N., Shishodia, S., 2006. 10 Curcumin-Biological and Medicinal Properties.

3. Aggarwal, B.B., Kumar, A., Bharti, A.C., 2003. Anticancer potential of curcumin: preclinical and clinical studies. Anticancer Res. 23, 363–398.

4. Aggarwal, B.B., Surh, Y.-J., Shishodia, S., 2007. The molecular targets and therapeutic uses of curcumin in health and disease. Springer Science & Business Media.

5. Ak, T., Gülçin, İ., 2008. Antioxidant and radical scavenging properties of curcumin. Chem. Biol. Interact. 174, 27–37.
   https://doi.org/https://doi.org/10.1016/j.cbi.2008.05.003

6. Alam, M.N., Bristi, N.J., Rafiquzzaman, M., 2013. Review on in vivo and in vitro methods evaluation of antioxidant activity. Saudi Pharm. J. 21, 143–152. https://doi.org/https://doi.org/10.1016/j.jsps.2012.05.002

7. Anamika, B., 2012. Extraction of curcumin. J Env. Sci Toxicol Food Technol 1, 1–16.

8. Anand, P., Kunnumakkara, A.B., Newman, R.A., Aggarwal, B.B., 2007. Bioavailability of Curcumin: Problems and Promises. Mol. Pharm. 4, 807–818. https://doi.org/10.1021/mp700113r

9. Ang, L.F., Darwis, Y., Por, L.Y., Yam, M.F., 2019. Microencapsulation Curcuminoids for Effective Delivery in Pharmaceutical Application. Pharmaceutics 11, 451. https://doi.org/10.3390/pharmaceutics11090451

10. Araiza-Calahorra, A., Akhtar, M., Sarkar, A., 2018. Recent advances in emulsion-based delivery approaches for curcumin: From encapsulation to bioaccessibility.

Trends Food Sci. Technol. 71, 155–169.

https://doi.org/https://doi.org/10.1016/j.tifs.2017.11.009

11. Aziz, H.A., Peh, K.K., Tan, Y.T.F., 2007. Solubility of Core Materials in Aqueous Polymeric Solution Effect on Microencapsulation of Curcumin. Drug Dev. Ind. Pharm. 33, 1263–1272. https://doi.org/10.1080/03639040701483967

12. Bakshi, P.S., Selvakumar, D., Kadirvelu, K., Kumar, N.S., 2019. Chitosan as an environment friendly biomaterial – a review on recent modifications and applications. Int. J. Biol. Macromol. https://doi.org/https://doi.org/10.1016/j.ijbiomac.2019.10.113

13. Blanco-García, E., Otero-Espinar, F.J., Blanco-Méndez, J., Leiro-Vidal, J.M., Luzardo-Álvarez, A., 2017. Development and characterization of anti-inflammatory activity of curcumin-loaded biodegradable microspheres with potential use in intestinal inflammatory disorders. Int. J. Pharm. 518, 86–104. https://doi.org/http://dx.doi.org/10.1016/j.ijpharm.2016.12.057

14. Carvalho, D. de M., Takeuchi, K.P., Geraldine, R.M., Moura, C.J. de, Torres, M.C.L., 2015. Production, solubility and antioxidant activity of curcumin nanosuspension. Food Sci. Technol. 35, 115–119.

15. Chambin, O., Dupuis, G., Champion, D., Voilley, A., Pourcelot, Y., 2006. Colon-specific drug delivery: Influence of solution reticulation properties upon pectin beads performance. Int. J. Pharm. 321, 86–93. https://doi.org/http://dx.doi.org/10.1016/j.ijpharm.2006.05.015

16. Chattopadhyay, I., Biswas, K., Bandyopadhyay, U., Banerjee, R.K., 2004. Turmeric and curcumin: Biological actions and medicinal applications. Curr. Sci. 87, 44–53.

17. Chen, Z., Xu, J., Wu, Y., Lei, S., Liu, H., Meng, Q., Xia, Z., 2018. Diosgenin inhibited the expression of TAZ in hepatocellular carcinoma. Biochem. Biophys. Res. Commun. 503, 1181–1185. https://doi.org/10.1016/J.BBRC.2018.07.022

18. Cheng, B., Pan, H., Liu, D., Li, D., Li, J., Yu, S., Tan, G., Pan, W., 2018. Functionalization of nanodiamond with vitamin E TPGS to facilitate oral absorption of curcumin. Int. J. Pharm. 540, 162–170. https://doi.org/https://doi.org/10.1016/j.ijpharm.2018.02.014

19. Chirio, D., Gallarate, M., Peira, E., Battaglia, L., Serpe, L., Trotta, M., 2011.

Formulation of curcumin-loaded solid lipid nanoparticles produced by fatty acids coacervation technique. J. Microencapsul. 28, 537–548. https://doi.org/10.3109/02652048.2011.590615

20. Christenhusz, M., Byng, J., 2016. The number of known plant species in the world and its annual increase, Phytotaxa. https://doi.org/10.11646/phytotaxa.261.3.1

21. Daas, P.J.H., Meyer-Hansen, K., Schols, H.A., De Ruiter, G.A., Voragen, A.G.J., 1999. Investigation of the non-esterified galacturonic acid distribution in pectin with endopolygalacturonase. Carbohydr. Res. 318, 135–145. https://doi.org/https://doi.org/10.1016/S0008-6215(99)00093-2

22. de Vos, P., Faas, M.M., Spasojevic, M., Sikkema, J., 2010. Encapsulation for preservation of functionality and targeted delivery of bioactive food components. Int. dairy J. 20, 292–302.

23. Dhaneshwar, S.S., Mini, K., Gairola, N., Kadam, S.S., 2006. Dextran: A promising macromolecular drug carrier. Indian J. Pharm. Sci. 68, 705.

24. Dong, R., Guo, J., Zhang, Z., Zhou, Y., Hua, Y., 2018. Polyphyllin I inhibits gastric cancer cell proliferation by downregulating the expression of fibroblast activation protein alpha (FAP) and hepatocyte growth factor (HGF) in cancer-associated fibroblasts. Biochem. Biophys. Res. Commun. 497, 1129–1134. https://doi.org/10.1016/J.BBRC.2018.02.193

25. Drews, J., 2000. Drug discovery: a historical perspective. Science (80-.). 287, 1960–1964.

26. Duan, J., Mansour, H.M., Zhang, Y., Deng, X., Chen, Y., Wang, J., Pan, Y., Zhao, J., 2012. Reversion of multidrug resistance by co-encapsulation of doxorubicin and curcumin in chitosan/poly(butyl cyanoacrylate) nanoparticles. Int. J. Pharm. 426, 193–201. https://doi.org/10.1016/j.ijpharm.2012.01.020

27. F. Gibbs Inteaz Alli, Catherine N. Mulligan, Bernard, S.K., 1999. Encapsulation in the food industry: a review. Int. J. Food Sci. Nutr. 50, 213–224. https://doi.org/10.1080/096374899101256

28. Fang, Z., Bhandari, B., 2010. Encapsulation of polyphenols – a review. Trends Food Sci. Technol. 21, 510–523. https://doi.org/https://doi.org/10.1016/j.tifs.2010.08.003

29. Floegel, A., Kim, D.-O., Chung, S.-J., Koo, S.I., Chun, O.K., 2011. Comparison of ABTS/DPPH assays to measure antioxidant capacity in popular antioxidant-rich US foods. J. Food Compos. Anal. 24, 1043–1048. https://doi.org/https://doi.org/10.1016/j.jfca.2011.01.008

30. Flutto, L., 2003. Pectin | Properties and Determination, in: Caballero, B.B.T.-E. of F.S. and N. (Second E. (Ed.),. Academic Press, Oxford, pp. 4440–4449. https://doi.org/https://doi.org/10.1016/B0-12-227055-X/00901-9

31. Fraeye, I., Colle, I., Vandevenne, E., Duvetter, T., Van Buggenhout, S., Moldenaers, P., Van Loey, A., Hendrickx, M., 2010. Influence of pectin structure on texture of pectin–calcium gels. Innov. Food Sci. Emerg. Technol. 11, 401–409. https://doi.org/https://doi.org/10.1016/j.ifset.2009.08.015

32. Gangurde, A., Amin, P., 2015. Enhancement of solubility and dissolution rate of curcumin by eudragit epo-based solid dispersions prepared by hot melt extrusion and spray drying technology.

33. Garcea, G., Jones, D.J.L., Singh, R., Dennison, A.R., Farmer, P.B., Sharma, R.A., Steward, W.P., Gescher, A.J., Berry, D.P., 2004. Detection of curcumin and its metabolites in hepatic tissue and portal blood of patients following oral administration. Br. J. Cancer 90, 1011–1015. https://doi.org/10.1038/sj.bjc.6601623

34. Gharib, R., Greige-Gerges, H., Fourmentin, S., Charcosset, C., Auezova, L., 2015. Liposomes incorporating cyclodextrin–drug inclusion complexes: Current state of knowledge. Carbohydr. Polym. 129, 175–186. https://doi.org/https://doi.org/10.1016/j.carbpol.2015.04.048

35. Gómez-Estaca, J., Gavara, R., Hernández-Muñoz, P., 2015. Encapsulation of curcumin in electrosprayed gelatin microspheres enhances its bioaccessibility and widens its uses in food applications. Innov. Food Sci. Emerg. Technol. 29, 302–307. https://doi.org/https://doi.org/10.1016/j.ifset.2015.03.004

36. Grant, G.T., Morris, E.R., Rees, D.A., Smith, P.J.C., Thom, D., 1973. Biological interactions between polysaccharides and divalent cations: The egg-box model. FEBS Lett. 32, 195–198. https://doi.org/10.1016/0014-5793(73)80770-7

37. Günter, E.A., Popeyko, O. V, 2016. Calcium pectinate gel beads obtained from callus

cultures pectins as promising systems for colon-targeted drug delivery. Carbohydr. Polym. 147, 490–499. https://doi.org/https://doi.org/10.1016/j.carbpol.2016.04.026

38. Hamid, A.A., Kaushal, T., Ashraf, R., Singh, A., Chand Gupta, A., Prakash, O., Sarkar, J., Chanda, D., Bawankule, D.U., Khan, F., Shanker, K., Aiyelaagbe, O.O., Negi, A.S., 2017. (22β,25R)-3β-Hydroxy-spirost-5-en-7-iminoxy-heptanoic acid exhibits anti-prostate cancer activity through caspase pathway. Steroids 119, 43–52. https://doi.org/10.1016/J.Steroids.2017.01.001

39. Holder, G.M., Plummer, J.L., Ryan, A.J., 1978. The Metabolism and Excretion of Curcumin (1,7-Bis-(4-hydroxy-3-methoxyphenyl)-1,6-heptadiene-3,5-dione) in the Rat. Xenobiotica 8, 761–768. https://doi.org/10.3109/00498257809069589

40. Hu, L., Jia, Y., Niu, F., Jia, Z., Yang, X., Jiao, K., 2012. Preparation and Enhancement of Oral Bioavailability of Curcumin Using Microemulsions Vehicle. J. Agric. Food Chem. 60, 7137–7141. https://doi.org/10.1021/jf204078t

41. Joe, B., Lokesh, B.R., 1994. Role of capsaicin, curcumin and dietary n — 3 fatty acids in lowering the generation of reactive oxygen species in rat peritoneal macrophages. Biochim. Biophys. Acta - Mol. Cell Res. 1224, 255–263. https://doi.org/https://doi.org/10.1016/0167-4889(94)90198-8

42. Jovanovic, S. V, Steenken, S., Boone, C.W., Simic, M.G., 1999. H-atom transfer is a preferred antioxidant mechanism of curcumin. J. Am. Chem. Soc. 121, 9677–9681.

43. Keshari, P., Sonar, Y., Mahajan, H., 2019. Curcumin loaded TPGS micelles for nose to brain drug delivery: in vitro and in vivo studies. Mater. Technol. 34, 423–432. https://doi.org/10.1080/10667857.2019.1575535

44. Kiuchi, F., Goto, Y., Sugimoto, N., Akao, N., Kondo, K., Tsuda, Y., 1993. Nematocidal activity of turmeric: synergistic action of curcuminoids. Chem. Pharm. Bull. 41, 1640–1643.

45. Li, M., Ma, Y., Ngadi, M.O., 2013. Binding of curcumin to β-lactoglobulin and its effect on antioxidant characteristics of curcumin. Food Chem. 141, 1504–1511. https://doi.org/https://doi.org/10.1016/j.foodchem.2013.02.099

46. Lin, J.-K., Pan, M.-H., Lin-Shiau, S.-Y., 2000. Recent studies on the biofunctions and biotransformations of curcumin. BioFactors 13, 153–158.

https://doi.org/10.1002/biof.5520130125

47. Lucas, J., Ralaivao, M., Estevinho, B.N., Rocha, F., 2020. A new approach for the microencapsulation of curcumin by a spray drying method, in order to value food products. Powder Technol. 362, 428–435.
https://doi.org/https://doi.org/10.1016/j.powtec.2019.11.095

48. Mangolim, C.S., Moriwaki, C., Nogueira, A.C., Sato, F., Baesso, M.L., Neto, A.M., Matioli, G., 2014. Curcumin–β-cyclodextrin inclusion complex: Stability, solubility, characterisation by FT-IR, FT-Raman, X-ray diffraction and photoacoustic spectroscopy, and food application. Food Chem. 153, 361–370.
https://doi.org/https://doi.org/10.1016/j.foodchem.2013.12.067

49. Nedovic, V., Kalusevic, A., Manojlovic, V., Levic, S., Bugarski, B., 2011. An overview of encapsulation technologies for food applications. Procedia Food Sci. 1, 1806–1815. https://doi.org/http://dx.doi.org/10.1016/j.profoo.2011.09.265

50. Nguyen, A.T.-B., Winckler, P., Loison, P., Wache, Y., Chambin, O., 2014. Physico-chemical state influences in vitro release profile of curcumin from pectin beads. Colloids Surfaces B Biointerfaces 121, 290–298.
https://doi.org/http://dx.doi.org/10.1016/j.colsurfb.2014.05.023

51. Okuyama, K., Noguchi, K., Kanenari, M., Egawa, T., Osawa, K., Ogawa, K., 2000. Structural diversity of chitosan and its complexes. Carbohydr. Polym. 41, 237–247.
https://doi.org/https://doi.org/10.1016/S0144-8617(99)00142-3

52. Pandey, A., Srivastava, R., Shukla, A.K., Saksena, A., 2011. Physico-chemical studies on molecular interactions of curcumin with mono and divalent salts at different temperature. Int. J. Smart Home 5, 7–23.

53. Paradkar, A., Ambike, A.A., Jadhav, B.K., Mahadik, K.R., 2004. Characterization of curcumin–PVP solid dispersion obtained by spray drying. Int. J. Pharm. 271, 281–286. https://doi.org/http://dx.doi.org/10.1016/j.ijpharm.2003.11.014

54. Paramera, E.I., Konteles, S.J., Karathanos, V.T., 2011. Stability and release properties of curcumin encapsulated in Saccharomyces cerevisiae, β-cyclodextrin and modified starch. Food Chem. 125, 913–922.
https://doi.org/https://doi.org/10.1016/j.foodchem.2010.09.071

55. Pillay, V., Fassihi, R., 1999. In vitro release modulation from crosslinked pellets for site-specific drug delivery to the gastrointestinal tract: II. Physicochemical characterization of calcium–alginate, calcium–pectinate and calcium–alginate–pectinate pellets. J. Control. Release 59, 243–256. https://doi.org/https://doi.org/10.1016/S0168-3659(98)00197-7

56. Prieto, M.A., Oswald, K., Torres, E., Allgeuer, T.T., 2015. PE-based crosslinked elastomeric foam with high filler loadings for making shockpads and articles used in footwear and flooring applications.

57. Rafiee, Z., Nejatian, M., Daeihamed, M., Jafari, S.M., 2019. Application of curcumin-loaded nanocarriers for food, drug and cosmetic purposes. Trends Food Sci. Technol. 88, 445–458. https://doi.org/https://doi.org/10.1016/j.tifs.2019.04.017

58. Ravindranath, V., Chandrasekhara, N., 1981. Metabolism of curcumn-studies with [3H]curcumin. Toxicology 22, 337–344. https://doi.org/https://doi.org/10.1016/0300-483X(81)90027-5

59. Ravindranath, V., Chandrasekhara, N., 1980. Absorption and tissue distribution of curcumin in rats. Toxicology 16, 259–265. https://doi.org/https://doi.org/10.1016/0300-483X(80)90122-5

60. Ribas, M.M., Sakata, G.S.B., Santos, A.E., Dal Magro, C., Aguiar, G.P.S., Lanza, M., Oliveira, J.V., 2019. Curcumin cocrystals using supercritical fluid technology. J. Supercrit. Fluids 152, 104564. https://doi.org/https://doi.org/10.1016/j.supflu.2019.104564

61. Ringman, J.M., Frautschy, S.A., Teng, E., Begum, A.N., Bardens, J., Beigi, M., Gylys, K.H., Badmaev, V., Heath, D.D., Apostolova, L.G., Porter, V., Vanek, Z., Marshall, G.A., Hellemann, G., Sugar, C., Masterman, D.L., Montine, T.J., Cummings, J.L., Cole, G.M., 2012. Oral curcumin for Alzheimer's disease: tolerability and efficacy in a 24-week randomized, double blind, placebo-controlled study. Alzheimers. Res. Ther. 4, 43. https://doi.org/10.1186/alzrt146

62. Santana, Á.L., Macedo, G.A., 2019. Challenges on the processing of plant-based neuronutraceuticals and functional foods with emerging technologies: Extraction, encapsulation and therapeutic applications. Trends Food Sci. Technol. 91, 518–529.

https://doi.org/https://doi.org/10.1016/j.tifs.2019.07.019

63. Santos, S. dos, Medronho, B., Santos, T. dos, Antunes, F.E., 2013. Amphiphilic Molecules in Drug Delivery Systems, in: Coelho, J. (Ed.), Drug Delivery Systems: Advanced Technologies Potentially Applicable in Personalised Treatment. Springer Netherlands, Dordrecht, pp. 35–85. https://doi.org/10.1007/978-94-007-6010-3_2

64. Seo, S.-W., Han, H.-K., Chun, M.-K., Choi, H.-K., 2012. Preparation and pharmacokinetic evaluation of curcumin solid dispersion using Solutol® HS15 as a carrier. Int. J. Pharm. 424, 18–25.
https://doi.org/https://doi.org/10.1016/j.ijpharm.2011.12.051

65. Shahgholian, N., Rajabzadeh, G., 2016. Fabrication and characterization of curcumin-loaded albumin/gum arabic coacervate. Food Hydrocoll. 59, 17–25.
https://doi.org/https://doi.org/10.1016/j.foodhyd.2015.11.031

66. Sharma, R.A., Gescher, A.J., Steward, W.P., 2005. Curcumin: The story so far. Eur. J. Cancer 41, 1955–1968. https://doi.org/https://doi.org/10.1016/j.ejca.2005.05.009

67. Shin, G.H., Li, J., Cho, J.H., Kim, J.T., Park, H.J., 2016. Enhancement of Curcumin Solubility by Phase Change from Crystalline to Amorphous in Cur-TPGS Nanosuspension. J. Food Sci. 81, N494–N501.

68. Siepmann, J., Siepmann, F., 2008. Mathematical modeling of drug delivery. Int. J. Pharm. 364, 328–343.
https://doi.org/http://dx.doi.org/10.1016/j.ijpharm.2008.09.004

69. Sneharani, A.H., Karakkat, J. V, Singh, S.A., Rao, A.G.A., 2010. Interaction of Curcumin with β-Lactoglobulin—Stability, Spectroscopic Analysis, and Molecular Modeling of the Complex. J. Agric. Food Chem. 58, 11130–11139.
https://doi.org/10.1021/jf102826q

70. Song, I.-S., Cha, J.-S., Choi, M.-K., 2016. Characterization, in Vivo and in Vitro Evaluation of Solid Dispersion of Curcumin Containing d-α-Tocopheryl Polyethylene Glycol 1000 Succinate and Mannitol. Molecules 21, 1386.
https://doi.org/10.3390/molecules21101386

71. Sriamornsak, P., Nunthanid, J., 1998. Calcium pectinate gel beads for controlled release drug delivery: Int. J. Pharm. 160, 207–212.

https://doi.org/http://dx.doi.org/10.1016/S0378-5173(97)00310-4

72. Steinhauser, E. V, 2015. Turmeric curcumin: Discover the amazing health benefits and healing power of turmeric curcumin. Xilytics, LLC.

73. Suri, S., Ruan, G., Winter, J., Schmidt, C.E., 2013. Chapter I.2.19 - Microparticles and Nanoparticles, in: Ratner, B.D., Hoffman, A.S., Schoen, F.J., Lemons, J.E.B.T.-B.S. (Third E. (Eds.),. Academic Press, pp. 360–388. https://doi.org/https://doi.org/10.1016/B978-0-08-087780-8.00034-6

74. T. Reintjes, 2011. Solubility Enhancement with BASF Pharma Polymers: Solubilizer Compendium. Germany.

75. Tapal, A., Tiku, P.K., 2012. Complexation of curcumin with soy protein isolate and its implications on solubility and stability of curcumin. Food Chem. 130, 960–965. https://doi.org/https://doi.org/10.1016/j.foodchem.2011.08.025

76. Tønnesen, H.H., 2002. Solubility, chemical and photochemical stability of curcumin in surfactant solutions. Studies of curcumin and curcuminoids, XXVIII. Pharmazie 57, 820—824.

77. Tønnesen, H.H., Karlsen, J., 1985. Studies on curcumin and curcuminoids. Zeitschrift für Leb. und Forsch. 180, 402–404. https://doi.org/10.1007/BF01027775

78. Tønnesen, H.H., Másson, M., Loftsson, T., 2002. Studies of curcumin and curcuminoids. XXVII. Cyclodextrin complexation: solubility, chemical and photochemical stability. Int. J. Pharm. 244, 127–135. https://doi.org/https://doi.org/10.1016/S0378-5173(02)00323-X

79. Van Parys, M., 2006. Smart Textiles Using Microencapsulation Technology. Funct. Coatings, Wiley Online Books. https://doi.org/doi:10.1002/3527608478.ch7

80. Vareed, S.K., Kakarala, M., Ruffin, M.T., Crowell, J.A., Normolle, D.P., Djuric, Z., Brenner, D.E., 2008. Pharmacokinetics of curcumin conjugate metabolites in healthy human subjects. Cancer Epidemiol. Biomarkers Prev. 17, 1411–1417. https://doi.org/10.1158/1055-9965.EPI-07-2693

81. Wahlström, B., Blennow, G., 1978. A Study on the Fate of Curcumin in the Rat. Acta Pharmacol. Toxicol. (Copenh). 43, 86–92. https://doi.org/10.1111/j.1600-0773.1978.tb02240.x

82. Wandrey, C., Bartkowiak, A., Harding, S.E., 2010. Materials for encapsulation, in: Encapsulation Technologies for Active Food Ingredients and Food Processing. Springer, pp. 31–100.

83. Wang, Y.-J., Pan, M.-H., Cheng, A.-L., Lin, L.-I., Ho, Y.-S., Hsieh, C.-Y., Lin, J.-K., 1997. Stability of curcumin in buffer solutions and characterization of its degradation products. J. Pharm. Biomed. Anal. 15, 1867–1876.

84. Willats, W.G.T., Knox, J.P., Mikkelsen, J.D., 2006. Pectin: new insights into an old polymer are starting to gel. Trends Food Sci. Technol. 17, 97–104. https://doi.org/https://doi.org/10.1016/j.tifs.2005.10.008

85. Xiao, B., Si, X., Zhang, M., Merlin, D., 2015. Oral administration of pH-sensitive curcumin-loaded microparticles for ulcerative colitis therapy. Colloids Surfaces B Biointerfaces 135, 379–385.
https://doi.org/https://doi.org/10.1016/j.colsurfb.2015.07.081

86. Yan, A., Von Dem Bussche, A., Kane, A.B., Hurt, R.H., 2007. Tocopheryl polyethylene glycol succinate as a safe, antioxidant surfactant for processing carbon nanotubes and fullerenes. Carbon N. Y. 45, 2463–2470.
https://doi.org/https://doi.org/10.1016/j.carbon.2007.08.035

87. Yang, K.-Y., Lin, L.-C., Tseng, T.-Y., Wang, S.-C., Tsai, T.-H., 2007. Oral bioavailability of curcumin in rat and the herbal analysis from Curcuma longa by LC–MS/MS. J. Chromatogr. B 853, 183–189.
https://doi.org/https://doi.org/10.1016/j.jchromb.2007.03.010

88. Yoon, H.-G., Kim, H.-Y., Lim, Y.-H., Kim, H.-K., Shin, D.-H., Hong, B.-S., Cho, H.-Y., 2000. Thermostable chitosanase from Bacillus sp. strain CK4: cloning and expression of the gene and characterization of the enzyme. Appl. Environ. Microbiol. 66, 3727–3734.

89. Zhang, Z., Tan, S., Feng, S.-S., 2012. Vitamin E TPGS as a molecular biomaterial for drug delivery. Biomaterials 33, 4889–4906.
https://doi.org/https://doi.org/10.1016/j.biomaterials.2012.03.046

90. Zuidam, N.J., Nedovic, V., 2010. Encapsulation technologies for active food ingredients and food processing.

APPENDIX
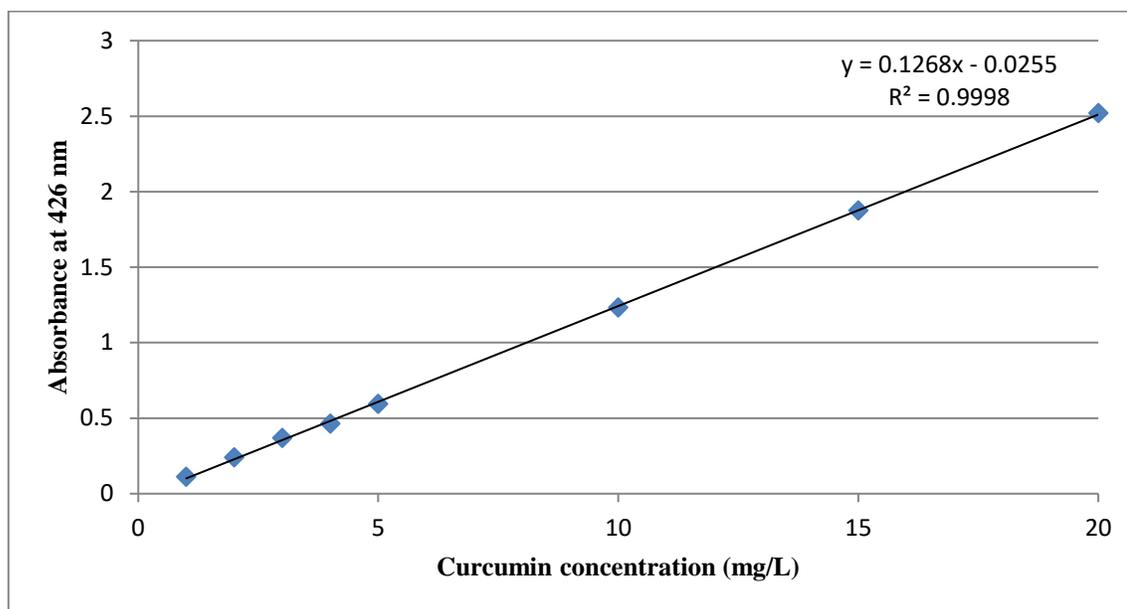
Figure 208. Calibration curve of solubilized curcumin in deionized water containing 5 g/L Kolliphor® HS 15 at absorbance 426 nm (remettre n° de figure dans le texte)
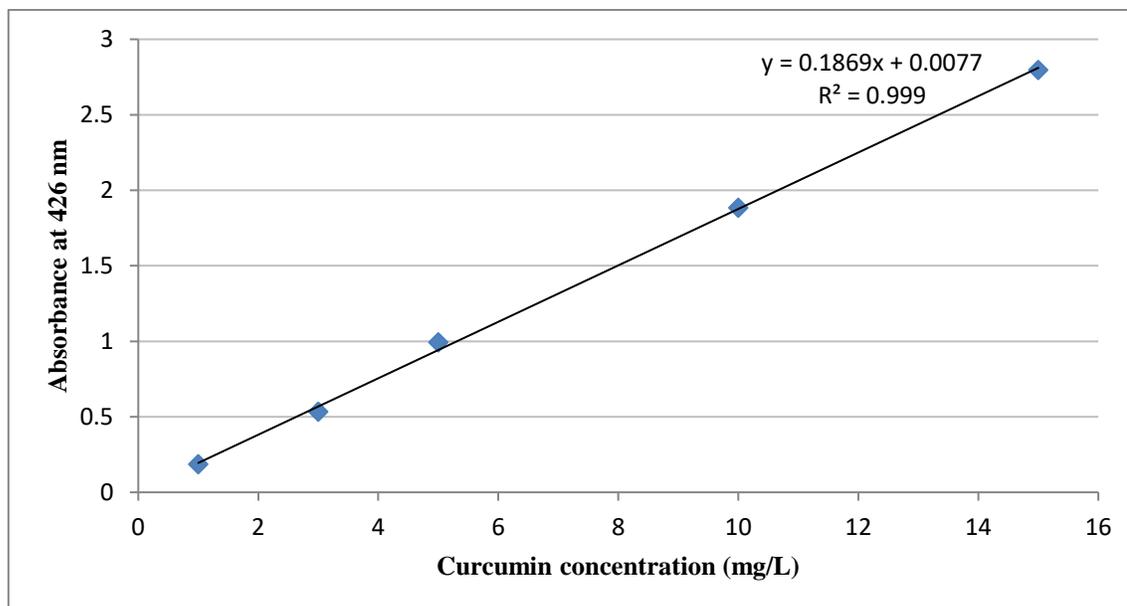

**Figure 209.** Calibration curve of solubilized curcumin in EtOH 96% at absorbance 426 nm
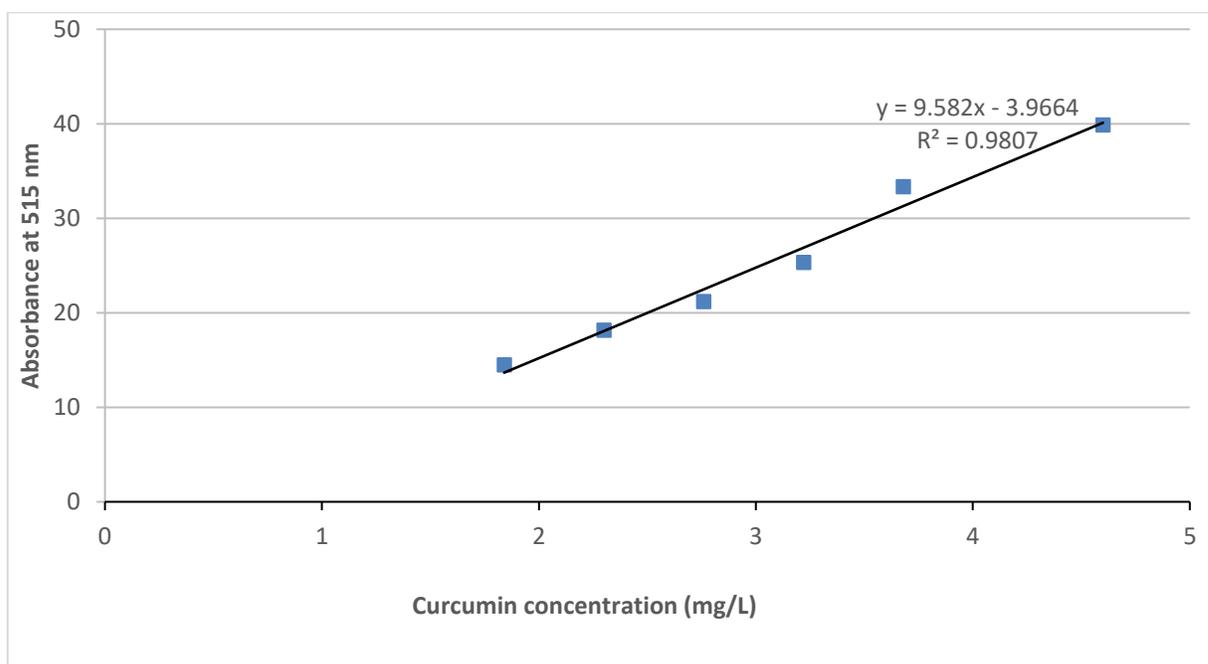
Figure 210. Calibration curve of solubilized curcumin in EtOH 96% containing 5 mL of DPPH in EtOH 96 % solution at absorbance 515 nm

GENERAL CONCLUSION

Since saponins are secondary metabolites manufactured from various plants species because of their potentials, researchers are continuing to isolate new saponins from natural sources, together with structural determination, reported also on biological activities. In order to continue research for new biologically active and completing the chemotaxonomic data about saponins, three species including *W.* x "Bristol ruby", *W. florida* "Pink poppet" and *W. florida* "Jean's gold" and from genus *Cordyline*, thus family Asparagaceae, along with two species including *C. fruticosa* "Fairchild red" and *Dracaena braunii* were phytochemically studied. This investigation led to an isolation of 35 saponins using various chromatographic methods. Nine triterpenoid saponins are previously undescribed derived from the acid oleanolic and hederagenin which were further biologically investigated, among with 18 steroidal saponins including 7 new spirostane-types and 6 new furostane-types. The biological tests on cancer cell lines were further carried out on saponins extracted from three *Weigela* species. The biological tests on cancer cell lines were further evaluated on saponins extracted from three *Weigela* species. The relationship between structure and cytotoxic activity was described. It seems that aglycone and sugar part of saponin plays an important role for cytotoxicity. The presence of sequence β-D-xylopyranosyl-(1→3)-α-L-rhamnopyranosyl-(1→2)-β-D-xylopyranosyloleanolic acid or β-D-xylopyranosyl-(1→3)-α-L-rhamnopyranosyl-(1→2)-arabinopyranosyloleanolic acid responded for enhancements of cytotoxicity. In contrary, the cytotoxic activity of hederagenin-type triterpenoid saponins were pointed out as inactive *in vitro*, but those saponins exhibited an inferior *in vivo* antitumor activity due to literature. This knowledge contributes to complete the chemotaxonomic data about saponins and it will interresting to evaluate the *in vivo* cytotoxic activity of this type saponins in the further study. On the other hand, biological investigation will be further carried out on steroidal saponins extracted from *C. fruticosa* "Fairchild red" and *Dracaena braunii*. This will interesting to analyse biological results as well as their relationship between structure and bioactivity.

In order to overcome limitations and enhance therapeutic efficacy of natural hydrophobic agents, curcumin as a model drug, a phenolic compound isolated from turmeric powder

which posscess significant biological and pharmacological activities, was chosen to assess the interest of encapsulation for natural products. An encapsulation process was carried out using ionotropic gelation method with the presence of different surfactants. Different beads were manufactured successfully and characterized for physicochemical characteristics. High encapsulation efficiency was achieved in all case of beads produced. The crystallinity of curcumin was tranformed into amorphous state during the production process based on DSC profile results. The improvement of curcumin solubility was demontrated with Kolliphor® and TPGS® and the matrix encapsulation has a great potential to control the release properties in intestinal medium. This study exhibited that surfactants are significantly effective in order to enhance the solubility and protect antioxidant capacity of curcumin and that their choices are essential.

The same strategy could be applied for microencapsulation of other bioactive ingredients, particularly natural compounds as saponin, in the development of functional foods and pharmaceutical products.

This work gives opening perspectives:

- Study on biological properties of diosgenin as a model of aglycone and set up a suitable encapsulation method.

- Try to discover new saponins with biological activities from other plants in Asian countries.

- Investigate new encapsulation techniques to preserve the natural compounds and optimize their bioavailability.

- Evaluate the interest to use saponin as surfactant in curcumin encapsulation with pectin.

LIST OF PUBLICATION, ORAL PRESENTATION AND POSTER

Publications

1. Nguyen, D.H., Mitaine-Offer, A.-C., Maroso, S., Papini, A.-M., Paululat, T., Bellaye, P.-S., Collin, B., Chambin, O., Lacaille-Dubois, M.-A. (2019). Cytotoxic glycosides from the roots of *Weigela* x "Bristol Ruby." *Fitoterapia* 137, 104242. https://doi.org/10.1016/j.fitote.2019.104242

2. Nguyen, D.H., Mitaine-Offer, A.-C., Miyamoto, T., Tanaka, C., Bellaye, P.-S., Collin, B., Chambin, O., Lacaille-Dubois, M.-A. (2020). Phytochemical analysis of two *Weigela florida* cultivars, "Pink Poppet" and "Jean's Gold." *Phytochemitry Letters* 37, 85–89. https://doi.org/10.1016/j.phytol.2020.04.009

Posters and Oral presentation

1. 11th World Meeting on Pharmaceutics, Biopharmaceutics and Pharmaceutical Technology, APV - APGI, ADRITELF (Poster 1)
   Influence of surfactant upon curcumin encapsulation in pectinate matrices, Granada 19-22 March 2018, Spain.

2. 24th Forum des Jeunes Chercheurs (FJC2018) (Poster 2)
   Phytochemistry of Dracaena braunii from Vietnam, Besançon 14-15 June 2018, France.

3. 25th Forum des Jeunes Chercheurs (FJC2019) (Oral communication)
   Cytotoxic glycosides from the roots of Weigela x "Bristol Ruby", Dijon 13-14 June 2019, France.